

# Sheffield Hallam University

*Detection of Alzheimer's disease biomarkers and mycotoxins using spectroscopic ellipsometry.*

MUSTAFA, Mohd Kamarulzaki.

Available from the Sheffield Hallam University Research Archive (SHURA) at:

<http://shura.shu.ac.uk/20106/>

## A Sheffield Hallam University thesis

This thesis is protected by copyright which belongs to the author.

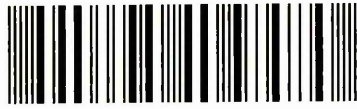
The content must not be changed in any way or sold commercially in any format or medium without the formal permission of the author.

When referring to this work, full bibliographic details including the author, title, awarding institution and date of the thesis must be given.

Please visit <http://shura.shu.ac.uk/20106/> and <http://shura.shu.ac.uk/information.html> for further details about copyright and re-use permissions.

Learning and Information  
Adsetts Centre, City Campus  
Sheffield S1 1WD

101 990 552 2



**REFERENCE**

ProQuest Number: 10697413

All rights reserved

INFORMATION TO ALL USERS

The quality of this reproduction is dependent upon the quality of the copy submitted.

In the unlikely event that the author did not send a complete manuscript and there are missing pages, these will be noted. Also, if material had to be removed, a note will indicate the deletion.



ProQuest 10697413

Published by ProQuest LLC (2017). Copyright of the Dissertation is held by the Author.

All rights reserved.

This work is protected against unauthorized copying under Title 17, United States Code  
Microform Edition © ProQuest LLC.

ProQuest LLC.  
789 East Eisenhower Parkway  
P.O. Box 1346  
Ann Arbor, MI 48106 – 1346

Detection of Alzheimer's Disease  
Biomarkers and Mycotoxins using  
Spectroscopic Ellipsometry

Mohd Kamarulzaki Mustafa

**A thesis submitted in partial fulfilment of the requirements of  
Sheffield Hallam University  
for the degree of Doctor of Philosophy.**

April 2011

# Declaration

I hereby declare that this thesis submitted for the degree of PhD is the result of my own research and that this thesis has not been submitted for a higher degree to any University or Institution.

Signed

**Mohd Kamarulzaki Mustafa**

# Abstract

Neurological diseases such as Alzheimer's, Parkinson's, MS, which are common around the world and particularly in developed countries with high proportion of elderly, stimulate the development of bio-sensors for early diagnostics of such diseases. For instance the treatment of Alzheimer's patients constitutes a substantial proportion of NHS budget nowadays. Therefore, the development of highly sensitive optical devices for early diagnoses of Alzheimer's disease (AD) will be beneficial to society. This PhD is mainly dedicated to the application of the method of Spectroscopic Ellipsometry for AD diagnostics. Total Internal Reflection Ellipsometry (TIRE) was utilized in this work as an immunosensor for detection of Amyloid Precursor Protein 770 (APP<sub>770</sub>) and beta amyloid peptide (A $\beta$ <sub>1-16</sub>). The detection of low concentrations of APP<sub>770</sub> in a complex medium containing other proteins, salts, and amino acids was achieved using the method of TIRE in direct immuno assay with monoclonal DE2 antibodies. The calibration of TIRE with a complementary QCM measurements in air allowed the evaluation of (originally unknown) concentration of APP<sub>770</sub> as 121 *pmol/l*. The immune reaction between APP<sub>770</sub> and DE2 antibodies was also tested using QCM technique operating in liquid. The application of TIRE was extended to the detection of much smaller peptide A $\beta$ <sub>1-16</sub> which bind to the same DE2 antibody. The results were very encouraging since low concentrations (0.05ng/ml) of A $\beta$ <sub>1-16</sub> were detected; this showed good prospects for detection of A $\beta$ <sub>40-42</sub>, an actual marker of AD.

The second part of this work was dedicated to detection of mycotoxins, a hazardous contaminant in agriculture products (grains) and associated food and feed. Two mycotoxins, namely Aflatoxins B1 and Zearalenone, were detected in TIRE direct immunoassay. Zearalenone was also detected using TIRE competitive assay. The obtained limits of detection of 0.04 ng/ml for Aflatoxin and 0.1 ng/ml for Zearalenone are well below the legislation limit. Such remarkable results are due to a combination of high sensitivity of TIRE method and the aggregation of hydrophobic molecules of mycotoxins in aqueous solutions. A new method of purification of substances contaminated with mycotoxins based on the use of polyelectrolyte microcapsules functionalized with specific antibodies was successfully tested in this work.

# Acknowledgements

I would like to thank my Director of Studies, Dr. Alexei Nabok, for all of his encouragement, help and support during this work. I greatly enjoyed the learning process and worthwhile research studies under him.

I am grateful to my supervisors, Prof. David Parkinson and Dr. Aseel Hassan, for their ideas and suggestions to make this work meaningful.

My sincere gratitude belongs to Dr. Anna Tsargorodskaya and our collaborators, Prof. Nikolai Starodub (National University of Life and Environmental Sciences of Ukraine), Prof. Victor Erokhin (Department of Physica, University of Parma) and Prof. Andras Szekac (Plant Protection Institute, Hungarian Academy of Science, Hungary) for their contributions and advice in this work.

Thanks are also due to all MERI support staff, especially Gary Robinson and Deeba Zahoor, for their technical help and support throughout this work.

Special thank to my wife, Murni, and all my children, Azraei, Khairie and Yasmin Putrie, for their loving support, patience and understanding throughout the course of my studies. Your sacrifices allowed me to pursue this endeavour.

# Dedication

To my parent, my wife and my children.

# Contents

Declaration	ii
Abstract	iii
Acknowledgement	iv
Dedication	v
Contents	vi
Lists of Publications	x
Lists of Abbreviations	xii

## CHAPTER

## TOPICS

<b>1</b>	<b>INTRODUCTION</b>	
	1.1 Alzheimer's Disease (AD) And Methods Of Detection	1
	1.2 Diagnosis of Alzheimer's Disease	4
	1.3 Mycotoxins review and detection of low molecular weight toxins	6
	1.3.1 Detection of Mycotoxins	10
	1.3.2 Toxin purification	12
	1.4 Aims and Objectives	13
<b>2</b>	<b>BIOSENSORS THEORY, BACKGROUND AND APPLICATIONS</b>	
	2.1 Biosensors review	15
	2.1.1 The need of label free detection	19
	2.2 Affinity Biosensors	20
	2.2.1 Antigen-antibody interaction	21
	2.2.2 Nucleic Acids Interaction	23
	2.2.3 Enzyme-substratum Interaction	24

2.2.4	Avidin–Streptavidin Interaction	25
2.3	Immunosensors	26
2.3.1	Antibody immobilization	27
2.4	Immunoassays format for immunosensors	28
2.5	Piezoimmunosensors; Quartz Crystal Microbalance (QCM)	30
2.6	Spectroscopic Ellipsometry for sensing applications	32
2.7	Summary	34
<b>3</b>	<b>OPTICAL IMMUNOSENSING EXPERIMENTAL METHODS: TOTAL INTERNAL REFLECTION ELLIPSOMETRY (TIRE)</b>	
3.1	Theoretical background of evanescent wave technique	35
3.1.1	Ellipsometry Method	37
3.1.2	Surface Plasmon Resonance (SPR)	41
3.2	Total Internal Reflection Ellipsometry (TIRE)	44
3.2.1	Theoretical background of TIRE	45
3.2.2	TIRE experimental set-up	48
3.2.3	TIRE measurements and fitting protocol	50
3.2.4	Further improvement of TIRE data analysis	53
3.2.5	TIRE kinetics analysis	56
3.3	Summary	58
<b>4</b>	<b>COMPLEMENTARY EXPERIMENTAL METHODS AND TECHNOLOGIES</b>	
4.1	Piezoelectric resonator: Quartz Crystal Microbalance (QCM)	59
4.2	Crystal Quality Factor	63
4.3	QCM operates in liquid	64
4.3.1	Viscoelastic effect	65

4.3.2	Special Sauerbrey equation in liquid medium	66
4.3.3	Impedance Analysis	66
4.3.4	Butterworth van dyke (BVD) equivalent circuit model	67
4.3	QCM in Microfluidics flow	70
4.4	Atomic Force Microscope (AFM)	73
4.5	Scanning Electron Microscopy (SEM)	76
4.6	Summary	77
<b>5</b>	<b>THE STUDY OF IMMUNE REACTIONS FOR ALZHEIMER'S DISEASE DIAGNOSTIC</b>	
5.1	Sample preparation	78
5.2	Detection of Amyloid Precursor Protein (APP <sub>770</sub> ) by Total Internal Reflection Ellipsometry (TIRE) method	79
5.3	Calibration of unknown concentration of APP using Quartz Crystal Microbalance (QCM) dry technique	83
5.4	QCM measurements in liquid	88
5.4.1	QCM in Microfluidics	88
5.4.2	QCM impedance analysis of the immune reactions between DE2 and APP	92
5.5	Detection of Amyloid beta peptide 1-16 (A $\beta$ <sub>1-16</sub> ) by TIRE method	98
5.6	TIRE kinetic analysis and evaluation of affinity constant for A $\beta$ <sub>1-16</sub>	102
5.7	Morphology Analysis for APP and A $\beta$ <sub>1-16</sub>	106
5.8	Summary	119
<b>6</b>	<b>THE DETECTION OF ZEARALENONE MYCOTOXINS USING TIRE METHOD</b>	
6.1	Sample Preparation	120
6.2	TIRE Direct Immunoassay for detection of ZON	121
6.3	TIRE Competitive Immunoassay for ZON	123
6.4	TIRE Kinetics Measurement for ZON	125
6.5	Polyelectrolyte Microcapsules for ZON Purification	128

6.5.1	Microcapsules Preparation	128
6.5.2	SEM Analysis of MnCO <sub>3</sub> Microcapsule	129
6.5.3	ZON Purifying Result by UV-vis Spectrophotometer	131
6.6	Summary	132
<b>7</b>	<b>DETECTION OF AFLATOXIN B1 (AFT) USING TIRE COMBINED WITH DIRECT IMMUNOASSAY</b>	
7.1	Sample preparation	134
7.2	TIRE spectra for Aflatoxins direct immunoassay	135
7.3	TIRE data fitting for Aflatoxin B1 direct immunoassay	138
7.4	Kinetics of the Aflatoxin Immune Reaction	140
7.5	Summary	143
<b>8</b>	<b>CONCLUSIONS AND FUTURE WORK</b>	
8.1	Conclusions	145
8.2	Recommendations for future work	148
	References	149

# Lists of Publications

## *Journals publications;*

1. A. Nabok, A. Tsargorodskaya, M.K. Mustafa, I. Székács, N.F. Starodub, A. Székács, 'Detection of low molecular weight toxins using an optical phase method of ellipsometry', *Sensors and Actuators B: Chemical*, In Press, Corrected Proof, Available online 10 February 2010.
2. Alexei Nabok, Mohd Kamarulzaki Mustafa, David Parkinson, Anna Tsargorodskaya, 'Ellipsometric Immunosensor for Detection of Amyloid Precursor Protein with a View of Alzheimer's Disease Diagnostics', *Sensors & Transducers Journal* (ISSN 1726-5479), Vol.120, Issue 9, September 2010, pp.53-61.
3. M.K. Mustafa, A. Nabok, D. Parkinson, I.E. Tothill, F. Salam, A. Tsargorodskaya, 'Detection of B- amyloid peptide (1-16) and amyloid precursor protein (APP770) using Spectroscopic Ellipsometry and QCM techniques: a step forward towards Alzheimer's disease diagnostics', *Biosensors and Bioelectronics*, Volume 26, Issue 4, 15 December 2010, pp. 1332-1336.
4. A.V. Nabok, M.K. Mustafa, A. Tsargorodskaya, N.F. Starodub, 'Detection of Aflatoxin B1 with a label free ellipsometry immunosensor', *BioNanoScience*, (Springer), 2011 (in press).
5. A.V. Nabok, M.K. Mustafa, V. Erokhin, S. Erokhina, A. Szekacs, ' Purification of substances contaminated with mycotoxins using functionalysed microparticles' *IEEE sensors*, 2011 (in press).

## *Publications in Conference Proceedings:*

1. 13<sup>th</sup> International Conference on Organized Molecular Films, 18-21 July 2010, Quebec City, Canada, (Poster and Oral Presentation).
2. Proceeding of Eurosensors XXIII conference, 2009, *Procedia Chemistry*, Vol. 1, Issue 1, 1491-1949.

3. Proceeding of 5<sup>th</sup> Workshop on Ellipsometry, 2-4 March 2009, Zweibrucken, Germany.
4. Proceeding of 1<sup>st</sup> Bio-sensing Technology Conference, 10-12 Nov. 2009, Marriot Bristol City Centre, Bristol.
5. Proceeding of X Conference on Optical Chemical Sensors and Biosensors (Eurotrode X), 28-31 March 2010, Prague, Rep. Check.
6. Proceeding of 10th World Biosensors Congress, 26-28 May 2010, Glasgow, UK.

***Presentations on National and International Conferences and Seminars:***

1. Faculty of Health and Wellbeing Research Day, 17 Dec 2008, Millennium Gallery, Sheffield (Poster Presentation)
2. 5<sup>th</sup> Workshop on Ellipsometry, Zweibrucken, Germany 2-4 March 2009 (Poster Presentation)
3. Applications of Micro and Nanosensors in Security, Health and Environmental Monitoring, NPL, 26 March 2009 (Poster Presentation)
4. Eurosensors XXIII, Lausanne, Switzerland, 6-9 Sept 2009 (Poster Presentation).
5. Applications of Micro & nano technology in biosensing & diagnostics seminar, Cranfield University, 17 Sept 2009 (Poster Presentation).
6. 1<sup>st</sup> Bio-sensing Technology Conference, 10-12 Nov. 2009, Marriot Bristol City Centre, Bristol (Oral Presentation)
7. X Conference on Optical Chemical Sensors and Biosensors (Eurotrode X), 28-31 March 2010, Prague, Rep. Check (Poster Presentation).
8. 10th World Biosensors Congress, 26-28 May 2010, Glasgow, UK (Oral and Poster Presentation)

# Lists of Abbreviation

AD	Alzheimers Disease
AFM	Atomic force microscopy
AFT	Aflatoxin
APP	Amyloid Precursor Protein
A $\beta$	Amyloid Beta Peptide
Ab	Antibody
BSA	Bovine Serum Albumin
BVD	Butterworth Van-Dyke
CM	Complete medium
DNA	Deoxyribonucleic acid
ELISA	Enzyme-linked immunosorbent assay
ESI	Electrospray ionization
FAO	Food authority organization
IgG	Immunoglobulin G
K <sub>A</sub>	Association constant
K <sub>D</sub>	Dissociation / affinity constant
LC	Liquid chromatography
LOD	Limit of detection
MALDI	Matrix assisted laser desorption/ionization
MnCO <sub>3</sub>	Magnesium carbonate
MS	Mass spectroscopy
MSE	Mean square error

OWLS	Optical waveguide light spectroscopy
PAH	Poly(allylamine) hydrochloride
PSS	Poly-styrene sulfonate
QCM	Quartz Crystal Microbalance
SEM	Scanning electron microscopy
SERS	Surface enhanced Raman scattering
SP	Senile plaque
SPR	Surface Plasmon Resonance
SPW	Surface Plasmon Wave
TIRE	Total internal reflection ellipsometry
TLC	Thin layer chromatography
TSM	Thickness Shear Mode
WHO	World health organization
ZON	Zearalenone

# CHAPTER 1

## INTRODUCTION

The main focus of this project is further development of optical bio-sensing methods for medical applications. Two main biomedical applications are discussed in this chapter. The first is the diagnostic of Alzheimer's Disease (AD), which involves statistics about AD patients, AD biomarkers, and methods of detection. The second is the study of mycotoxins, which is mostly dedicated to detection methods of low molecular weight toxins. The chapter concludes by providing a brief description of the aim and objectives of this work.

### 1.1 Alzheimer's Disease (AD) And Methods Of Detection

Alzheimer's Disease is a degenerative disease which was first described by the German psychiatrist and neuropathologist Dr Alois Alzheimer in 1906. He presented his findings about a patient who had suffered mental decline prior to her death. AD is part of the dementia family and is commonly accompanied by neuro-psychiatric symptoms; these include agitation (60%-70%), apathy (60%-70%), depression (50%), anxiety (50%), irritability (50%), delusion disorders and psychosis (40%-50%), disinhibition (30%) and hallucination (10%) [1]. At a severe stage, AD patients can develop impaired judgement, disorientation, confusion, behaviour changes, language breakdown, difficulty swallowing and problems walking. At worst AD can lead to emotional extremes of aggressiveness, anxiety and despair [2,3].

Studies have estimated that in 2000 about 25 million people had dementia, projected to rise to 63 million by 2030 and 114 million by 2050, assuming no geographic variation and age-specific prevalence rates [4]. Generally AD has been diagnosed in people over

65 years old; cases below the age of 60 are very rare. Cost for about 224 000 elderly people with cognitive impairment living in institutions has been estimated at £4.6 billion annually, or 0.6% of UK gross domestic product. According to the Global Burden of Disease estimates for the 2003 World Health Report, dementia contributes 11.2% years lived with disability in people aged 60 years and older; this is more than stroke (9.5%), musculoskeletal disorders (8.9%), cardiovascular disease (5.0%), and all forms of cancer (2.4%) [5]. This growth is phenomenal, especially in developing countries, including India, China, South Asia and the Western Pacific, which will experience 300% growth in the number of dementia patients [6].

An autopsy by Dr Alois revealed that there were amyloid plaque, neurofibrillary tangles and arteriosclerosis changes in his patient's brain which suggest that the deposition of  $\beta$  amyloid ( $A\beta$ ) in the form of senile plaques (SPs) and often in the walls of cerebral and meningeal blood vessels is one of the major neuropathological hallmarks of Alzheimer's disease (AD) [6]. The central core of SPs consists of an insoluble deposit of 1-42 amino acid peptide known as  $\beta$ -Amyloid peptide or  $A\beta$  [7,8]. Until recently it was believed that aberrant processing gives rise to deposition of  $A\beta$  and hence AD, but it has now been shown that  $A\beta$  is produced under normal circumstances in healthy cells *in-vitro* [9-11] and can be detected in the cerebrospinal fluid of healthy individuals [11,12].  $A\beta$  is derived from a larger trans-membrane spanning protein known as amyloid precursor protein (APP), the role of which is not clearly identified. APP consists of a single trans-membrane spanning domain, a large extracellular N terminus and a short intracellular C terminus [13]. APP comes in several forms and can be cut apart by enzymes to form beta amyloid, as in Fig. 1.1. Eventually, the cut pieces of APP aggregate as amyloid plaque and injure nerve cells. The difference between a normal and AD patient brain pattern is shown in Fig. 1.2.

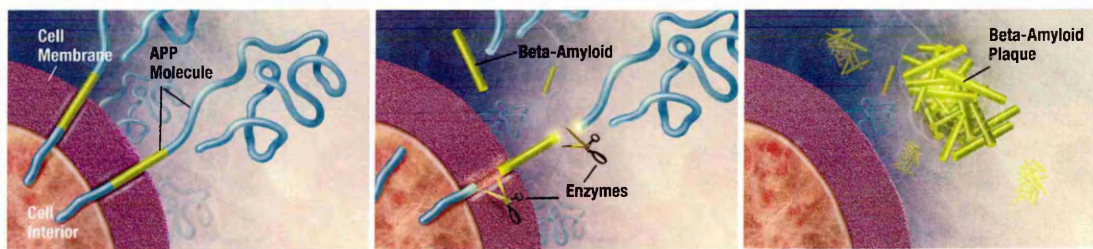


**Fig. 1.1.** The process of beta amyloid production from APP secretase [14].

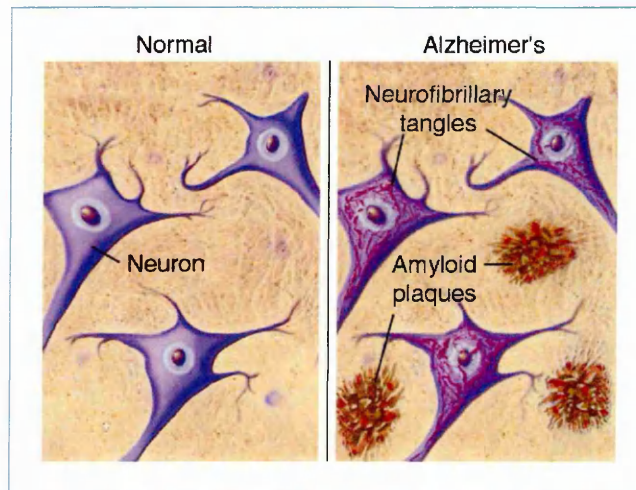


**Fig. 1.2.** The pattern of normal and AD patient brains [14].

The A $\beta$  region of APP corresponds to amino acids 11-15 of the trans-membrane domain and 28 amino acids of the extracellular domain [13]. Alternative splicing of the APP gene gives rise to at least 10 protein isoforms. Three of the APP isoforms known to contain A $\beta$  are APP<sub>770</sub> (full length APP), APP<sub>751</sub> (minus exon 8) and APP<sub>695</sub> (minus exons 7 and 8). APP is cleaved by three types of protease which are  $\alpha$ ,  $\beta$  and  $\gamma$  secretases (Fig. 1.3). Processing by  $\beta$  and  $\gamma$  secretases cleaves on N and C terminal ends of A $\beta$  respectively releasing A $\beta$  whereas  $\alpha$  secretase cleaves within A $\beta$  sequence. There are several closely associated morphologic changes in the brains of AD patient; neurofibrillary tangles (NFT) within neurons, plaques consisting of various proportions of amyloid cores surrounded by neuritic degeneration, a variable degree of congophilic angiopathy, and widespread neuronal loss and glial cyst in areas affected by NFT and plaque formation [15].

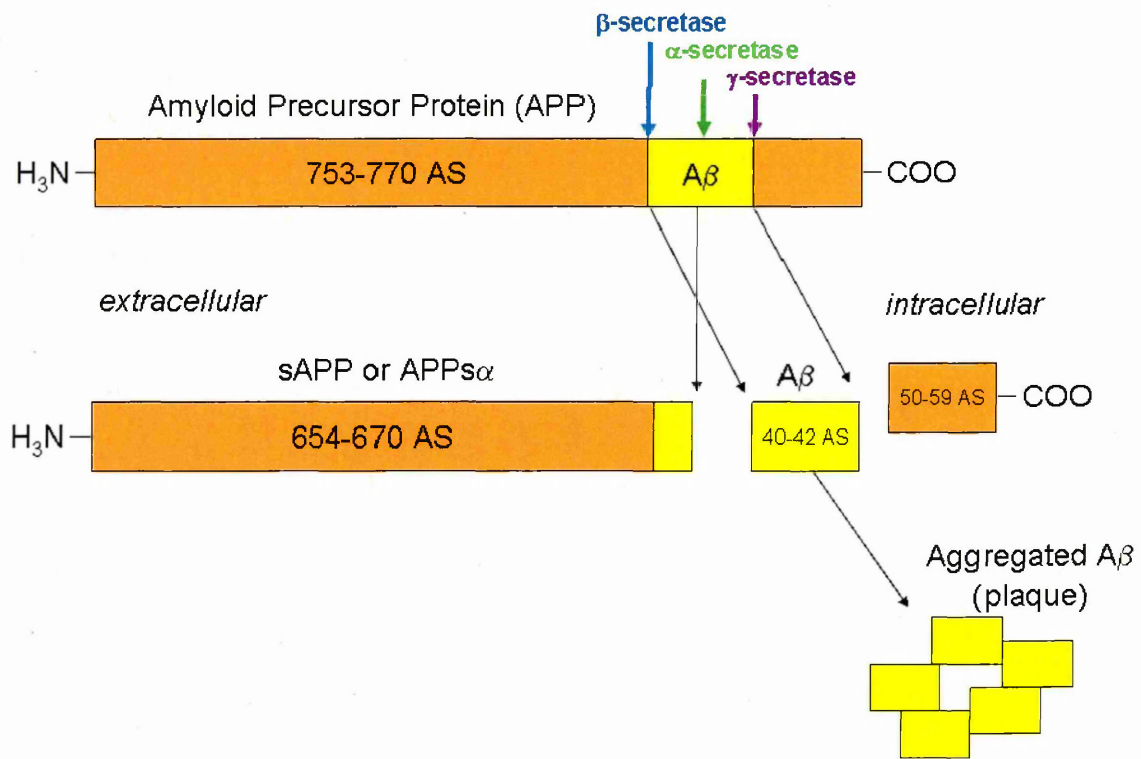


**Fig. 1.3.** Biochemistry of Amyloid Precursor Protein.

A $\beta$  has been shown to interact with a number of intracellular and extracellular molecules, but the relative contribution of these interactions to the toxicity of A $\beta$  is not well understood. An artificial step in characterising the importance of this interaction is the ability to measure both the affinity and the kinetics of these interactions. Currently AD can only be diagnosed definitively by post mortem identification of neuritic plaques and neurofibrillary tangles in central nervous system tissue. The development of rapid and cost-effective methods for AD diagnostics (particularly at early stages of AD) is in great demand nowadays, considering the ageing population of developed countries.

## 1.2 Diagnosis of Alzheimer's Disease

Apart from post mortem examination, mentioned above, and well-developed questionnaires and physiological tests for establishing early stages of AD, there are a number of bio-sensing methods available. Current clinical practice of AD diagnostics is

based upon detection of  $A\beta_{1-42}$  in ELISA sandwich immunoassay [16]. Studies of circulating  $A\beta$  in blood provide insights into  $A\beta$  equilibrium between the brain and the periphery. The ELISA method in sandwich assay has been employed to investigate the level of  $A\beta$  oligomers and monomeric  $A\beta$  in plasma and brain tissue of AD patients. Plasma samples were taken from 36 patients varying from normal to those with mild cognitive impairment. A significant reduction in plasma  $A\beta_{42}$  level showed the direct relationship of plasma  $A\beta$  to amyloid formation in the brain. This method is quite reliable but expensive and laborious; furthermore it is not suitable for early diagnosis of AD [17].

Conventional techniques of mass spectroscopy (MS) face difficulty in detecting  $A\beta$  fibrils. Usually MS technique has to be combined with other secondary methods. Electrospray ionization (ESI) ion trap has been identified as more suitable for analyzing amyloid solution compared to matrix assisted laser desorption ionization-time of flight (MALDI-TOF) and atmospheric pressure ion trap (AP) MALDI [18].

Direct and label-free measurement provides an alternative approach for protein aggregation detection using physical methods such as piezoelectric or quartz crystal microbalance (QCM) method. Amyloid growth on a sensing surface causes mass increase which affects the resonance frequency of quartz crystal. The protein aggregation process has to be directed onto the sensing surface in order for this method to be more effective. The functionalisation of a crystal surface was achieved by covalently attaching small pre-form  $A\beta_{1-40}$  fibrils. For this purpose, surface functionalisation is crucial to create a specific growth site on the surface. It has been reported that aggregation rates could be measured for concentrations of peptide as low as 500 nM [19].

The well-established method of surface plasmon resonance (SPR) has attracted great deal of attention because of its high sensitivity in bio-chemical analysis. Surface enhanced Raman spectroscopy (SERS) has been employed to detect the conformation transition of  $A\beta$   $\alpha$ -helical to  $\beta$ -sheet structure. A modification that has been made to increase sensitivity is to introduce gold nanoparticles in nano fluidic devices. Since the diameter of gold particles used is 60 nm compared to 40 nm for the depth of the shallow

nanochannel, the particles are trapped and form a cluster at the nanochannel entrance. In the SERS method, surface plasmon resonance frequency is shifted to near infrared region. This technique provides significant Raman signal intensity through the electromagnetic field and chemical enhancement due to adsorption of molecules on the metal surface [20].

Evidence has been presented that amyloid beta causes mitochondrial dysfunction and neuronal cell death through the direct interaction of A $\beta$  with catalytically active 17 beta-hydroxysteroid dehydrogenase type 10 (17 $\beta$ -HSD10). The detection of 17 $\beta$ -HSD10 on polyclonal antibody and the binding of 17 $\beta$ -HSD10 enzyme to amyloid beta 40 have been investigated using multi channel SPR. Results show that higher sensor response was observed for the reaction of A $\beta$ 40 to 17 $\beta$ -HSD10 enzyme compared to polyclonal antibody [21]. Several SPR biosensors have been reported to detect Alzheimer's disease [13,22,23]. AD is subject of interest because of the complexity of biological fluid, and real need for reliable biosensor detection methods that can offer high sensitivity at low cost.

Amongst the abundance of recent publications related to AD, only one publication was found that registered using the ellipsometry method for the monitoring of plaque formation on different proteins. The absorption kinetics of lipoprotein was investigated *in-situ* as a function of  $\beta$ -amyloid presence and apolipoprotein E isoform. The increased deposition rate which can be seen from kinetic measurement in the presence of  $\beta$ -amyloid is compatible with previous literature, thus suggesting the potential of this method for studies mimicking Alzheimer's plaque formation [24].

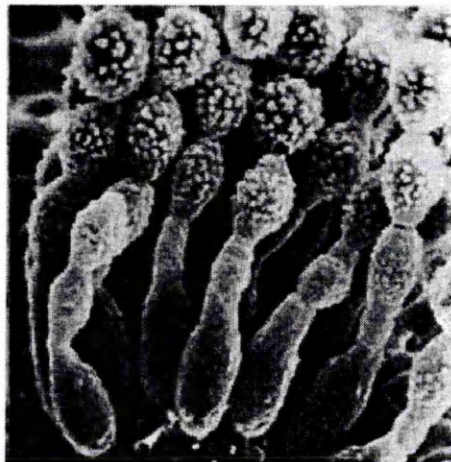
### **1.3 Mycotoxins review and detection of low molecular weight toxins**

Mycotoxins contaminate the diet of a large proportion of the world's population, especially in low income and developing countries. In 1985 the World Health Organization (WHO) estimated that approximately 25% of the world's grain was contaminated with mycotoxins. This figure has most certainly grown since then due to an increase in global import and export of grains. Mycotoxins are toxic chemical

compounds found in certain fungi that can grow on crops in the field, after harvest or during storage. Since they are produced by fungi, mycotoxins are associated with mouldy crops. Fungi that are available in food have a great significance in the health of humans and livestock. Nowadays there are hundreds of mycotoxins of different chemical structures and different modes of action, but only five of them are regularly found in staple foods and animal foodstuffs such as grains and seeds. These mycotoxins are aflatoxins, zearalenone, ochratoxins, fumonisins and deoxynivalenol/nivalenol. T-2 mycotoxins can also be found in varieties of grain apart from the five most frequent toxins found in staple food. Indeed, the large scale production of T2 has been used as a biological warfare agent. Table 1.1 describes the five most important mycotoxins, the staple food affected, fungal species which produce them, and their chemical structure and molecular weight. Most mycotoxins are hydrophobic molecules of low molecular weight and are thus not soluble in water but in organic solvents such as methanol, chloroform, acetone and acetonitril.



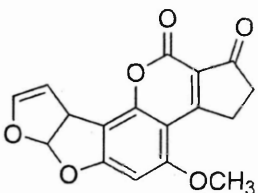
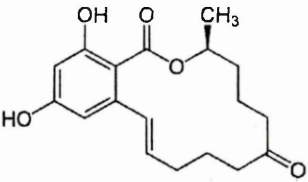
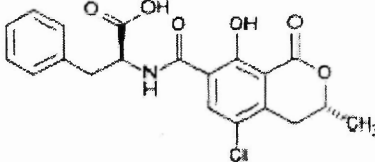
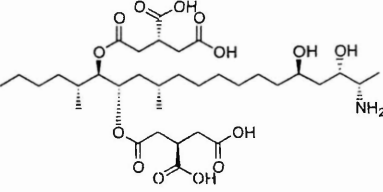
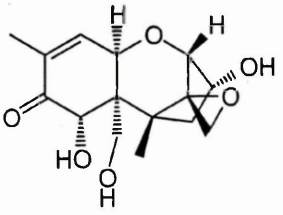
(a)



(b)

**Fig. 1.4.** *Aspergillus flavus* (mag. 1000x) (b). *Aspergillus paraciticus* (mag. 3000x) [25].

**Table 1.1.** Most dangerous mycotoxins, their sources, and chemical structures.

Mycotoxins	Commodities	Fungal source	Chemical structure
Aflatoxin	Maize, peanut, seeds, spices,	Aspergillus flavus, Aspergillus parasiticus.	 <p>MW = 312-346 g/mol</p>
Zearalenone	Maize, wheat	Fusarium graminearum, Fusarium crookwellence, Fusarium culmorum	 <p>MW = 318.36 g/mol</p>
Ochratoxin	Barley, wheat	Aspergillus ochraceus, Penicillium verrucosum	
Fumonisin B1	maize	Fusarium moniliforma	
Deoxynivalenol /nivalenol	Wheat, maize, barley	Fusarium graminearum, Fusarium crookwellence, Fusarium culmorum	

Aflatoxin is a common and naturally widespread mycotoxin that is produced by species of *Aspergillus* fungi, most notably *A. flavus* and *A. paraciticus*, and contaminates a variety of staple foods (Fig. 1.4). Favourable host plants for aflatoxin formation are grain cultures and cereals (maize, rice, wheat, etc.), spices (chilli and black pepper, coriander, ginger), high oil content nuts (almond, pistachio, walnut, coconut, Brazil nut) as well as coffee, cocoa, and fruit products [26-28]. The toxin can also be found in milk and milk products of animals that are fed contaminated food [29-31]. Within the aflatoxin group, the most dangerous toxin is aflatoxin B1 (LD50 = 6.5-16.5 mg/kg). The toxicity of AFB1 is ten times that of potassium cyanide, 68 times that of arsenic and 416 times that of melanine [32]. It can colonize and contaminate grain before harvest or during storage.

All mycotoxins are dangerous to human and animal health in connection with high hepato- and nephro-toxicity, and carcinogenic, genotoxic, cytotoxic, and mutagenic actions [33,34]. Human poisoning by aflatoxin, or aflatoxicosis, in countries where maize is consumed for daily meals is associated with fatality for daily consumption of food with more than 1000 ppb [31,35]. Aflatoxin has been extensively studied in relation to liver cancer. Studies suggested more than 600 000 people die of liver cancer worldwide each year, the majority of them in China and South East Asia [36]. Some other toxins have side effects on the kidneys, liver or immune system and some are carcinogenic.

Zearalanone (ZON) is the product of the *Fusarium* fungus *Gibirella*; it is less toxic but appears as a potent estrogenic metabolite dangerous to poultry and swine [37]. This mycotoxin can be found in grain products, i.e. maize, barley, oats, wheat, rice, sorghum, as well as in related food products (muesli, cereal, bread) stored at high humidity and temperatures. Current maximum levels set by the European Commission are 20, 75, and 100 µg/kg for baby food, cereal flour and unprocessed cereals respectively [38-40].

Quite high standards for the maximum concentration of mycotoxins, typically in the part per billion (ppb) range, are established by environmental legislation in the EU, US and worldwide. Established maximum concentration limits for aflatoxins in monitored commodities range from 5 µg/kg (in Eastern Europe) to 20 µg/kg (in the USA). The European Union is much stricter, and has established a maximum level of 4 µg/kg for

aflatoxins in agricultural commodities (2 µg/kg for aflatoxin B1). In 1993, the International Agency for Cancer Research (IARC) assessed and classified aflatoxin B1 as a class 1 human carcinogen [41]. The European Commission Regulation (EC No. 1525/98) on aflatoxins came into force in January 1999 and established the above limits for aflatoxin B1 and total aflatoxins in groundnuts, nuts, dried fruit and cereals, as well as a limit of 0.05 µg/kg for aflatoxin M1 in milk and dairy products [42]. Various governments have set limits for mycotoxins in food and animal foodstuffs presented for sale or import, such as 4 to 50 g/kg (ppb) for aflatoxins. Most developed countries will not permit the import of commodities containing an amount of mycotoxins above specified limits. Therefore mycotoxins also have an impact on trade between nations.

### **1.3.1 Detection of Mycotoxins**

The detection and monitoring of mycotoxins, which may naturally occur in agricultural products, food, and feed stored in inappropriate conditions, is of great interest nowadays and depends on precise and reliable analytical methods. The monitoring process benefits not only consumers but also producers of raw products prior to costing processing and transportation. The detection of mycotoxins in low concentration is a difficult task because of their low molecular weight. The use of biosensors to ease rapid detection of pathogens and toxins is a promising technology for food safety due to its simplicity, flexibility and efficiency [43]. The fluorescent properties of aflatoxins when induced by laser at 360 nm can also be exploited as a detection mechanism.

The conventional method for the detection of mycotoxins is by using chromatography techniques. Thin layer chromatography (TLC) has been used to determine aflatoxins in various food matrices, peanut butter, paprika and pistachios. The measurements using this technique provide a limit of detection (LOD) ranging from 0.1 µg/kg to 0.7 µg/kg for Aflatoxin B1, B2, G1 and G2 [44]. High Performance Liquid Chromatography (HPLC) method has been selected for the detection of Aflatoxins B1 and Ochratoxin A produced in bee pollen with detection limits of 0.49 µg/kg and 0.20 µg/kg respectively [45]. Liquid Chromatography Quadrupole Mass Spectroscopy (LC-MS/MS) allows simultaneous detection of a large range of mycotoxins; 87 mycotoxins in wheat and maize [46], 18 mycotoxins and metabolites in cows' milk [47], and 16 mycotoxins in

fungal cultures [48]. Traditional methods have the disadvantages of being expensive and time-consuming, associated with steps taken for sample clean up, pre-concentration, and analyte derivatisation, and require trained personnel. Although most validated detection methods are chromatographic, alternative detection means based on bio sensing principles are more promising for regular diagnostics.

Piezoelectric devices based on quartz crystal microbalance (QCM) have the advantage of being label free but struggle to detect the small molecules of mycotoxins, especially in direct assay format. Indirect assay is more dominant in this technique, such as competitive assay, which introduces conjugated antibodies to boost the resonance frequency. Further amplification of the changes of resonance frequency corresponding to the deposited mass on a QCM surface is possible to increase sensitivity. In recent work, piezoimmunosensors were developed using indirect competitive assay for the detection of AFB1. Horseradish peroxidase, labelled G-anti-MsIgG, which was bound to the anti-AFB1, acted as biocatalyst for oxidative precipitation resulting in an obvious frequency change corresponding to the levels of AFB1 analyte [49]. Gold nanoparticles have also been utilized to amplify the sensitivity of QCM immunosensors. Amplification by 20 nm gold nanoparticles for the detection of AFB1 in milk using competitive assay format produced a better limit of detection, down to 0.01 ng/ml [50].

Several optical methods have been used for mycotoxin immunosensors. Some of them require labels such as fluorescence, and some others rely on the changes of optical properties of a sensing surface. The Surface Plasmon Resonance (SPR) method is based on the changes in optical density after a reaction takes place on the sensing surface. Commercially available SPR (BIAcore 2000) is only able to detect 10 - 15 kDa or high refractive index substances using direct detection method [51]. In order to be able to detect low molecular weight toxins, an indirect assay has been proposed as well as developing a highly sensitive SPR device. SPR-based competitive immunoassay has been utilized for the detection of Aflatoxin B1. A conjugate consisting of AFB1-BSA was immobilized on dextral gel surface. Competition occurred between immobilized AFB1 conjugate and free AFB1 injected into the cell during the assay. It was reported that the assay had a linear range of 3.0 - 98.0 ng/ml with good reproducibility [52].

Due to the linear relationship of shifted resonance angle and reflected light intensity at selected wavelengths to analyte concentration, an SPR immunosensor has been developed to determine Fumonisin B1 concentration in a spike sample. The detection limit of 50 ng/ml was obtained by direct assay in an analysis time of 10 minutes [53]. SPR also has been utilized for the detection of mycotoxins such as Deoxynivalenol [54], Zearalenone [51] and Ochratoxins A [55].

Evanescent wave principle has been exploited in fibre optic immunosensors for the detection of fumonisin and aflatoxins in maize using competitive and non-competitive formats. Among the advantages of this sensing method are high specificity, freedom from EM interference, ease of miniaturization, real time monitoring, biocompatibility, and adaptability for remote sensing [56].

Optical waveguide light spectroscopy (OWLS) exploited evanescent field to measure the variations in refractive index due to changes of layer thickness. Since direct assay format did not provide low LOD, a competitive approach was used. In this measurement a detection range of 0.5 ng/ml to 10 ng/ml was recorded for Aflatoxin B1 and Ochratoxins A which were obtained from real samples [57].

### **1.3.2 Toxin Purification**

The problem of purification of substances contaminated with mycotoxins has not been explored as extensively as detection. Several methods of decontamination of mycotoxins are used especially for food purification. Physical processes involve separation of the contaminated fraction, removal and inactivation of the toxins by physical means such as UV light, heat and radiation [58,59]. Chemical degradation of aflatoxin using chlorine, hydrogen peroxide, ozone and ammonia has been investigated [59-61] while biological methods for detoxication of zearalenone and aflatoxin have also been explored [62,63].

The introduction of micro- and nanometer-size capsules [64,65] attracted attention in diverse areas of biotechnology. The preparation of capsules by layer by layer (LbL) technique [66] is of particular interest due to the customization of properties (size,

composition, porosity, stability, surface functionality etc.) to needs. In this work an alternate deposition of positively and negatively charge polymers was developed on a calcium and magnesium carbonate core templates. Such polyelectrolyte capsules modified on the surface with antibodies specific to mycotoxins were used for purification of solutions contaminated with mycotoxins. Layer by layer deposition on a 6  $\mu\text{m}$  templates was started with negatively charged PSS and followed by PAH; after depositing 4 bilayers of PSS/PAH, the capsules were further functionalized with Protein A and anti-zearalenone. The immobilized capsules were introduced to a liquid containing zearalenone toxins. The presence of zearalenone was monitored with UV-vis absorption spectra measurements taken at different incubation times. The results showed that modified capsules can be used in the purifying process of contaminated liquid.

These processes, however, must ensure that the decontamination process retains the nutritive values and will not result in the introduction of new toxic substances. Apart from that, it must be technically and economically feasible for compliance with Food Authority Organization (FAO). One of the requirements is that the decontamination process must be able to destroy, deactivate or remove the toxins.

#### **1.4 Aims and Objectives**

The main goal of this research is to develop optical sensors for biomedical applications particularly for AD diagnostics and detection of mycotoxins. To achieve this aim, seven tasks were identified:

- i. To design and develop a small volume Total Internal Reflection Ellipsometry (TIRE) cell suitable for different bio-sensing applications.
- ii. To employ TIRE method for the detection of Amyloid Precursor Protein (APP<sub>770</sub>), (Mw = 115 kDa) in direct immune assay with DE2 antibody.
- iii. To employ QCM as a secondary method for calibration of TIRE for amyloid precursor protein (APP).

- iv. To employ TIRE method for the detection of Amyloid beta peptide ( $A\beta_{1-42}$ ) (Mw = 1955 Da) in direct assay with DE2 antibody in regards to Alzheimer Disease (AD) diagnostic.
- v. To employ TIRE method for the detection of mycotoxins, aflatoxins & zearalenone.
- vi. To investigate microcapsule technology for purification of substance contaminated with mycotoxins and its possibilities for biomedical application.
- vii. To investigate the morphology of sensing surfaces using Atomic Force Microscope (AFM) and nano-SEM techniques.

# CHAPTER 2

## BIOSENSORS THEORY, BACKGROUND AND APPLICATIONS

This chapter describes biosensors in detail; biosensing theory, principles, background and applications. Affinity sensors, particularly immunosensors, are explained in detail, including the production of antibodies and immobilization techniques. Further discussion on immune assay format is also reviewed. The applications of QCM and Ellipsometry methods in biosensing are describes in the last part of this chapter.

### 2.1 Biosensors Review

In the early days, biosensors were called bio electrodes, enzyme electrodes or bio catalytic membrane electrodes [67,68]. A biosensor is a device consisting of two parts, which are a bio-element and a sensor. Figure 2.1 shows the layout of a biosensor which comprises the analyte, bioelement, and transducer. The bioelement is where the recognition or biochemical reaction occurs. The bioelement can be an enzyme, antibody, living cell or tissue, but usually biosensors exploit either enzymes or antibodies as the bioelements. Enzymes specifically catalyse the reaction of decomposition of the substratum while antibodies specifically bind target molecules. Specific bioelements recognise certain analytes and are directly connected to transducer which transform the reaction to a measurable sensor signals.

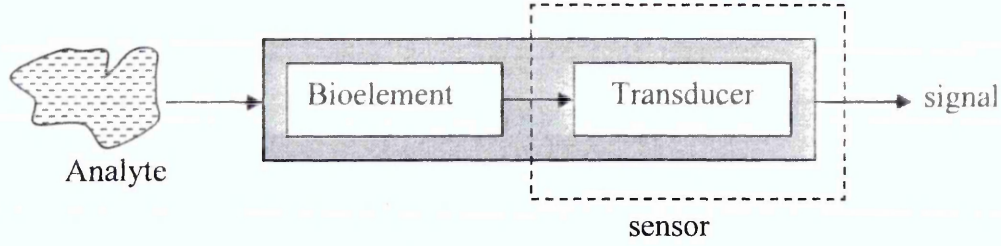
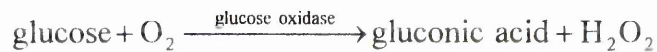


**Fig. 2.1.** The layout of a biosensor

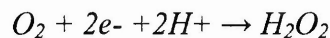
Transducers transform the reaction into physical parameters. There are several types of transducers [146]:

- i. Optical transducers are based on optical phenomena of light, absorption, reflection, interference, polarization, etc. They provide a quantitative characterization utilizing changes in the amplitude and/or phase of electromagnetic waves, optical density and complex refractive index.
- ii. Acoustic (gravimetric) transducers are based on the interaction of acoustic waves in piezoelectric materials with analytes. There are three types of gravimetric sensors, which are quartz crystal microbalance (QCM), bulk acoustic wave (BAW) and surface acoustic wave (SAW).
- iii. Thermal transducers are based on the response to an incident energy rate (proportional to molar enthalpy of the material). Generally, the response which is related to the adsorption or emission of heat is slow. Thermal transducers are constructed by combining immobilized enzymes with temperature sensors. When the analyte (substratum) is decomposed in the presence of enzyme the amount of heat produced (or consumed) during the enzyme reaction is measured and calibrated against the analyte concentration. The total amount of heat produced or absorbed is proportional to the molar enthalpy and the total number of molecules in the reaction.
- iii. Photon transducers are based on the response to incident photon rate. They operate in a wide spectral range, respond quickly ( $\mu\text{s}$  or faster) and can be single or multi channel.

The first biosensor was developed by Clark and Lyon in 1962 to detect glucose levels in blood (Fig. 2.2), was called enzyme electrodes. Glucose biosensors are based on the oxidation of glucose to gluconic acid catalysed by the enzyme glucose oxidase (GOD).



A platinum electrode was used to detect oxygen produced by the enzyme reaction. The enzyme GOD was placed very close to the surface of platinum; it is physically trapped against the electrodes with a sandwich of teflon and cellophane membranes. The reaction at the electrode is described as:



The current which is proportional to the oxygen concentration is measured when voltage is applied between platinum (Pt) and silver (Ag) electrodes. The concentration of glucose is then proportional to the decrease in the current.

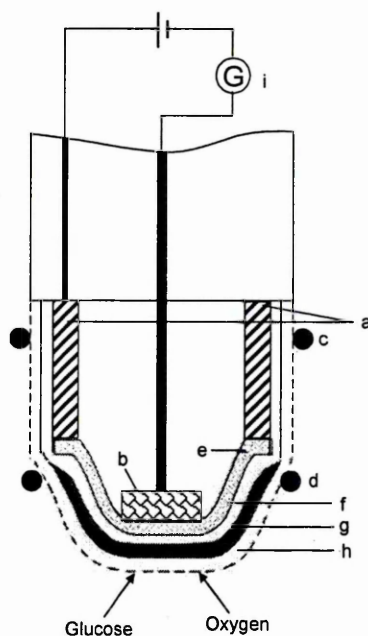


**Fig. 2.2.** Clark and Lyon's first glucose biosensors, consisting of Ag electrode (a), Pt electrode (b), rubber ring support (c,d), electrolyte gel (e), teflon membrane (f), glucose oxidase on nylon net (g), cellophane membrane (h), galvanometer (i). (Reconstructed from [68]).

Examples of biosensor applications can be seen in the areas of health care, industrial processes control, and environmental monitoring. However the application of biosensors in the medical field has been the most significant. Blood glucose testing gave

major revenue to biosensor companies which saw various types of blood glucose sensors available in the market.

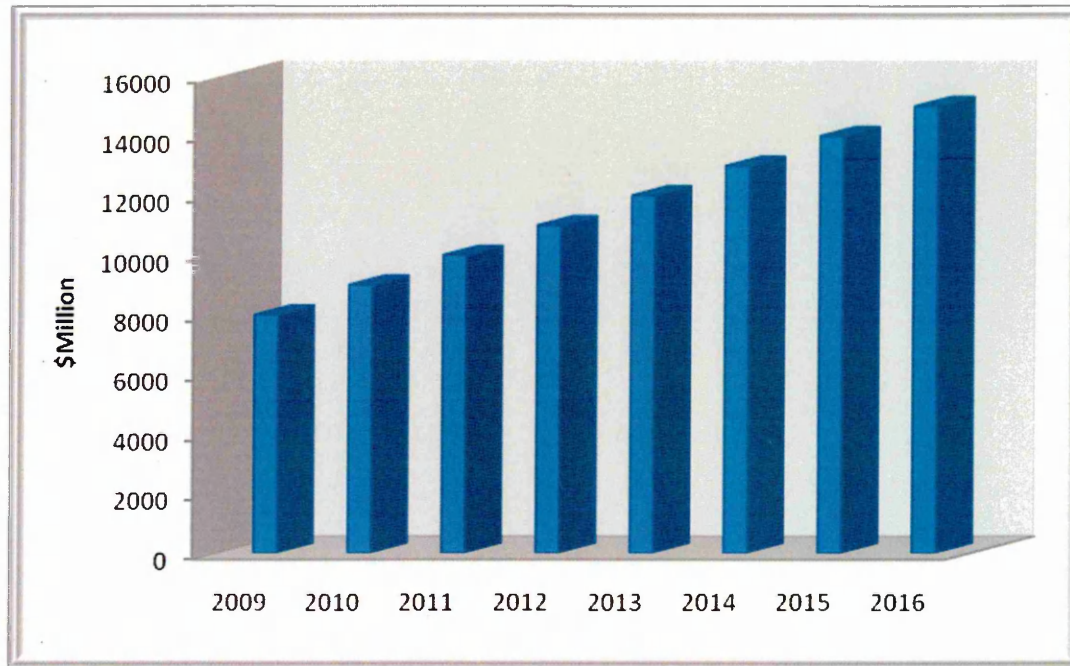


**Fig. 2.3.** The total biosensors market showing the world revenue forecast for 2009–2016.

Disease diagnostics as a whole represents a very large, well-established and continuously expanding market. Particularly with the awareness that ‘prevention is better than cure’, the need for sensitive, easy-to-use, and low cost sensor devices is a requirement for monitoring diseases at an early stages. The chart in Fig. 2.3 shows the percentage of revenues from the markets of environmental control, security, bio-defence and home diagnostic continues the growth trend up to 2016. Point of care diagnostics continues to be the largest market for biosensors and it is likely to dominate to 2016 and beyond. It has been estimated that global revenue from the biosensors market will continue to exhibit strong growth and will exceed USD 14 billion in the next seven years (Fig. 2.4) [69]. Other reports say that the USA and Europe dominate the global market for medical biosensors, collectively capturing a 70% share, estimated in 2008. The Asian Pacific will see exponential growth to reach USD 794 million by the year 2012 [70].

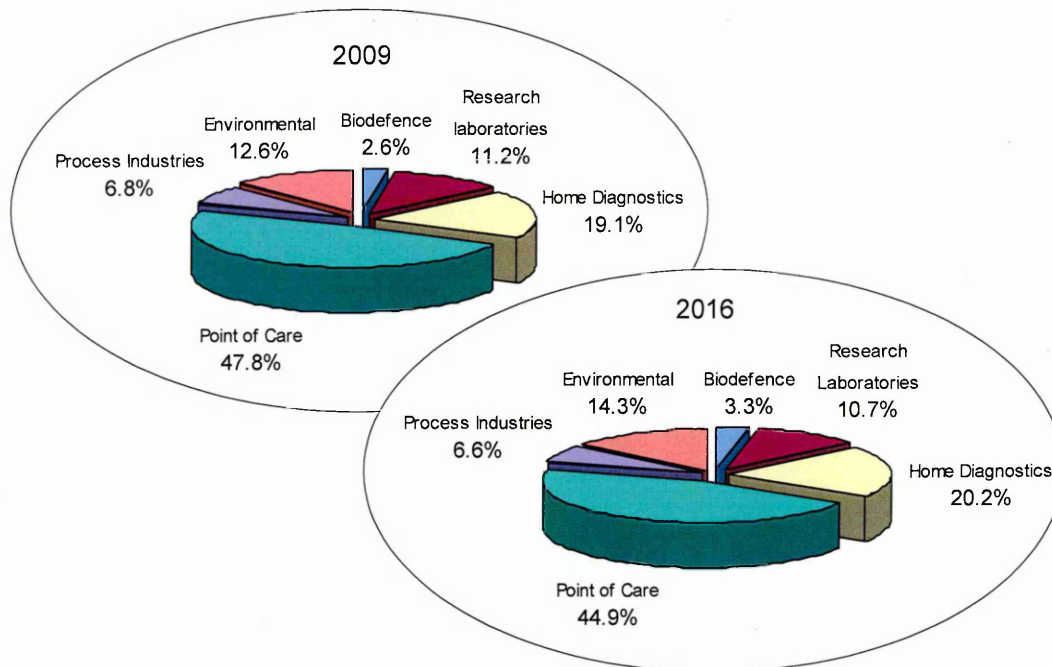


**Fig. 2.4.** Biosensors world market that shows the percent of revenue in different area of applications in 2009 and 2016 [69].

### **2.1.1 The need for label-free detection**

Nowadays, the development of biosensors faces the challenges of detection of very low concentrations (in fg – pg/ml range) of traditional analytes such as antibodies, peptides, DNA oligomers, and low molecular weight (300 – 1000 Da) analytes such as toxins.

Due to the difficulties of detecting biological analytes directly through their intrinsic properties such as size, mass, electrical impedance, or dielectric permittivity, labels that attach to one or more molecules have been used [71,72]. A label, which is typically designed to be easily detected by its colour or fluorescence acts as a surrogate to indicate the presence of the analyte. For example, fluorescent dyes conjugated with DNA or proteins can be used as a label when the fluorescence is excited with a laser [73].

The use of nanoparticles [74], enzymes [75], and radioactive [76,77] labels are among the popular techniques to highlight biological interaction. In practical terms, label-based assays possess several potential problems. There is a need to reduce the cost of raw

materials (assay-related cost) and the complexity of assays while at the same time providing more quantitative information.

Label-free detection generally involves a transducer capable of measuring directly some physical properties of biological objects, e.g. DNA, peptides, proteins, cell, etc. Physical properties, such as mass, volume, viscoelasticity, dielectric permittivity, conductivity, etc., can be utilized to indicate the presence of these molecules. Label-free detection removes experimental uncertainty induced by the effect of the label or molecular conformation, blocking active sites, steric hindrance, or inability to find an appropriate label that functions equivalently for all molecules in the experiment. Label-free detection is able to reduce the time and cost required for the assay development while removing experimental artifacts from quenching and background fluorescence.

## **2.2 Affinity Biosensors**

Affinity sensors are analytical devices that use antibodies, DNA-sequence, or receptor proteins interfaced to a signal transducer to measure the binding event [78]. This interaction behaviour is called affinity. The two binding partners can be separated again by changes in pH, salt concentration, heat or additional hydrogen bond destabilizer [79]. This separation is also called regeneration. The affinity receptors such as antibodies are commonly used in immunosensing [80].

Affinity and avidity are two common parameters describing the strength of interaction between receptors and analytes. Affinity is the strength of the binding site of the antibody (called paratope or Fab-fragment) and epitope of the antigen. In the case of antibody-antigen binding, the parameter of affinity describes the binding strength of monovalent binding (e.g. binding of a Fab-fragment to one epitope on an antigen). Avidity is a measure of stability of a complex formed as a result of antigen-antibody binding (Fig. 2.5). A measure of avidity includes the sum of the affinities for the multivalent interaction. In addition to the sum of affinities, avidity also measures the general strength of binding, which includes the structural arrangement of both molecules. Low-affinity antibodies will bind weakly with the antigen and will dissociate

easily, but high-affinity antibodies will bind the antigen tightly and can remain bound longer.

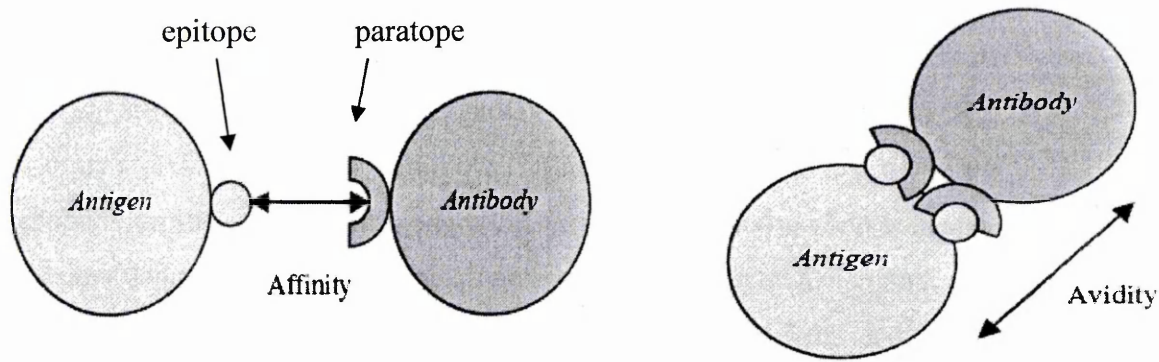


**Fig. 2.5.** The difference between affinity and avidity interactions of antibody and antigen [81].

The time required to reach equilibrium depends on the rate of diffusion and the affinity of the antibody towards the antigen, and these parameters can vary widely. The affinity constant for antibody-antigen binding can span over a wide range, from below  $10^5 \text{ M}^{-1}$  to above  $10^{12} \text{ M}^{-1}$ , and can be affected by temperature, pH, and type of buffers used.

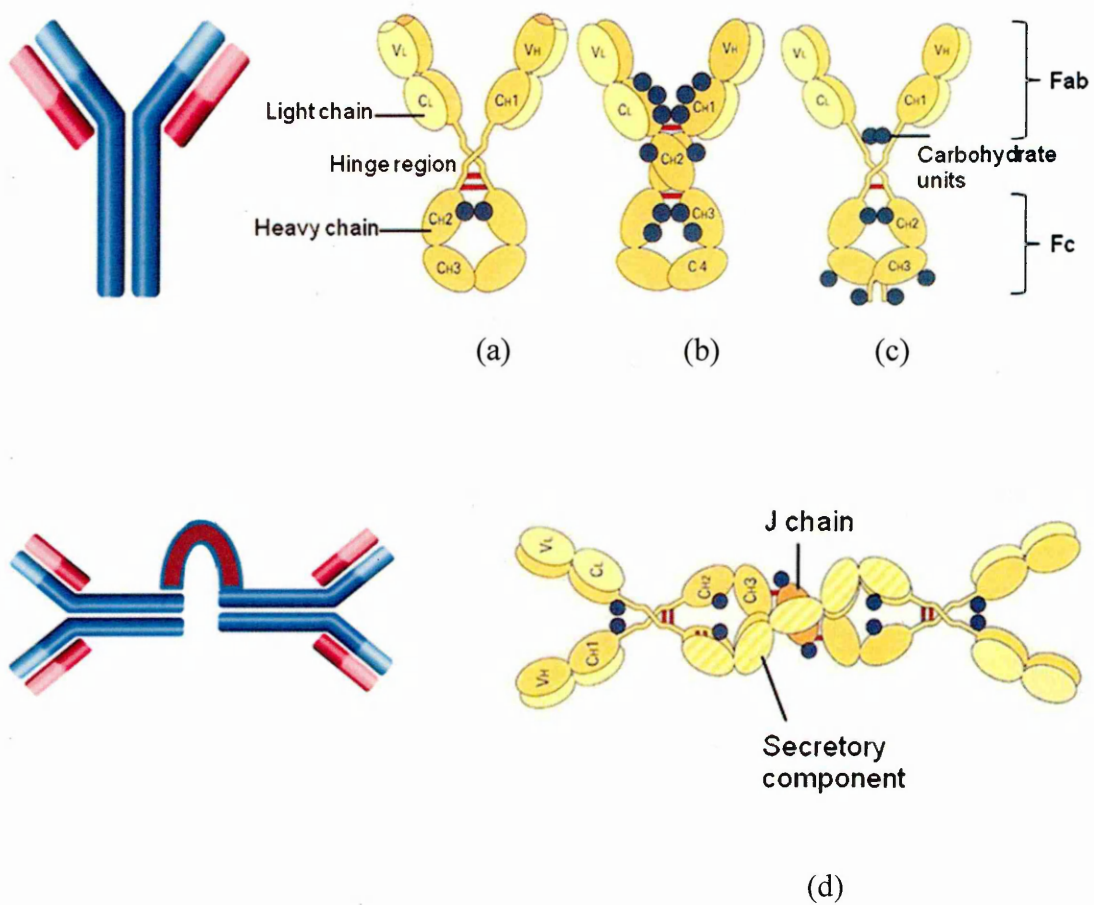
### 2.2.1 Antigen-antibody interaction

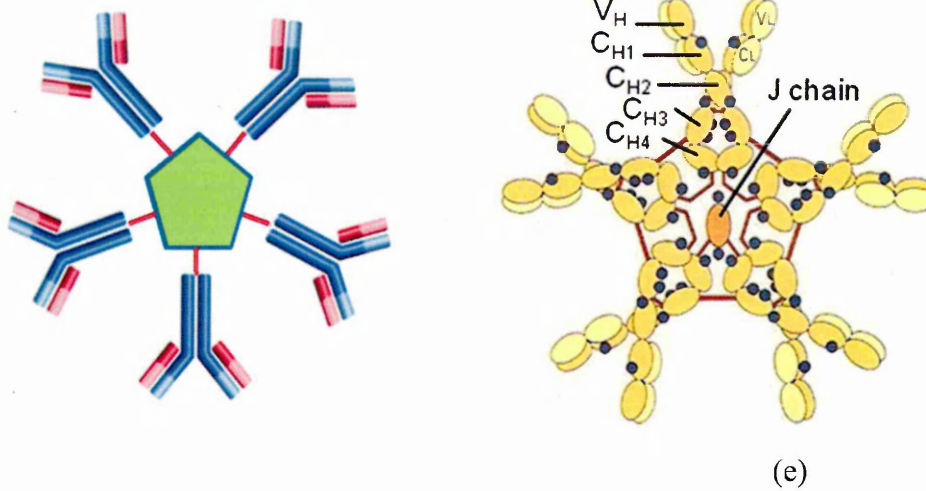
Antigen-antibody reactions are widely used, not only in medical diagnostics but also in environmental analysis, forensic analysis, food industry, veterinary, military etc. The combination of a biosensor approach with an antigen-antibody reaction seems to be more suitable and promising because of the following unique characteristics of antibodies [82]:

- i. The binding site of an antibody is derived from a huge number of potential combinations of 22 amino acid sequences which are able to bind a wide range of chemicals, bio-molecules, cells and viruses.
- ii. High specificity of antibody-antigen binding.

- iii. The binding between antibody and its target is non-covalent which allows recovering the sensor by breaking the antibody-antigen complex, for example at low pH.

Basically, there are five major classes of antibodies secreted in serum, namely IgG, IgD, IgE, IgA and IgM. IgG is the most abundant class in serum and is about 80% of total serum immunoglobulin (Fig. 2.7). The antibodies differ in size, charge, amino acids sequence and carbohydrate content [83]. The basic structure of an antibody consists of two identical heavy polypeptide chains paired with two identical shorter light chains forming a flexible Y shape. The chains are subdivided into domains consisting of approximately 110 amino acids which are linked by a variable number of disulfide bonds, giving a total molecular mass of approximately 150 kDa. Immunoglobulin G (IgG) antibody is the most abundant antibody in serum [82].





$V_H, V_L$  = Heavy and light chain variable region

$C_L$  = Light chain constant region and divided into  $C_{H1}, C_{H2}, C_{H3}$

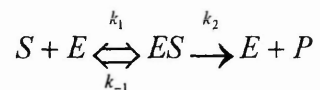
**Fig. 2.7.** The structure of antibody Isoforms: (a) IgG, (b) IgE, (c) IgD, (d) IgA (e) IgM [83].

### 2.2.2 Nucleic Acids Interaction

Nucleic acids operate in the same way as antibodies. The specific base pairings between strands of nucleic acids give rise to the genetic code which determines the replicating characteristics of all parts of living cells and thus the inherited characteristics of individual members of a species. DNA is formed of relatively simple polymers involving sequences of nucleotides derived from four bases; adenine (A), cytosine (C), guanine (G) and thymine (T), which are carriers of biological information. DNA probes can be used to detect genetic disease, cancers and viral infections. They are used either in a short synthetic form or the long form produced by cloning. They can recognize other nucleotides via non-covalent interaction, termed base pairing. DNA assay often involves the addition of labelled DNA to the assay. The labelling can be radioactive [76],[77], photometric [84], enzyme [85], or electroactive [86,87] which provide a variety of biosensor types. Label-free DNA assay has also been reported for the detection of different species of fish and other applications such as DNA-protein and DNA-drug interactions [69].

### 2.2.3 Enzyme-substrate Interaction

Enzymes are large and complex macromolecules consisting largely of proteins, usually containing a prosthetic group, which often includes one or more metal atoms. The mode of action may involve oxidation or reduction which can be detected electrochemically [68]. The basic enzyme catalysis mechanism is:



Where S = substrate, E = enzyme, ES = enzyme substrate complex and P = end product.

The enzyme reacts selectively with a specific molecule called a substrate. The substrate binds to the enzyme active site to form enzyme-substrate complex; the substrate is then decomposed into several reaction products and released from the active site. Two simultaneous processes control the reaction: (i) the enzymatic alteration of the substrate to the product(s) and (ii) the diffusion of the product(s) from the enzyme later. The enzyme reaction is usually accompanied by changes in pH, heat emission and the production of other compounds, such as ammonia or oxygen, which can be detected by transducer. The advantages and disadvantages of using enzymes as a bio-element are as follows [68]:

Advantages:

- i. they bind specifically to the substrate
- ii. they are highly selective
- iii. they have catalytic activity, thus improving sensitivity
- iv. they are fairly fast acting
- v. they are the most commonly used biological components

Disadvantages:

- i. They are expensive. The cost of extracting, isolating and purifying enzymes is very high and sometimes the cost of the source for the enzyme may also be high. However, a very wide range of enzymes is available commercially, usually with well-defined assay characteristics.

- ii. There is often a loss of activity when they are immobilized on a transducer.
- iii. They tend to lose activity owing to deactivation after a relatively short period of time

#### 2.2.4 Avidin–Streptavidin Interaction

The avidin-biotin system has been established as a powerful tool in life science. Due to the strength and specificity of an avidin-biotin complex with an extraordinary affinity ( $K_A = 10^{15} \text{ M}^{-1}$ ) [88], this system was also exploited as affinity matrix in several works [89-91]. The development of new methods and reagents to biotinylated antibodies and other molecules [92,93] allowed the transfer of the avidin-biotin system to a wide range of biotechnological applications. Many biotin molecules can be coupled to protein, enabling the biotinylated protein to bind more than one molecule of avidin.

There are several distinctive advantages to using the avidin-biotin system:

- i. The biotin molecule retains its biological and physical characteristics after modification. This allows the modification of any biological active compound with biotin.
- ii. Avidin has four binding sites (tetrameric structure) for biotin which provides the possibility of use of a multifaceted system. (Fig. 2.8), and signal amplification.

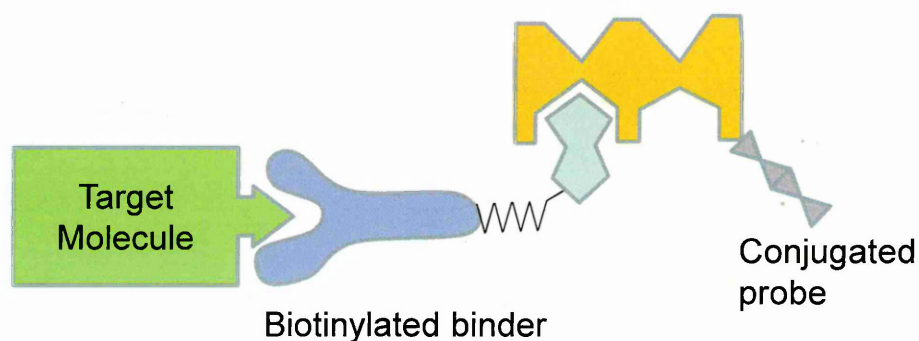


**Fig. 2.8.** Avidin-biotin interaction in biosensing application

## 2.3 Immunosensors

Immunosensor is a device for the detection of immune reaction, deploying antibodies as bio-receptors. The use of antibodies as a recognition element is justified by their higher affinity, versatility and commercial availability [94]. Antibody is typically an immunoglobulin (glycoprotein, with a molecular weight of ~150,000 daltons) which is capable of specific binding with its specific antigen. Antibodies play an important role in the human immune system and they are also a powerful diagnostic and research tool. Rapid and accurate determination of the activity and binding properties of antibodies is crucial in the estimation of their performance in various applications. The process of antibody-antigen binding is based on non-covalent interactions such as; Van der Waals forces, Coulombic interactions, hydrophobic interactions, and hydrogen bonding [95]. This combination of interactions can make the antigen-antibody binding very specific. For instance, if two very similar antigens, A and B, are present where A has an additional hydrogen bond which B does not have, the strength of the interaction of A to the antigen compared to B can be 1,000 times greater. The affinity for monoclonal antibodies to their antigens is typically in the range of  $10^6$ - $10^8$  mol/l.

Antibodies are generated in response to the challenge of an immunogen in the host animal. Antibodies derived from the serum of an immunized animal, arising from separate cell lines which recognise various regions on the immunogen, are termed as polyclonal antibodies. Antibodies derived from a single cell line are known as monoclonal antibodies and recognise a single specific region (epitope) on the immunogen compared with a polyclonal antibody in which each clone in the total mix recognized a different epitope (Fig. 2.9). Both of these antibodies have certain advantages and limitations for use in immunosensing.

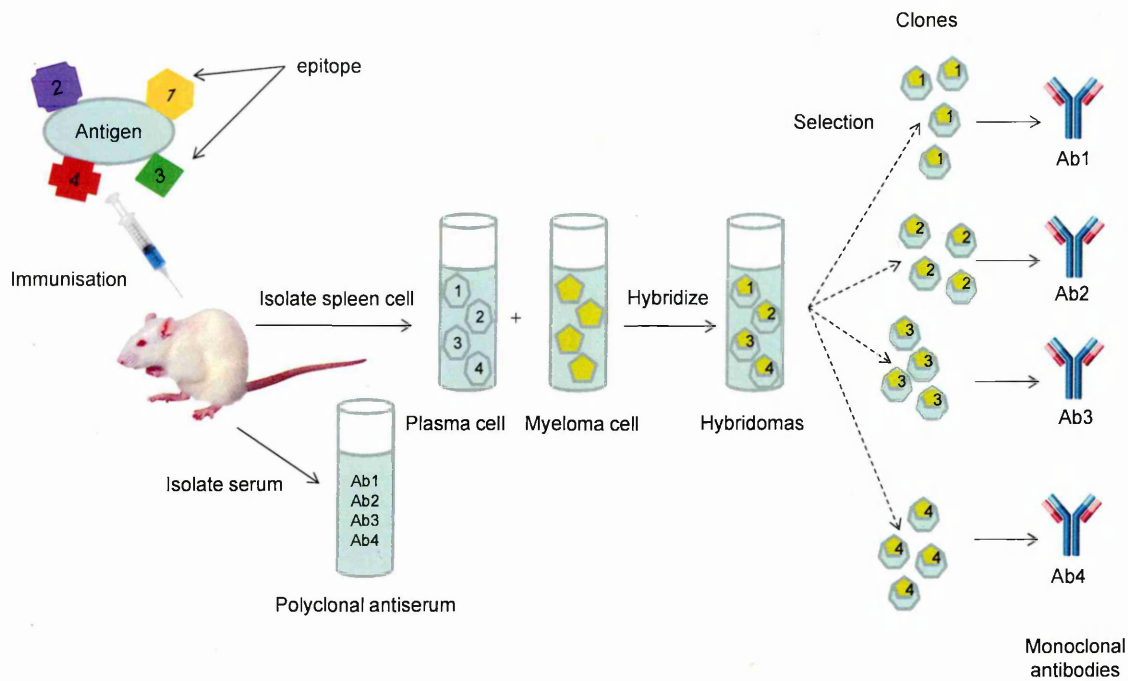


**Fig. 2.9.** The production of antibodies by immunizing an animal.

### 2.3.1 Antibody immobilization

An antibody has four possible orientations on the solid surface: “end on” (Fc closer to chip surface), “side on” (Fc and one of the Fabs closer to the surface), “head on” (Fabs closer to chip surface) and “lying on” (Fc and two of the Fabs closer to the surface) orientations [96-98]. The desired “end on” orientation can be achieved using a powerful interaction of Fc region with other functional compounds [99], protein A or protein G adsorbed on the surface.

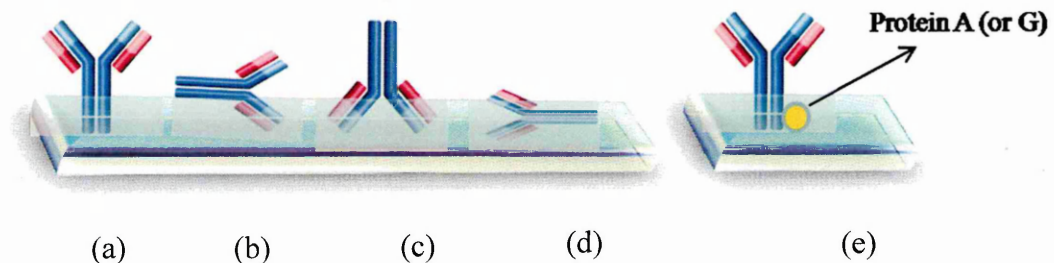


**Fig. 2.10.** The orientation of antibody on surface “end on” (a), “side on” (b), “head on” (c), “laying on” (d), antibody “end on” position supported with the binding of Protein A (or G) at Fc fragment (e).

The orientation of an antibody towards an antigen can be optimized by its binding to protein A or protein G at the Fc fragment of the antibody. The association of protein A (or G) and the antibody has three significant characteristics [96,97].

- i. Binding sites of protein A (or G) and antibodies are located on the Fc fragment of the antibody; the association capacity of an antibody with an antigen cannot be changed.
- ii. Protein A (or G) will resume its character readily
- iii. The affinity of protein A (or G) to antibody is very high; however, the association of protein A (or G) with an antibody will be lost in acidic solutions.

#### **2.4 Immunoassays format for immunosensors**

An immunoassay is a biological test for monitoring of binding of an antibody to its antigen. Immunoassays are classified by the method of detection which depends on the nature of the target analyte, analytical sample, sensitivity and application. Generally there are three types of the assay format [100].

Direct immunoassay (Fig. 2.11 (a)), which involves direct binding of antigen to antibody, is the simplest technique. The antigen or antibody is immobilised directly on the sensor's surface and the analyte will binds to the immobilized antigen or antibody. This is the simplest and the most inexpensive assay that can offer reasonable sensitivity. This method is useful for the detection of large molecules with molecular weight larger than 10 kDa [101]. The response signal due to the binding of the analyte to antibody is proportional to the concentration of the analyte. Usually this technique is not suitable for detection of small molecules and often a sandwich assay is selected. This technique has also been reported by [102,103].

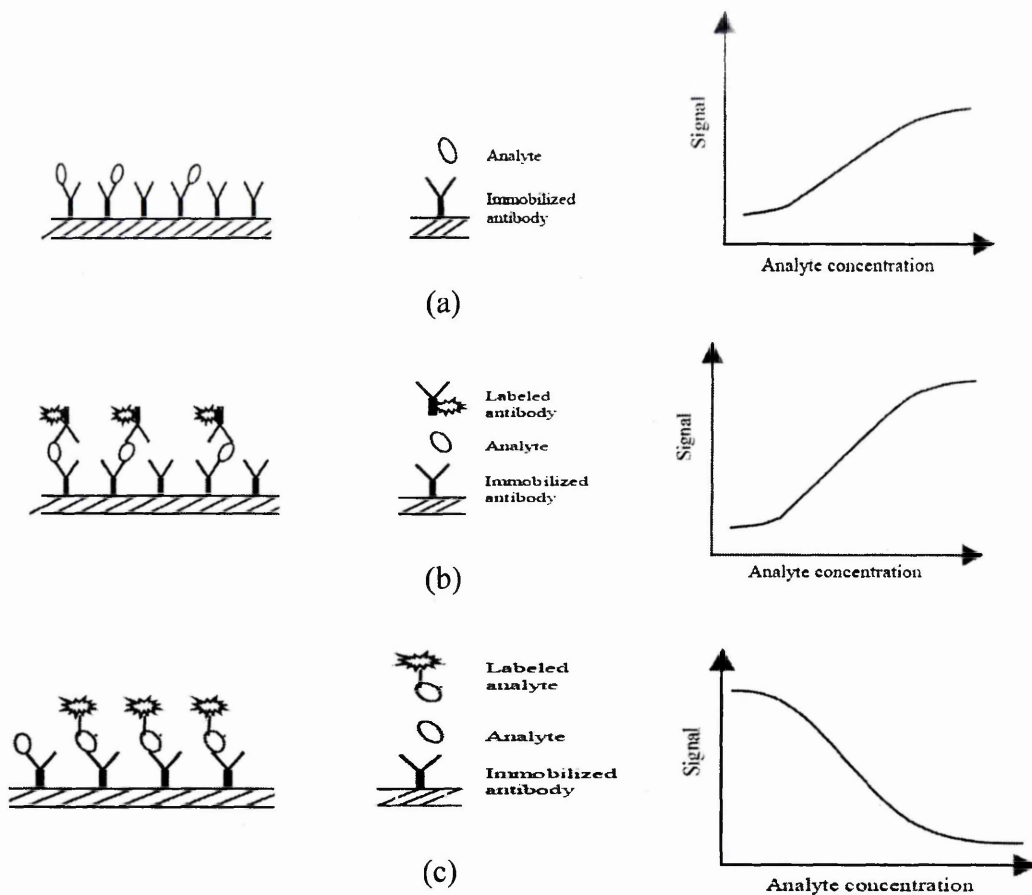


**Fig. 2.11:** The different formats of immunoassay used in immunosensor and the corresponding response signals for: (a) Direct immunoassay format; (b) Sandwich immunoassay format; (c) Competitive immunoassay format [100].

A sandwich assay (Fig. 2.11 (b)) consists of two steps: first, antibodies immobilized on sensor surface are allowed to bind with particular analytes. Then secondary antibodies are added to the system to bind with the previously captured analyte. Labelling the second antibody is used in sandwich assay. The response signal due to the binding interaction between analyte and antibody is proportional to the concentration of the analyte, but it is much higher compared to the direct format.

In competitive immunoassay format (Fig. 2.11 (c)), the immobilized antibodies on the sensor surface have to compete for the labelled analytes introduced in the sample. The response signal is high at low concentration label analyte and gets lower at a high concentration before reaching a plateau.

Other type of assay called competitive inhibition assay format [104,105] which required the immobilization of an antigen on sensing surface. This assay requires the inhibition of antigen with the respective antibodies prior to injection. Normally 5 to 10 minutes is allows for the mixture to inhibit. The mixture of antibodies and low concentration of antigen during inhibition, produce high response due to access of antibodies to compete with antigen immobilized on the surface. At high concentration of antigen, there are fewer antibodies available to react with antigen on surface, thus produce low sensor response.

The main strategy for immunosensor construction is to place antibody molecules in close contact with the transducer surface in order to obtain high sensitivity and to minimize the measurement time. Furthermore a greater use of the immobilized antibodies-antigen on the transducer will also increase the effective area of the transducer surface [94].

## **2.5 Piezoimmunosensors; Quartz Crystal Microbalance (QCM)**

Typically piezo sensors operate in dry conditions, either in gases or a vacuum and are based on direct relationship of added mass and oscillation frequency given by the Sauerbrey equation. Contact between the quartz crystal and liquid leads to the attenuation of crystal oscillation and therefore limited application in biosensing. However, the used of thickness shear mode (TSM) resonators allowed overcoming the difficulties of employing quartz crystal for probing the liquid media. Since then piezo sensors have been widely used in biosensing in many areas, especially as immunosensors.

The first piezoimmunosensors were employed to detect the binding of BSA on immobilized anti-BSA on a quartz crystal [106]. A combination of dry and wet techniques was employed for the detection of *S. typhimurium* with anti-Salmonella antibody. The deposition of protein A and polyethylenimine-glutaraldehyde (PEI-GA) on quartz crystal prior to immobilization of antibodies in dry assay was tested. Then anti-Salmonella antibodies immobilized on protein A were used to bind with *S.*

typhimurium in a wet chamber which showed a decreased frequency [107]. A number of works on QCM immunosensors have been reported [94, 108 -110].

The mechanical properties of resonators can be figured out by the measurements of whole impedance spectra of a TSM resonator and fitting the experimental data to the ButterworthVan-Dyke (BVD) equivalent circuit model. In this model, the resistance (R) represents the energy loss from viscous effect; the inductance (L) is related to initial mass and thus to the oscillation frequency and capacitance (C) represents the mechanical elasticity of the quartz. In this method the effect of energy dissipation from the viscosity effect provides additional information to the mass loading for the analysis of QCM measurements.

QCM Impedance sensing of hexane and toluene organic vapours has been achieved by coating TSM resonators with calixarene films which are capable of adsorption of the above analytes in the nanoporous structure of calixarene films. Fitting of experimental data to a BVD equivalent circuit allows simultaneous monitoring of changes in both the mass and viscoelastic properties of a sensitive membrane in the course of absorption of organic vapour [111].

In another work, the impedance analysis of QCM has been used to study anti-human immunoglobulin G (anti-h IgG) adsorption and the subsequent human immunoglobulin (hIgG) or rabbit immunoglobulin G (rIgG) affinity reaction with polystyrene in aqueous solution. Time-dependencies of R, L, C parameters were obtained by fitting the impedance spectra to BVD equivalent circuit. It was found that the motional resistance (R) increases while the resonance frequency ( $f$ ) decreases during both anti-hIgG immobilization and the subsequent affinity process [112].

It has been shown that the QCM method is suitable for mass sensitive measurements in air as well as in liquid, but it is still difficult to measure the binding of small molecules in many cases. For example, the detection limit of label-free QCM immunosensors for bacteria generally is about  $10^5 - 10^7$  CFU/ml [59]. The detection of smaller molecules using both direct and competitive assays for the detection of herbicide 2,4-dichlorophenoxyacetic acid has been reported at 0.5 ng/ml and 0.01 ng/ml respectively [110].

Competitive immunoassay was always selected to realize the detection of small molecules. In addition, nanoparticles conjugated with the secondary antibody have been employed to amplify the response.

QCM is a most regular technique for DNA sensing as it allows real time measurements of DNA binding and hybridization at sub-nanogram level. It was reported that the amplification by 50 nm gold nanoparticles for the detection of DNA increased the sensitivity significantly up to  $10^{-14}$  M. The sensitivity increase was attributed to a larger mass of nanoparticles and the larger surface area occupied by each gold nanoparticle [113].

## **2.6 Spectroscopic Ellipsometry for sensing applications**

Ellipsometry is an analytical tool which is a well-established for thin film and surface characterization. This method relies on two parameters  $\psi$  and  $\Delta$  corresponding, respectively, to the light intensity ratio and phase shift of p and s components of polarized light. With respect to organic materials, spectroscopic ellipsometry has been extensively used in studying polymer thin films [114,115], self-assembled layers [116,117], LB films [118,119] and liquid crystal [115,120]. The majority of these applications however focus on the surface characterization. Ellipsometry is well known in thin film industry for in-situ monitoring of film deposition to control layer thickness, growth rate and layer quality. However the method of ellipsometry in general is recognised as a optical properties measurements tool but not as a sensor.

Due to the high sensitivity to the thickness increment (in the range of 0.01 nm) this method was recently adopted for the measurement of molecular layer adsorbed on solid surface which naturally leads to sensing applications. The advantages of the ellipsometry method in sensing applications are [121]:

- i. The measurements are based on reflection of polarized light; no reference beam or labels are needed.
- ii. It is possible to measure a very thin molecular layer (0.01 nm) adsorbed on the surface with fast response (within seconds).

- iii. Even higher sensitivity can be gained by observing the parameter  $\Delta$  (phase shift between p and s components of polarized light).
- iv. The method is capable of *in-situ* dynamic monitoring of both parameters  $\psi$  and  $\Delta$  in the course of bio-reactions such as affinity binding reactions.
- v. Molecular multilayers representing consecutively adsorbed (bound) molecules can be studied using the advanced the multilayer modelling facilities usually available in modern spectroscopic ellipsometry instruments.

The only drawback of ellipsometry is that it is an indirect method which needs an optical model for quantitative analysis and requires experience personnel to do the fitting. On the other hand, recent ellipsometry instruments such as J.A. Woollam equipment provide a library of models and algorithms for thin film analysis on different materials.

Spectroscopic ellipsometry method has been reported in various bio-sensing applications including the detection of Hepatitis B,  $\alpha$ -fetoprotein, and DNA hybridization. Detection limit of 0.1 ng/ml, 0.01 ng/ml and 10 amol/ml were achieved respectively [122,123].

In biosensing applications, the use of porous materials is a good approach providing a large surface area for immobilization of reagents. For this purpose, ellipsometric methods were successfully employed to study a porous surface of silicon [124] which then had been suggested as a support for enzyme based glucose sensor [125].

Further advances in spectroscopic ellipsometry for bio-sensing applications were achieved in its total internal reflection mode (TIRE). The idea of using ellipsometry in internal reflection mode was first realised experimentally by Wesphal [126] where the prism was used to couple the light beam into a thin metal film thus combining the ellipsometric principle of detection with the phenomenon of surface plasmon resonance. The increase in the sensitivity was achieved, and the method was originally called surface plasmon enhanced ellipsometry. This method was further explored and theoretically explained by Arwin [127] and got the current name of total internal reflection ellipsometry (TIRE). Further development of the method of TIRE was carried out by Nabok and his colleagues; the detailed modelling showed 10 fold gain of the

sensitivity with the use of  $\Delta$  spectra (as compared to  $\Psi$  spectra and traditional SPR measurements).  $\Delta$  and  $\Psi$  spectra is a phase shift and intensity ratio of  $p$  and  $s$  polarized light respectively. The method of TIRE was then successfully used in a number of bio-sensing applications and particularly in detection of low molecular weight molecules such as pesticides Simazine and Atrazine [128], T2 mycotoxin [129] and nonylphenol [130]. The detection of T2 mycotoxins in a wide range of concentrations from 100  $\mu\text{g/ml}$  down to 0.15  $\text{ng/ml}$  was observed.

## 2.7 Summary

In this work the method of TIRE was developed further (through improvements in the experimental set-up and data processing protocol) and used as the main experimental method in the study of another two mycotoxins (zearalenone and aflatoxin B1) as well as in the detection of amyloid precursor protein and beta-amyloid peptide involved in Alzheimer's disease. QCM is selected as secondary method to provide further analysis.

# CHAPTER 3

## OPTICAL IMMUNOSENSING EXPERIMENTAL METHODS: TOTAL INTERNAL REFLECTION ELLIPSOMETRY (TIRE)

This chapter outlines the basic theory of evanescent waves which is the main mechanism for a number of optical sensors. The methods of ellipsometry and surface plasmon resonance (SPR) are described and the similarities between them highlighted. The background of TIRE method (a combination of ellipsometry and SPR) is given; the experimental setup, measurements protocol and analysis are explained in detail.

### 3.1 Theoretical background of evanescent wave technique

Optical methods based on the evanescent field phenomenon combined with thin film nano-technology give some novel opportunities in the area of bio-sensing. Such methods can be label-free and suitable for express *in-situ* and in-field analysis. Usually parameters detected by this method are the intensity and/or phase shift of the reflected light. Very often optical evanescent field sensors use thin metal film as the transducing elements. Evanescent field methods link well with thin film nanotechnology capable of depositing few molecular layers on a surface. The evanescent field is associated with the electric field propagated along the interface between two materials at the condition of total internal reflection, as shown in Fig 3.1 (a). The amplitude of the electric field decays exponentially in the direction perpendicular to the interface. (Fig. 3.1(b)).

$$n_1 > n_2$$

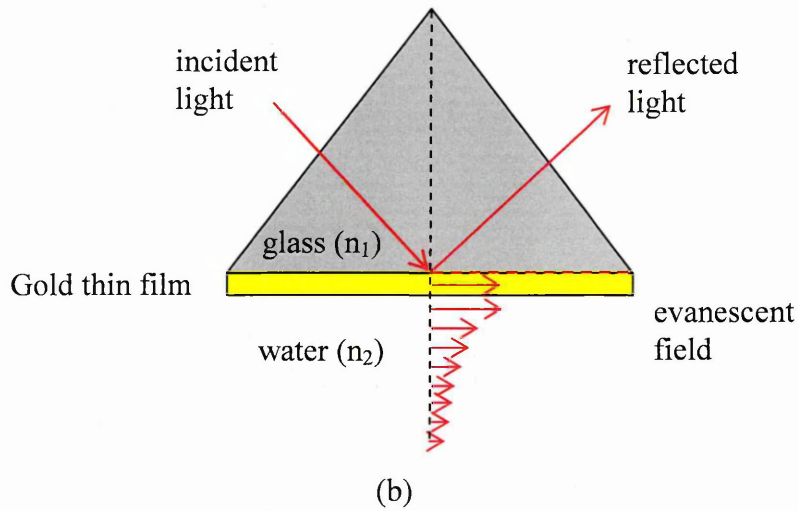
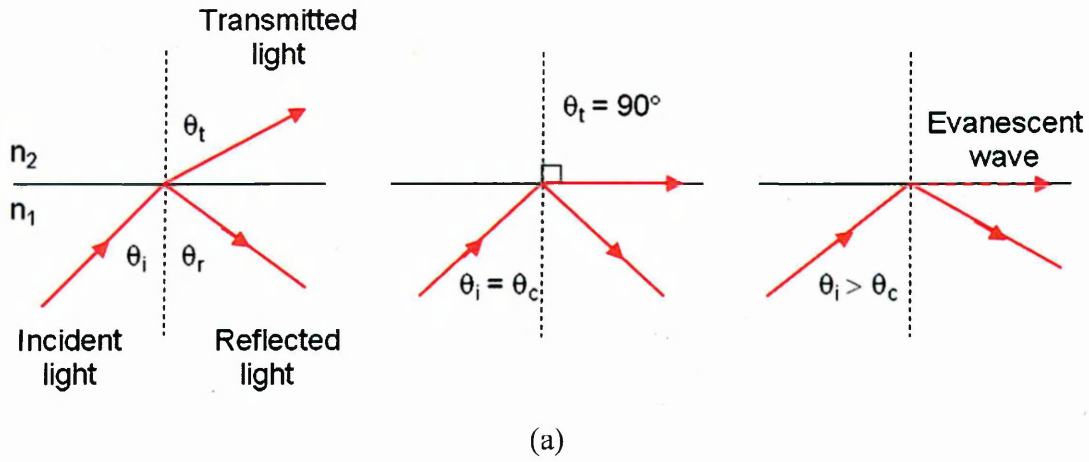


**Fig. 3.1:** (a) The formation of evanescent wave at total internal reflection with the condition of the refractive index,  $n_1 > n_2$ .  $\theta_i, \theta_r, \theta_t$  and  $\theta_c$  corresponds to angle of incident, reflection, transmission and critical angle respectively. (b) Evanescent wave in the presence of metal film on the interface; penetration of evanescent field in the direction perpendicular to the interface.

The general equation for the evanescent field is given by

$$E_t = E_{ot} \exp[i\omega t - iq_1(x \sin \theta_1 + z \cos \theta_1)] \quad 3.1$$

where  $q_1 = 2\pi \frac{ni}{\lambda}$ ,  $\theta$  is incident angle and  $n$  is an integer number.  $E_{ot}$  is the field at an interface,  $\omega$  is angular velocity,  $t$  is time and  $x, z$  are the coordinates along and

perpendicular to the interface. Derivation from the equation gives the relation for the decay of the wave in direction  $z$ . The depth of penetration,  $d_z$  at which the evanescent field has decayed from its initial value, is given by:

$$\begin{aligned} \frac{1}{d_z} &= \frac{2\pi}{\lambda} \left[ (n_1 \sin \theta_1)^2 - n_2^2 \right]^{1/2} \\ &= \frac{2\pi n_2}{\lambda} \left[ \left( \frac{\sin \theta_1}{\sin \theta_c} \right)^2 - 1 \right]^{1/2} \\ d_z &= \frac{\lambda / n_2}{2\pi \left[ \sin^2 \theta_1 - \left( n_2 / n_1 \right)^2 \right]^{1/2}} \end{aligned} \quad 3.2$$

where  $\theta_1$  = incident angle at medium 1 and  $\theta_c$  = critical angle.

### 3.1.1 Ellipsometry Method

Ellipsometry is a non-destructive optical method to determine the optical properties of materials. The idea of ellipsometry lies in measurements of changes of polarized light upon its reflection from a sample. As light reflects from a sample surface the state of polarized light changes from linear to elliptical, as in Fig. 3.2.

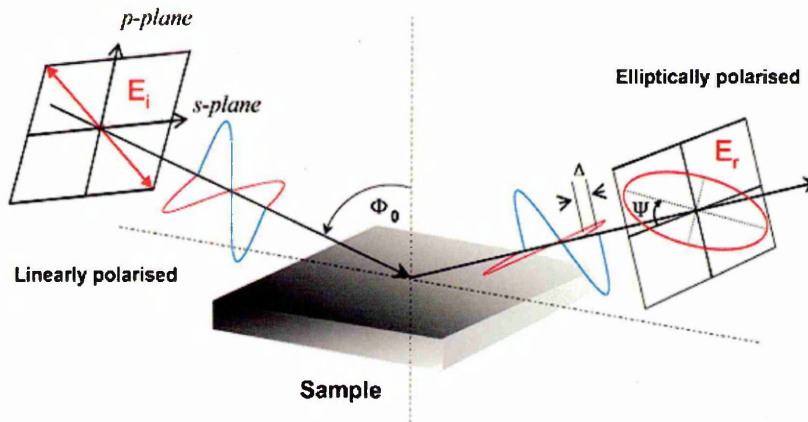


Fig. 3.2: The changes in polarization of light reflected from the surface [131].

Ellipsometry techniques do not measure directly the optical properties of the material but the angles of ( $\psi$ ) and ( $\Delta$ ). Psi ( $\psi$ ) and delta ( $\Delta$ ) are defined as a ratio, ( $\rho$ ), of complex reflection coefficients  $r_p$  and  $r_s$  for electric vectors, p (parallel) and s (perpendicular) to the plane of incidence [127].

$$\rho = \frac{r_p}{r_s} = \frac{|r_p| \exp(i\delta_p)}{|r_s| \exp(i\delta_s)} = \tan \psi \exp(i\Delta) \quad 3.1$$

In eq. 3.1,  $\psi$  represents the amplitude ratio of p and s components of polarized light while  $\Delta$  is the phase difference between p and s components.

$$\tan \psi = \frac{|r_p|}{|r_s|} \quad \Delta = \delta_p - \delta_s \quad 3.2$$

In the case of reflection / transmission at the interface between two media with respective indices  $N_0$  and  $N_1$ , the reflection and transmission coefficients are described by Fresnel's formula [132];

$$r_s = \left( \frac{E_{0r}}{E_{0i}} \right)_s = \frac{n_i \cos \theta_i - n_t \cos \theta_t}{n_i \cos \theta_i + n_t \cos \theta_t} \quad r_p = \left( \frac{E_{0r}}{E_{0i}} \right)_p = \frac{n_i \cos \theta_i - n_t \cos \theta_t}{n_i \cos \theta_i + n_t \cos \theta_t} \quad 3.3$$

$$t_s = \left( \frac{E_{0t}}{E_{0i}} \right)_s = \frac{2n_i \cos \theta_i}{n_i \cos \theta_i + n_t \cos \theta_t} \quad t_p = \left( \frac{E_{0t}}{E_{0i}} \right)_p = \frac{2n_i \cos \theta_i}{n_i \cos \theta_i + n_t \cos \theta_t} \quad 3.4$$

Substitution of  $r_p$  and  $r_s$  in equation (3.2), their values from (3.3) and Snell's Law,  $N_0 \sin \theta_0 = N_1 \sin \theta_1$ , yields;

$$N_1 = N_0 \tan \theta_0 \left[ 1 - \frac{4\rho}{(1+\rho^2)} \sin^2 \theta_0 \right]^{1/2} \quad 3.5$$



Solving the main ellipsometric equation is quite a difficult task. Two approaches are typically used, namely, forward and reverse ellipsometry problems. In forward ellipsometry problems, the values of  $\psi$  and  $\Delta$  can be found from known parameters  $N_0, N_1, N_2, d_1, \theta_0, \lambda$  and by solving Fresnel equations analytically, which is a rather straightforward procedure. Solving the reverse ellipsometric problem, i.e. finding the parameters of the reflective system such as refractive index ( $N_1$ ) and thickness ( $d_1$ ) of the film, can be obtained from the experimental values of  $\psi_{\text{exp}}$  and  $\Delta_{\text{exp}}$  and is much more complex. It can be tackled using some of the least square techniques which involve solving a forward problem (Fresnel equation) several times and finding the theoretical values ( $\psi_{\text{the}}$  and  $\Delta_{\text{the}}$ ) and subsequent minimizations of the error function.

The approach is based on finding the mean square error (MSE) between the experimental values of  $\psi_i^{\text{exp}}$  and  $\Delta_i^{\text{exp}}$  and theoretical (modelled) ones  $\psi_i^{\text{mod}}$  and  $\Delta_i^{\text{mod}}$  as given, for example [131]:

$$MSE = \frac{1}{2N - M} \sum_{i=1}^N \left[ \left( \frac{\Psi_i^{\text{mod}} - \Psi_i^{\text{exp}}}{\sigma_{\Psi_i}^{\text{exp}}} \right)^2 + \left( \frac{\Delta_i^{\text{mod}} - \Delta_i^{\text{exp}}}{\sigma_{\Delta_i}^{\text{exp}}} \right)^2 \right] = \frac{1}{2N - M} \chi^2$$

A smaller MSE implies a better fit. MSE is weighted by the error bars of each measurement, so noisy data are weighted less.

There are several types of ellipsometry instrumentation developed within the last 4 – 5 decades ranging from simple fixed angle, single wavelength units to modern spectroscopic ellipsometric instruments. Spectroscopic ellipsometers can be split into two major categories: instruments that use rotating optical elements (analyzer or compensator) and instruments that use a photoelastic modulator. For example, the J. A. Woollam M2000 spectroscopic ellipsometric instrument exploits the principle of a rotating compensator, which consists of a wide spectral range of light source (370 – 1000 nm), polarizer, rotating compensator, analyzer and a photodetector, as shown in Fig. 3.4.

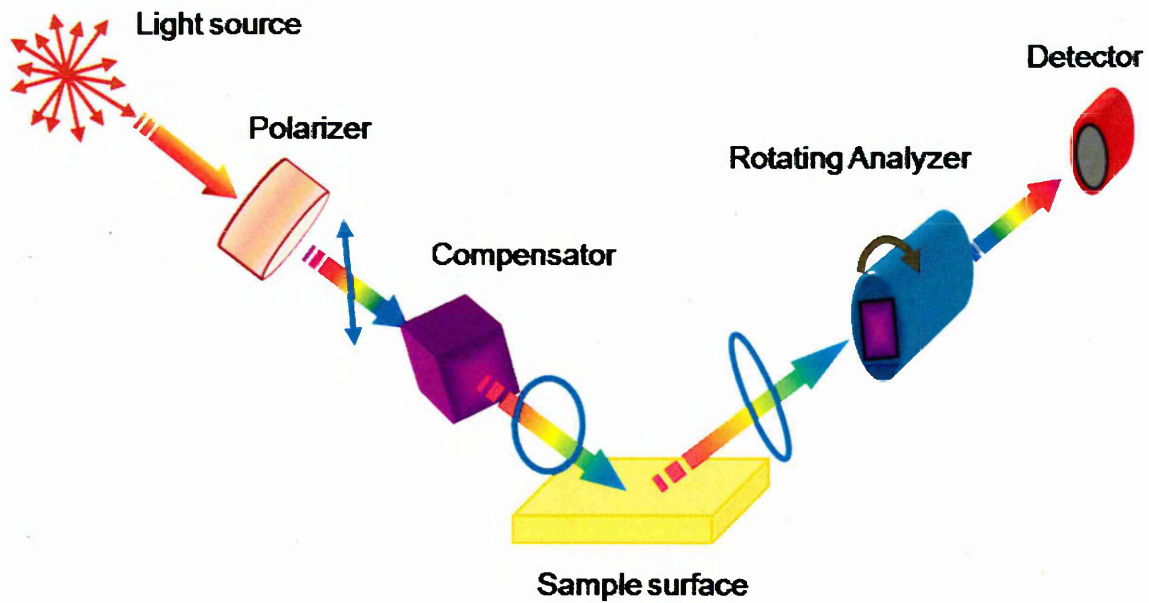
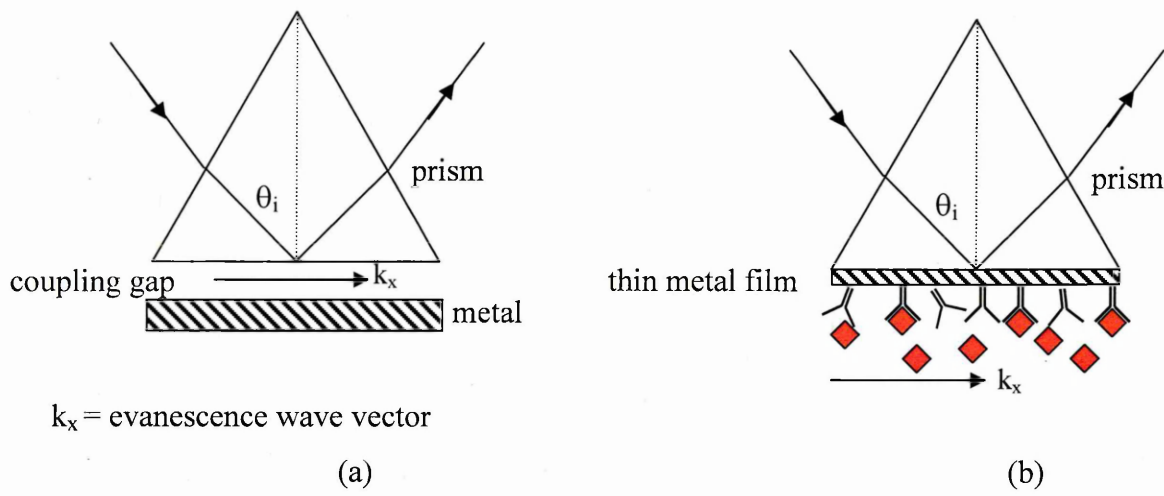


**Fig. 3.4.** The schematic of rotating analyzer spectroscopic ellipsometry

### 3.1.2 Surface Plasmon Resonance (SPR)

The most popular and widely-used design of SPR sensor is based on a prism coupler in attenuated total reflection (ATR) mode which was introduced by Otto [133] and Kretschmann,[134] (Fig. 3.5). Of the two, Kretschmann geometry setup has been found very convenient and suitable for bio-sensing applications. In this setup, the electromagnetic wave of light is totally reflected at the interface between a prism and the investigated medium. A thin metal film (20-40 nanometers in thickness) has little effect on the conditions of total internal reflection, but plays a crucial role when the energy of incident light matches the energy of plasmon oscillation in metal.



$k_x$  = evanescence wave vector

**Fig. 3.5:** SPR setup configurations by Otto [133] (a) and Kretschmann [134] (b).

The wave vector of the evanescent field,  $K_{ev}$  is given by [124];

$$K_{ev} = k_0 n_{glass} \sin \theta \quad 3.11$$

Where  $k_0 = \frac{2\pi}{\lambda}$  is the wave vector in a vacuum,  $n_{glass}$  is the refractive index of the glass prism and  $\theta$  is the angle of incidence of incoming light. The wave vector for surface plasmons wave,  $K_{spw}$  can be written by;

$$K_{spw} = k_0 \sqrt{\frac{\epsilon_m n_d^2}{\epsilon_m + n_d^2}} \quad 3.12$$

Where  $\epsilon_m = R_i \epsilon_m + I_m \epsilon_m$  is the dielectric function of the metal and  $n_d$  is the refractive index of the dielectric. The excitation of resonance plasmon can happen if;

$$K_{spw} = K_{ev} \quad 3.13$$

This causes the transfer of the energy of incident light to surface plasmon oscillation or wave (SPW) and therefore to energy dissipation in the metal film, resulting in a reduction of the intensity of reflected light, which can be detected as a sharp dip (Fig. 3.6). There are several types of SPR experiment set-up, which can be based either on the principle of prism rotation (like the original Kretschmann set-up) [135] or on the use of a white light source and recording the whole spectrum with a photodiode array [136, 137]. Depending on the type of SPR used, the SPR graph can be presented as a

dependence of the reflected light intensity on the angle of incidence or as an SPR spectrum, e.g. reflected intensity vs wavelength (as shown in Fig. 3.6).

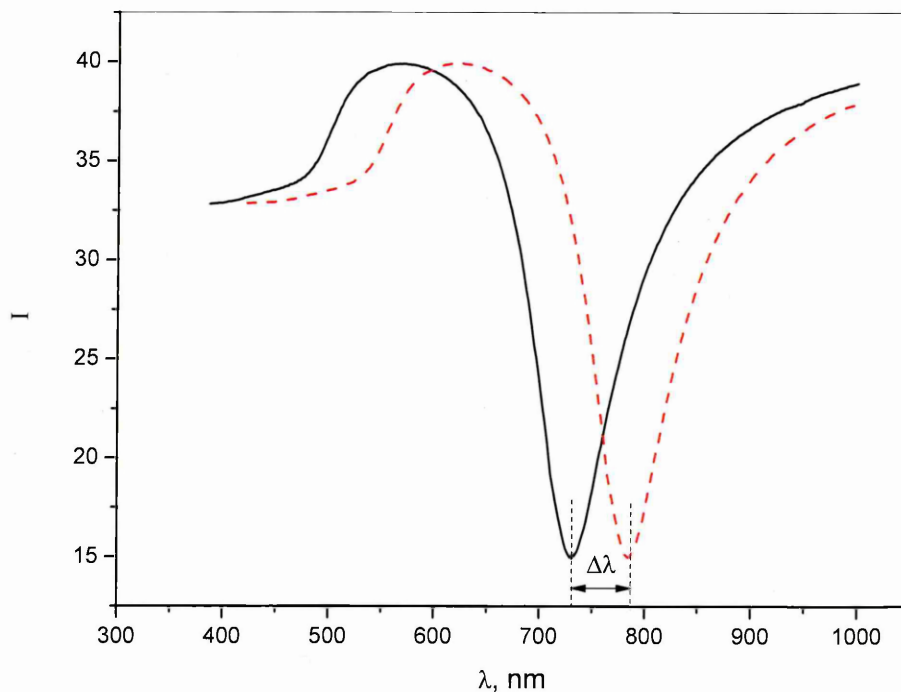


**Fig. 3.6.** Typical SPR spectra. The spectral shift is caused by the presence of a thin film (such as an adsorbed molecular layer) on the surface of gold.

Fig. 3.6 shows typical SPR spectra: one corresponding to a surface of bare gold and the other (red shifted) corresponding to the added layer on the gold surface. This layer could be a molecular layer adsorbed on the surface. Any changes in this adsorbed layer caused, for example, by immune binding can therefore be recorded and further quantified. For instance, the value of a spectral shift depends on the thickness and optical properties of the adsorbed layer such as refractive index,  $n$ , and extinction coefficient,  $k$ . Similar to ellipsometry, these parameters can be found by fitting the SPR spectra to Fresnel's equation using a least square technique. Furthermore, by monitoring the intensity of the reflected light at a fixed wavelength (or angle of incidence), the kinetics of molecular adsorption (or immune binding) can be investigated.

This is why the method of SPR has become a popular analytical tool in biochemistry. BIACORE, which was first introduced in 1990 by Biacore Ab. (Uppsala, Sweden), is the SPR instrument used most extensively nowadays [138].

Extensive review papers of the fundamental principles and advanced developments in SPR biosensors have been published [138,139] which expand on their use in various bio-sensing applications including food analysis [140], immunosensors [141], molecular binding and kinetics analysis [142] and disease detection [143].

### **3.2 Total Internal Reflection Ellipsometry (TIRE)**

The main drawback of using traditional ellipsometry for bio-sensing applications is the propagation of light through the investigated medium. The use of different biochemicals in different buffer solutions having different refractive indices may affect the measurements, especially *in-situ* measurements of adsorption (or binding) kinetics. Apart from the effect of the medium, the cell is usually large (which is a serious drawback for the majority of bio-sensing tasks) and may also require non-polarising transparent windows. Other factors that could seriously affect the ellipsometry measurements are the use of cloudy fluids or fluid turbidity produced by injection of liquid or vibration. The current trend of utilising combining particles to amplify the sensor response is almost impossible due to light scattering.

The method of Total Internal Reflection Ellipsometry offers a solution to the above problems by introducing upside down geometry when the light is coupled to thin gold films through a glass prism in conditions close to total internal reflection. In that case, the light penetrates very little into the investigated medium and can be separated from direct interaction with the investigate medium.

Combination of the advantages of SPR and ellipsometry, called surface plasmon resonance enhanced ellipsometry (SPEE) [126], was first explored in 2002 to investigate a biomolecular layer of antibody and DNA hybridization. The setup, as shown in Fig. 3.9, consisted of a liquid cell attached with a gold coated glass slide and 70° prism to provide the condition of total internal reflection. It was reported as

sensitive enough to detect changes in the effective thickness of biomolecular layers of less than 10 ppm.

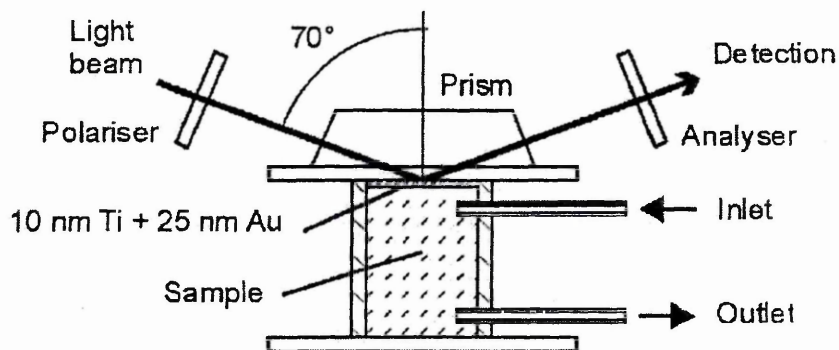


**Fig. 3.9:** Experimental setup for surface plasmon resonance enhanced ellipsometry [126].

Later TIRE principle and its applications in bio-sensing were reviewed in 2004 [127]. Spectroscopic TIRE in *in-situ* investigation of protein adsorption on a thin film was investigated. A light source of a xenon lamp went through a polarizer and was then refracted into a  $60^\circ$  glass prism in optical contact with a glass slide with a thin metal layer. After reflection, the light passed through the analyzer and the polarization was determined by analysing the signal from the detector. Various concentrations of ferritin protein from 1 mg/ml up to 2 mg/ml were injected to the cell. Optical properties values from the modelling showed a good agreement between experiment and literature [144].

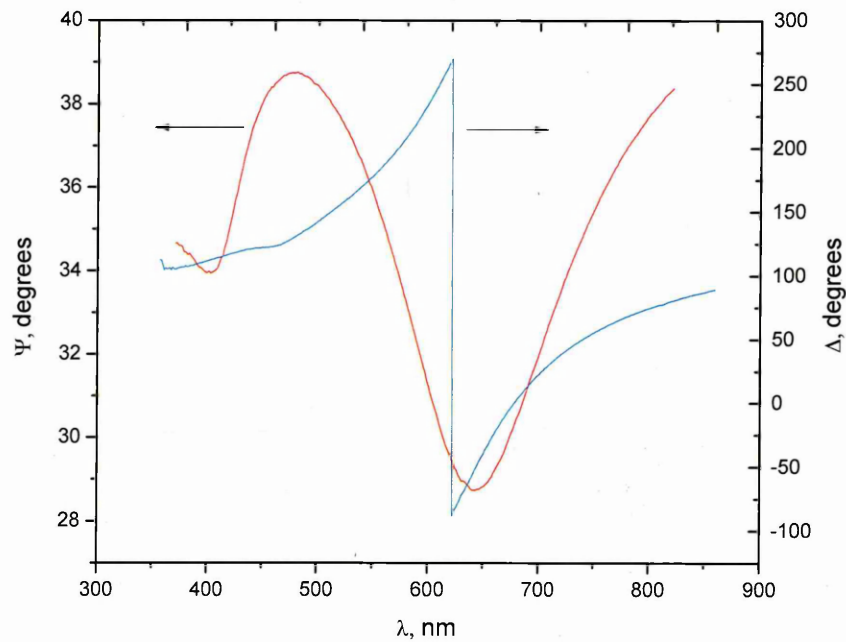
### 3.2.1 Theoretical background of TIRE

TIRE employs a prism coupler technique which combines the advantages of spectroscopic ellipsometry and the experimental convenience of Kretschmann SPR configuration. The angle of incidence selected should be close to the angle of total internal reflection, which needs to use a suitable prism, and can be calculated by [127]:

$$\theta = \arcsin \left[ \frac{1}{N_1} \sqrt{\frac{\epsilon_m N_2^2}{\epsilon_m + N_2^2}} \right] \quad 3.14$$

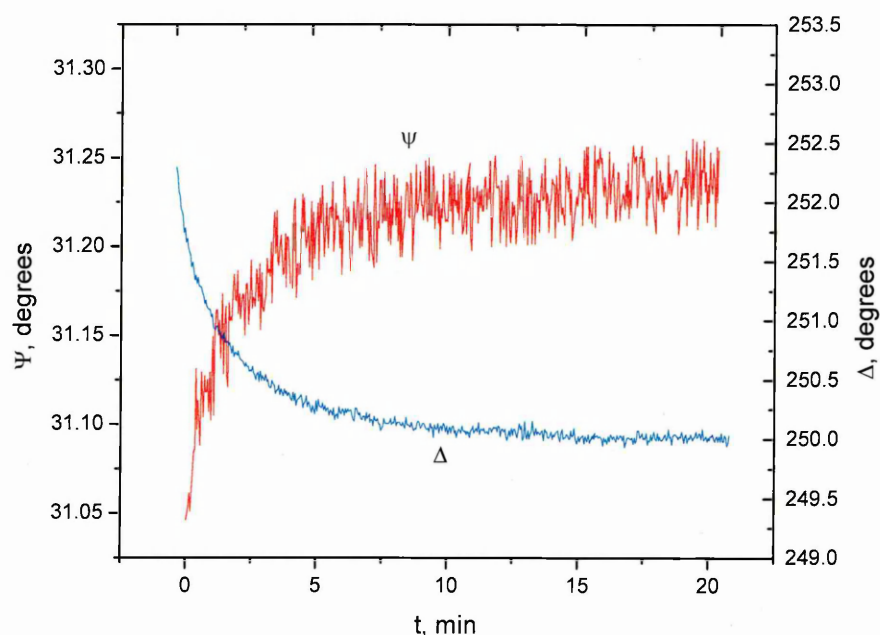
where  $N_1$  and  $N_2$  are the refractive index of glass and dielectric film respectively,  $\epsilon_m$  is the real part of dielectric constant of metal film.

In contrast to the conventional bio-sensing analytical tool of SPR based upon monitoring the intensity of reflected p polarised light, the TIRE method detects the two parameters  $\Psi$  and  $\Delta$  related, respectively, to the amplitude ratio and the phase shift of p and s components of polarised light. Two types of TIRE measurements can be performed: (i) Single spectroscopic scans, which are always performed in the same buffer solution in steady state conditions after completion of each adsorption (or binding) step; such measurements are used for evaluation of the thickness and optical constants of adsorbed layers; (ii) Dynamic spectral measurements, which are performed in the course of adsorption (binding) and require recording a number of spectra after certain time intervals.



**Fig. 3.7.** Typical TIRE spectra bare gold film on glass.

The typical  $\psi$  and  $\Delta$  spectra from single spectroscopic measurement are shown in Fig. 3.7. The  $\psi$  spectrum resembles typical SPR spectra with the maximal intensity corresponding to the conditions of total internal reflection while the minimum is due to the surface plasmon resonance. At the same time, the  $\Delta$  spectrum experiences a sharp drop from  $270^\circ$  to  $90^\circ$  near the plasmon resonance. From the spectra given in Fig. 3.7, it is quite obvious that the parameter of  $\Delta$  is more sensitive than  $\psi$  to small variations of the position of spectra cause by molecular binding. The comparison of  $\psi$  and  $\Delta$  spectra for TIRE in different media shows that TIRE is about 10 times more sensitive towards the changes in both the thickness,  $d$ , and refractive index,  $n$ , of thin films as compared to conventional external reflection ellipsometry [145].



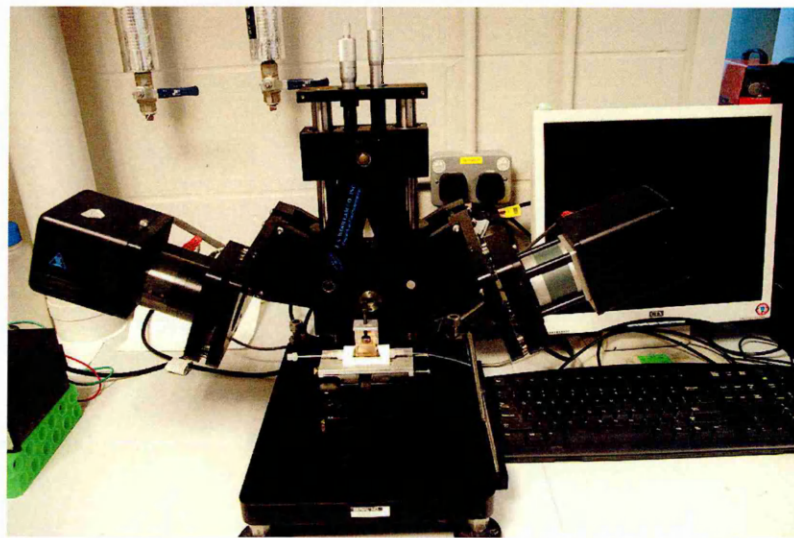
**Fig. 3.8.** Typical time dependencies of  $\psi$  and  $\Delta$  extracted from dynamic TIRE scans at selected wavelength.

Figure 3.8 shows typical dynamic spectra during immune reaction. From the large number of data recorded, only the spectra of  $\psi$  and  $\Delta$  at certain wavelengths (typically near the plasmon resonance) were selected. For example, the selection of the wavelength at 600 nm in Fig. 3.7 gives a rising  $\psi$  signal and decaying  $\Delta$  signal. As one can see in Fig. 3.8, the  $\Delta$  kinetic curve is less noisy than the  $\psi$  one, and therefore  $\Delta(t)$  characteristics were selected for further analysis of the molecular adsorption kinetics.

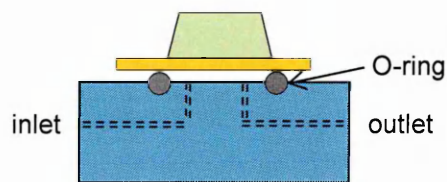
Further analysis of the absorption (binding) kinetics was required for the evaluation of the affinity constants of the immune reaction studied [145]. The exact procedure for kinetics analysis is given in Section 3.2.5.

### 3.2.2 TIRE experimental set-up

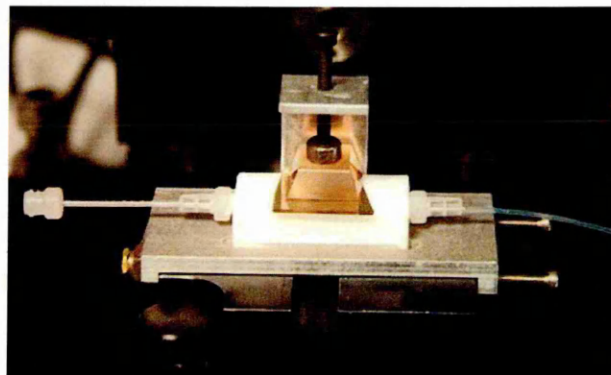
The TIRE experiment setup was based on the basis of commercial M2000 J. A. Woollam Spectroscopic Ellipsometry operating in the 370 – 1000 nm spectral range and exploiting the rotating compensator principle (Fig. 3.9 (a)).



(a)



(b)



(c)

**Fig. 3.9.** (a) J.A.Woollam M2000 Ellipsometer (b) Newly designed TIRE cell (c) Zoomed in TIRE cell with a 68° prism attached on an ellipsometer sample stage.

In order to use the instrument as a biosensor operating in liquid, a special small-volume TIRE cell was designed and machined from polytetrafluoroethylene (PTFE) material. The 200  $\mu\text{l}$  volume of the cell substantially reduces consumption of bio-liquids, which is a very important factor in bio-sensing experiments. A silicon O-ring was used to seal the gold slide against the cell, as shown in Fig 3.9 (b).

Another key element of TIRE is the glass prism which couples the light beam into a thin gold film. Fig. 3.9 (c) shows the TIRE cell with attached 68° prism on a J. A. Woollam sample stage. The choice of a 68° prism was made to provide the condition of total internal reflection on a glass – water interface. A gold-coated glass slide was brought into optical contact with the prism via index matching liquid to avoid an air gap.

TIRE data processing requires building an optical model corresponding to a sample. Dielectric functions of some layers (namely; BK7 glass, gold, water) are known and can be selected from the WVASE software library [131]. Parameters of unknown layers (i.e. thickness and dispersion of  $n$  and  $k$ ) can be found by fitting the experimental data to the model layer which can be selected from the WVASE library. The most common model for adsorbed molecular layers is Cauchy [176].

Fig. 3.10 shows the TIRE measurement protocol, which typically started with a single spectroscopic scan of the sample of a bare gold film in a standard Tris-HCl buffer for TIRE routine. The measurements started with the single spectroscopic in a buffer solution (pH 7.5) to obtain the effective thickness and dispersion curves for optical parameters  $n(\lambda)$  and  $k(\lambda)$  of the Chromium–Gold layer. A three-layer model consisting of ambient (BK7 glass), gold, and substrate (water) was used, where the parameters for glass and water are fixed but the thickness and optical constants of the metal layer are varied. The dispersion parameters of  $n(\lambda)$  and  $k(\lambda)$  for gold as well as the thickness of evaporated gold layer were taken as initial guess values. The effective parameters for the Cr/Au layer obtained by fitting for that particular sample were then used as fixed parameters for further fitting of data obtained on the same sample.

### 3.2.3 TIRE measurements and fitting protocol

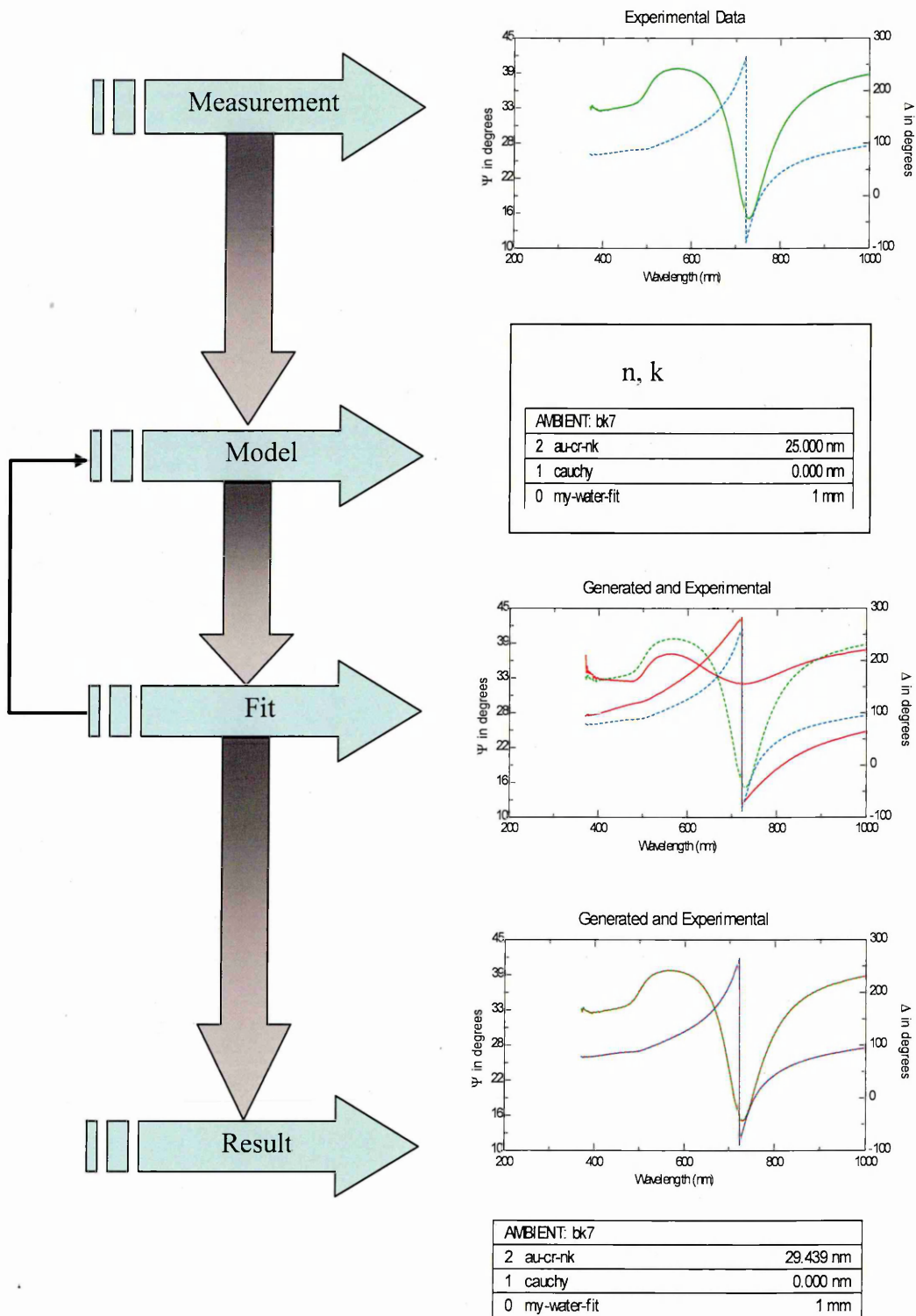
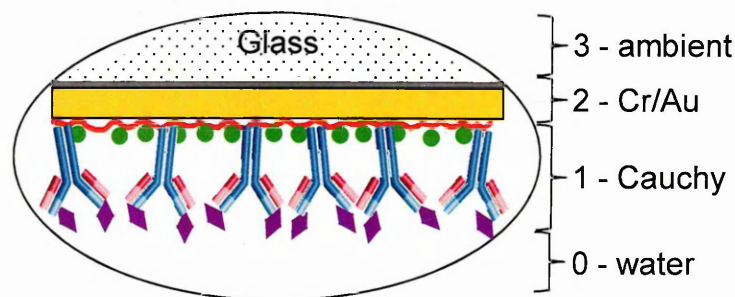


Fig. 3.10. The flowchart of data analysis in TIRE.

Ellipsometry data fitting requires a great deal of experience and the outcomes depend on the selection of a physically adequate model as well as the choice of initial parameter fitting routine, i.e. the use of ‘normal fit’, ‘global fit’, or ‘spectral fit’ option, limiting the range of variable parameters, removing ‘anomalous’ data points, etc. In order to achieve reliable results, the fitting procedure needs to be repeated several times (preferably from different initial conditions) until consistent values of thickness ( $d$ ), refractive index ( $n$ ) and extinction coefficient ( $k$ ) are achieved. In some cases a good fit cannot be achieved due to the following reasons [132]:

- (i) the measurements of  $(\psi, \Delta)$  spectra are inaccurate.
- (ii) inappropriate electric functions selected in data analysis
- (iii) the optical model in data analysis is not suitable
- (iv) depolarization effect from the sample

Further TIRE measurements consisted of recording single spectroscopic scans in the same buffer solution after completing each step of adsorption (or binding). Parameters of adsorbed molecular layers ( $d$ ,  $n$  and  $k$ ) were obtained by data-fitting to the four-layer model (see Fig. 3.11). In this model, the glass (prism and glass slide) acts as ambient (3) then the light goes through the Cr/Au film (2) adsorbed molecular layer (1) and finally reaches the aqueous buffer solution in a cell which acts as a substrate (0). The molecular layer is modelled by the Cauchy dispersion function [132].



**Fig. 3.11.** Illustration of the four-layer model for TIRE data fitting.

**Table 3.1.** The four-layer model for TIRE data fitting

No.	Layer	Parameters
3	BK-7 glass (ambient)	$n, k$ dispersions from WVASE32 library $n = 1.515, k = 0$ at 633nm
2	Cr/Au film	$n = 0.359 \pm 0.078; k = 2.857 \pm 0.114$ at 633nm $d$ is varied in the range of 25 – 30 nm
1	Adsorbed layer	Cauchy model: $A = 1.396, B = 0.01, C = 0$ $n = 1.42, k = 0$ at 633nm
0	Water	$n, k$ dispersions from WVASE32 library, $n = 1.33, k = 0$ , at 633nm

The four-layer model is given in more detail in Table 3.1. As mention before, the optical dispersion characteristics for BK7 glass (3) and water (0) were taken from the J. A. Woollam material library and were always fixed. The characteristic values of  $n$  and  $k$  for glass and water are given in Table 3.1 at the wavelength 633 nm (corresponding to HeNe laser). The effective values of thickness and refractive index dispersion for Cr/Au were found earlier by fitting TIRE data for a bare gold surface. TIRE measurements were always performed on the bare gold surface before deposition of a molecular layer. Then the obtained values of thickness ( $d$ ), and dispersion functions for  $n$  and  $k$  were kept fixed in further TIRE fittings on this sample after deposition of molecular layers. Such a procedure had to be repeated for every new sample. For organic layers deposited on the sensing surface, the Cauchy dispersion function was used;

$$n = A + \frac{B}{\lambda^2} + \frac{C}{\lambda^4} + \dots, k = 0 \quad 3.15$$

During fitting, the parameters of  $A, B$  and  $C$  were fixed at 1.396, 0.01 and 0 respectively, giving a value for  $n$  of about 1.42, which is typical for organic materials. A zero value for coefficient ( $k = 0$ ) was used since all molecular layers were considered to be optically transparent in the spectral range used (370 – 1000 nm). The only variable parameter was the thickness,  $d$ . In such approximation, all changes (mostly spectral shifts) in the TIRE spectra are associated with changes in film thickness.

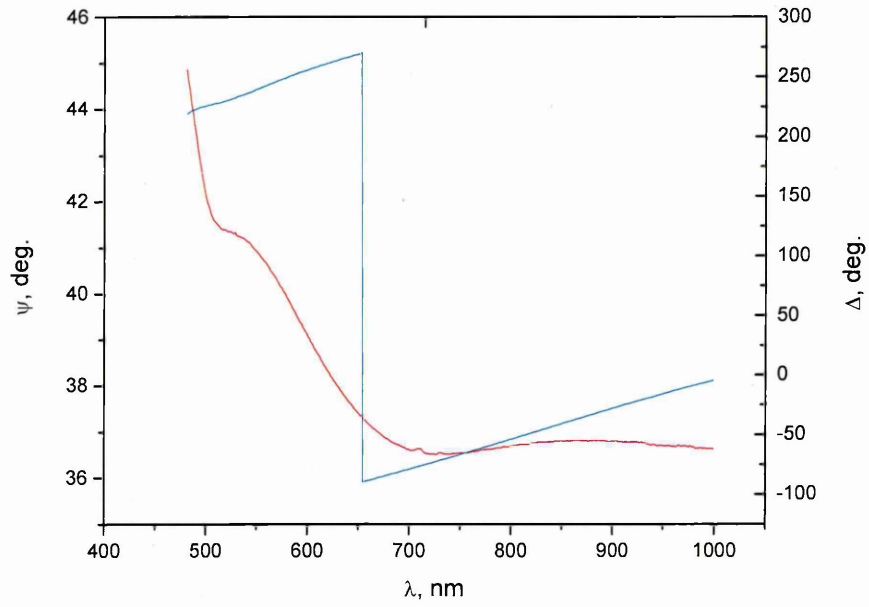
The proposed approach in data analysis (i.e. fixing the values of  $n$  and  $k$ ) is not strictly correct but was enforced by natural limitations of both ellipsometry and SPR methods for thin (thinner than 10 nm) dielectric films [146]. It has to be said that common practice in bio-sensing [147] was to fix the film thickness and relate all the changes to the refractive index. However, recent experimental work has shown that the refractivity increments caused by adsorption of different bio-molecules represent only 0.1-0.14% of the refractive index,  $n$ , and therefore the spectral changes are associated mainly with thickness [148]. A similar value ( $n = 1.44$ ) of the fixed refractive index was used in detection of *E. coli* phospholipids using Bruggeman's effective medium approximation and resulted in the measurements of the effective thickness of lipids immobilized on silicon oxide [149].

A similar dispersion function was used to measure protein multilayers system on silicon substrate with up to 20 alternating layers of biotinylated bovine serum albumin and streptavidin. A slightly lower refractive index of 1.385 was found [150].

#### **3.2.4 Further improvement of TIRE data analysis**

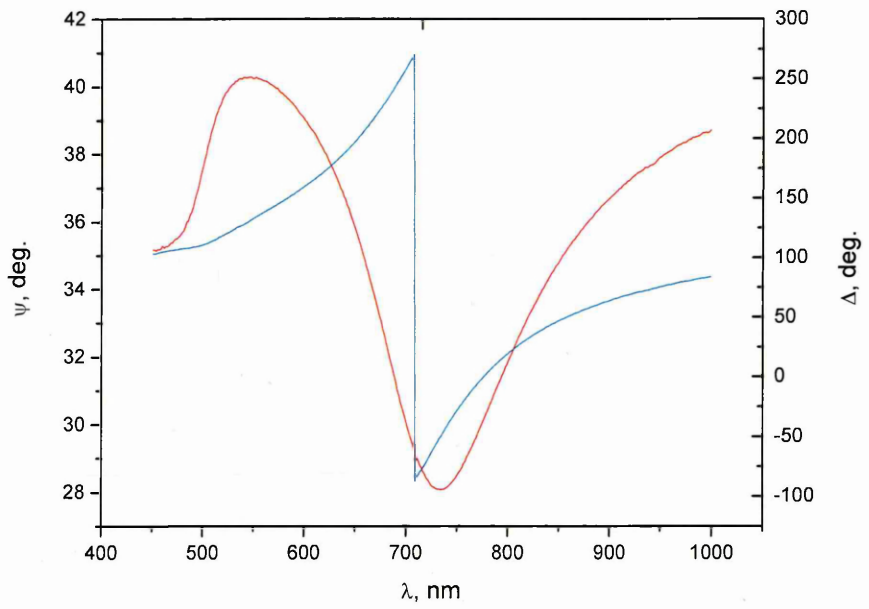
The shift of  $\psi$  and  $\Delta$  spectra to the higher wavelength was caused by the increase in thickness of the sensing surface. The increase in average layer thickness was correlated with the molecular size (or weight) of the bound analyte. The shifted spectra have been used as an indicator for the bio-reaction, i.e. antigen-antibody binding.

The parameters of the Cr/Au under layer have a significant effect on the general shape of TIRE spectra and subsequent data fitting. Figures 3.12 (a) and (b) show  $\psi(\lambda)$  and  $\Delta(\lambda)$  spectra of bare gold in a Tris-HCl buffer at different thicknesses of the Au layer of 15.280 nm and 27.720 nm respectively.



Cr/Au = 15.280, MSE =  $6.085 \times 10^{-10}$

(a)



Cr/Au = 27.720 nm, MSE =  $6.713 \times 10^{-10}$

(b)

**Fig. 3.12.** Typical  $\psi(\lambda)$  and  $\Delta(\lambda)$  curves for a 15 nm (a) and 28 nm (b) thick gold layer.

The number of revolutions of the compensator has an effect on the noise level. The use of a large number of revolutions per measurement (100 or higher) can significantly improve signal-to-noise ratio and therefore the subsequent data fitting of  $\Delta(\lambda)$  and  $\psi(\lambda)$  spectra. The higher the number of revolutions per measurement, the longer the time needed for single spectrum scan. The latter fact is tolerable for steady state measurements but a large number of revolutions cannot be used in dynamic spectral measurements (here the number of revolutions is typically 10-20).

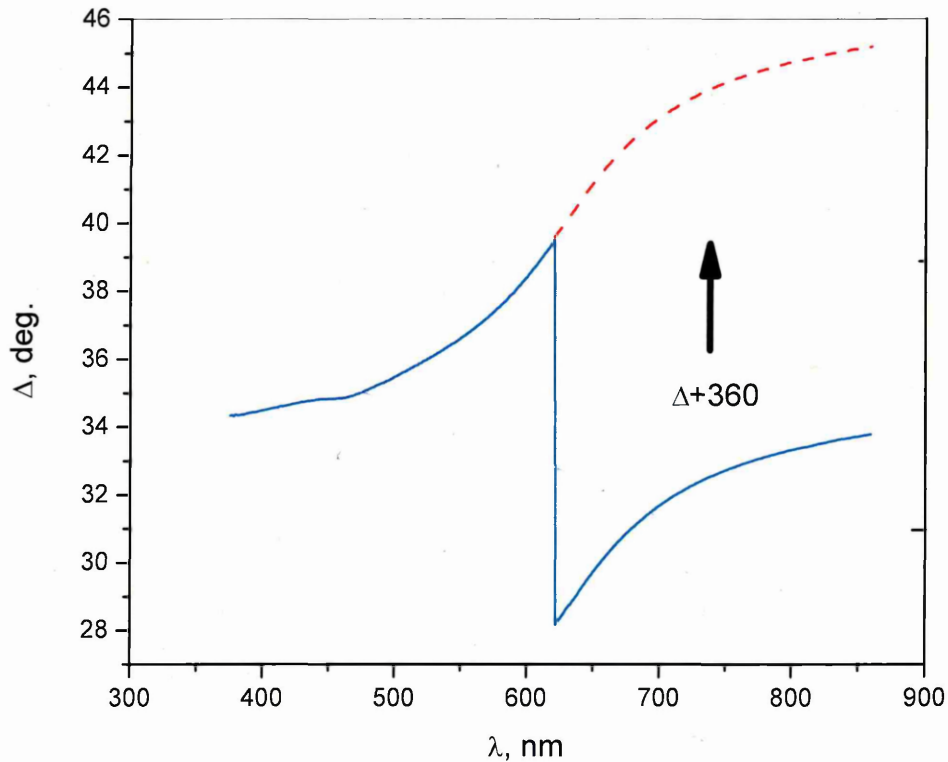


**Fig. 3.13.** The correction of TIRE  $\Delta(\lambda)$  spectra

As has been mentioned earlier, in the TIRE method, typical  $\Delta(\lambda)$  spectra exhibit a sharp phase drop from  $270^\circ$  down to  $-90^\circ$ . This effect is characteristic of the particular ellipsometric instrument used (J. A. Woollam in this work) while in theory  $\Delta(\lambda)$  varies between 0 and 360 [132]. The drawback of such a sharp change in  $\Delta$  is that a spectral shift smaller than the wavelength step (1.4 nm in the M2000 instrument) cannot be detected experimentally. The data fitting always gives a small thickness increment while there is no spectral shift detected. The correction of negative values of  $\Delta(\lambda)$  by adding

360° transforms the  $\Delta(\lambda)$  spectrum into an almost linear curve (Fig. 3.13) and eventually improves the resolution of TIRE measurements. Small spectral shifts (smaller than the wavelength increment) become visible after such alteration and the results of data fitting and spectral shift are now in good agreement.

### 3.2.5 TIRE kinetic analysis

TIRE dynamic spectral measurements are based on recording a number of spectra of both  $\psi$  and  $\Delta$  after a certain time intervals during the adsorption (or binding) processes. The resulting time dependencies of  $\psi$  and  $\Delta$  at selected wavelengths (similar to those presented in Fig. 3.8) are utilized for *in-situ* monitoring of all stages and molecular adsorption and biochemical reactions, i.e. immune reactions. TIRE dynamic spectral measurements followed by subsequent data processing allow the evaluation of the association and affinity constants of bio-reactions. The analysis of adsorption kinetics, which was originally outlined in several literature reports [145,151-153] was further improved and simplified in this work.

Adsorption of molecules to binding sites of concentration  $N$  on the surface is described by the following equation:

$$\frac{dn}{dt} = k_a C(N - n) - k_d n \quad 3.16$$

Where  $k_a [Mol^{-1}s^{-1}]$ ,  $k_d [s^{-1}]$  are adsorption and desorption rates, respectively,  $C [Mol]$  is the concentration of analyte (i.e. antigen) in the environment (solution),  $n [Mol \cdot m^{-2}]$  is the concentration of adsorbed analyte on the surface, and  $N [Mol \cdot m^{-2}]$  is the concentration of binding sites (i.e. antibodies) on the surface. Consequently,  $N - n$  is the concentration of available binding sites on the surface. The solution of this equation is given as:

$$n = N \frac{k_a C}{k_a C + k_d} \left[ 1 - e^{-(k_a C + k_d)t} \right] \quad 3.17$$

It can be expressed in terms of sensor response, or, in our case, in terms of the recorded values of  $\psi$  and  $\Delta$ . For example, a rising exponential function of  $\psi$  can be described as:

$$\Psi = \Psi_{\max} \frac{k_a C}{k_a C + k_d} \left[ 1 - e^{-(k_a C + k_d)t} \right] \quad 3.18$$

While a decaying exponential dependence for  $\Delta$  is given as:

$$\Delta = \Delta_{\max} \frac{k_a C}{k_a C + k_d} e^{-(k_a C + k_d)t} \quad 3.19$$

The time constant in the above dependencies can be introduced as:

$$\tau = \frac{1}{k_a C + k_d} \quad 3.20$$

The reciprocal value of  $S = \frac{1}{\tau} = k_a C + k_d$  depends linearly on the concentration of analyte, the rates of adsorption ( $k_a$ ) and desorption ( $k_d$ ) can therefore be evaluated as a gradient and intercept of the graph  $S$  vs  $C$  respectively. Then the association constant can be found as a ratio of  $k_a$  and  $k_d$  ( $K_A = \frac{k_a}{k_d}$ ) and the affinity constant is the reciprocal of  $K_A$  ( $K_D = K_A^{-1} = \frac{k_d}{k_a}$ ).

In order to find values of  $K_A$  or  $K_D$ , TIRE dynamic measurements have to be performed at different concentrations of analytes and the time constant ( $\tau$ ) has to be found by fitting every time dependence to the equation  $\exp(-t/\tau) + b$ . The reciprocal values  $S = 1/\tau = k_a C + k_d$  have to be plotted against the concentration of the analyte (or antigen), ( $C$ ). Linear fit of such dependence yields the values of  $k_a$  and  $k_d$  and consecutively  $K_A$  and  $K_D$ .

The correct analysis of the immune reaction kinetics has to be performed for different concentrations of antigen binding to originally empty binding sites i.e. antibodies freshly immobilized on the surface. Such a procedure is however lengthy, expensive (because of the large amount of antibodies used) and thus not practical. In this work, the consecutive adsorption (binding) steps started from the smallest concentration of

analytes (or antigen). This approach is much more practical but it has to be justified. If  $N_0$  is the initial concentration of binding sites (antibodies) on the surface, the concentration of molecules adsorbed on the surface after the first stage of adsorption is given as:

$$n_1 = N_0 \frac{k_a C_1}{k_a C_1 + k_d} [1 - \exp(-(k_a C_1 + k_d)t)] \quad 3.21$$

and  $N_i = N_{i-1} - n_{i\max}$ ,  $n_{i\max} = N_{i-1} \frac{k_a C_i}{k_a C_i + k_d}$  until all binding sites are occupied and eventually  $N_i = 0$ . It is important to note that only the concentration of available binding sites on the surface ( $N_{i-1}$ ) is varied during such consecutive adsorption steps, while the time constant  $\tau_i = \frac{1}{k_a C_i + k_d}$  remains the same, as in the case of single stage adsorption [145], and depends only on the parameters  $k_a$ ,  $k_d$  and the concentration of antigen in solution ( $C_i$ ). Thus we can conclude that the procedure of the evaluation of  $k_a$  and  $k_d$  from graph  $1/\tau_i$  vs.  $C_i$  described in [151] is still valid in the case of consecutive adsorption. The above procedure was implemented for the immune analysis throughout the work and particularly for the detection of mycotoxins.

### 3.3 Summary

TIRE was employed as a main detection method in this work. A newly designed TIRE cell which consumes only 200  $\mu$ l volume of liquid reduce significantly the amount of bio-chemical needed to perform the measurements. Since TIRE  $\Delta(\lambda)$  spectra is more sensitive, it was selected for the analysis throughout this work. There are two types of measurements that were performed; single spectroscopic and kinetic measurements for the evaluation of shifted spectra and affinity calculation respectively.

# CHAPTER 4

## COMPLEMENTARY EXPERIMENTAL METHODS AND TECHNOLOGIES

This chapter outlines other experimental methods employed in this study. The method of Quartz Crystal Microbalance (QCM) in both dry and liquid phase was explored in this study as a complementary technique for investigation of the immune reactions. In particular, two types of QCM techniques operating in liquid phase, QCM in microfluidic flow and QCM impedance analysis, are described here. Other methods, used for surface morphology analysis, were Atomic Force Microscopy (AFM) and Scanning Electron Microscopy (SEM).

### 4.1 Piezoelectric resonator: Quartz Crystal Microbalance (QCM)

The piezoelectric effect is a reversible process of generation of internal electrical charges (or electrical field) in response to mechanical deformation of the material, or vice versa. Piezo-electricity is typically associated with non-centro symmetric crystals such as quartz. Fig. 4.1 shows the relationship between mechanical and electrical variables on quartz crystal.

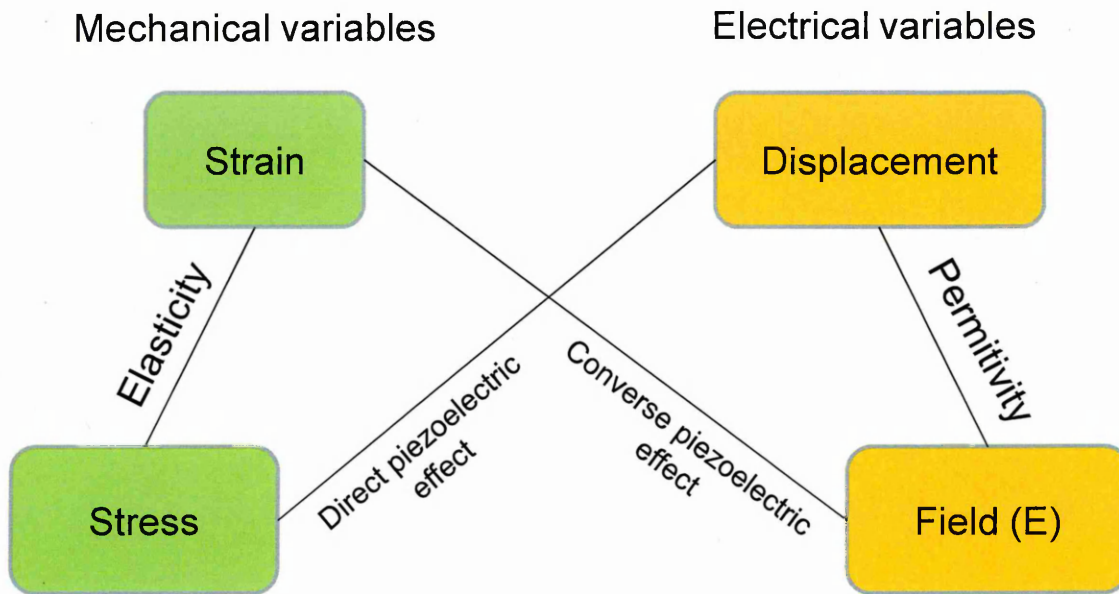


**Fig. 4.1** The relation between mechanical and electrical properties of QCM [154].

AC voltage applied between two electrodes deposited on the opposite sides of a quartz crystal causes mechanical oscillations in the crystal. Since the piezoelectric effect is reversible, mechanical oscillations in quartz crystals generate alternating voltage on the electrodes. The condition when the frequency of the AC signal matches the frequencies of mechanical standing waves in a quartz crystal is called resonance, and thus the devices are called piezoelectric resonators. A piezoelectric quartz crystal resonator is a piece of a natural or synthetic crystal of bulk quartz cut precisely along certain crystallographic directions, as illustrated in Fig. 4.2.

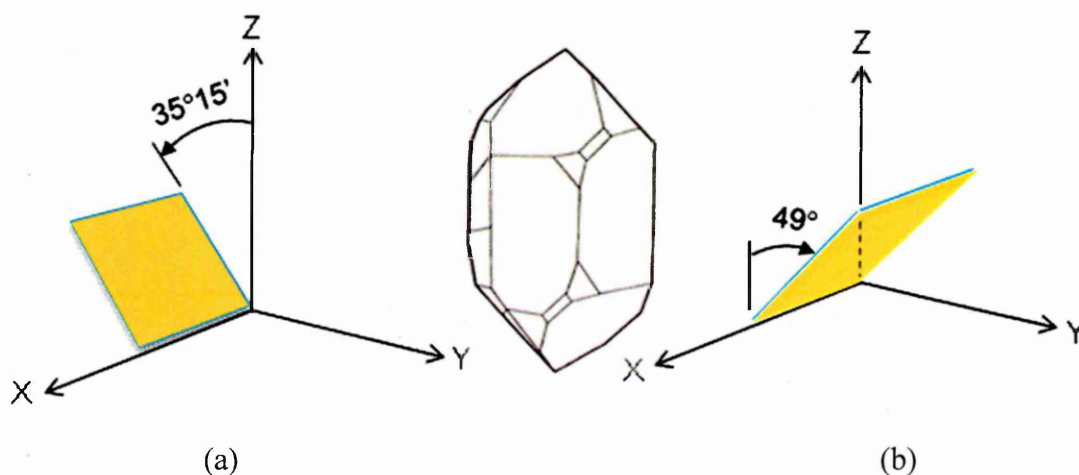


**Fig. 4.2.** Cutting angle for quartz crystal (a) AT cut (b) BT cut [155].

The major differences between the AT and BT cuts are in the type of acoustic oscillations, the values of the oscillation frequency values, and stability acoustic characteristics. In BT cut crystals, the mechanical (acoustic) waves propagate perpendicularly to the surface, while lateral vibrations are excited in AT cut crystals. Generally a BT cut crystal is thicker than an AT cut crystal of the same frequency, so a higher frequency can be obtained using BT cut crystals. The stability of mechanical oscillations is much better in AT-cut crystals, since they are practically independent on temperature and they are less affected by the presence of vicous environment (such a liquid).

One of the popular applications of quartz crystal resonators is the quartz crystal microbalance (QCM) which is based on the fact of linear relation of the resonance oscillation frequency of quartz crystal on the added mass, i.e. the mass of material deposited on metal electrodes. AT cut is widely used in quartz crystal microbalance (QCM) transducers, with gold electrodes evaporated on both sides and connected to the wires with clamps, as shown in Fig. 4.3. The term ‘Quartz Crystal Microbalance’ (QCM) is in fact not strictly accurate, as in some situations the ‘QCM’ does not act as a microbalance (if the oscillation frequency is not directly proportional to the added mass). The QCM devices are often called as thickness-shear mode (TSM) resonator, which means the use of AT cut crystal which undergoes lateral oscillations.

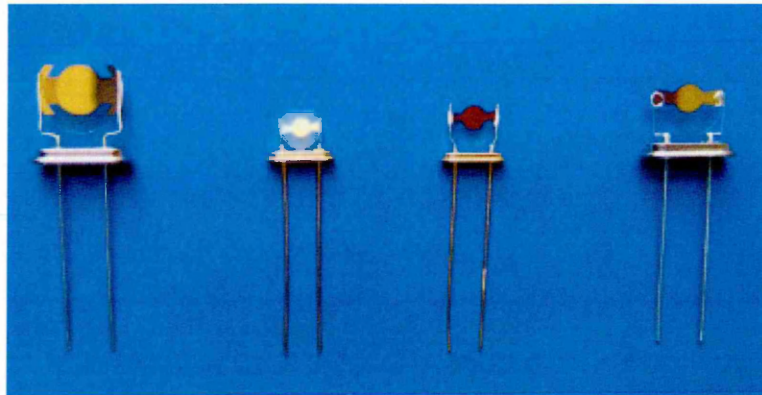


**Fig. 4.3:** The commercially-available quartz crystals

By applying electrical alternating voltage of a certain (e.g. resonance) frequency between the electrodes, a standing shear wave is produced due to the piezoelectric properties of quartz, as shown in Fig. 4.4. The acoustic wave propagates in a direction

perpendicular to the crystal surface [156]. The amplitude is greatest in the centre of the electrode and monotonically decreases with the radius.

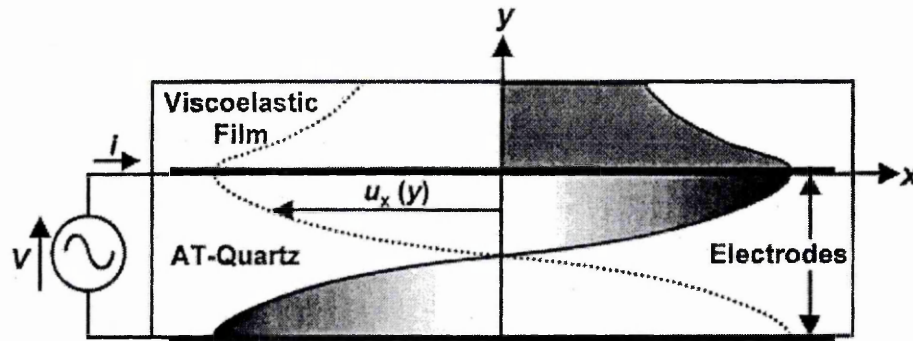


**Fig. 4.4.** The schematic cross-sectional diagram of deformation standing waves in TSM quartz resonator with a viscoelastic film coating the upper surface. [157]

As has been mentioned above, the operational principle of QCM lies in the measurements of a resonance frequency of a quartz crystal which is directly proportional to the added mass. Small changes in the mass due to film deposition at the surface of the resonator cause a reduction in the oscillation frequency.

Let us consider the electro-acoustic resonance in quartz crystals in more detail. The resonance in the crystal occurs when the total phase shift of the standing wave is at an integer of  $2\pi$  for constructive interference to happen. The following equation must apply:

$$h_c = N \frac{\lambda}{2} \quad 4.1$$

Where  $\lambda$  = wavelength and  $h_c$  = crystal thickness.

$$f_N = N \frac{v_c}{2h_c} \quad 4.2$$

Where  $f_N$  = resonance frequency,  $N$  = harmonic number and  $v_c$  = shear wave velocity.

The added mass affects directly the value of shear wave velocity, and eventually leads to so-called Sauerbrey equation [158]:

$$\Delta f = -\frac{2f_0^2}{A\sqrt{\rho_q\mu_q}}\Delta m = -\frac{2.3 \times 10^6 f_0}{A}\Delta m$$

4.3

where  $\Delta f$  is the changes of frequency,  $f_0$  is the original resonance frequency of quartz crystal,  $\rho_q = 2.646 \text{ gcm}^{-3}$  and  $\mu_q = 2.947 \times 10^{11} \text{ gcm}^{-1}\text{s}^{-2}$  are the density and shear modulus of the quartz respectively. Meanwhile  $A$  is the coated area of overlapping gold electrodes.

The linear relation of frequency and mass (Sauerbrey equation) is only applicable under two conditions: firstly, the total mass of the adsorbed film should be small as compared to the weight of the crystal, and secondly, the adsorbed film should be rigid and homogeneous.

## 4.2 Crystal Quality Factor

The quantity used to describe mechanical and electrical resonators is the quality factor,  $Q$ , that provides information about the energy dissipation in relation to the energy that is stored in the oscillator.

The behaviour of a quartz crystal resonator (QCR) in liquid diverges essentially from that in a vacuum or in gaseous media. Viscoelastic properties of macromolecular coating materials can also have a strong impact on the vibration behaviour of the crystal and diminish the  $Q$  factor. The dissipation of the acoustic energy due to the liquid contact translates into energy loss in the electrical circuit. The oscillations are therefore significantly damped, and the  $Q$  factor is reduced.

In general,  $Q$  factor of a LCR circuit can be defined as a ratio of reactive (either  $X_L$  or  $X_C$ ) and active ( $R$ ) components of the impedance  $Z = R + j(X_L - X_C)$ :

$$Q = \frac{X_C}{R} = \frac{X_L}{R}$$

4.4

which leads to a more practical formula for Q factor [159]:

$$Q = \frac{f_0}{B} \quad 4.5$$

where  $f_0$  is the oscillation frequency of quartz crystal and  $B$  is the bandwidth of the impedance spectrum measured between the points where the gain falls to  $\frac{1}{\sqrt{2}}$  or 0.707 times its maximum.

For a quartz crystal operating in a liquid environment, the Q factor is given by [160]:

$$Q = \frac{2\pi f_s L_1}{R_1} \quad 4.6$$

where  $f_s$ ,  $L_1$  and  $R_1$  are respectively mechanical frequency, motional inductance and motional resistance in the circuit.

From this equation,  $Q$  is inversely proportional to the motional resistance, which can also be described as energy dissipation factor. Energy dissipation is greater in liquid than in air. This is because liquids have higher density and are more viscous than air leading to a greater transfer of the acoustic energy from the crystal to the surrounding medium. This problem is unavoidable in biosensing applications. The other (more technical) problem is preventing electrical short-circuiting between the electrodes deposited on the opposite sides of a crystal surface which needs some form of sealant. Any other constraints imposed on the free and uniform mechanical oscillation of the crystal leads to further dissipation and lowering of the Q factor.

### 4.3 QCM operates in liquid

Since the quartz crystal resonator was first shown to be able to oscillate in liquid [161], the use of a TSM resonator in liquid phase has been exploited in a number of biosensing applications [162-164]. The operation of QCM can also be done when only one face of the quartz crystal is in contact with the liquid. The purpose of using one side of the

crystal is to remove the influences of dielectric constant and the conductivity of a liquid and also to reduce the liquid damping in order to attain a stable oscillation. QCM operating in liquids presents a challenge because several phenomena occur simultaneously. The effect of added mass on the frequency is the same as in the gas phase; however, the presence of a liquid causes substantial dumping of oscillations distorting the shape (the amplitude and half-width) of the resonance peak. As a result, the oscillation frequency becomes dependent not only on the added mass but also on the viscoelastic properties of the liquid, and the Sauerbrey equation is not valid.

#### 4.3.1 Viscoelastic effect

An important consideration in biosensing applications is the viscoelastic film deposited on the resonator surface. In bio-sensing applications, many coating materials (especially those made of soft materials such as polymers, organic films and proteins) do not act as a thin rigid layer. They exhibit viscoelastic characteristics which may cause significant differences in the sensor response as compared to a rigid mass layer. When this material is subjected to sinusoidal deformation, the characteristics of viscoelastic material can be expressed by the complex shear modulus [165]:

$$G = G' + jG'' \quad 4.7$$

Where the real part ( $G'$ ) is the stress component in phase with the strain which leads to energy storage. The imaginary component ( $G''$ ) is the stress component which is  $90^\circ$  out of phase. When resonance occurs, the part of the coating materials in contact with the crystal surface oscillates synchronously but the outer section of the layer may lag behind and produce a phase shift, ( $\phi$ ) between them. In this condition the sensor response depends strongly on the material's properties.

The resultant frequency shift caused by viscoelastic coating materials invalidates deposited mass calculation. This extra perceived frequency shift leads to an over-estimation of the mass accumulation unless viscoelastic contributions are taken into consideration. The viscoelastic materials also cause an increase in the resistance created by the introduction of loss moduli  $G''$  [154].

### 4.3.2 Special Sauerbrey equation in liquid medium

When the crystal operates in liquid, the relation of  $f$  and  $\Delta m$  is no longer linear and correction of Sauerbrey is needed. The frequency will change drastically once the crystal surface is brought into contact with the liquid. A shear motion on the surface generates motion in the liquid near the interface. The oscillation surface generates a plane laminar flow in the liquid which causes a decrease in the frequency proportional to  $(\rho\eta)^{1/2}$ . The relation is given by [155]:

$$\Delta f = f_0^{3/2} \left( \frac{\rho\eta}{\pi\rho_q\eta_q} \right)^{1/2} \quad 4.8$$

where  $f_0$  = fundamental frequency of unloaded crystal,  $\rho$  = liquid density,  $\eta$  = liquid viscosity,  $\rho_q$  = crystal density,  $\eta_q$  = crystal viscosity.

### 4.3.3 Impedance Analysis

There are four measuring principles of QCM in liquid: Active Oscillator-based measurement, impedance analysis, reference crystal method and QCM-D (dissipation) [159]. For impedance analysis in particular, a spectrum analyzer with a frequency generator is used to excite the crystal oscillation near resonance while monitoring the complex electrical impedance and admittance upon the applied frequency. By fitting the recorded spectrum to an equivalent circuit model, both mass load and energy dissipation can be distinguished. More information about acoustic conditions at the quartz surface can be obtained from the measurements of the electrical admittance or impedance spectrum of the quartz crystal near its resonance frequency [166].

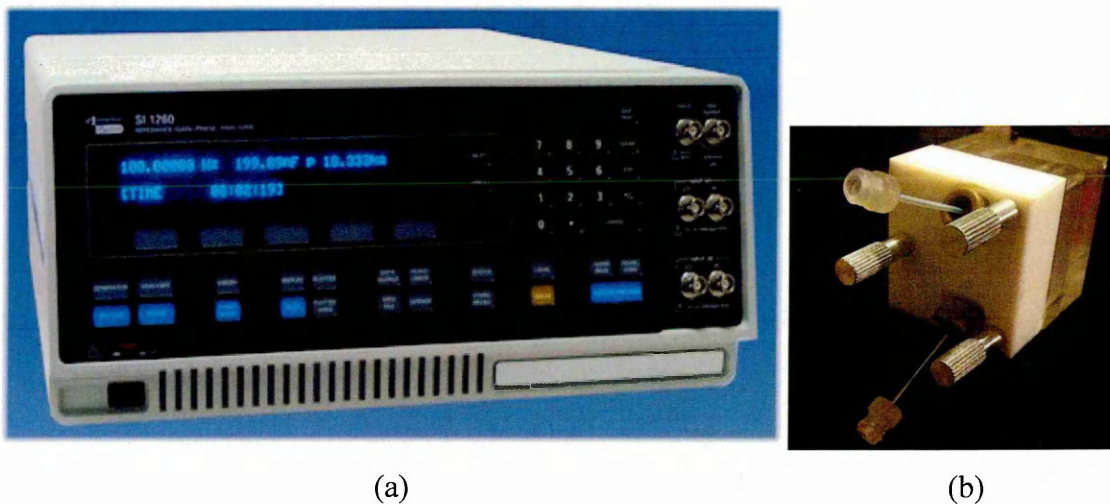


**Fig. 4.5.** Solartron Impedance Analyzer and liquid cell

A spectrum analyzer with an internal frequency generator can be used to stimulate the quartz and monitor the complex electrical impedance which is a reciprocal of electrical admittance parameter depending on the applied frequency. In this work, a Solartron Impedance analyzer was utilized for impedance measurement of quartz crystals operating in liquid (Fig. 4.5 (a)). In order to operate crystals in liquid, a special cell of 100  $\mu\text{l}$  in volume was designed and fabricated as shown in Fig.4.5 (b). An AT-cut quartz crystal chip (QCMA) from Sierra Sensors Ltd. (Germany) with a fundamental frequency of 19.5 MHz was used. SMaRT software V-3.0.1 allowed the recording of impedance (or admittance) spectra in a selected frequency range, and further data analysis for the purpose of *in-situ* monitoring of the kinetics of biochemical reactions. The information such frequency, impedance and admittance magnitudes and phases, and capacitance can be retrieved through using this software.

#### **4.3.4 Butterworth van dyke (BVD) equivalent circuit model**

An equivalent circuit model that can accurately distinguish between electrical and mechanical properties of the resonator was first introduced by the three ports Mason model [167]. The general one-dimensional model that has been suggested is to provide a basis for the theoretical description of complex composite resonators as they apply in bio-sensing applications. In this particular case, the Mason model can easily be

transformed near resonance into an equivalent circuit with lump elements, called a Butterworth Van Dyke (BVD) circuit.

A BVD model (Fig. 4.6) consists of four parameters; resistance (R), inductance (L), serial capacitance (C<sub>s</sub>) and parallel capacitance (C<sub>p</sub>). Resistance (R) represents energy loss arising from the effect of a viscous medium, initial friction, and damping. Inductance (L) is the initial mass/motional inertia of the system. 'C' is the mechanical elasticity of the quartz, while C<sub>p</sub> consists of the capacitance of the quartz between electrodes and the parasitic capacitance of the crystal fixture. The parallel capacitance C<sub>p</sub> dominates the admittance spectra away from the quartz resonance.

$$C_p = \epsilon_q \frac{A}{h_q} \quad 4.9$$

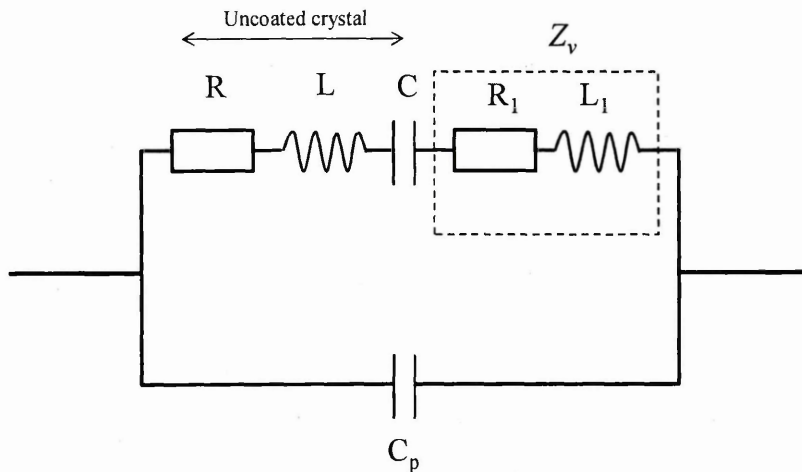


**Fig.4.6.** BVD equivalent circuit model of TSM resonator with additional impedance, Z<sub>v</sub> representing viscoelastic loading [111].

A BVD circuit can be used to model an unloaded crystal. From the circuit, admittance ( $Y$ ) value can be determined.

$$Y(\omega) = j\omega C_p + \frac{1}{z_m} \quad 4.10$$

Where  $z_m(\omega) = R + j\omega L + \frac{1}{j\omega L}$

When  $R \rightarrow 0$ , two resonance frequencies appear: serial resonance frequency,  $f_s$  where the motional reactance is zero; and parallel resonance frequency,  $f_p$  where the total reactance is zero. This corresponds to the minimum and maximum admittance which can be defined as:

$$f_s = \frac{1}{2\pi\sqrt{LC}} \quad 4.11$$

$$f_p = \frac{1}{2\pi} \sqrt{\left[ \frac{1}{L} \left( \frac{1}{C} + \frac{1}{C_p} \right) \right]} \quad 4.12$$

The deposition of a viscoelastic film onto a crystal surface can be described by the additional elements  $R_1$  and  $L_1$ , which measure of energy dissipation in the film and mass loading, respectively [111] in the BVD circuit.

The admittance spectra  $Y(\omega)$ , generated from the BVD model can be expressed by [157], [168];

$$Y(\omega) = G + jB = \frac{1}{Z_m + Z_v} + j\omega C_p \quad 4.13$$

$$Z_m(\omega) = R + j\omega L + \frac{1}{j\omega C} \quad 4.14$$

$$Z_v = R_1 + j\omega L_1 \quad 4.15$$

Where  $\omega = 2\pi f$

QCM impedance analysis was used in this work as a complementary method to study the immune reactions between DE2 antibodies and APP770. The analysis of the obtained results was rather qualitative without using BVD fitting.

#### 4.4 QCM in Microfluidic flow



**Fig. 4.7.** QCMA-1 Microfluidics, Sierra Sensors instrument

Another QCM-based technique used in this work is the measurements of the oscillation frequency of two quartz crystals (one of them used as reference) in conjunction with a microfluidic system.

A fully-automated QCM microfluidics instrument, QCMA-1, which includes a QCM sensor chip from Sierra Sensors GmbH is shown (Fig. 4.7). This instrument is able to process dozens of samples in a single unattended run. Sample analysis can either be fully automated, or the injections can be run on demand using scripted testing procedures. Real time molecular interaction can be monitored in terms of changes of the oscillation frequency of the QCM in the main channel in respect to the reference oscillator. In this instrument, the frequency response was inverted in order to produce the effect of added mass due to molecular adsorption.

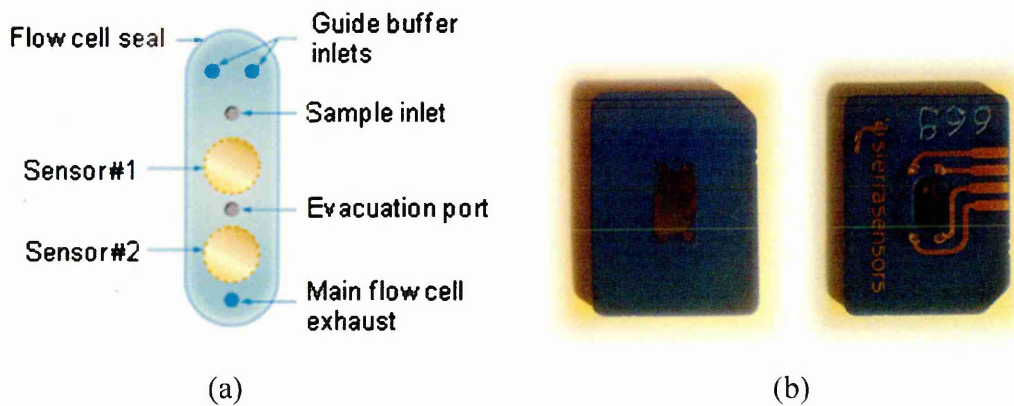


**Fig. 4.8.** QCMA-1 sensor chip (a) the structure of QCMA-1 sensor chip (b) real fabrication of QCMA-1 sensor chip.

The QCMA-1 chip combines two sensing spots on the same AT-cut quartz crystal with a fundamental frequency 19.5 MH, enabling *in-situ* monitoring of both sensing channels simultaneously. Fig. 4.8 (a) shows the structure of the QCMA-1 sensor chip, which comprises two sensing spots, and all the inlets and outlets for tested analyte and buffer. The fabrication of QCMA-1 sensor chips with electrical connection as shown in Fig. 4.8 (b) makes the crystal easy to handle.

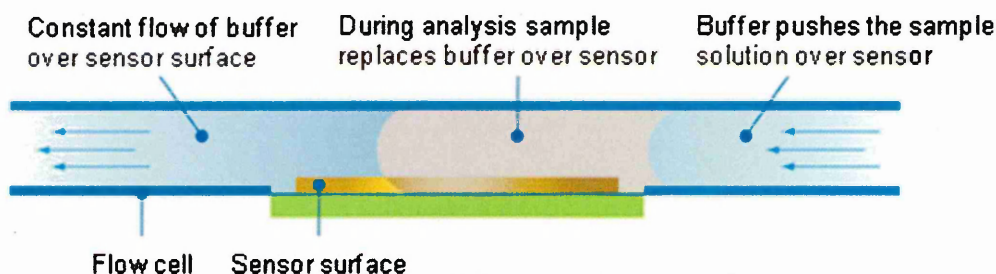


**Fig. 4.9.** QCMA-1 sample delivery [169]

The Sierra sensor has a unique microfluidic sample delivery system called hydrodynamic isolation, as illustrated in Fig. 4.9. It can deliver highly discrete microlitre volumes of a sample within a continuous flow of liquid to any sensing location. Microfluidic pumps and automated valves precisely control the delivery of all samples, buffers and reagent solutions to the sensor surface.

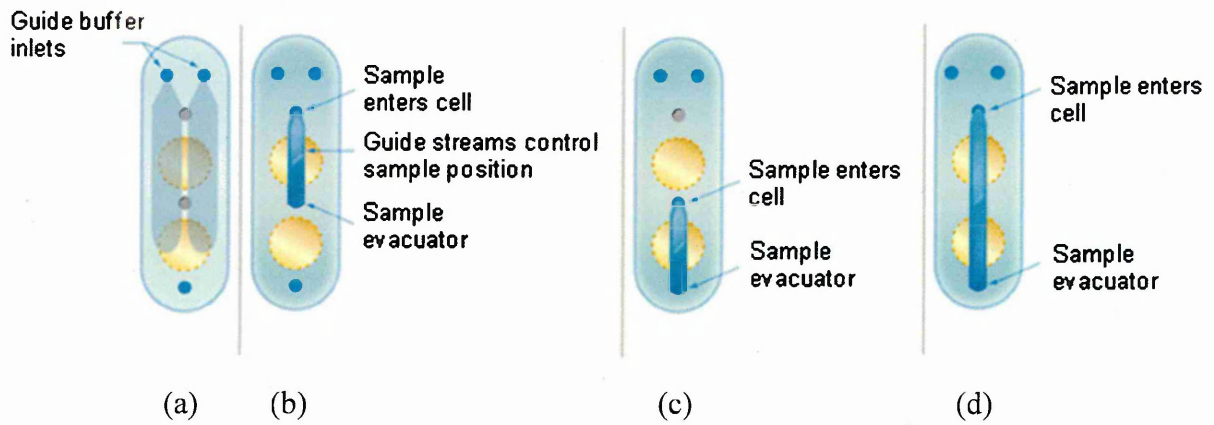


**Fig. 4.10.** Sample addressing in a two-sensor spot flow cell: (a) buffer streams in flow cell; (b) sample addressing to sensor spot #1; (c) sample addressing to sensor spot #2; (d) sample addressing to both sensors [169].

Fig. 4.10 shows the sample delivery system in a QCMA-1 sensing chip. Stage (a) shows a buffer stream filling the whole cell through the guide buffer inlets; stages (b) and (c) show the sample addressing sensor spot No. 1 and sensor spot No. 2 respectively through different evacuation channels, while stage (d) shows the sample addressing both sensing spots simultaneously in order to reduce overall assay time.

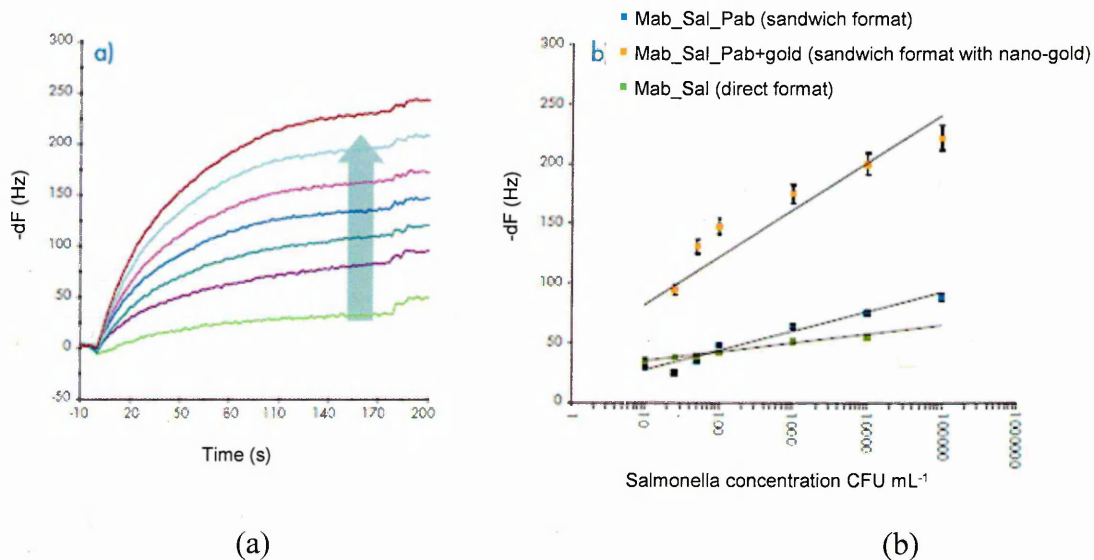


**Fig. 4.11.** (a) The changes of frequencies due to the binding of a salmonella cell on immobilized antibodies at a QCMA-1 sensor chip surface (b) Comparison of different assay formats using a QCMA-1 sensor chip [170].

This method has been successfully utilized for the detection of salmonella bacteria using direct and sandwich assay [170]. Fig. 4.11 (a) shows the higher frequency response ( $-\Delta f$ ) for a larger number of salmonella cells in the sample. The comparison of different immunoassay formats, i.e. direct, sandwich and nanogold-conjugated sandwich assay, using the above method, is shown in Fig. 4.11 (b).

#### 4.5 Atomic Force Microscope (AFM)

Atomic Force Microscopy (AFM) is a microscopy technique that can quantify surface morphology down to atomic resolution. It works by measuring the deflection of the cantilever during its scanning across the surface of a material. An AFM provides much more topographical information as compared to optical microscopy and scanning electron microscopy (SEM). The advantage of an AFM over the other scanning nano-probe techniques (STM, SNOM) is that it can be used for imaging almost any type of surface, including polymers, ceramics, composites, glass, and biological samples [171]. An AFM is capable of detecting the changes in the thin film morphology caused by biochemical reactions which can be used as a complementary bioanalytical method.

The operating principle of an AFM lies in the detection of an interactive force between the sample and the tip. The main part of an AFM is a microscale cantilever with a sharp tip (probe) at its end that is used to scan the sample surface. When the tip is brought into contact with the sample surface, forces between the tip and the sample lead to a deflection of the cantilever according to Hooke's law

$$F = kx \quad 4.14$$

where  $F$  is the force,  $k$  is the stiffness of the cantilever and  $x$  is the deflection distance of the lever. Typically, the deflection is measured using a laser beam reflected from the top surface of the cantilever into an array of photodiodes, as shown in Fig. 4.12.

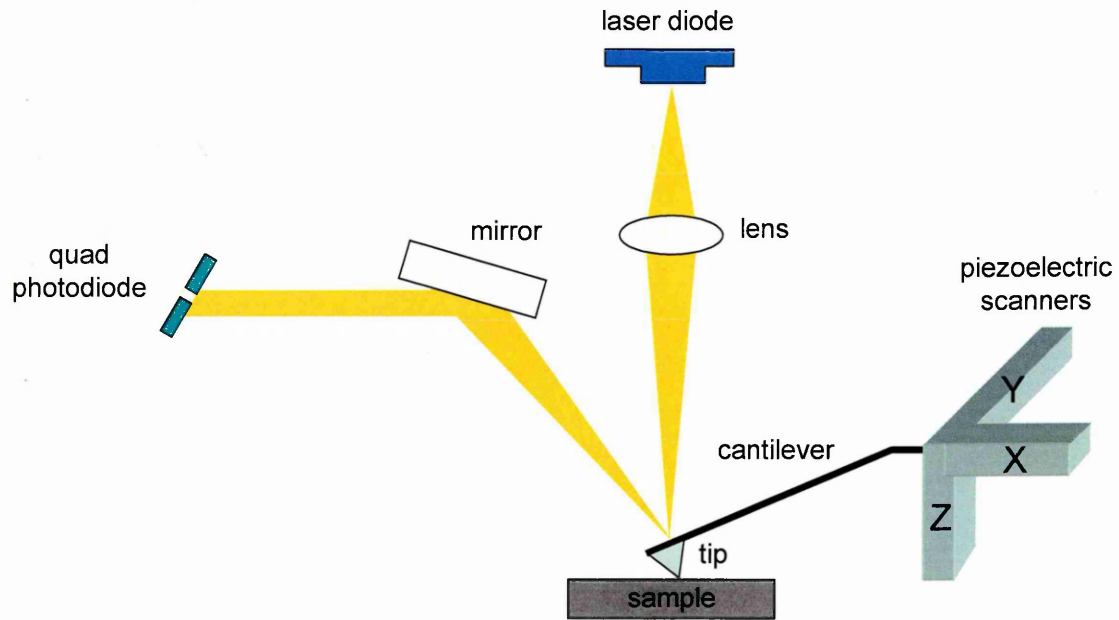


**Fig. 4.12:** Schematic diagram of Atomic Force Microscope

An AFM can be operated in a number of modes, depending on the application. Normally it is used in contact or tapping modes. In contact mode, the probe scans across the surface, keeping a constant force between tip and sample, maintained by a feedback control. The amount of movement required to keep the constant force is then used to create an image of the surface. In tapping mode, the cantilever vibrates, and both the amplitude and phase of oscillations can be affected when the tip approaches the surface so that surface profile data can be obtained from changes in the oscillation amplitude. Changes in the oscillation phase can provide additional information of viscoelastic properties of the sample. AFM cantilevers are microfabricated from silicon using standard microelectronics technology and the tips are made of either silicon or silicon nitride. Typical tip radius ranges from a single nanometer to tens of nanometers.

The force measured in an AFM is an inter-atomic (Van der Waals) force. The dependence of Van der Waals force on the cantilever deflection is shown in Fig. 4.13. In the contact region, the cantilever is held less than a few Angstroms from the sample surface and inter-atomic force between the cantilever and the sample is repulsive. In the non-contact region, the cantilever is far away (tens to hundreds of angstroms) from the

sample surface and the inter-atomic force between the cantilever and sample is attractive.

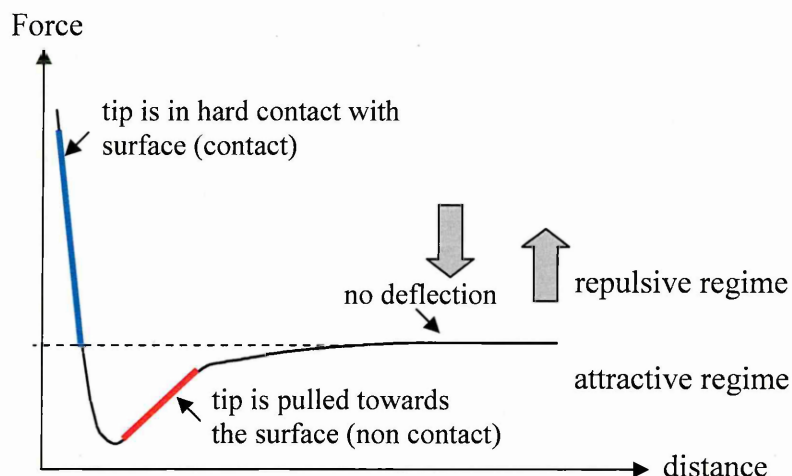


**Fig. 4.13:** Van der Waals force versus distance between tip and surface.

The minimum in Fig. 4.13 corresponds to the equilibrium between repulsive and attractive forces. In contact mode, an AFM operates in the repulsive force range, while in tapping mode the range of deflection is much wider around the minimum. The commercially available AFM Nanoscope IIIa apparatus from Digital Instruments Inc. was used in this research. It comes with software capable of presenting images in different forms such as line scans, 2D, and pseudo-3D images, and performs statistical analysis of images including roughness and particle analysis.

#### **4.4.1 Contact Mode**

This mode is widely used. As the tip is raster-scanned across the surface, it is deflected as it moves over the surface corrugation. In a constant force mode, the tip is constantly adjusted to maintain a constant deflection, and therefore a constant height above the surface. Because the tip is in close contact with the surface, the stiffness of the lever needs to be less than the effective spring constant holding atoms together, which is in the order of 1 - 10 nN/nm. Most contact mode levers have a spring constant of  $< 1\text{N/m}$ . The advantages of contact mode are a faster scan process and the possibility of scanning rough samples with extreme changes in vertical surface morphology. However, this

regime can be damaging to the sample, which is particularly important for soft materials such as organic films, polymers and bio-samples.

#### **4.4.2 Tapping Mode**

This mode is also referred to as intermittent-contact or by the more general term Dynamic Force Mode (DFM) [172]. A stiff cantilever is oscillated closer to the sample than in non-contact mode. Part of the oscillation extends into the repulsive regime, so the tip intermittently touches or “taps” the surface. Very stiff cantilevers are typically used, as tips can get “stuck” in the water contamination layer. The advantage of tapping the surface is improved lateral resolution on soft samples. Lateral forces such as drag, common in contact mode, are virtually eliminated. For poorly adsorbed specimens on a substrate surface the advantage is clearly seen.

In tapping mode the cantilever is driven to oscillate up and down at near its resonance frequency by a small piezoelectric element mounted in the AFM tip holder. The amplitude of this oscillation is greater than 10 nm, typically 100 to 200 nm, with the frequency in the range of 200-400 kHz. Due to the interaction of forces acting on the cantilever when the tip comes close to the surface, Van der Waals or dipole-dipole interaction causes the amplitude of this oscillation to decrease as the tip gets closer to the sample.

#### **4.6 Scanning Electron Microscopy (SEM)**

The scheme of SEM operation is shown in Fig. 4.14 which consists of an electron gun as an electron source, two condenser lenses, an objective lens attached with scanning coils which deflect the beam in x and y axes, detectors for backscattered and secondary electrons, and the specimen. A SEM operates in a vacuum with a high energy electron beam (2 – 25 kV) produced by an electron gun. The beam is focused by two condenser lenses into a nano-meter (0.5 – 5 nm) spot.

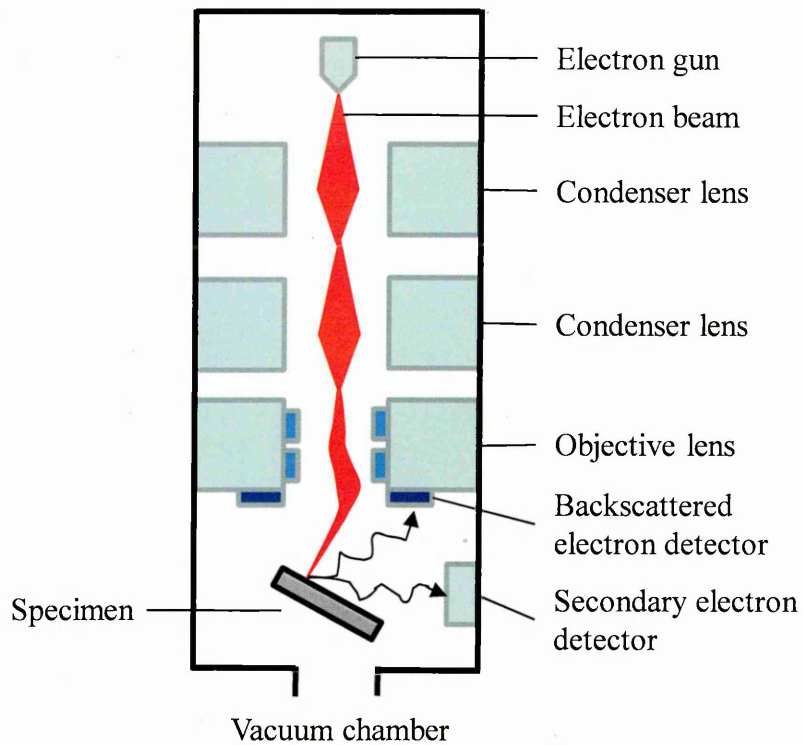


**Fig. 4.14.** The scheme of a scanning electron microscope (SEM), [173]

The reflected electrons from the specimen, backscattered or secondary electrons, are collected by a detector to provide an image of the specimen. In many cases, backscattered electrons reflected from the sample are used in analytical SEM due to the relation of intensity and atomic number ( $z$ ) of materials. The limitation of SEM resolution is caused by beam diameter and image distortion due to the short electron wavelength. Also depth from which backscatter occurs.

#### 4.7 Summary

QCM was used in this work as complementary method to study immune reactions between DE2 antibody and APP770. The analysis of QCCM in air helps to calibrate the unknown concentration of APP770. The results from QCM operate in liquid rather qualitative without further analysis or fitting to BVD circuit. Established AFM and SEM techniques were utilized for morphology analysis on sample surface.

# CHAPTER 5

## THE STUDY OF IMMUNE REACTIONS FOR ALZHEIMER'S DISEASE DIAGNOSTIC

This Chapter is dedicated to the detection of Amyloid Precursor Protein (APP770) and Amyloid beta peptide ( $A\beta_{1-16}$ ) in the direct immune assay with monoclonal DE2 antibodies raised against  $A\beta_{1-16}$ .  $A\beta_{1-16}$  is a small 16 amino acids fragment of much larger APP consisting of 770 amino acids. The detection of APP 770 gives additional challenges of unknown concentration of APP and high possibility of unspecific binding of other proteins present in complete medium solution of APP. In order to calculate the original concentration of APP, a complementary method of QCM was exploited. Three types of QCM techniques have been explored; QCM in air, QCM in microfluidic and QCM impedance analysis. Later the TIRE method was also employed for the detection of  $A\beta_{1-16}$  using the same DE2 antibody. Although an actual biomarker for AD is  $A\beta_{1-42}$ , the detection of small molecule of  $A\beta_{1-16}$  shows great prospects of detection of larger  $A\beta$  fragments in biological fluids. Furthermore the evaluation of the affinity constant for  $A\beta_{1-16}$  to DE2 antibody has been carried out by TIRE kinetic measurements. The morphology of sensing surface after binding of APP and  $A\beta_{1-16}$  was analyzed using Atomic Force Microscope (AFM).

### 5.1 Sample preparation

Cr/Au coated glass slides for TIRE measurements were prepared by consecutive thermal evaporation of chromium ( $3\pm 1$  nm) and gold ( $25\pm 3$  nm) layers onto standard microscopic glass slides without breaking the vacuum of about  $10^{-6}$  Torr, using the

Edwards E306A evaporation unit. The presence of thin Cr layer improves the adhesion of Au layer to glass. Prior immobilisation of antibodies, the surface of gold was modified with the layer of mercaptoethyl sodium sulfonate to enhance the negative surface charge on sensing surface [174].

The method of electrostatic layer-by-layer deposition [175,176] was used for immobilisation of proteins on the surface. DE2 antibodies were electrostatically attached to the surface via the polycationic layer of poly(allylamine hydrochloride) (PAH, 2 mg/ml). An intermediate layer of Protein G (0.02 mg/ml) molecules at pH 7.5 (charge = -2.2) having a binding site to the second domain of IgG was used to orient DE2 with their Fab-fragments towards the solution; such procedure improves the sensitivity in about 3 times as compared to randomly adsorbed antibodies [177].

Tris-HCl buffer pH 7.5 was used for rinsing the cell after molecular binding as well as for dilution of A $\beta$ <sub>1-16</sub> while complete medium (CM) solution was used for dilution of APP. Similar treatment was used to modify the surface of gold electrodes of quartz resonators.

## **5.2 Detection of Amyloid Precursor Protein (APP<sub>770</sub>) by Total Internal Reflection Ellipsometry (TIRE) method.**

The immunoreaction of APP<sub>770</sub> with monoclonal DE antibodies was detected using TIRE method. The unknown stock concentration of APP was diluted up to 16 times using complete medium. Figures 5.1 and 5.2 show, respectively, typical set of TIRE  $\psi$  ( $\lambda$ ) and  $\Delta$ ( $\lambda$ ) spectra recorded in a standard Tris-HCl buffer solution (pH 7.5) on bare gold surface and after completing every adsorption (binding) steps in the following sequence: PAH, Protein G, DE2 antibodies, APP<sub>770</sub> in different concentrations starting from 1:16 diluted stock solution of APP.

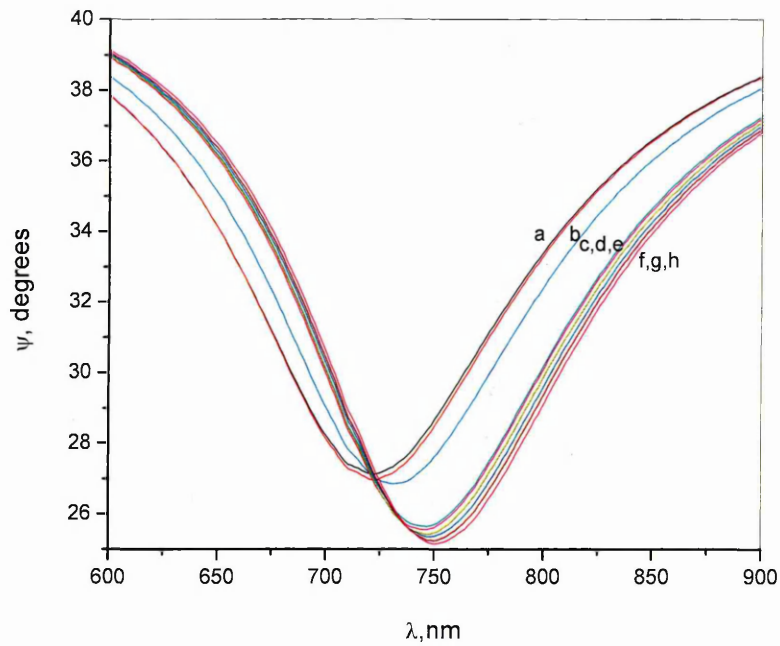


**Fig. 5.1.** A set of TIRE  $\psi(\lambda)$  spectra measured on bare gold surface (a) and after adsorption of PAH (b), Protein G (c), antibodies DE2 (d), and after binding APP770 of different dilution: 1:16 (d), 1:8 (e), 1:4 (f); 1:2 (g); 1:1 (h).

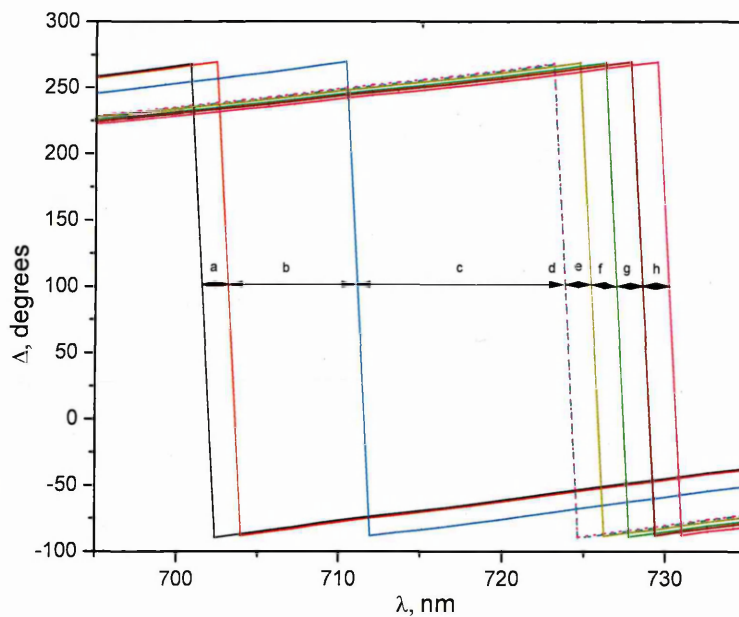


**Fig. 5.2.** A set of TIRE  $\Delta(\lambda)$  spectra measured on bare gold surface (a) and after adsorption of PAH (b), Protein G (c), antibodies DE2 (d), and after binding APP770 of different dilution: 1:16 (d), 1:8 (e), 1:4 (f); 1:2 (g); stock APP concentration (h).

As one can see,  $\psi(\lambda)$  spectra in Fig. 5.1 shows very small shift; so it is very difficult to distinguish between the curves. In contrast the shift of  $\Delta(\lambda)$  spectra in Fig. 5.2 is much more pronounced. Further analysis will focus on  $\Delta(\lambda)$  spectra since it is more sensitive as compared to  $\psi(\lambda)$  spectra.

**Table 5.1.** The results of TIRE data fitting.

Adsorption stage	$D(\text{nm})$	$\Delta d(\text{nm})$
PAH	0.462	0.462
Protein G	5.211	4.749
DE2	1cv1.887	6.676
APP770 (1:16)	12.115	0.228
APP770 (1:8)	12.684	0.569
APP770 (1:4)	13.550	0.866
APP770 (1:2)	14.546	0.996
APP770 (1:1)	15.362	0.816

Parameters of the adsorbed layers such as thickness ( $d$ ) and refractive index ( $n$ ) can be evaluated by fitting TIRE spectra to the model system using the J.A. Woollam software [131]. During the fitting, the parameters of  $n$  and  $k$  were fixed (as discussed in Chapter 3). This is not strictly correct, but it is close to the real situation where the refractive index ( $n$ ) for all organic layers studied was closed to 1.42 (at 633 nm). A four-layer upside down model for TIRE measurements, which has been described in Chapter 3 was used. Table 5.1 shows the values of thickness and thickness increment for every stage of adsorption.

It is clear that the thickness increment ( $\Delta d$ ) increases from 0.462 nm for the smallest PAH molecules (molecular weight for repeated unit is 93.5, molecular weight of the polymer MW=70,000), to 4.749 nm for larger Protein G (MW=25,000), and up to 6.676 nm for much larger DE2 molecules (MW=120,000). Decreasing the concentration of APP770 leads to a smaller response (e.g. thickness increment), which has practically disappeared for 1:16 diluted APP770. The latter fact means that concentration of APP770 in the stock solution was rather small. Control TIRE measurements were carried out by adsorbing pure complete medium (CM) solution (e.g. not containing

APP770) on top of immobilised DE2 antibodies. No noticeable spectral shift was detected in this test as shown in Fig. 5.3. Further control test has been done to ensure the specificity of DE2 antibody using 400 ng/ml Aflatoxin as an antigen.

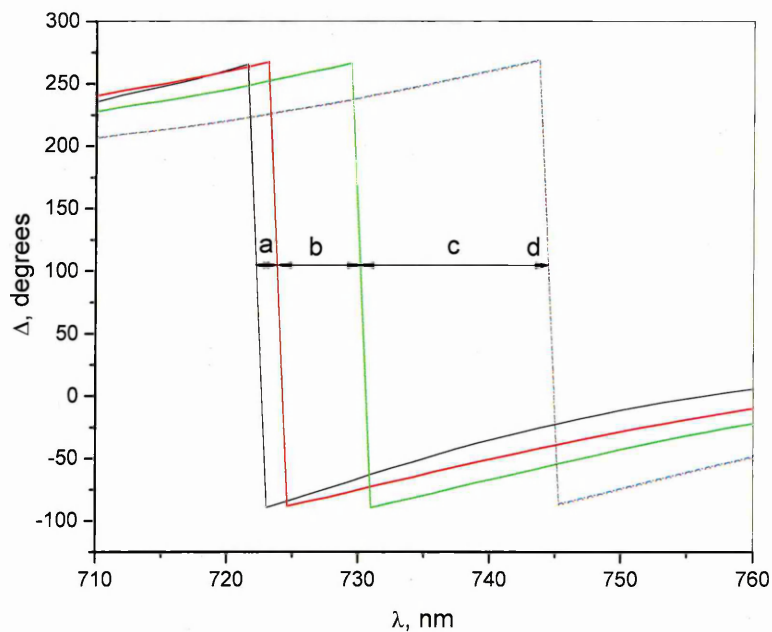


**Fig. 5.3.** A set of TIRE  $\Delta(\lambda)$  spectra measured on bare gold surface (a), after adsorption of PAH (b), Protein G (c), antibodies DE2 and (d) complete medium (CM).

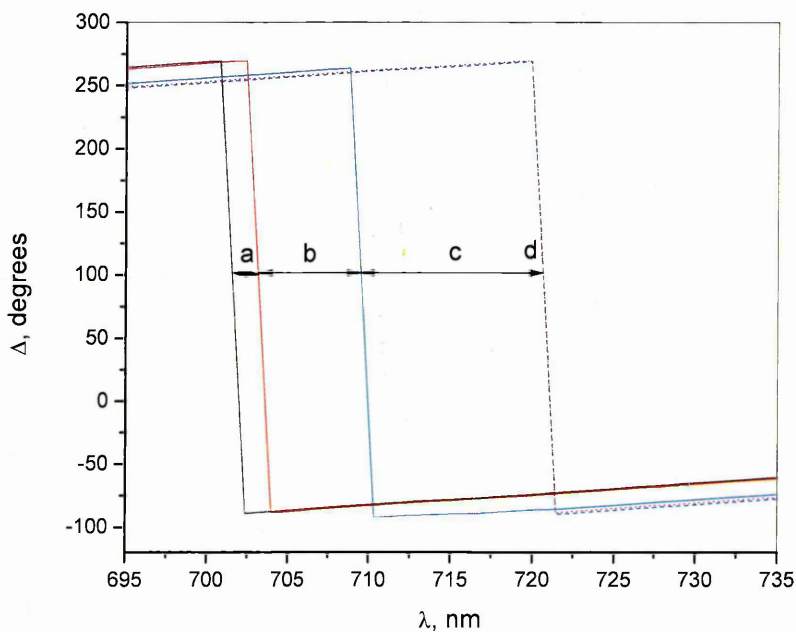


**Fig. 5.4.** A set of TIRE  $\Delta(\lambda)$  spectra measured on bare gold surface (a), after adsorption of PAH (b), Protein G (c), antibodies DE2 and (d) 400ng/ml AFT.

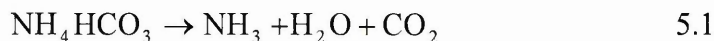
The result in Fig. 5.4 shows coinciding  $\Delta$  spectra indicating that no binding occurred between DE2 antibody and Aflatoxins. In fact the layer thickness gathered from TIRE fitting become smaller after injection of Aflatoxins. The decrease of absorbed layer is probably due to toxicity of Aflatoxins causing partial desorption of biomolecules.

The calibration of the TIRE biosensor was not possible at this stage because the concentration of APP770 in stock solution was not known. For the same reason TIRE dynamic spectral measurements could not be used for the evaluation of the association and affinity constants for immune reaction between DE2 and APP770. Therefore Quartz Crystal Microbalance (QCM) measurements were performed to solve the above problems.

### **5.3 Calibration of unknown concentration of APP using Quartz Crystal Microbalance (QCM) dry technique.**

Complementary measurements of the oscillation frequency were performed on dry quartz crystals coated sequentially with PAH, protein A, DE2, and APP770 (from stock solution) in order to evaluate the added mass due to molecular adsorption. Quartz crystals having fundamental frequency of 10 MHz were purchased from EuroQuartz UK. This method relies on the changes of resonance frequency caused by absorbed mass on the crystal surface. Batches of ten quartz crystals were immersed in the solution consecutively in a reaction well array specially designed for this technique (see Fig.5.5 (a)). At first, frequency was recorded on bare crystals before they were immersed consecutively in solution of PAH, Protein G, DE2 antibodies and APP. Twenty minutes of incubation time was allowed for the binding of each compound to reach the plateau. Fig. 5.5 (b) shows the front view of the crystal when it was hung up in the well during the absorption process. After completion of absorption, the crystals were rinsed thoroughly with ammonium bicarbonate buffer at pH 7.0 and last with deionized water to wash out non-bound molecules on the surface. Ammonium bicarbonate buffer was selected because of the volatility of the end product to avoid salt deposition on the crystal surface and thus extra added mass. Ammonium bicarbonate liberates protonated amine, water and carbon dioxide when exposed to nitrogen gas and the solution become alkaline, in the reaction as shown by chemical equation 5.1. Drying of quartz crystal

was carried out in a steady flow of nitrogen gas parallel to the crystal plane as shown in Fig. 5.5 (c) before it was connected to the oscillator circuit for frequency measurements. The drying process was carried out in a steady nitrogen flow over the crystal surface to dry off any water trapped on the surface. The frequency measurements were performed at room temperature throughout the experiment.



After drying, the quartz crystals were connected to the oscillation circuit for frequency recording. The mass absorbed on the crystal surface slows down crystal oscillation thus reducing the resonance frequency as described by Sauerbrey equation on Chapter 4. Typical variations of the resonance frequency of quartz crystals at different stages of adsorption are shown in Fig. 5.6. As one can see the variation of frequency after each absorption is proportional to the size of the molecules. For example, deposition of DE2 antibody, which is the largest molecule, shows a steep of frequency drop.

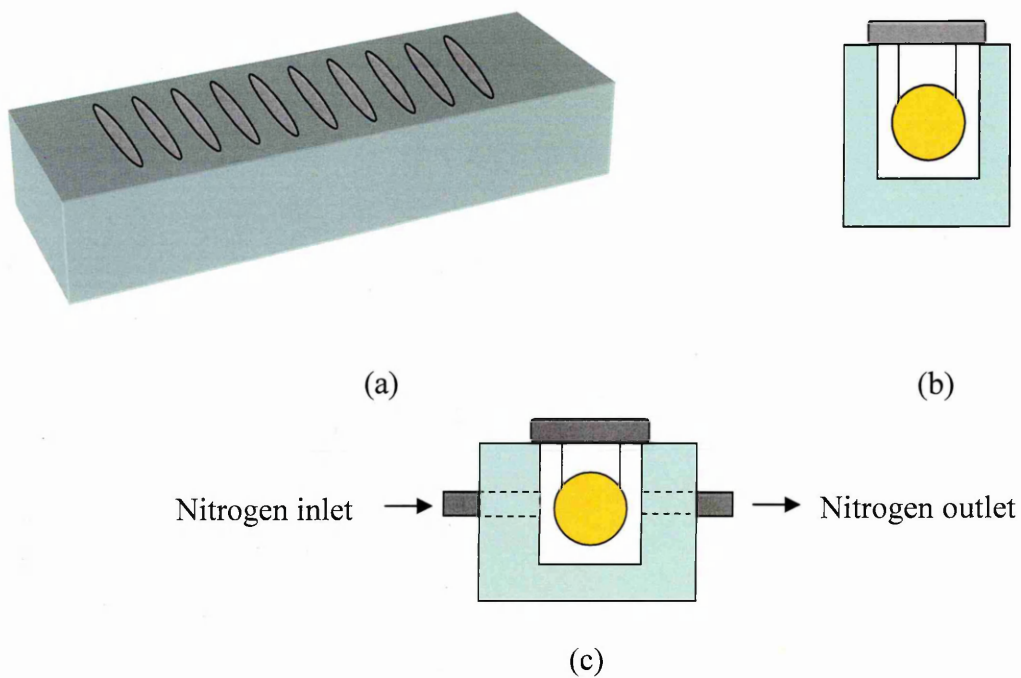


**Fig 5.5.** (a) Ten well array for QCM dry technique (b) front view of the well (c) Cell for drying process.

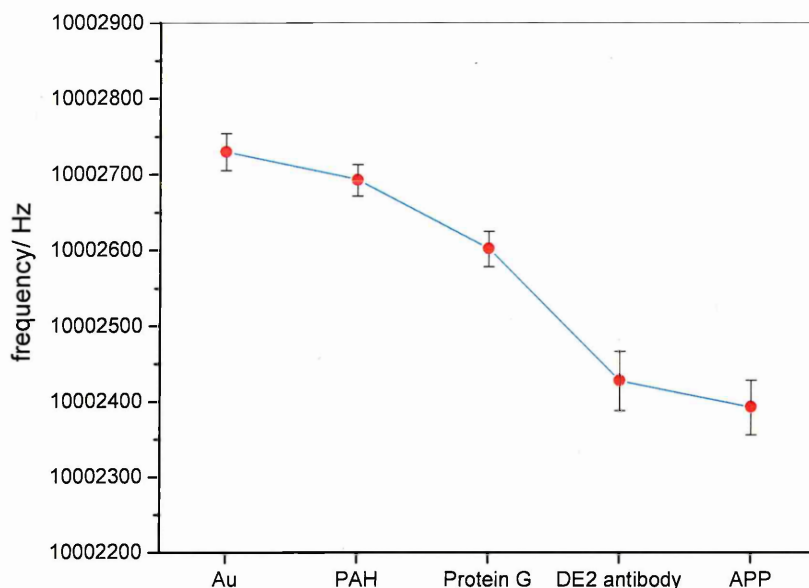


**Fig. 5.6.** Resonance frequency of quartz crystals after different stages of adsorption

**Table 5.2.** QCM data on the sequential adsorption of PAH, Protein G, DE2, and APP770

Layer	Added mass $\Delta m (\times 10^{-7} \text{ g/cm}^2)$	Molar concentration $C (\times 10^{-12} \text{ M})$
PAH	$1.8229 \pm 1.4488$	$2.4349 \pm 1.3349$
Protein G	$3.2578 \pm 0.8950$	$13.7823 \pm 2.9740$
DE2	$7.4337 \pm 2.4371$	$4.73 \pm 0.86$
APP770	$1.0026 \pm 0.7544$	$0.18 \pm 0.03$

From the frequency measurements, the values of added mass  $\Delta m (\text{g/cm}^2)$  were calculated using Sauerbrey equation (the procedure was explained in detail in Chapter 4). The obtained mass values as well as molar concentration of adsorbed molecules ( $C = \Delta m / MW$ ) are given in Table 5.2. As can be seen from the table the standard deviation for PAH is about 70% which is quite high. The absorption of PAH on the crystal surface was not consistent most likely due to poor electrostatic deposition of molecules onto gold surface, which was not treated for enhancing negative surface

charge. An example of the calculation of mass absorbed per surface area using Sauerbrey equation for PAH is given below:

$$\begin{aligned}\Delta m(g/cm^2) &= \frac{\Delta f}{2.26 \times 10^{-6} f_o^2} A \\ &= \frac{(10002716 - 10002675)}{2.26 \times 10^{-6} (10002716)^2} \\ &= \frac{41}{2.26 \times 10^8} = 1.81 \times 10^{-7} gcm^{-2}\end{aligned}$$

Concentration of absorbed PAH molecules is therefore equal to:

$$\begin{aligned}C &= \frac{\Delta m}{Mw} \\ &= \frac{1.81 \times 10^{-7}}{70000} = 2.59 \times 10^{-12} M\end{aligned}$$

All the values of deposited mass per surface area for PAH, Protein G, DE2 antibody and APP were calculated in a similar way and shown in Table 5.2.

The surface concentrations of DE2 antibodies ( $N$ ) and adsorbed APP770 molecules ( $n$ ) can be found by multiplying the concentration,  $C$  to Avogadro's number:

$$\begin{aligned}N &= 4.73 \times 6 \cdot 10^{23} = (2.84 \pm 0.86) \times 10^{12} cm^2 \\ n &= 0.18 \cdot 10^{-12} \times 6 \cdot 10^{23} = (1.08 \pm 0.03) \times 10^{11} cm^2\end{aligned}$$

In general, molecular adsorption is described by a following differential equation [68]:

$$\frac{dn}{dt} = k_a(N - n)C - k_d n \quad 5.2$$

where  $n$  and  $N$  are the concentrations of adsorbed molecules and binding sites, respectively,  $C$  is the concentration of analyte molecules,  $k_a$  and  $k_d$  are rates for adsorption and de-sorption, respectively. The solution of the above is given as [68]:

$$n = N \frac{k_a C}{k_a C + k_d} \left[ 1 - e^{-(k_a C + k_d)t} \right]$$

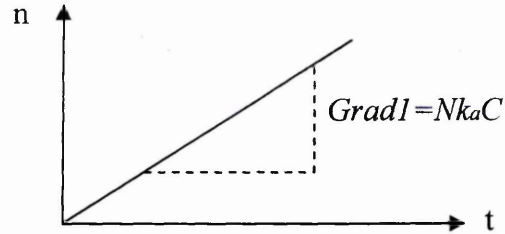
5.3

From this equation, two cases can be considered:

**(i). At small  $t$ , beginning of adsorption process**

$$1 - e^{-x} \approx x \text{ when } x \rightarrow 0,$$

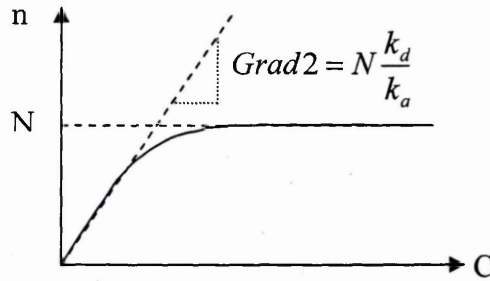
$$\text{So, } n \approx N \frac{k_a C (k_a C + k_d) t}{k_a C + k_d} = N k_a C t$$



**(ii). At large  $t$ , end of adsorption process or saturation**

$$1 - e^{-x} \approx 1, \text{ when } x \rightarrow \infty$$

$$\text{So, } n = N \frac{k_a C}{k_a C + k_d} = \frac{N}{1 + \frac{k_d}{k_a C}}$$



After transformations one can obtain:

$$C = \frac{k_d}{k_a} \frac{n}{N - n}$$

if  $C$  is large,  $C \rightarrow \infty$ ,  $n \rightarrow N$

if  $C$  is small,  $C \rightarrow 0$  when  $n \ll N$

$$C = \frac{k_d}{k_a} \frac{1}{\frac{N}{n} - 1} \approx \frac{k_d}{k_a} \frac{n}{N} \text{ or } n = CN \frac{k_a}{k_d}$$

In this case, assuming that binding process was complete after an incubation time of 15–20 minutes (from TIRE kinetic measurement) where  $t$  value is large;  $1 - e^{-x} \approx 1$ , when  $x \rightarrow \infty$  the maximal concentration of APP is therefore given by:

$$C = \frac{k_d}{k_a} \frac{n}{N - n} \text{ or } = K_D \frac{n}{2N - n} \quad 5.4$$

where  $K_D = k_d / k_a$  is known as the affinity constant. Factor 2 in eq. (5.4) appeared because every antibody has two binding sites. Typically for monoclonal IgG-based antibodies such as DE2 the value of  $K_D$  is in the range of  $10^{-7}$  (mol/l) or even smaller [151]. Therefore, taking the values of  $N = 2.84 \times 10^{12} \text{ cm}^{-2}$  and  $n = 1.08 \times 10^{11} \text{ cm}^{-2}$  from QCM measurements, we can estimate the concentration  $C_0$  for APP770 in stock solution as:

$$C_0 = K_D \frac{n}{2N - n} = 1.94 \times 10^{-9} \text{ mol/l} \quad 5.5$$

This allowed the calibration of TIRE measurements by defining the concentration scale. The minimal concentration of APP770 detected with TIRE biosensor for this particular batch of bio-chemicals DE2 antibody and APP770 can be estimated as  $C_0/16 = 121 \times 10^{-12} \text{ mol/l}$  or  $121 \text{ pM}$

## 5.4 QCM measurements in liquid

### 5.4.1 QCM in Microfluidics

The immune reaction between APP<sub>770</sub> and DE2 antibodies immobilised on the surface was studied with the QCM micro-fluidic method. A fully automated QCMA-1 biosensor instrument and sensor chips from Sierra Sensors GmbH were used. QCMA-1 chips combine two sensing spots on the same AT-cut quartz crystal with a fundamental frequency of 19.5 MHz enabling *in-situ* monitoring of both the active and control sensor channels simultaneously. The operating temperature of the QCM sensor chip was maintained at 25 °C throughout the experiments.

The surface of QCM chips was functionalized in 0.1 M mercapto-ethyl sodium sulfonate solution in methanol (chips were kept for overnight) to enhance negative surface charge similar to the TIRE sample preparation. Then the chip was docked to the QCMA-1 instrument and primed with running buffer (10 mM PBS, pH 7.4) at a flow rate of  $50 \mu\text{l min}^{-1}$ .

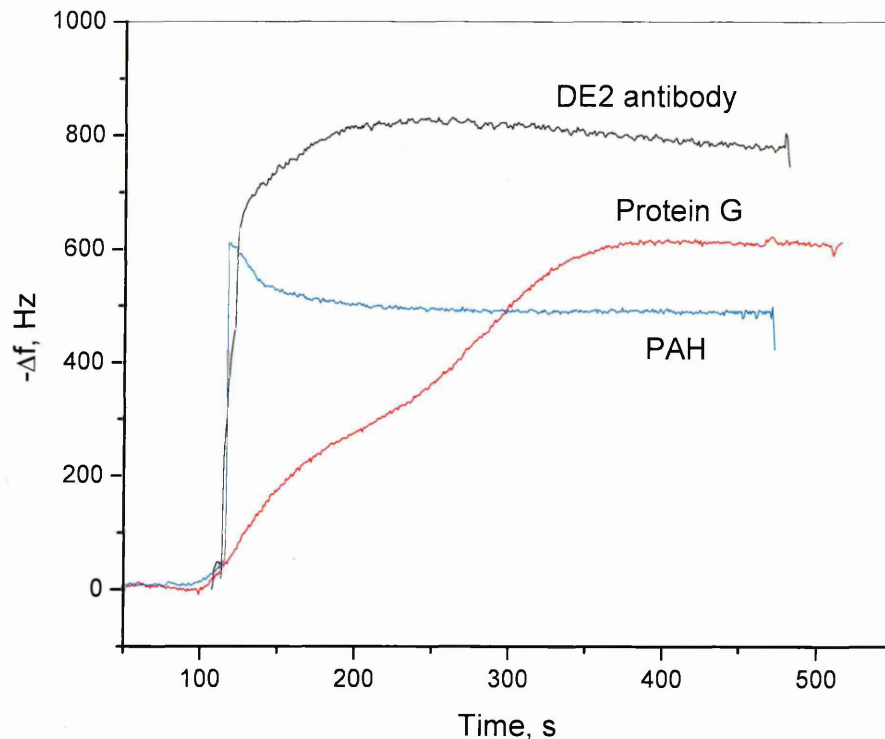


**Fig. 5.7.** Frequency responses (in active channel) during the different adsorption (or immobilization) stages.

In these measurements, in order to improve electrostatic binding, high concentration of PAH (10 mg/ml) was used. The solutions were first injected using automated programme injection needle and were kept at both channels for 400 s. The same incubation time and flow rate has been used for subsequent immobilization of Protein G and DE2 antibody. DE2 antibody was not introduced in the control channel. Figure 5.7 shows frequency responses during adsorption of layers of PAH, Protein G and DE2 antibody in the active channels. The response pattern was the same at control channel except DE2 antibody signal. The response for PAH was very fast and reaches saturation quickly because of a high concentration of PAH (10 mg/ml) in this experiment. Low concentration of PAH (2 mg/ml) (as was used in TIRE) were not enough to give the saturation at the particular incubation time (5 min) in this experiment. Protein G shows a gradual increase upon binding before reaching the saturation at 250 sec. Monoclonal DE2 antibody saturates much faster suggesting that the binding of large molecules was optimized using the flow delivery system with the

right flow rate. The main advantage of using a flow injection system is the constant refreshing the solution in the cell and thus keeping the concentration of reagent near the sensing surface constant.

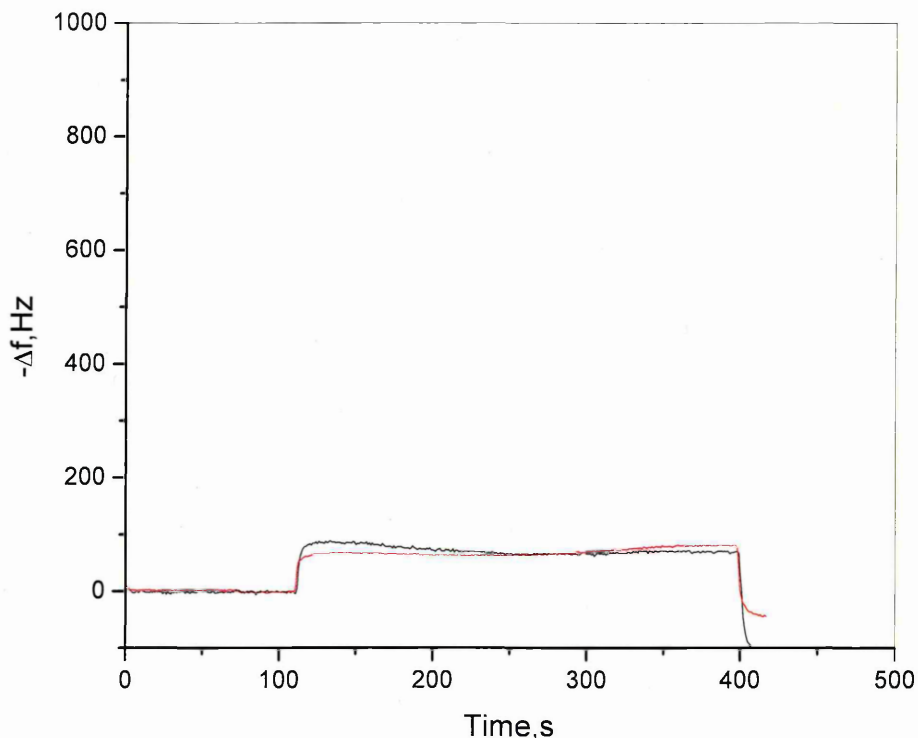


**Fig. 5.8.** Control experiment: The changes in QCM frequency during injection of pure CM solution in active (red curve) and control (black curve) channels.

Before the assays started, the response of QCM-1 sensor to binding of APP<sub>770</sub> from its solution in CM was recorded simultaneously in both active and control channels for 300 s at the same flow rates as in control experiments. The results are shown in Fig. 5.8. Since  $-\Delta f$  vs  $t$  dependencies were recorded, all the absorption or binding reaction appeared as the increase in the frequency signal. There is a frequency increase of about 50 Hz frequency in both channels but that it is much smaller than that during adsorption of layers PAH, Protein G and DE2 antibody and might be due to instrumentation error during measurement. The comparison of responses to the binding of CM in the active channel (coated with DE2) and the reference channel (without DE2) showed practically no difference. This proves the insignificance of non-specific binding of other proteins present in CM.

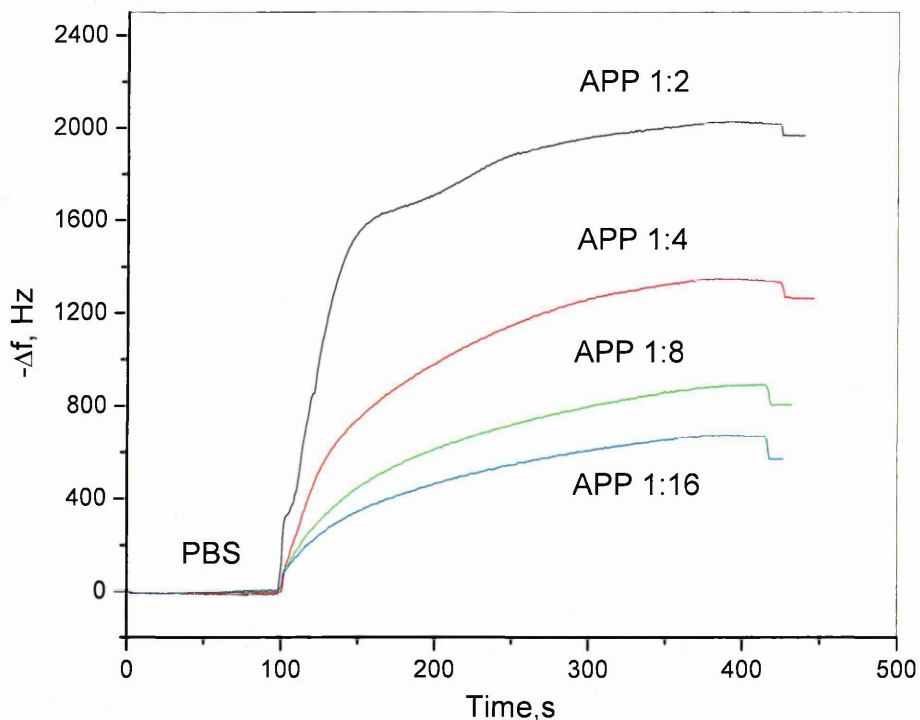


**Fig. 5.9.** Typical QCMA-1 sensor responses to binding of APP<sub>770</sub> of different concentrations (dilutions) in CM to DE2 antibodies immobilised on the surface at active channel.

Figure 5.9 shows changes in the resonance frequency in the active channel of QCMA-1 for 2, 4, 8, and 16 times dilution of APP<sub>770</sub> in CM. As one can see 300s is sufficient to achieve the saturation of responses. The response was proportional to the concentration of APP<sub>770</sub> (MW = 115 kDa). The baseline was recorded during injection of pure PBS buffer solution. Each binding steps in the immune assay were ended with the surface regeneration using 0.1 M HCl to remove antigen molecules and allow further immune binding. Since the Sauerbrey equation is not valid in liquid environment, this method just shows the binding event for immune assay without further analysis.

#### 5.4.2 QCM impedance analysis of the immune reactions between DE2 and APP

Another method introduced in the study of APP is quartz crystal microbalance (QCM) impedance measurement in liquid phase. The QCM impedance setup is based on Solartron Impedance Analyzer 1260 which offers 10  $\mu$ Hz to 32 MHz range of frequency (see details in Chapter 4). The original set-up was designed to perform measurements of impedance spectra of quartz crystals in air. It also was capable of providing a real time data fitting to the BVD equivalent circuit model and thus the *in-situ* monitoring of the parameters L and R of the equivalent circuit which are related respectively to the frequency shift and viscoelastic properties of the absorbed layer.

In order to operate in liquid, a special cell was designed to accommodate the single sided sensor chips (Sierra Sensors QCMA) from Sierra Sensors Ltd (Germany) with a fundamental frequency of 19.5 MHz which were utilized in this work. Dedicated SMART software was used to control and record impedance spectra of QCMA chips for the purpose of *in-situ* monitoring of kinetics of immune reaction between DE2 and APP. The sweep frequency range from 1945000 Hz to 1955000 Hz containing 200 data points was typically used. With such settings it takes about 6 minutes to record the spectrum. The spectra of impedance, admittance and capacitance parameters can be measured simultaneously.

Measurements in air and water of QCMA were performed initially to compare the efficiency oscillation of quartz crystal in these two media. Fig. 5.10 and Fig. 5.11 show the spectra of the impedance phase and magnitude in both media. The amplitude spectrum shows two characteristic peaks at 19469761.8 Hz and 19484203.9 Hz corresponding to the parallel and series resonance respectively while the phase spectrum shows a single peak at 19476230.1 Hz in between the resonances. Impedance phase measurements gives a negative values of phase (typical for capacitive circuit) which peaks near the fundamental frequency of the crystal. Both amplitude and phase spectra shows much sharper peaks in air than those in water, it is believed due to the damping of shear mode oscillations in the liquid environment. Also, the phase spectrum was shifted to lower frequency. More detailed information could be obtained by performing the data fitting to BVD model and extracting parameters of the equivalent circuit.

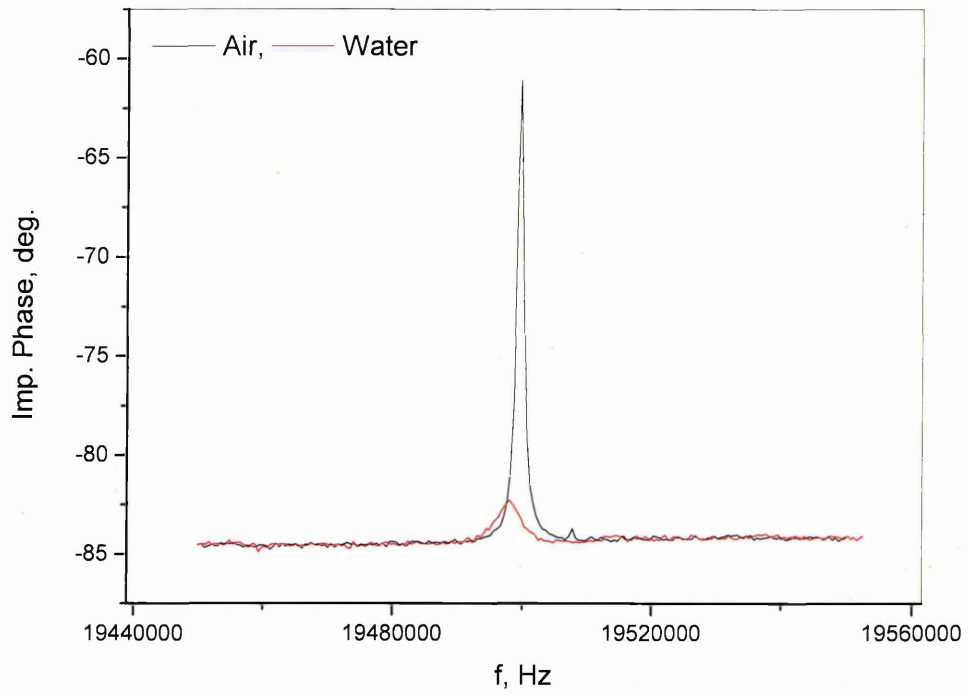


**Fig. 5.10.** Impedance Phase spectra for air and water.

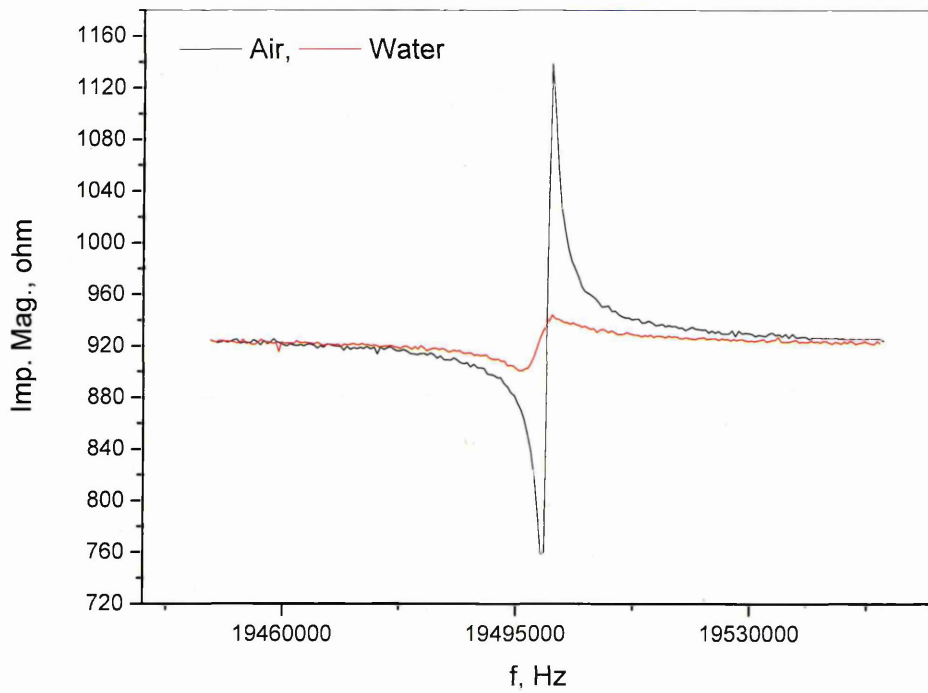


**Fig. 5.11.** Impedance Magnitude spectra for air and water

In this study for a purpose of qualitative analysis, a general spectral features were assessed. Although the Sauerbrey equation is not applicable for QCM oscillating in liquid, it is still possible to separate the effect of added mass causing a negative shift of the resonance frequencies and the damping which causes the reduction of amplitudes and phase shift. The efficiency of oscillation of QCM crystal can be accessed by the quality factor (Q) which indicates the ratio of energy losses to the energy stored in the oscillator and is equal to the ratio between resonance frequency ( $f_0$ ) and bandwidth (B):

$$Q = \frac{f}{B} \quad 5.1$$

The analysis of Q factor based on the impedance phase spectra is given in Table 5.3. It was found that the quality factor (Q) for the crystal oscillating in air was 10,355 which is nearly 4 times larger that (Q = 2,790) for the oscillation in water. The damping of oscillations in water is substantially larger than in air, but it is still possible to perform measurements and carry out analysis of immune reactions in liquid medium.

**Table 5.3:** Quality factor for QCM crystal in air and water (Impedance Phase).

Medium	Air	Water
Resonance frequency, $f_0$	19499780.8 Hz	19498168 Hz
Bandwidth, B (0.7071 of maximum peak)	$= f_2 - f_1$ $= 19500544.7 - 19498661.6$ $= 1883.1$ Hz	$= f_2 - f_1$ $= 19501235.6 - 19494247$ $= 6988.6$ Hz
Q factor	$\frac{f_0}{B} = \frac{19499780.8}{1883.1}$ $= 10,355.0$	$\frac{f_0}{B} = \frac{19498168.0}{6988.6}$ $= 2790.0$

The measurement of impedance for APP is using Sierra Sensors chip which was treated the same way as described in TIRE sample preparation to enhance a negatively charge on the sensing surface. Impedance spectra were always recorded in the same Triz-HCl buffer (pH 7.5) first on bare gold then after consecutive adsorption of layers of PAH, Protein G, DE2 and APP. The incubation time of 6 min was used followed by rinsing the cell in Triz-HCl except for PAH when by deionize water (Purelab Maxima 18.2 M $\Omega$ ) was used.

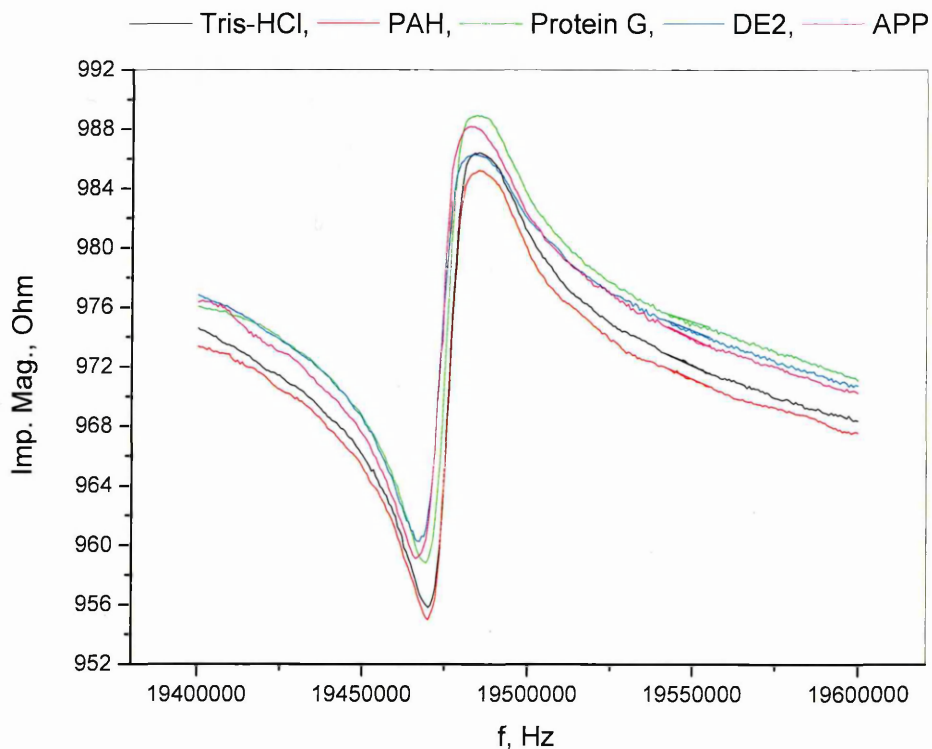


**Fig. 5.12.** Impedance mangitude spectra for Triz–HCl, PAH, Protein G, DE2 and APP.

Fig. 5.12 and Fig. 5.13 show respectively typical impedance phase and magnitude spectra respectively. Both spectra show a noticeable shift to the lower frequencies after each deposition which can be associated with the added mass.

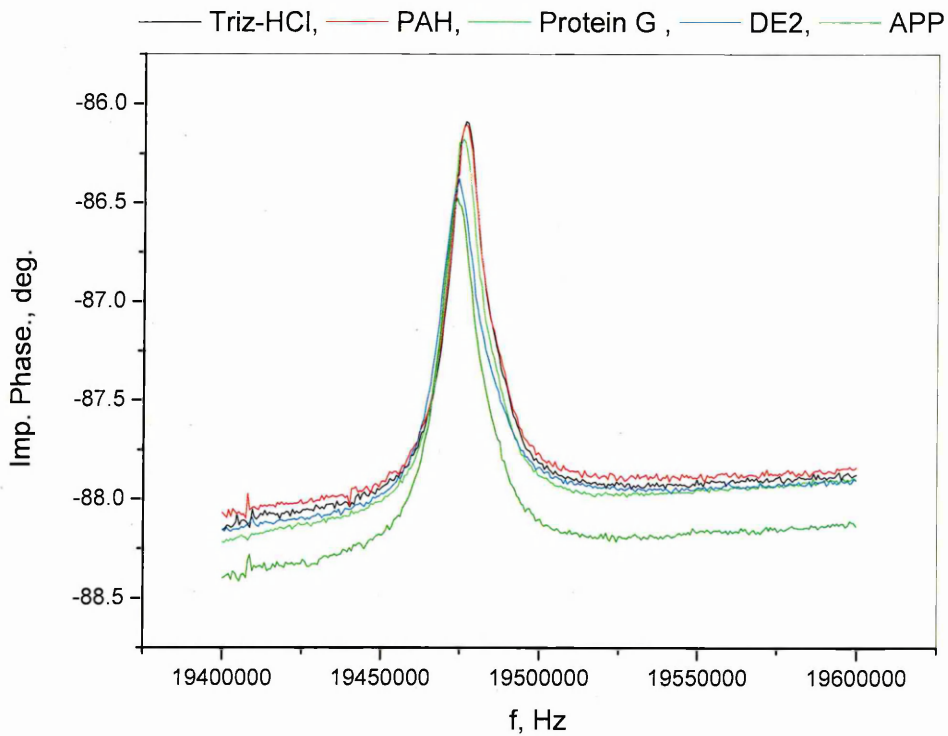


**Fig. 5.13.** Impedance phase spectra for Triz-HCl, PAH, Protein G, DE2 and APP.

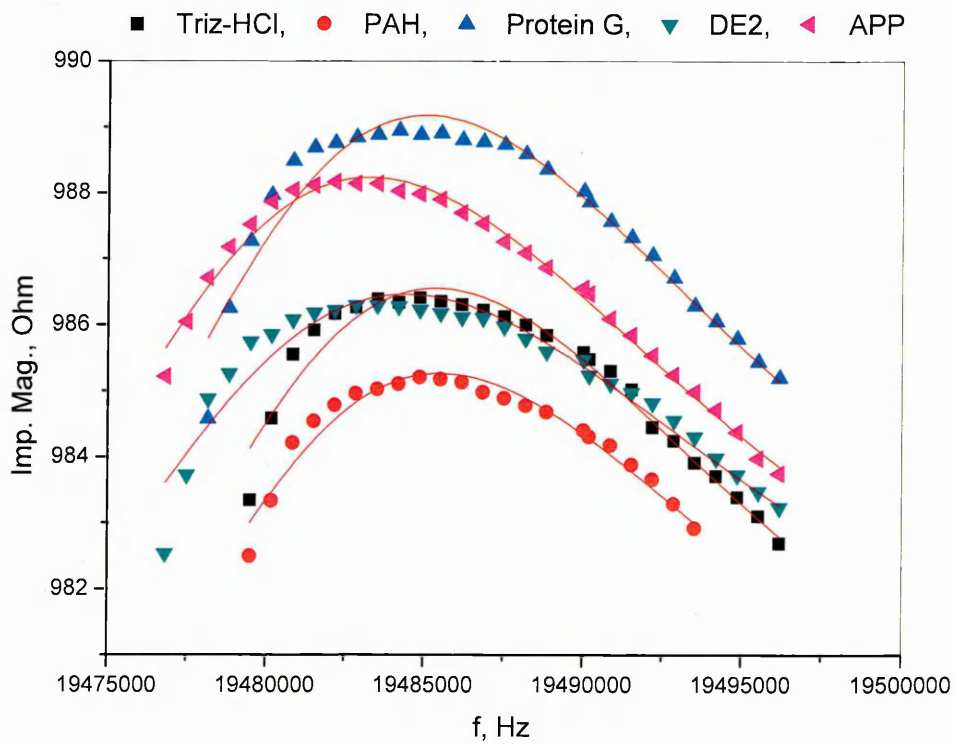


**Fig. 5.14.** Impedance magnitude spectra fitting for Triz-HCl, PAH, Protein G, DE2 and APP.

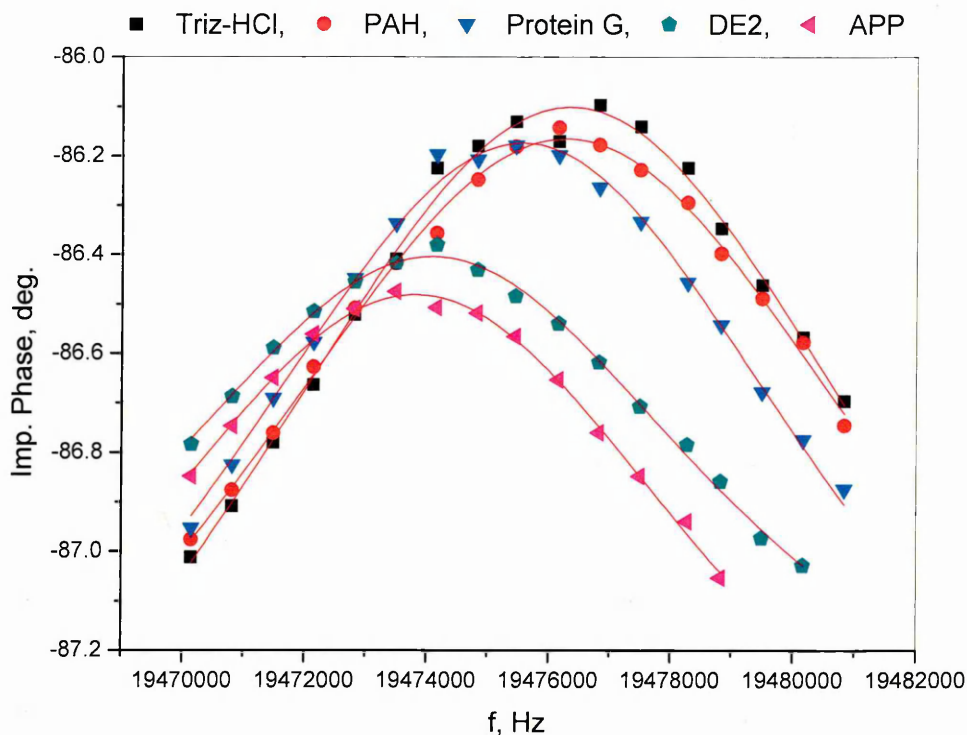


**Fig. 5.15.** Impedance phase spectra fitting for Triz-HCl, PAH, Protein G, DE2 and APP.

The variation of peak frequencies after deposition of layer of PAH, Protein G, DE2 and APP can be clearly seen on zoomed-in section of spectra near the maximum. In order to find precisely the position of maxima, polynomial fitting was performed. Fig. 5.14 and 5.15 shows experiment data points and polynomial fitting curves for the maximum of impedance phase and impedance magnitude respectively. It is obvious that the peak frequency of the crystal decreases as a result of deposition of molecular layers. The dependence of a frequencies shift in Fig. 5.16 is similar to that obtained on dry quartz crystals (see 5.3, Fig. 5.6) and correlated with the molecular weight of deposited molecules.

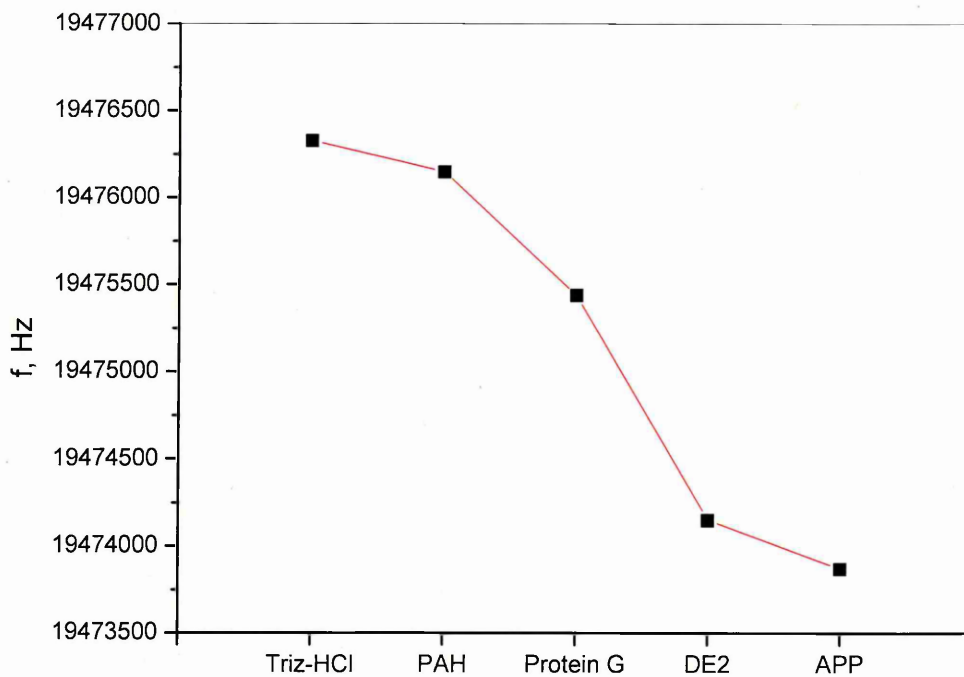


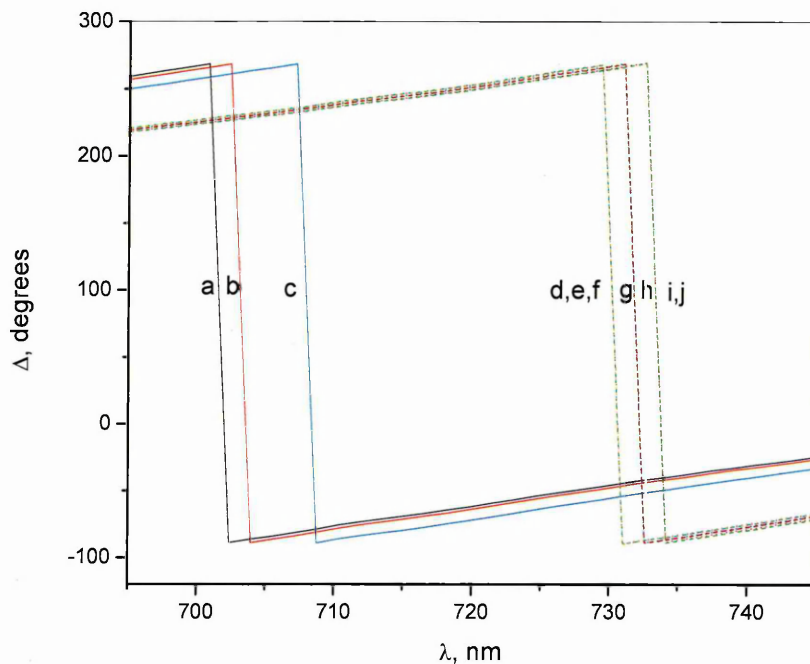
**Fig. 5.16.** Peak resonance frequency changes after consecutive absorption of PAH, Protein G, DE2 antibodies and APP.

### 5.5 Detection of Amyloid beta peptide 1-16 ( $A\beta_{1-16}$ ) by TIRE method.

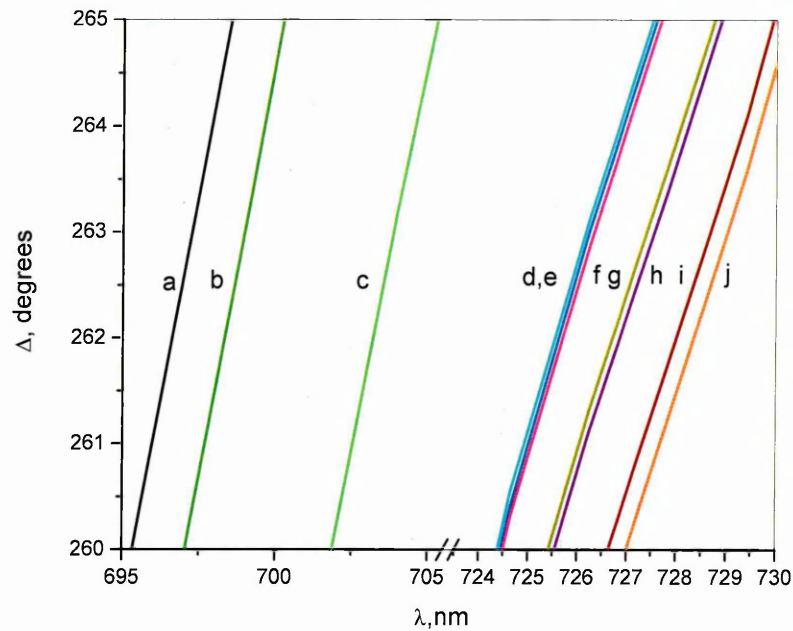
In this work  $A\beta_{1-16}$  was detected using the same monoclonal DE2 antibodies which were used for APP770 detection. The recording of single TIRE spectroscopic scans was performed in a standard Tris-HCl buffer solution (pH 7.5) after completing each adsorption (or binding) step. The cell was rinsed between adsorption steps by purging the same buffer solution ten times of the cell volume.

Figure 5.17 shows typical of  $\psi(\lambda)$  and  $\Delta(\lambda)$  spectra recorded in such TIRE measurements. Because of the spectral shift is smaller than the wavelength increment the direct observation cannot distinguish between spectra at different concentrations. Binding events in the assay was proved by TIRE fitting which shows the increase in the layer thickness after each injection. In order to improve this situation, the correction of negative values of  $\Delta$  spectra by adding  $360^\circ$  has been done as discussed in Chapter 3. After such correction, the spectral shift of  $\Delta(\lambda)$  is clearly noticeable in Fig. 5.18. All the

spectra were recorded in Tris-HCl buffer in the sequence of PAH, Protein G, DE2 antibody and  $A\beta_{1-16}$  at different concentration of 0.05 ng/ml, 0.5 ng/ml, 5 ng/ml, 50 ng/ml, 500 ng/ml and 5000 ng/ml.



**Fig. 5.17.** TIRE  $\Delta(\lambda)$  spectra recorded on of bare Au (a), after adsorption of PAH (b), Protein G (c), DE2 antibodies (d); and after consecutive binding of  $A\beta_{1-16}$  of different concentrations: 0.05ng/ml (e), 0.5ng/ml (f) 5 ng/ml (g) 50 ng/ml (h), 500 ng/ml (i), and 5  $\mu\text{g/ml}$  (j).



**Fig. 5.18.** Zoomed-in section of corrected  $\Delta(\lambda)$  spectra recorded on of bare Au (a), after adsorption of PAH (b), Protein G (c), DE2 antibodies (d); and after consecutive binding of  $A\beta_{1-16}$  of different concentrations: 0.05ng/ml (e), 0.5ng/ml (f) 5 ng/ml (g) 50 ng/ml (h), 500 ng/ml (i), and 5  $\mu$ g/ml (j).

**Table 5.3:** TIRE fitting results for immune reaction between DE2 and  $A\beta_{1-16}$ .

Asterisk (\*) sign indicates that the parameters were fixed during fitting. The values of  $n$  and  $k$  are given at the wavelength of 633nm.

$A\beta_{1-16}$ , accumulated concentration(ng/ml)	$d$ (nm)	$\Delta d$ (nm)	$n, k$ (at $\lambda=633$ nm)
0.05	12.599±0.018	1.094	$n^*=1.42; k^*=0$
0.55	12.649±0.002	1.145	$n^*=1.42; k^*=0$
5.55	13.115±0.001	1.463	$n^*=1.42; k^*=0$
55.55	13.184±0.011	1.680	$n^*=1.42; k^*=0$
555.55	13.637±0.017	2.133	$n^*=1.42; k^*=0$
5555.55	13.827±0.002	2.322	$n^*=1.42; k^*=0$

The obtained changes in the effective thickness of  $A\beta_{1-16}$  layer in respect to the layer of DE2 antibodies are summarized in Table 5.3. The thickness values ( $d$ ) represent effective thickness of molecular layers adsorbed on the surface. The increase in the effective thickness ( $\Delta d$ ) corresponds to the thickness increment caused by adsorption (binding) of respective molecules. Because the TIRE experiments on  $A\beta_{1-16}$  binding were carried out on the same sample (without surface regeneration) in the sequential increasing of  $A\beta_{1-16}$  concentration starting with the smallest concentration of 0.05 ng/ml, the accumulative concentration of  $A\beta_{1-16}$  was used in the Table 5.3 as well as in the calibration curve (Fig. 5.19).

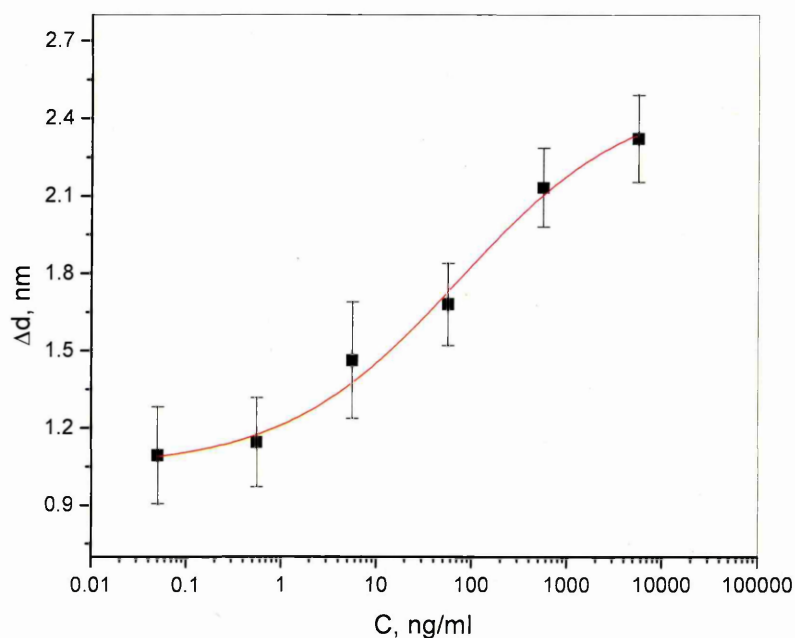


**Fig. 5.19.** Calibration curve for  $\beta$ -amyloid peptide 1-16.

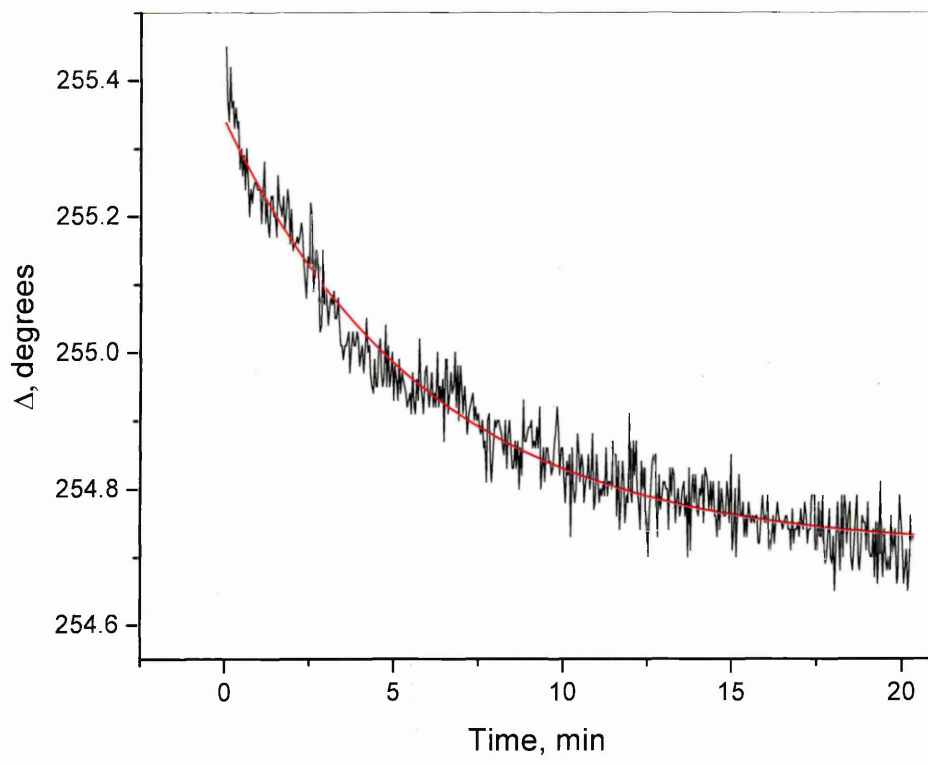
The values of thickness correlate with the size (or molecular weight) of adsorbed molecules as well as with their concentrations on the surface. The thickness increment ( $\Delta d$ ) increases from 0.756 nm for the smallest PAH molecules (molecular weight for repeated unit is 93.5, molecular weight of the polymer (MW=70 KDa), to 2.112 nm for Protein G (MW=25 KDa), and up to 8.637 nm for large DE2 molecules (MW=120 KDa).

The calibration curve in Fig. 5.19, i.e. the dependence of the increase in the effective thickness of adsorbed layer (Cauchy layer) vs the accumulative concentration of  $A\beta_{1-16}$ , appeared as a classical sigmoid curve typical for immune reactions. The linear range stretches from 2 to 500 ng/ml; and the trend to saturation is observed at concentrations higher than 5  $\mu$ g/ml. The minimal detected concentration of  $A\beta_{1-16}$  was 0.05 ng/ml.

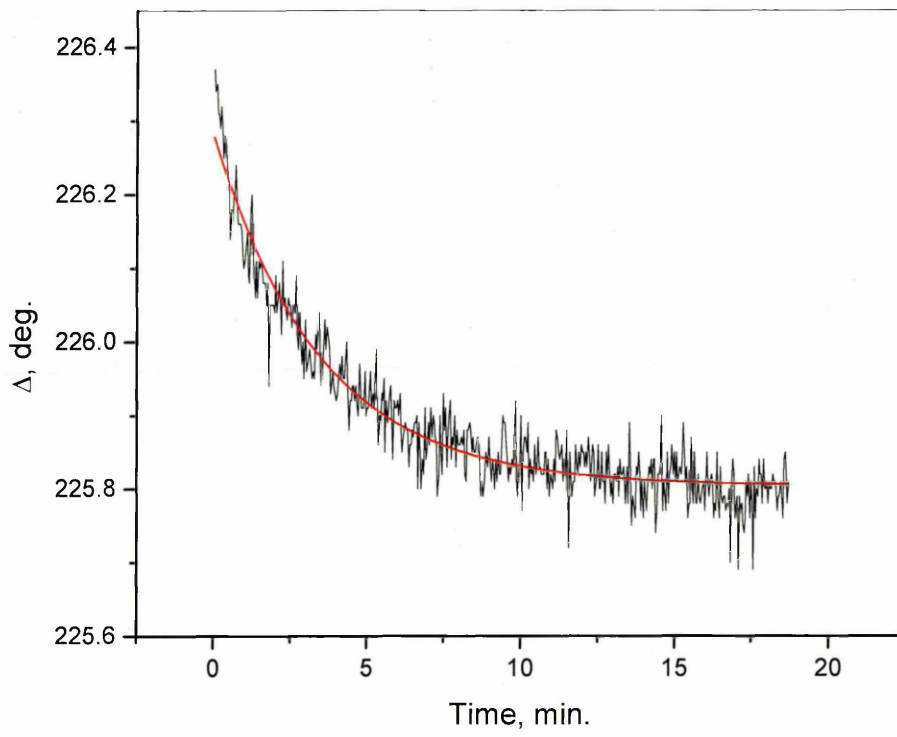
## 5.6 TIRE kinetic analysis and evaluation of affinity constant for $A\beta_{1-16}$

The kinetic of molecular adsorption (binding) has been monitored *in-situ* during the incubation period for each reagent using dynamic TIRE scans, i.e. recording a number of spectra after a certain time interval (typically 15 – 20 minutes). Then, the time dependencies of either  $\Psi$  or  $\Delta$  at a selected wavelength were extracted for the study of kinetics of molecular adsorption or binding.

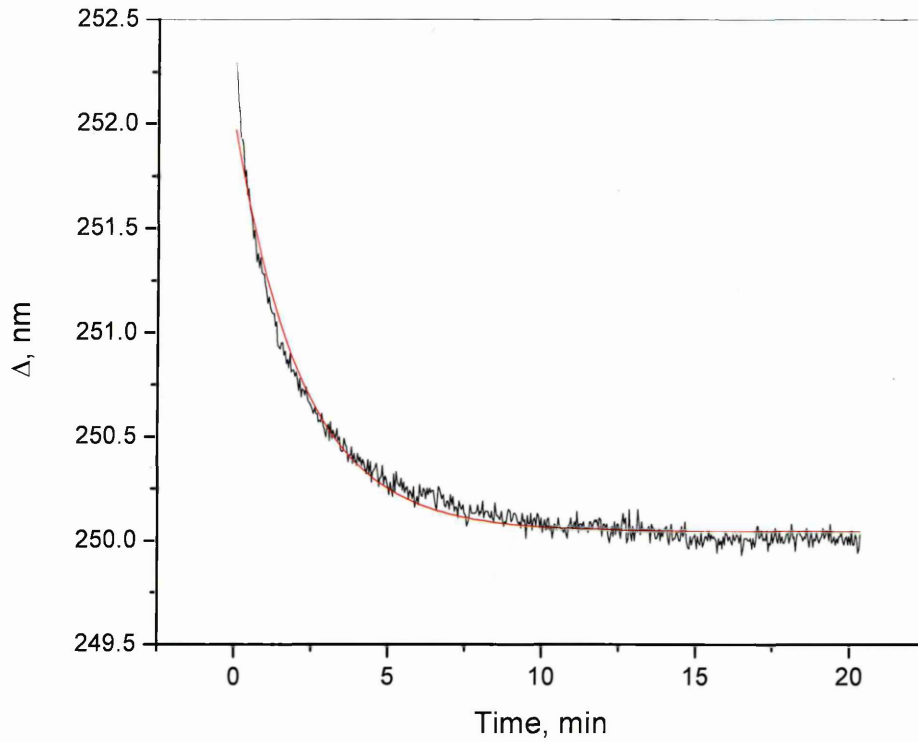
Time dependencies of  $\Psi$  and  $\Delta$  at 700 nm of different concentration of  $A\beta_{1-16}$  in the range of 0.05 ng/ml to 5  $\mu$ g/ml were extracted from TIRE dynamic spectral measurements during binding of  $A\beta_{1-16}$  molecules to DE2 antibodies immobilised on the surface. Typical kinetic curves for 0.05 ng/ml, 50 ng/ml and 500 ng/ml of  $A\beta_{1-16}$  are given in Figure 5.20 (a), (b) and (c) respectively. It was demonstrated that a 20 min incubation time was sufficient to reach the saturation for at the lowest concentration of  $A\beta_{1-16}$ .



(a)



(b)



(c)

**Fig. 5.20.** TIRE kinetic curves for binding of  $A\beta_{1-16}$  of different concentrations: (a) 0.05 ng/ml and (b) 50 ng/ml (c) 500 ng/ml.

Then a well-developed procedure of the evaluation of the rates of adsorption ( $k_a$ ) and desorption ( $k_d$ ) of the immune reaction was applied [145,151-153]. The characteristic time constant ( $\tau$ ) of the immune reaction was evaluated by fitting the data to the exponential function,  $a \cdot \exp(-t/\tau) + b$ . The inverse value of time constant

$S = \frac{1}{\tau} = k_a C + k_d$  was plotted against the concentration of the antigen ( $C$ ) in Figure

5.21, and the values of  $k_a$  and  $k_d$  were found, respectively, from the gradient and intercept of the linear graph. The values of  $k_a$  and  $k_d$  obtained from the graph in allowed

the calculation of the association and affinity constants as  $K_A = \frac{k_a}{k_d}$  and  $K_D = \frac{1}{K_A}$ ,

respectively.

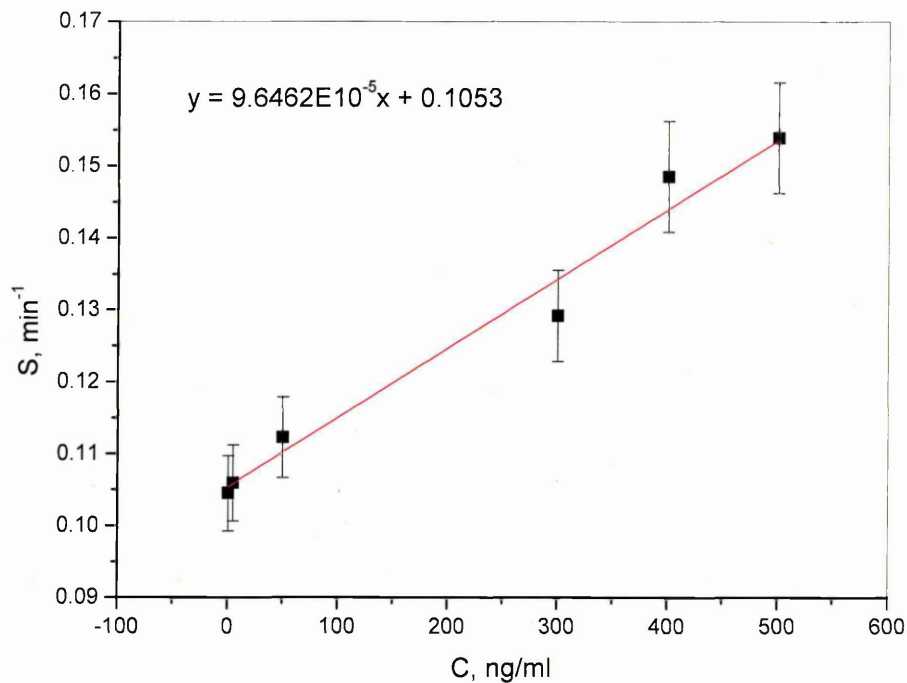


**Fig. 5.21.** The evaluation of the rates of adsorption ( $k_a$ ) and desorption ( $k_d$ ) from the kinetics of binding of  $A\beta_{1-16}$  to DE2 antibody.

The linear equation for the graph in Fig. 5.21 is :

$$S = 9.6462 \cdot 10^{-5} C - 0.1053$$

After adjusting the units and given the molecular weight for  $A\beta_{1-16}$  is 1955 Da;

$$k_a = 9.6462 \cdot 10^{-5} \left[ \frac{ml}{ng \cdot min} \right] = 9.6462 \cdot 10^{-5} \frac{10^{-3}}{10^{-9} \cdot 60} \left[ \frac{l}{g \cdot s} \right] = 1.6077 \left[ \frac{l}{g \cdot s} \right]$$

$$k_a = 1.6077 \cdot 1955 = 3.14 \cdot 10^3 \left[ \frac{l}{mol \cdot s} \right]$$

$$k_d = 0.1053 \left[ \frac{1}{min} \right] = \frac{0.1053}{60} = 1.76 \cdot 10^{-3} \left[ \frac{1}{s} \right]$$

The value of association constant is given by;

$$K_A = \frac{k_a}{k_d} \left[ \frac{l \cdot s}{mol \cdot s} \right] = \frac{3.14 \cdot 10^3}{1.76 \cdot 10^{-3}} = 1.78 \cdot 10^6 \left[ \frac{l}{mol} \right]$$

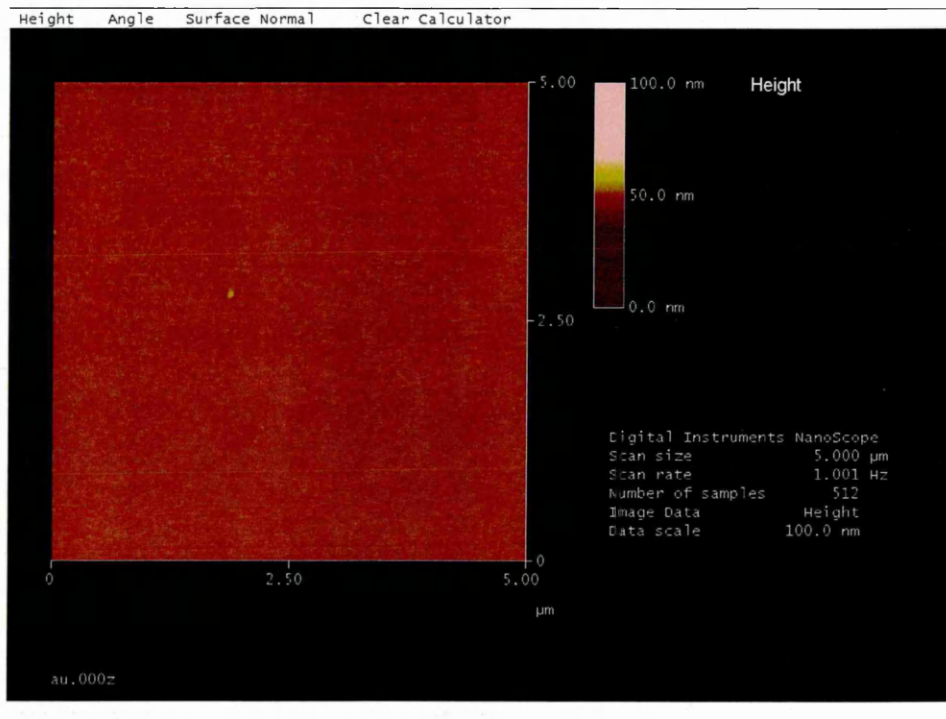
The value of dissociation constant is given by;

$$K_D = \frac{1}{K_A} = 5.61 \cdot 10^{-7} \text{ mol/l}$$

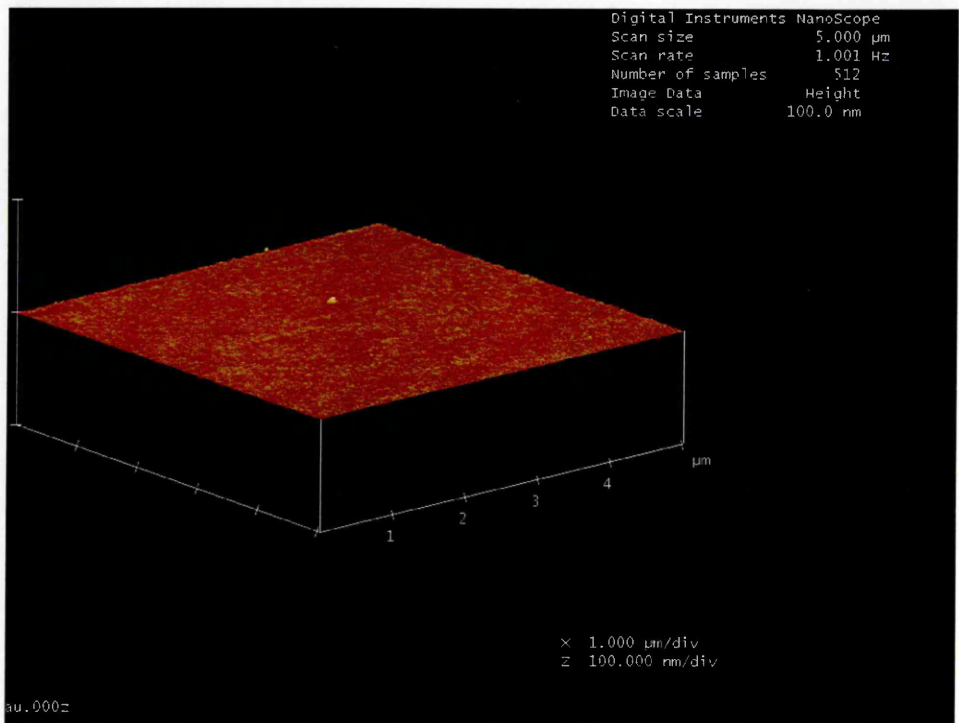
The obtained values of  $K_A = 1.78 \cdot 10^6 \text{ (l/mol)}$  and  $K_D = 5.61 \cdot 10^{-7} \text{ (mol/l)}$  are typical for highly specific immune reaction with monoclonal antibodies.

### 5.7 Morphology Analysis for APP and A $\beta_{1-16}$

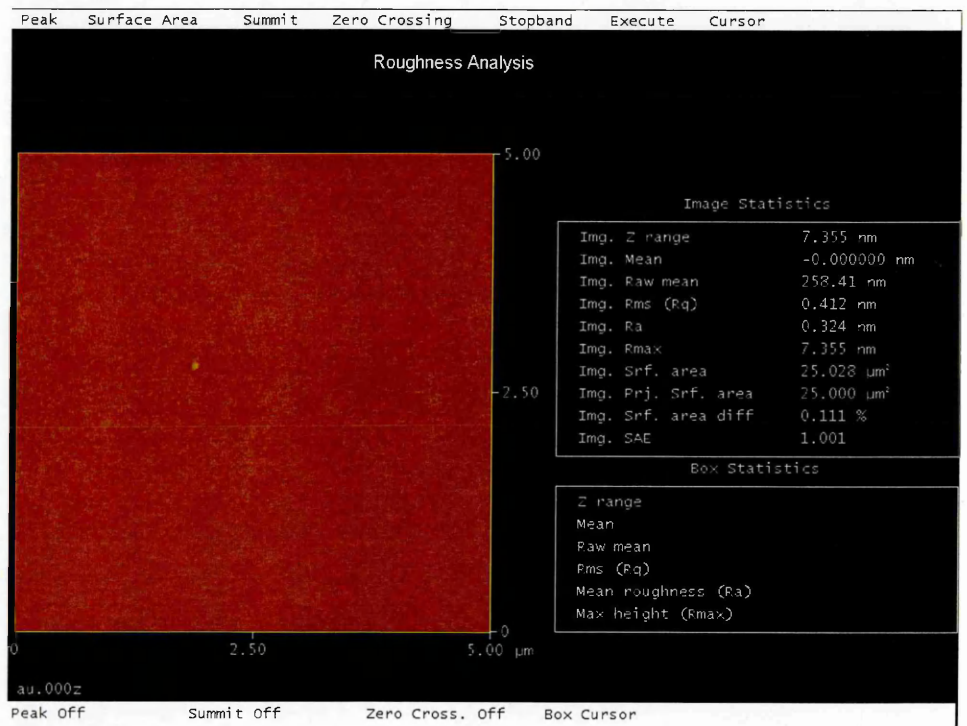
Atomic Force Microscope (AFM) technique is widely known for surface morphology analysis. Surface structure of the sensing layer used in this work was analyzed using Nanoscope IIIa from Digital Instrument. The tapping mode was employed using phosphorus doped Si tips with the oscillation frequency in the range of 240 – 330 Hz and typical radius of 10 nm. Surface area of  $25 \mu\text{m}^2$  was selected for analysis on every sample. All the images have  $100 \mu\text{m}$  data scale to compensate a flat and grainy area.



(a)



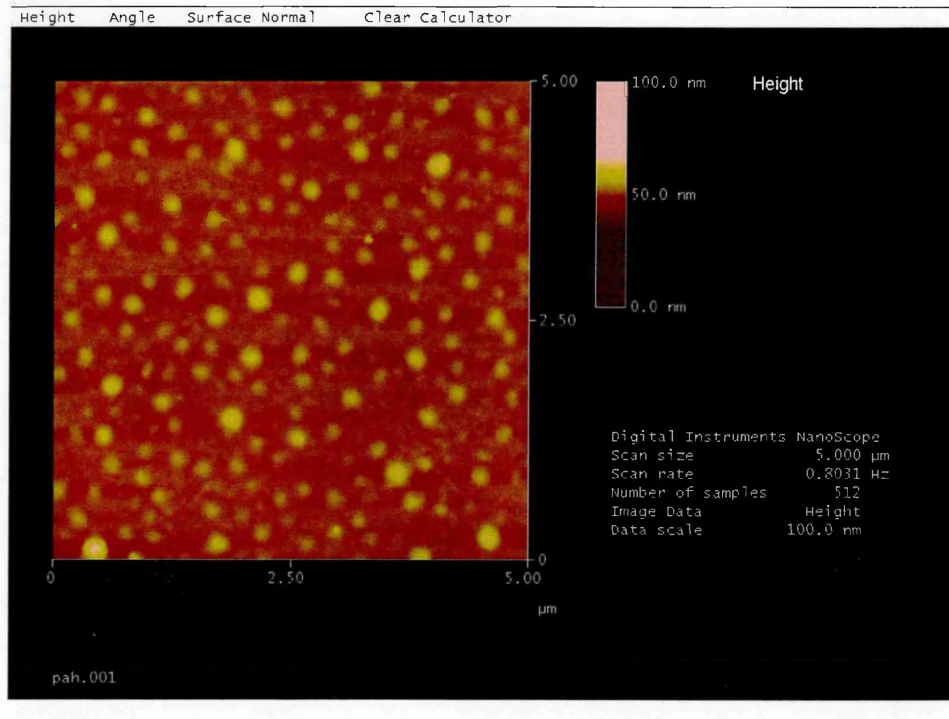
(b)



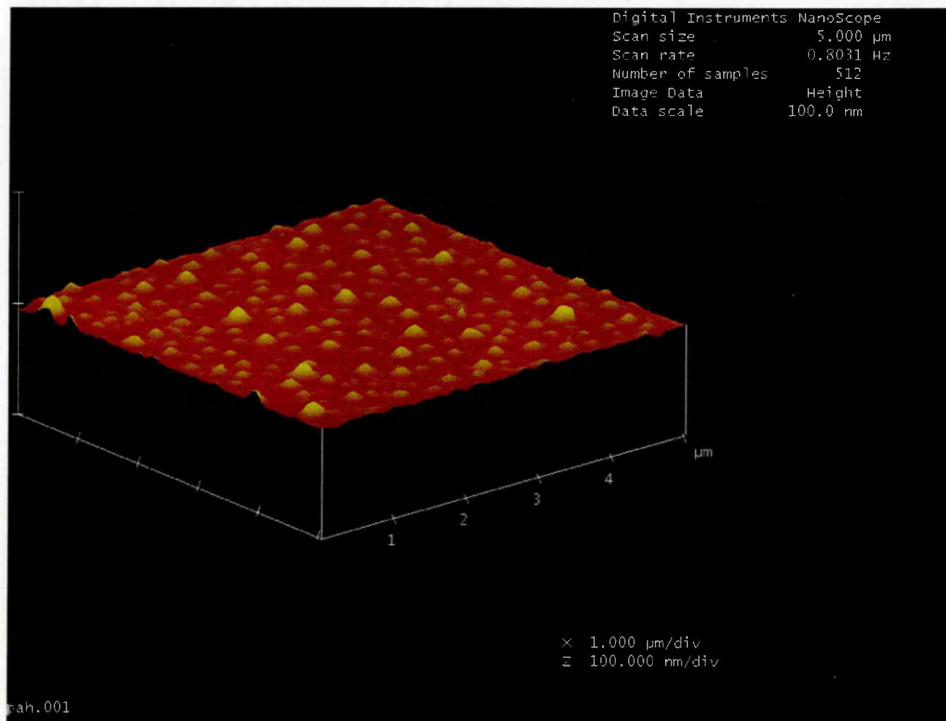
(c)

**Fig. 5.22.** Tapping mode AFM image of bare Au surface; Top view (a), 3D view (b) and surface roughness analysis (c).

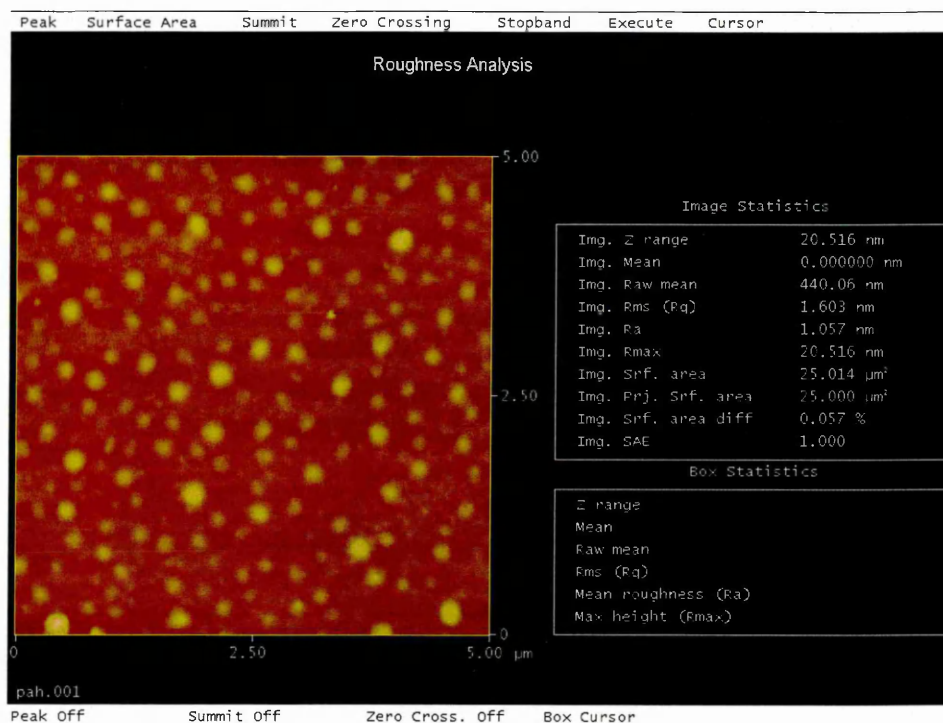
A typical AFM 2D image of bare gold surface is shown in Fig. 5.22 (a). The surface is very flat without any peak as revealed in psedo 3D AFM image in Fig. 5.22 (b). The roughness analysis in Fig. 5.22 (c) revealed with the mean roughness ( $R_a$ ) =  $0.4643 \pm 0.1915$  nm for all surface area studied.



(a)



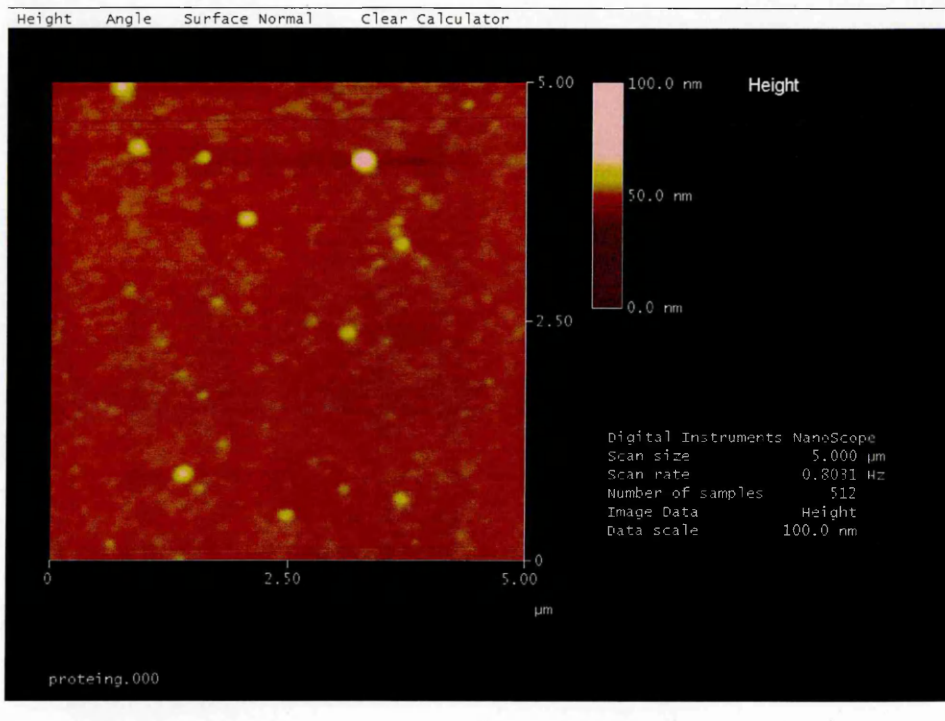
(b)



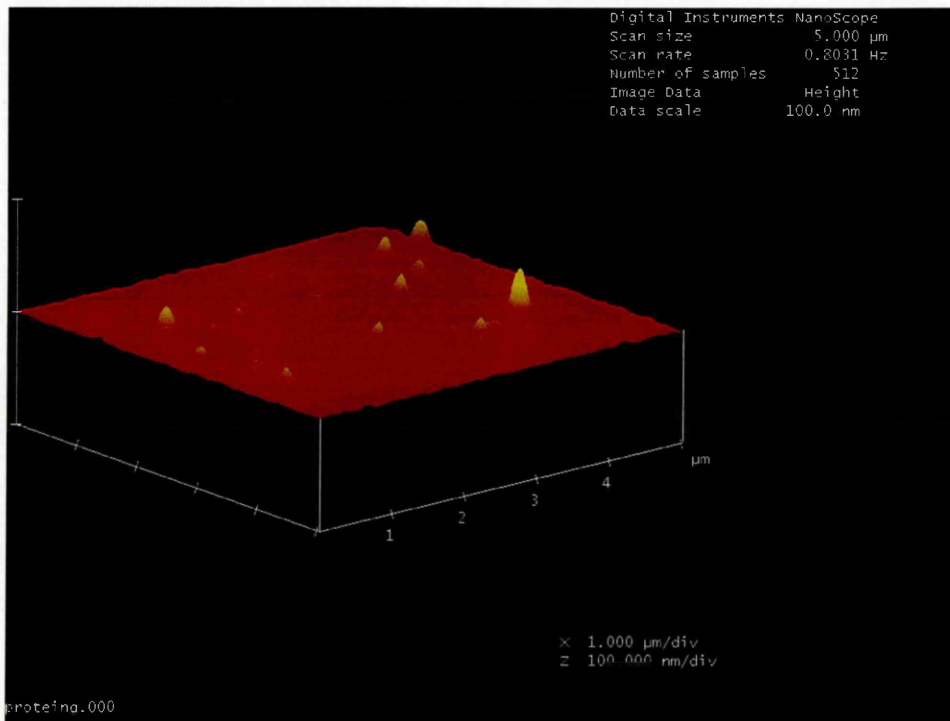
(c)

**Fig. 5.23.** Tapping mode AFM image of PAH surface; Top view (a), 3D view (b) and surface roughness analysis (c).

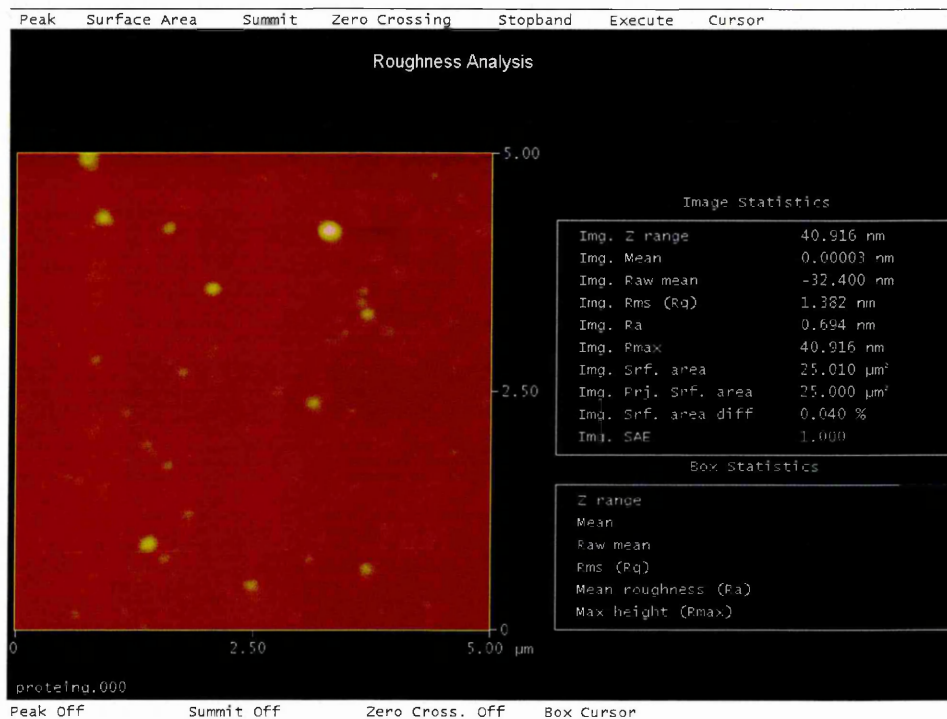
After deposition of layer of Poly-(allylamine hydrochloride), PAH ( $M_w = 70$  kDa), multiple spots appeared on the surface as shown in Fig. 5.23 (a). The pseudo 3D image of the surface presented more clearly a view of a grainy surface all over the area (Fig. 5.23 (b) which may have appeared as a result of aggregation of PAH chains. The PAH layer was relatively homogenous with the mean roughness of  $1.034 \pm 0.1023$  nm (Fig. 5.23 (c)).



(a)



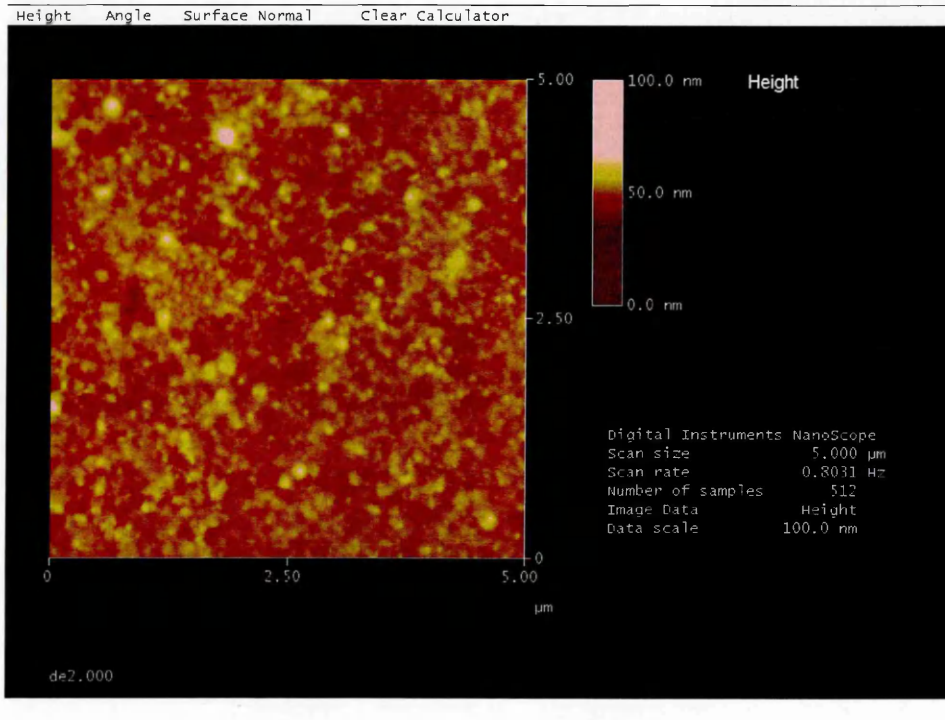
(b)



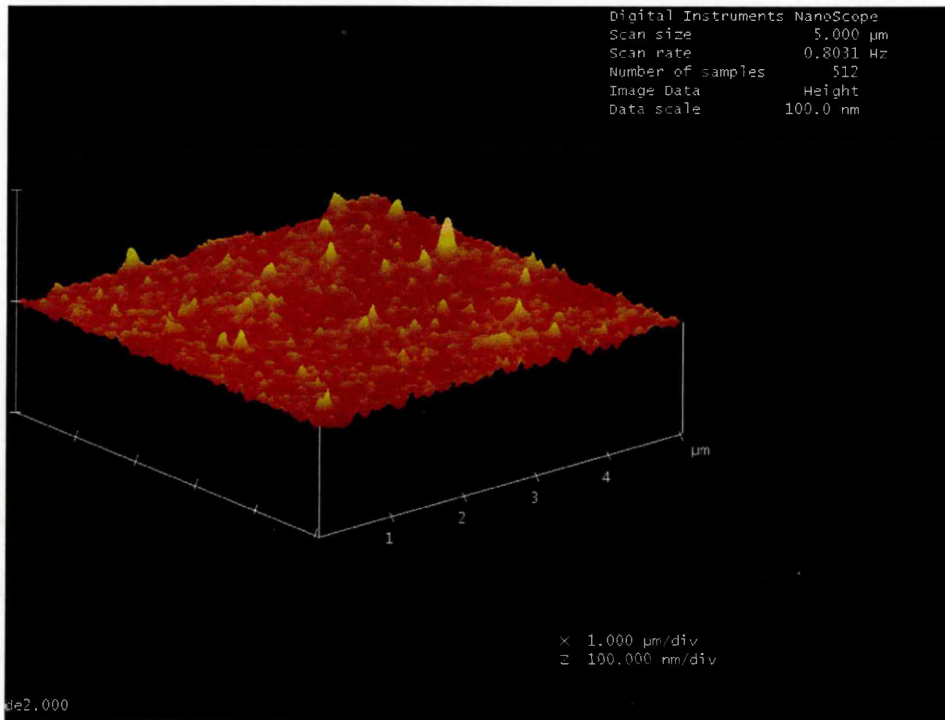
(c)

**Fig. 5.24.** Tapping mode AFM image of Protein G surface; Top view (a), 3D view (b) and surface roughness analysis (c).

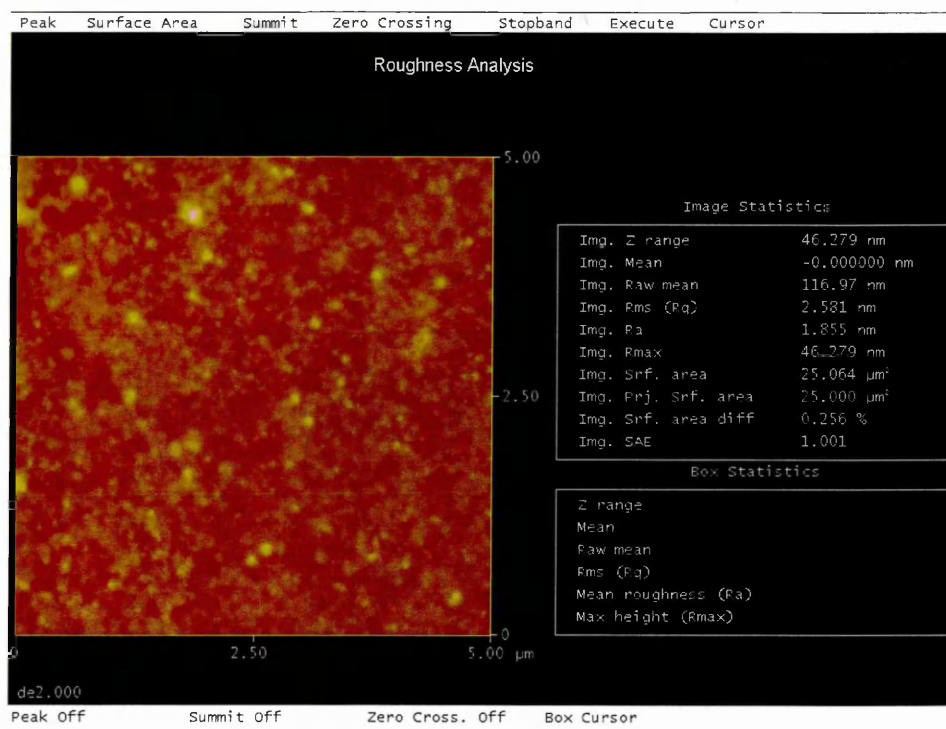
Figures 5.24 (a) and (b) shows respectively 2D and 3D AFM images of sensing surface after the deposition of Protein G (Mw = 25 kDa). The surface still looked flat and had some clear spots which may correspond to protein-PAH aggregates developed on the surface. Roughness analysis revealed that the surface was even smoother than the PAH layer with mean roughness value is  $0.7156 \pm 0.1487$  nm (Fig. 5.24 (c)). One can suggest that protein G molecules were located in the valleys between PAH molecules which caused more smooth and flatter surface.



(a)



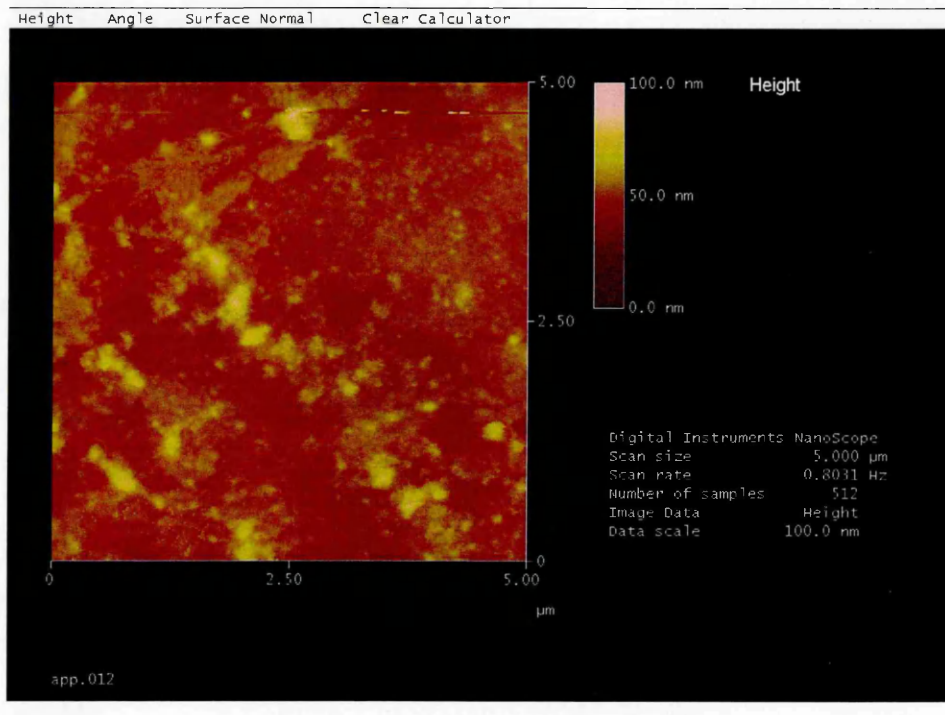
(b)



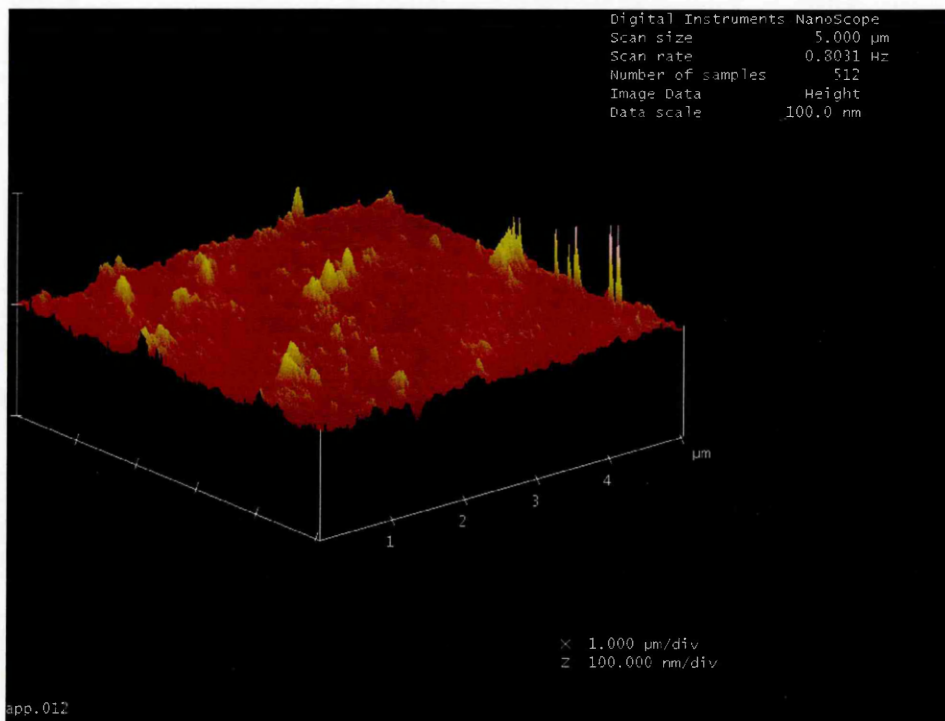
(c)

**Fig. 5.25.** Tapping mode AFM image of DE2 antibodies surface; Top view (a), 3D view (b), and surface roughness analysis (c).

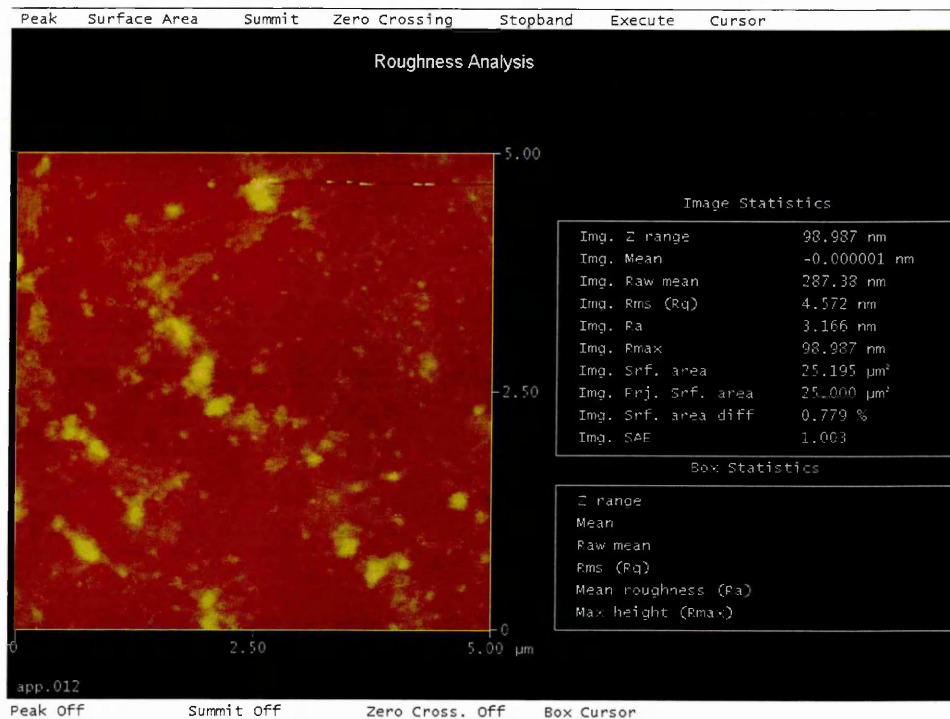
Deposition of DE2 antibodies ( $M_w = 120$  kDa) having Y shape with two binding sites (Fab fragment), transforms the AFM image dramatically. Top view image in Fig. 5.25 (a) shows the entire surface covered by multiple spots. The irregular surface with multiple peaks is clearly seen on 3D AFM image as in Fig 5.25 (b). Surface roughness analysis revealed much higher mean roughness value of  $1.867 \pm 0.1194$  nm (Fig. 5.25 (c)) on this sample.



(a)



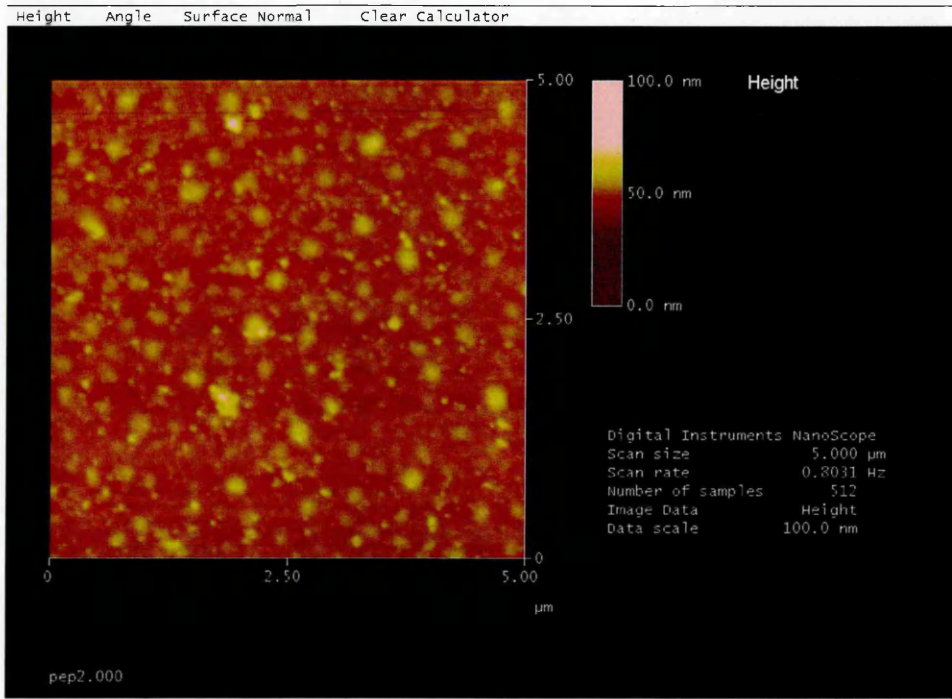
(b)



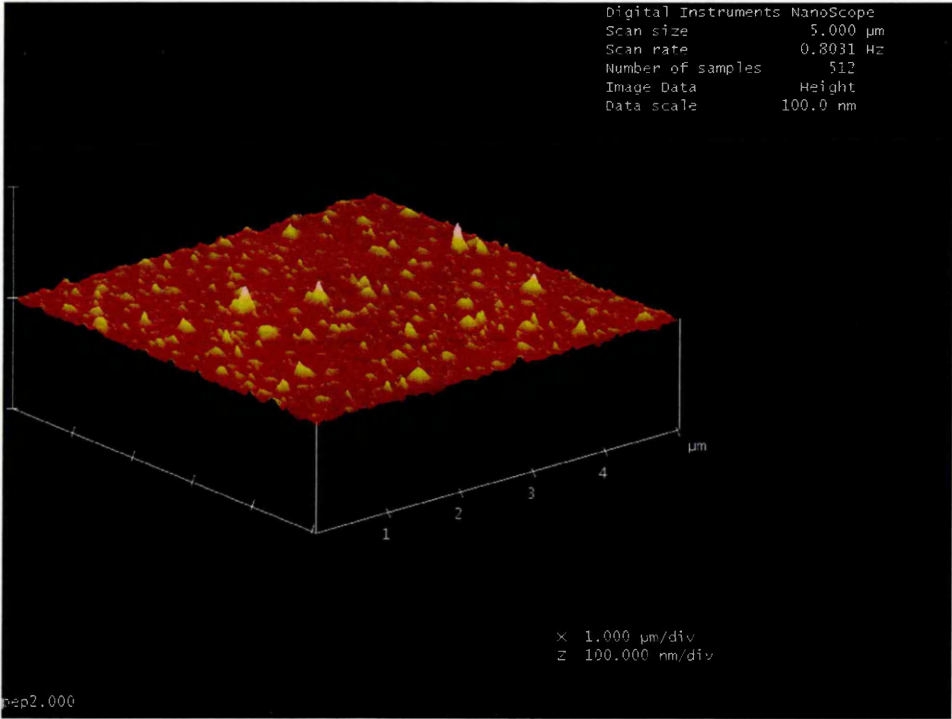
(c)

**Fig. 5.26.** Tapping mode AFM image APP surface; Top view (a), 3D view (b) and surface roughness analysis (c)

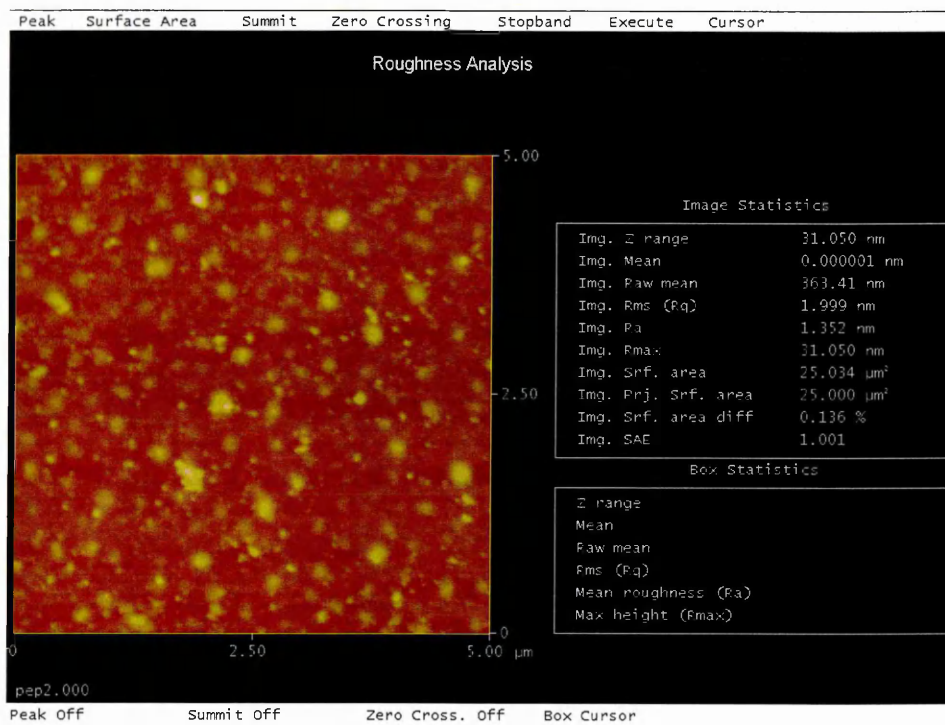
The morphology of sensing surface after the binding of APP770 to DE2 antibodies can be seen in Fig. 5.26. The surface is not covered homogeneously and contained quite large aggregates as reveals by 2D and pseudo-3D images in Fig. 5.26 (a) and (b). This may be due to further aggregation by folding of the long APP chains consisting of 770 amino acids and having binding sites at one end (first 1-16 amino acids). The increase of surface roughness up to  $R_a = 2.7063 \pm 0.3293$  nm (see Fig. 5.26 (c)) was a logical consequences of such aggregation.



(a)



(b)



(c)

**Fig. 5.27.** Tapping mode AFM image of  $A\beta_{1-16}$  surface; Top view (a), 3D view (b) and surface roughness analysis (c)

The same technique was applied for surface morphology analysis of sample after binding of much shorter antigens, e.g.  $A\beta_{1-16}$  to the same DE2 antibodies. The top view (2D) of AFM image after binding  $A\beta_{1-16}$  is shown in Fig. 5.27 (a) while pseudo-3D image is shown in Fig 5.27 (b). The surface morphology was not changed drastically as compared to the images in Fig. 5.25 giving similar values of the surface roughness  $1.491 \pm 0.2323$  nm. Such result is quite logical considering much shorter length (16 amino acids) of attached peptides  $A\beta_{1-16}$  as compared to APP 770.

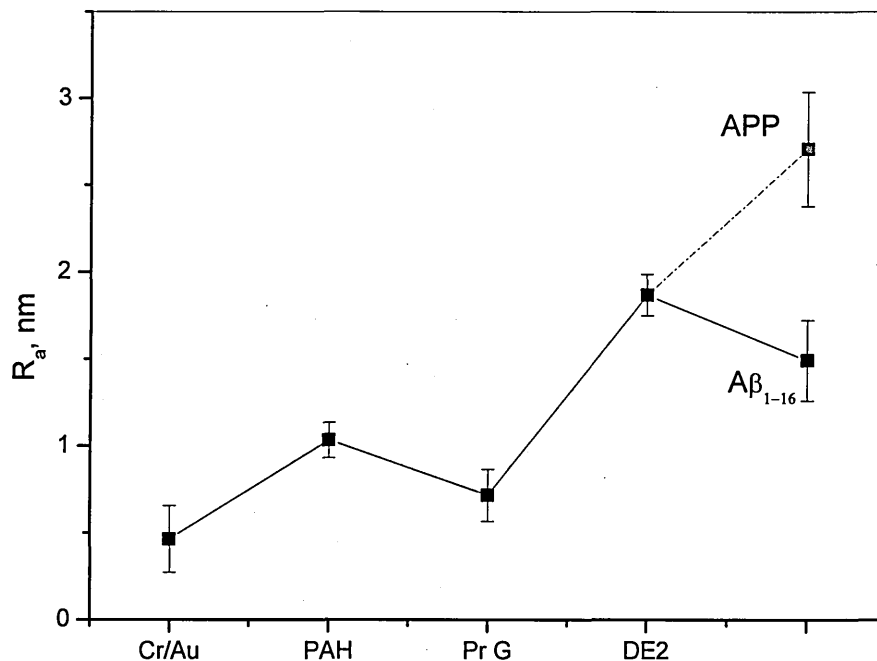


**Fig. 5.28.** Roughness analysis of APP770 and Aβ<sub>1-16</sub> by AFM.

Figure 5.28 summarises the changes in the mean roughness values after deposition of each layer. The surface roughness was increased after binding of PAH but slightly decreased after Protein G. Then it was increased substantially after the binding of large molecules of DE2 antibodies. The binding of APP 770 to DE2 antibodies caused further increase in the mean roughness, mostlikely due to folding of long protein chains of APP 770. On the other hand, the roughness value was slightly value decreased after binding of much shorter Aβ<sub>1-16</sub> peptide to DE2 antibodies. Aβ<sub>1-16</sub> molecules may occupy the 'vallies' between adsorbed antibodies; and therefore make the surface become smoother. Generally the values of surface roughness correlates to the size (or molecular weight) of absorbed the molecules; e.g. PAH = 70 kDa, Protein G = 25 kDa, DE2 antibody = 120 kDa, APP = 115 kDa and Aβ = 1955 Da.

## 5.8 Summary

The main achievement of this part is the use of TIRE for the detection of  $A\beta_{1-16}$  in direct immunoassay with DE2 antibodies. The achieved of 0.05 ng/ml limit is very impressive and its open a clear possibility for detection of AD marker  $A\beta_{1-42}$ .

The detection of APP in a complex complete medium solution is another highlight of this work which demonstrate a possibility of detection of AD markers in biological fluid (serum, blood, brain fluid). The combination of methods of QCM and TIRE allows the evaluation of concentration of APP in CM which was originally unknown.

Two types of QCM measurements in liquid were explored for the detection of APP. The fully automated QCM in microfluidics flow and QCM impedance measurement able to detect 16 times dilution of APP. The binding of molecular layer caused the changes of surface roughness which was measured by AFM technique.

# CHAPTER 6

## THE DETECTION OF ZEARALENONE MYCOTOXIN USING TIRE METHOD

This chapter describes the detection of zearalenone mycotoxin (ZON) in both direct and competitive immunoassays format by TIRE methods. A new technology of polyelectrolyte microcapsules was also explored for purification of substances contaminated with ZON.

### 6.1. Sample Preparation

Cr/Au coated glass slides for TIRE measurements with a typical thickness of  $25\pm 5$  nm were prepared by thermal evaporation as described previously in Chapter 5. The gold surface was treated overnight with mercaptoethyl sodium sulfonate to enhance negative charge on the sensing surface. PAH and Protein A (both from Sigma-Aldrich) were used in this work for immobilization of antibodies. Other chemicals, namely ZON toxins, ZON-CONA conjugate (ZON hapten conjugated with Bovine Serum Albumin (BSA) and Conalbumin (CONA)) and ZON polyclonal antibody were provided by our collaborators from Hungary. All proteins were prepared using Tris-HCl buffer pH 7.5; the same buffer was used as a medium for single spectroscopic TIRE measurements and also for rinsing the TIRE cell after each absorption step. Purelab Maxima, 18.2 M $\Omega$  de-ionized water was used this experiment for solution preparation as well as for rinsing the cell after absorption of PAH. Different dilutions, i.e. 1:1000, 1:2000, 1:4000 and 1:8000, of ZON antibodies were tested and it was found that 1:2000 gave the best response. Therefore ZON antibodies in 1:2000 dilution were selected for both direct and competitive immunoassay in this work.

## 6.2. TIRE Direct Immunoassay for detection of ZON

Aqueous solutions of zearalenone (ZON) of different concentrations (1  $\mu\text{g/ml}$ , 100  $\text{ng/ml}$ , 10  $\text{ng/ml}$ , 1  $\text{ng/ml}$ , and 0.1  $\text{ng/ml}$ ) were prepared by multiple dilutions of 1  $\text{mg/ml}$  stock solution of ZON in methanol.

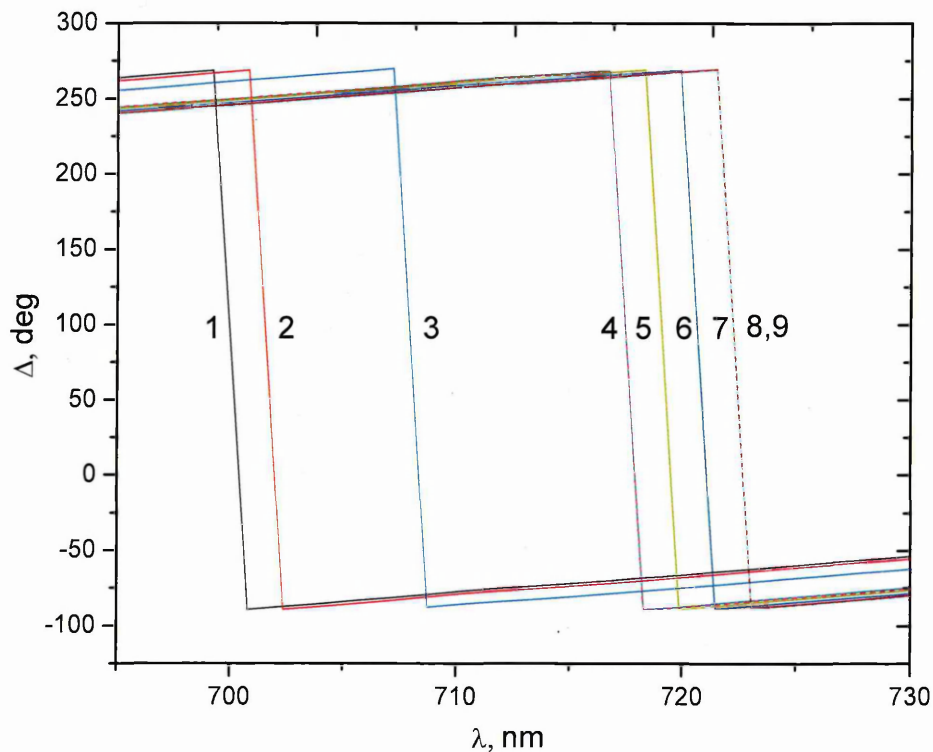


**Fig. 6.1.** TIRE spectra of  $\Delta$  recorded on bare Cr/Au surface (1), after adsorption of PAH (2), Protein A (3), Anti-ZON (4), and binding ZON from solutions of different concentration: 0.1  $\text{ng/ml}$  (5), 1  $\text{ng/ml}$  (6), 10  $\text{ng/ml}$  (7), 100  $\text{ng/ml}$  (8), and 1  $\mu\text{g/ml}$  (9).

A typical set of  $\Delta(\lambda)$  experimental spectra for ZON direct immunoassay in Fig. 6.1 shows a spectral shift caused by consecutive adsorption of layers of PAH, Protein A and ZON antibodies (anti-ZON) as well as by binding different concentrations of ZON to antibodies. The minimal detected concentration for ZON using direct immunoassay was 0.1  $\text{ng/ml}$ . TIRE data fitting allows the evaluation of the thickness values of the adsorbed layer using an established four-layer model as described in detail in Chapter 3. The calibration curve of thickness changes ( $\Delta d$ ) vs. ZON accumulated concentration ( $C$ )

obtained from the TIRE experiments is shown in Fig. 6.2. The thickness increment  $\Delta d$  was calculated in respect to the thickness of the absorbed layer after anti-ZON deposition (served as reference). The relatively large value of 2.5 nm for the maximal thickness changes (in comparison to the actual size of a ZON molecule of 0.5 – 0.7 nm) gives an insight into ZON molecule interaction and the formation of aggregates. The explanation of this fact may be related to the hydrophobicity of ZON molecules and thus their ability to form aggregates (similar to micelles) in aqueous solutions. The explanation of this fact may be related to the hydrophobicity of ZON molecules and thus their ability to form aggregates (similar to micelles) in aqueous solutions. As a result, antibodies bind not individual ZON molecules but to their aggregates. In terms of energy conservation, the  $\text{CH}_3$  groups tend to hide inside the micelle with their polar groups on the outer surface in contact with water. Such mechanism of the sensitivity boost was suggested earlier for T-2 mycotoxin and particularly for amphiphilic molecules of nonylphenol which form micelles in aqueous solutions [152,153].

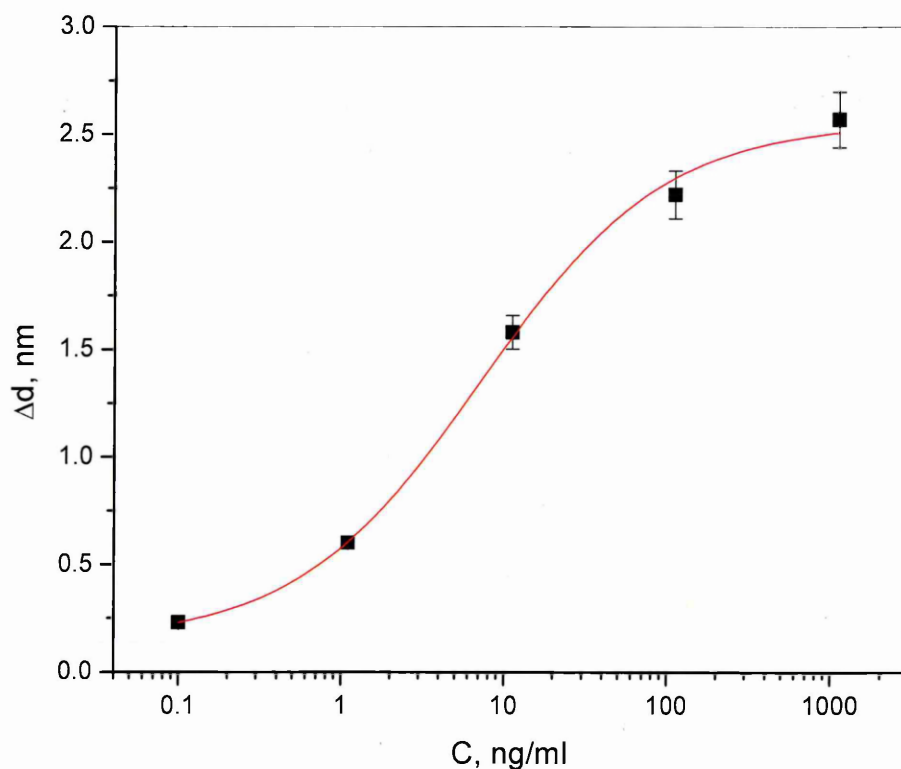


**Fig. 6.2.** TIRE calibration for direct immunoassay of Zearalenone.

### 6.3 TIRE Competitive Immunoassay for ZON

For competitive immunoassay, ZON-CONA conjugates, previously successfully applied in enzyme-linked immunosorbent assay (ELISA) format [178], were electrostatically immobilised on a surface of gold *via* a PAH layer. In order to block all remaining binding sites on the surface, an additional adsorption of ovalbumine (OVA) was carried out. Then a mixture of ZON antibodies (1:2000 diluted stock solution) and solutions of free ZON at different concentrations (100 ng/ml, 10 ng/ml, 1 ng/ml, 0.1 ng/ml, and 0.01 ng/ml) were injected into the cell. The mixtures were pre-incubated for 5 minutes before injecting.

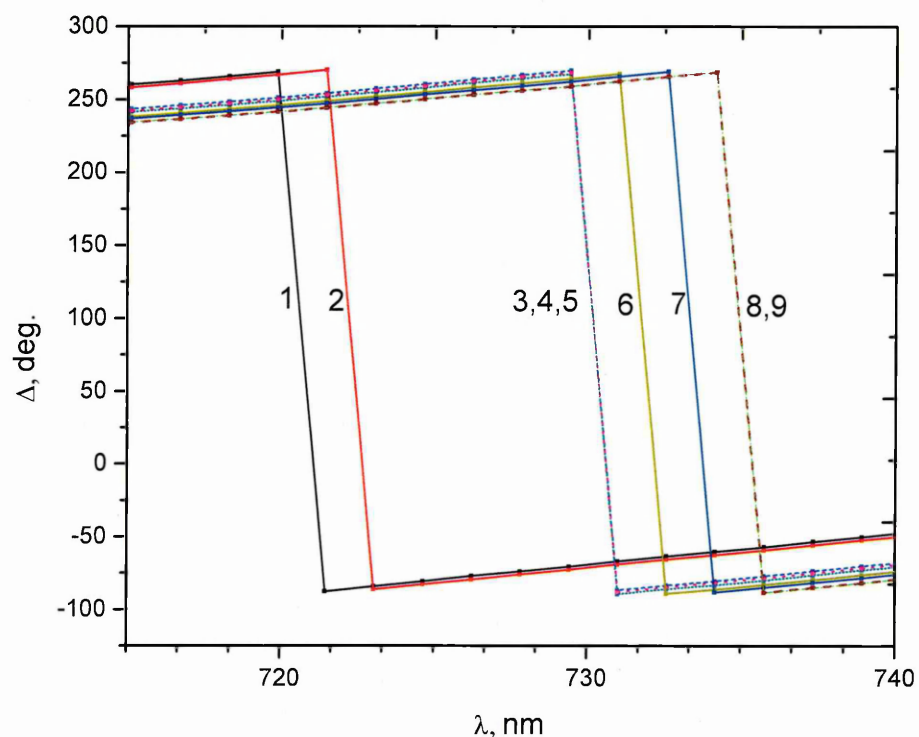


**Fig. 6.3.** Typical set of  $\Delta(\lambda)$  spectra measured on a bare Au surface (1), after adsorption of layers of PAH (2), ZON-CONA (3), OVA (4), and after binding ZON-Abs from pre-incubated mixtures containing ZON in different concentrations: 100 ng/ml (5), 10 ng/ml (6), 1 ng/ml (7), 0.1 ng/ml (8) and 0.01 ng/ml (9).

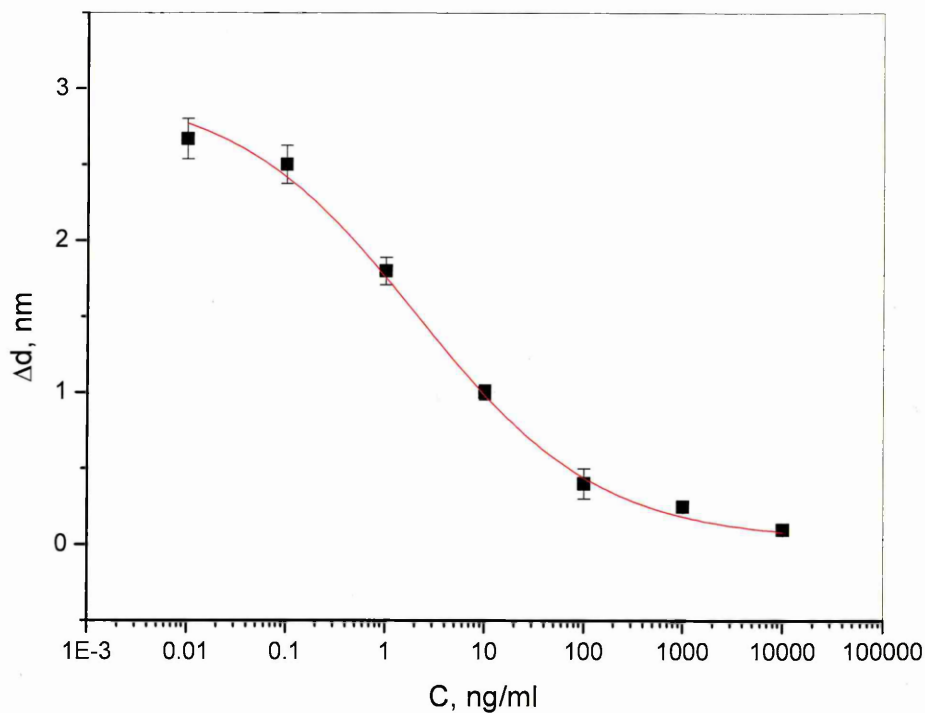


**Fig. 6.4.** Changes in the adsorbed layer thickness vs concentration of ZON (in the mixture with anti-ZON) obtained by fitting the TIRE data.

A typical series of  $\Delta(\lambda)$  spectra for ZON competitive immunoassay is shown in Fig. 6.3 in the sequence of Cr/Au, PAH, ZON-CONA, and anti-ZON mixed with free ZON at different concentrations of 100 ng/ml, 10 ng/ml, 1 ng/ml, 0.1 ng/ml, and 0.01 ng/ml. The dependence of the organic layer thickness increment ( $\Delta d$ ) obtained by TIRE data fitting against the concentration of ZON (10  $\mu\text{g/ml}$ , 1  $\mu\text{g/ml}$ , 100 ng/ml, 10 ng/ml, 1 ng/ml, 0.1 ng/ml, and 0.01 ng/ml) is shown in Fig. 6.4. The results given in Fig. 6.3 and 6.4 demonstrate the response is in reverse order to that shown for direct immunoassay in Fig. 6.1 and Fig. 6.2, where the highest concentration of ZON yields the lowest response. This is typical for competitive immunoassay, when ZON-CONA absorbed on the surface and free ZON molecules compete for antibodies in solution [178]. A detection limit of 0.01 ng/ml for ZON was found in this measurement. Usually, competitive immunoassay is about two to three orders of magnitude more sensitive than direct immunoassay. The obtained gain of just one order of magnitude might be due to

the aggregation of zearalenone molecules in aqueous solution, an effect which this time acted in the opposite direction.

#### 6.4 TIRE kinetics measurements for ZON

Typical kinetics of Anti-ZON interaction (direct immunoassay) are shown in Figs. 6.5 and 6.6 for 0.1 ng/ml and 100 ng/ml of ZON respectively. It is clearly seen that binding ZON from its 0.1 ng/ml solution to specific antibodies immobilised on the surface causes a measurable variation in  $\Delta$  values with a signal-to-noise ratio of about 7. It is important to note that changes in the variation of  $\Psi$  (with the same noise level) are about 10 times smaller than  $\Delta$ , which demonstrate once more the advantages of using phase dependent parameter,  $\Delta$ .

Following the procedure described in detail in Chapter 3, all kinetics curves recorded for different concentrations of ZON plotted in semi-logarithmic co-ordinates are linear with the slope (gradient)  $S$  linearly dependent on the analyte concentration ( $C$ ):

$$S = k_a C - k_d,$$

where  $k_a$  and  $k_d$  are the rates of adsorption and desorption, respectively.

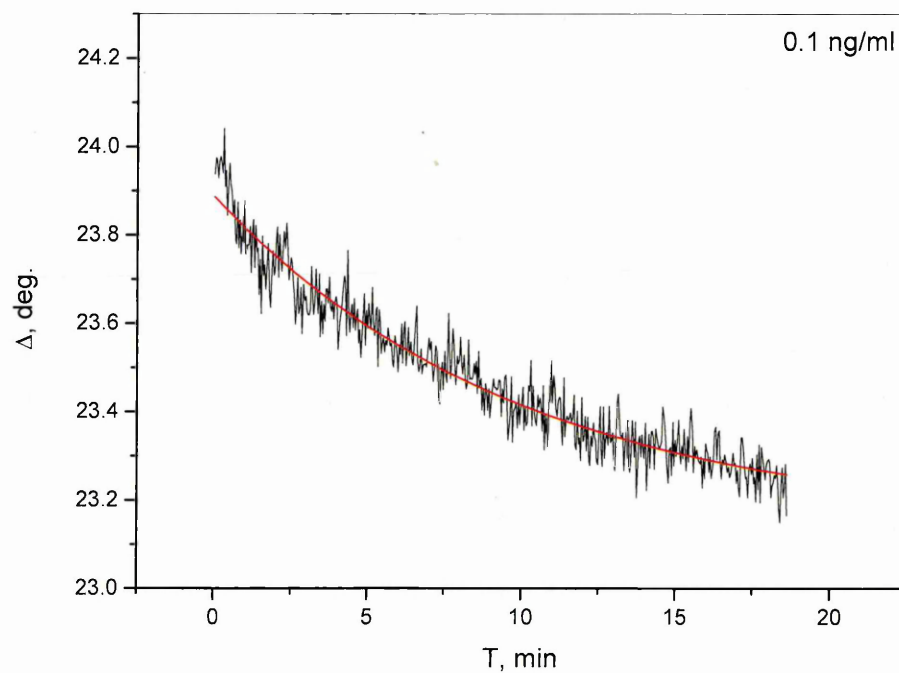
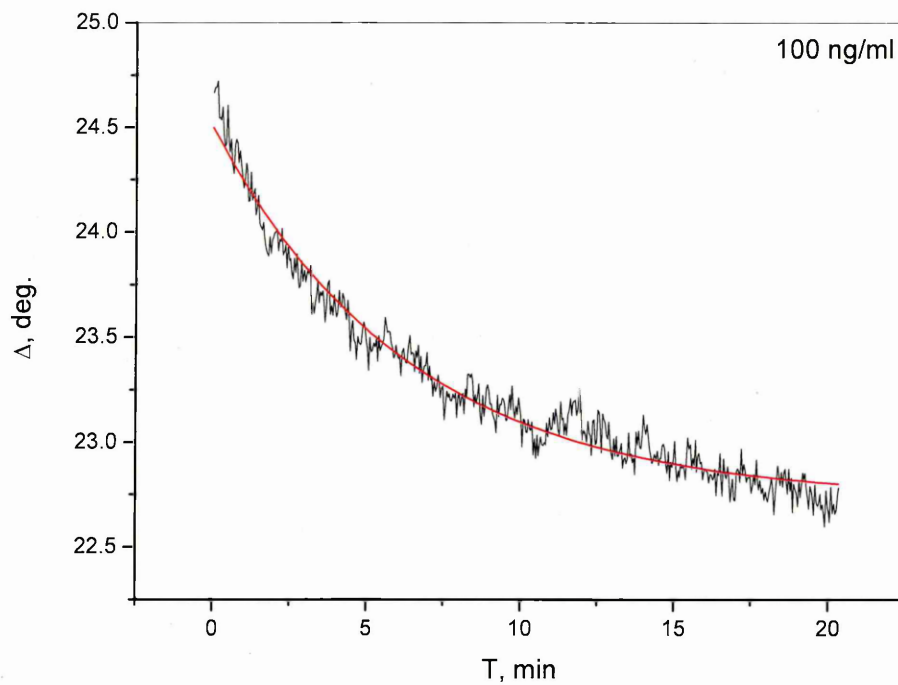
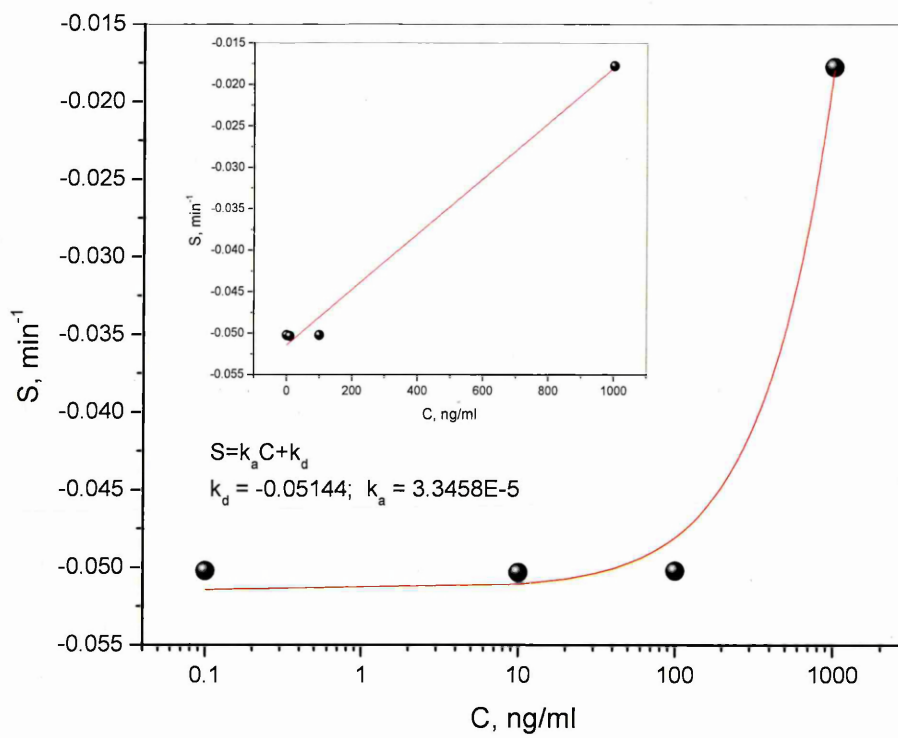


Fig. 6.5. TIRE  $\Delta$  kinetics during binding 0.1 ng/ml of ZON



**Fig. 6.6.** TIRE kinetic during binding 100 ng/ml of ZON



**Fig. 6.7.** Graphical evaluation of parameters  $k_a$  and  $k_d$ .

The  $S$  vs  $C$  graph obtained for ZON direct immunoassay is given in Fig. 6.7 in both linear and semi-logarithmic co-ordinates. The values of  $k_a = 177.52$  ( $l \cdot mol^{-1} \cdot s^{-1}$ ) and  $k_d = 8.57 \cdot 10^{-4}$  ( $s^{-1}$ ) were obtained, respectively, from the gradient and intercept of the linear graph. The value of the association constant  $K_A = k_a/k_d = 2.10^5$  ( $l \cdot mol^{-1}$ ) is therefore evaluated as calculated in detail in Table 6.1. This is slightly lower than the values of  $K_A$  in the range of  $10^6$ - $10^7$  ( $l \cdot mol^{-1}$ ) but still characteristically high for binding antigens to polyclonal antibodies.

**Table 6.1:** ZON Affinity calculation

$k_a, mol^{-1} \cdot l \cdot s^{-1}$ $k_d, s^{-1}$
$y_{result} = 3.3458 \cdot 10^{-5} x + 0.05144$ $k_a = 0.00003346 \left[ \frac{ml}{ng \cdot min} \right] = 0.00003346 \cdot \frac{10^{-3}}{10^{-9} \cdot 60} \left[ \frac{l}{g \cdot s} \right] = 0.5577 \left[ \frac{l}{g \cdot s} \right]$ $k_a = 0.5577 \cdot 318 = 177.52 \left[ \frac{l}{mol \cdot s} \right]$ $k_d = 0.05144 \left[ \frac{1}{min} \right] = \frac{0.05144}{60} = 0.000857 \left[ \frac{1}{s} \right]$ <p style="text-align: center;"><math>MW = 318</math> Da</p>
$K_A, l/mol, K_D, mol/l$
$K_A = \frac{k_a}{k_d} \left[ \frac{l \cdot s}{mol \cdot s} \right]$ $K_A = \frac{177.52}{0.000857} = 2.07 \cdot 10^5 \left[ \frac{l}{mol} \right]$ $K_D = \frac{1}{K_A} = \frac{1}{2.07 \cdot 10^5} = 4.83 \cdot 10^{-6} \left[ \frac{mol}{l} \right]$

## 6.5 Polyelectrolyte Microcapsules for ZON Purifying

In this work, a new approach of tackling the problem of contaminated liquid by mycotoxin was proposed by exploring polyelectrolyte micro-capsules which were invented quite recently [179] with the main purpose of controlled drug delivery [180]. The main idea of this is to use polyelectrolyte microparticles modified with antibodies which then bind specifically to particular mycotoxin molecules and remove them from the solution.

### 6.5.1 Microcapsules Preparation

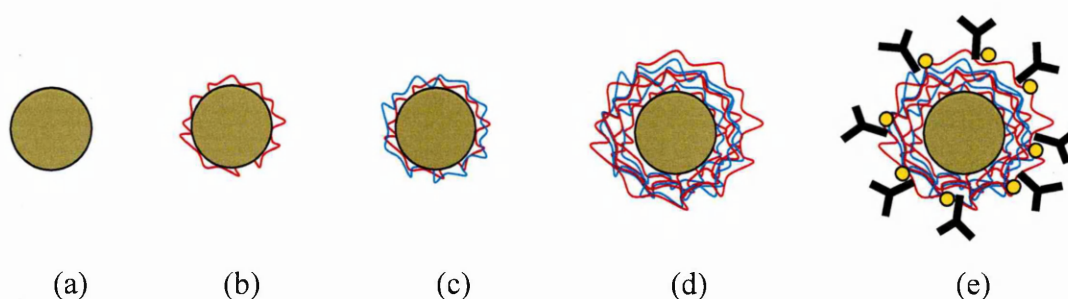


**Fig. 6.8.** Fabrication and functionalization of polyelectrolyte microcapsules.

The fabrication of polyelectrolyte-coated microparticles is shown schematically in Fig. 6.8. Functionalized microparticles were prepared by consecutive coating the  $\text{MnCO}_3$  core particles of 2, 4 and 6  $\mu\text{m}$  in diameter (PlasmaChem GmbH, Berlin) with layers of poly-styrene sulfonate (PSS) and poly-allylamine hydrochloride (PAH). The templates were first coated with a PSS layer by adding 2 mg/ml aqueous solution of PSS to the templates suspension in a ratio of 1:1, stage (b). After stirring the mixture for 5 minutes, the suspension was left undisturbed for 30 minutes. This time interval was sufficient for quite heavy particles of 2 and 4  $\mu\text{m}$  in diameter to sediment on the bottom of a sample tube, leaving a clear solution on top. This clear solution was then removed with a micropipette, the sample tubes were topped up with de-ionized water (Purelab Maxima, 18.2  $\text{M}\Omega$ ), and shaken for 5 minutes, then left to sediment for another 30 minutes. This rinsing procedure was repeated three times before adding 2 mg/ml aqueous solution of PAH. The procedure of depositing a PSS-PAH bilayer was repeated three to four times,

stage (c). After two bi-layers of PSS–PAH were deposited, 2 mg/ml solution of NaCl was added to the mixture with PAH and PSS; this increases the thickness of the shell and improves the adhesion between polyelectrolyte layers. After depositing another two PSS–PAH bi-layers containing NaCl the polyelectrolyte shell was complete, stage (d). Then the capsules were modified with layers of protein A and anti–ZON. Triple rinsing in Triz–HCl after immobilization of Protein A and anti-ZON was carried out using Triz–HCl buffer at pH 7.5, and finally the capsules were ready for use, stage (e).

### 6.5.2 SEM analysis of $\text{MnCO}_3$ microcapsule

Scanning Electron Microscope (SEM) microcapsule images were acquired using a Zeiss SUPRA 40 SEM instrument. In order to minimize electrical charging of the surface during SEM study, a low energy (1 keV) of electrons was used [181]. The samples for SEM study were prepared by casting the solution containing functionalized microparticles on clean pieces of a silicon wafer. For SEM study, antibodies were immobilised on the surface of microparticles via a layer of glutaraldehyde which provides much stronger covalent binding of antibodies.

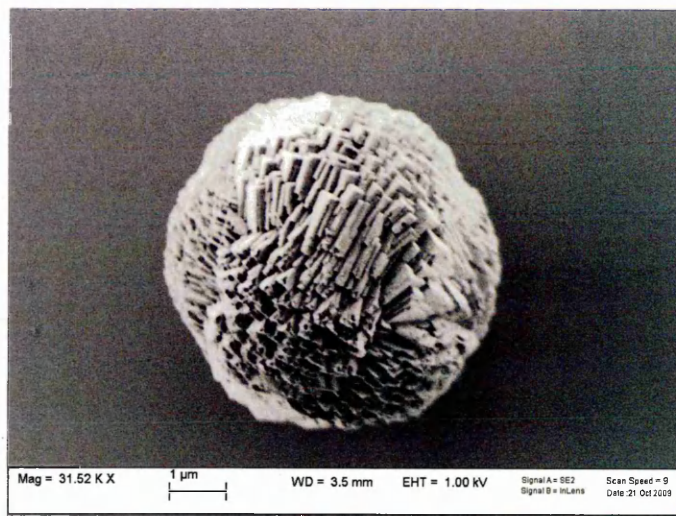


**Fig. 6.9.** SEM images of 6  $\mu\text{m}$   $\text{MnCO}_3$  microparticles coated only with polyelectrolyte layers.

SEM images in Fig. 6.9 show a 6  $\mu\text{m}$  polyelectrolyte coated microparticle; the same particles functionalized with Protein A and Anti-ZON are shown in Figs. 6.10 and 6.11 at different magnifications. The deposition of protein A and antibodies is clearly seen on SEM images as "goose bumps" with a size of 30 to 80 nm. These objects are slightly larger than individual protein molecules and most likely represent protein aggregates. Fig. 6.12 shows SEM image of capsules after exposure to ZON. As one can see, the outer layer of the capsules was splashed away after reaction with ZON.

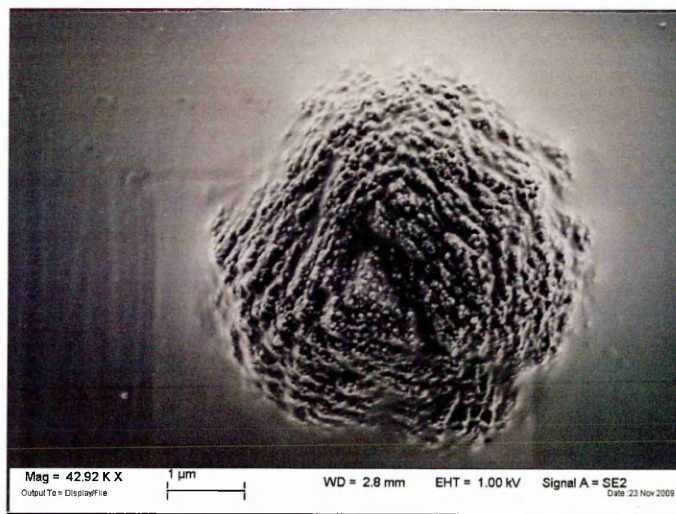


**Fig. 6.10.** A particle with antibodies to zearalenone immobilised on the surface via glutar aldehyde;

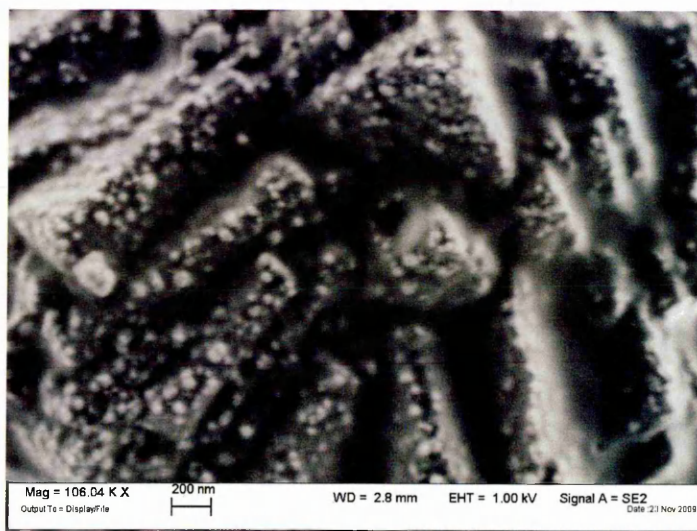


**Fig. 6.11.** The same object as in Fig.6.8 at higher magnification

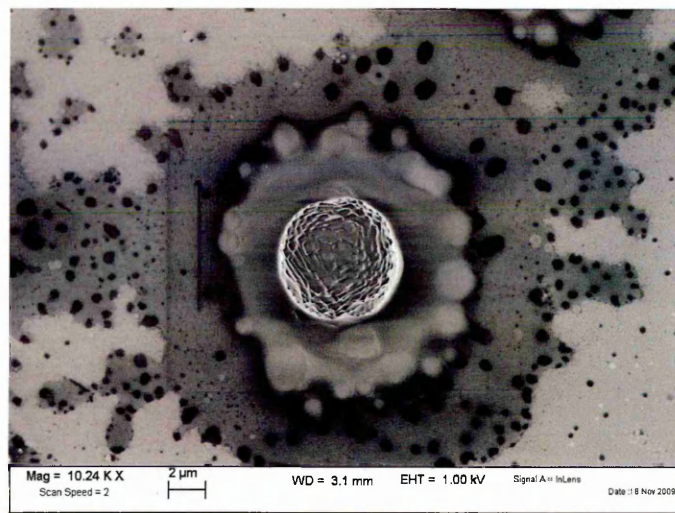


**Fig. 6.12.** Capsule splash reaction on glutar aldehyde.

### **6.5.3 ZON Purifying Result by UV-vis Spectrophotometer**

For extraction of ZON, the suspension of capsules modified with anti-ZON (as in Fig. 6.8) was mixed with a solution containing ZON. It was stirred for 5 minutes and then left undisturbed for up to 30 minutes. The optical absorption spectra were recorded on samples of untreated solution of ZON as well as after treatment with anti-ZON coated microcapsules using Cary 50 UV-vis spectrometer from Varian at various times. The results are shown in Fig. 6.13.

The original spectra of the solution containing 5  $\mu\text{g/ml}$  of ZON (curve 1, Fig. 6.13) shows three characteristic absorption bands of zearalenone at 235 nm, 270 nm, and 310 nm. The exposure of ZON solution to anti-ZON modified capsules for 1, 5, and 90 minutes resulted in a progressive reduction in the intensity of all three spectral bands; the reduction in the intensity of the first band (235 nm) is the most pronounced. This result is a clear indication of the reduction of concentration of ZON in the residual solution is caused by binding of ZON molecules to the anti-ZON on the surface of microcapsules followed by sedimentation of microcapsules and subsequent purification of the solution.

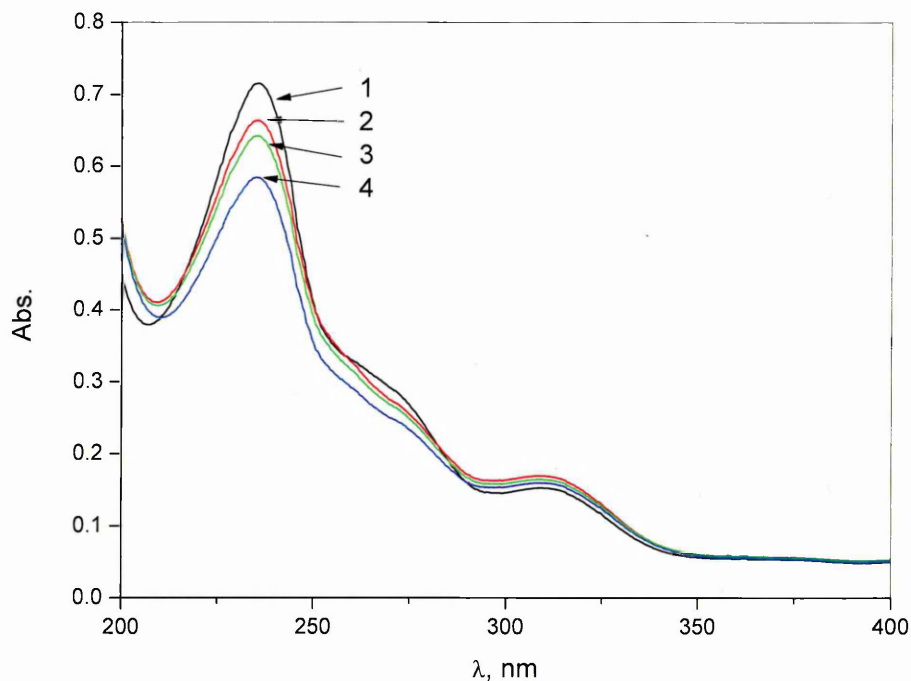


**Fig. 6.13.** UV–vis absorption spectra of 5 µg/ml aqueous solution of zearalenone: untreated ZON solution (1) and solution treated with polyelectrolyte microcapsules modified with Ant-ZON for 1 min (2), 5 min (3), and 90 min (4).

## 6.6 Summary

In this work, a small molecular weight mycotoxins, zearalenone (ZON), was detected using TIRE method. A comparison of results for direct and competitive assay showed the limits of detection obtained of 0.1 ng/ml and 0.01 ng/ml, respectively. Usually competitive assay gives much higher sensitivity, but in this case the immune reaction was affected by the aggregation of hydrophobic molecules of ZON. The aggregates (such as micelles) can be formed during the dilution of the original stock solution of ZON in methanol with water. The immune reaction actually happened between the antibody and the aggregate of a number of ZON molecules. It is interesting that such a reaction boosts the sensitivity of detection in the case of direct immunoassay, while reducing the response in competitive immunoassay experiments.

The affinity of ZON towards specific polyclonal antibodies was analyzed by TIRE kinetics and gave the association constant,  $K_A = 2.07 \cdot 10^5 \text{ l mol}^{-1}$ . This is not as high as typically observed for monoclonal antibodies and it could be explained by a combined results of aggregation of ZON molecules and the reduced affinity of polyclonal antibodies.

A toxin-filtering technique using functionalized polyelectrolyte microcapsules may provide an alternative way for toxin extraction from contaminated liquid. A capsule of 2 – 6  $\mu\text{m}$  in diameter functionalized with specific antibodies bind toxin molecules in contaminated liquid. After a certain period of time, the capsules with bound toxins sediment, leaving a clear solution behind. Further work is required for more detailed study of the reactions between microcapsules and toxins and possible future biomedical applications of this method.

## CHAPTER 7

### DETECTION OF AFLATOXIN B1 USING TIRE COMBINED WITH DIRECT IMMUNOASSAY.

This chapter describes the detection of Aflatoxin (AFT) B1 using cost effective direct immunoassay format. The method of TIRE allows the detection at very low concentrations of AFT which is not possible by any other optical method. The AFM images give evidence of aggregation of AFT molecules.

#### 7.1 Sample preparation

The same method of sample preparation for TIRE measurements was used here (see details in Chapter 5). Monoclonal antibodies specific to aflatoxin B1 were electrostatically attached to the surface via a polycation layer of poly(allylamine hydrochloride) (PAH). An intermediate layer of protein A molecules having a binding site to the second domain of the IgG-type antibodies were used to orient antibodies with their Fab fragments towards the solution. As described earlier in Chapter 5 and Chapter 6, the immobilization of antibodies (Abs) was carried out by consecutive injections of solutions of PAH, protein A, and antibodies into the cell. Then, the immune reaction between Abs and aflatoxin B1 (AFB1) was studied by performing a series of injections of solutions containing different concentrations of AFB1 (starting from the smallest concentration). An incubation time of 15 min was typically used in all adsorption and binding stages; the cell was rinsed after each adsorption step by purging Tris-HCl buffer solution (10 times the cell volume) through the cell. De-ionized water (Purelab Maxima, 18.2 M $\Omega$ ) was used for rinsing the cell after adsorption of PAH.

All the chemicals used were purchased from Sigma-Aldrich. A PAH solution of 2 mg/ml in de-ionized water was used; solutions of protein A (0.02 mg/ml) and Anti-AFT (1:1000) in Tris-HCl buffer pH 7.5 were selected. Aflatoxin B1 was provided by our collaborator from Ukraine. Aqueous solutions of aflatoxin B1 of different concentrations (400 ng/ml, 40 ng/ml, 4 ng/ml, 0.4 ng/ml, and 0.04 ng/ml) were prepared by multiple dilutions of the 1 mg/ml stock solution of aflatoxin B1 in methanol. Such dilutions, ranging from 1:2500 down to  $1:2.5 \cdot 10^7$ , give negligibly small residual concentration of methanol which cannot affect the activity of antibodies immobilized on the surface.

## 7.2 TIRE spectra for Aflatoxins direct immunoassay

TIRE experimental set-up described earlier in Chapter 3 and shown in Fig. 3.9 was used here. Figure 7.1 shows a typical set of  $\Delta(\lambda)$  spectra after consecutive absorption of PAH, Protein A, Anti-AFB1 and different concentrations of AFB1 (0.04 ng/ml – 400 ng/ml).

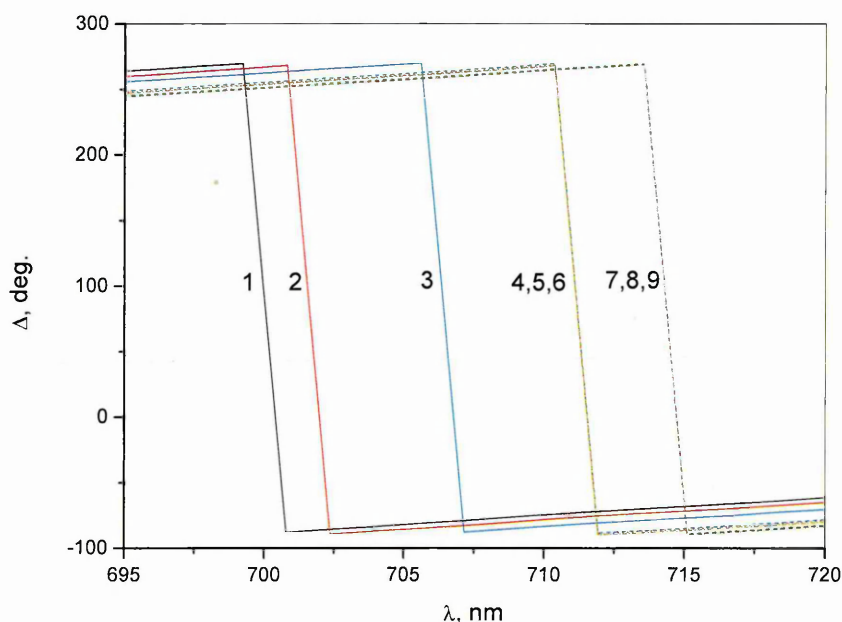


**Fig. 7.1.** Original set of  $\Delta(\lambda)$  spectra recorded on bare Cr/AU layer (1), after adsorption of PAH (2), Protein A (3), Anti-AFB1 (4), and after binding AFB1 of different concentrations: 0.04 ng/ml (5), 0.4 ng/ml (6), 4 ng/ml (7), 40 ng/ml (8), 400 ng/ml (9).

The correction of all negative values of  $\Delta$  by adding  $360^\circ$ , allowed us to improve the sensitivity of detection; the small spectral shift (smaller than the wavelength increment), which is normally not resolved in original  $\Delta(\lambda)$  spectra (Fig. 7.1), becomes visible after such alteration.

A typical set of corrected  $\Delta(\lambda)$  spectra in Fig. 7.2 shows the spectral shift caused by consecutive adsorption of layers of PAH, Protein A, antibodies specific to aflatoxin (Ab-AFB1), as well as by binding different concentrations of aflatoxin to Ab-AFB1 starting from the smallest, 0.04 ng/ml, up to 400 ng/ml. A small section of the  $\Delta$  spectra set was magnified to deliver the required resolution and is presented in Fig. 7.3. The values of thickness for all adsorbed layers were obtained by TIRE data fitting and are summarized in Table 7.1.

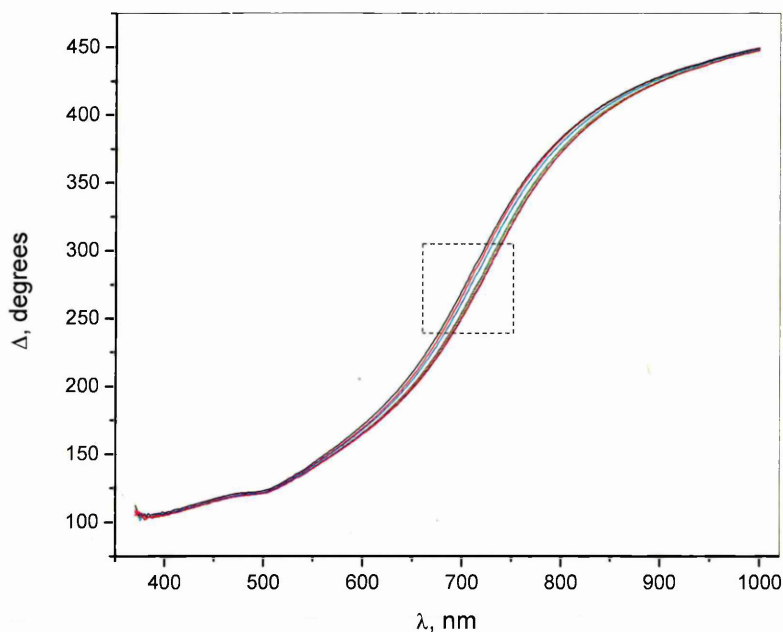


**Fig. 7.2.** A typical set of corrected  $\Delta(\lambda)$  spectra recorded on a bare surface of Cr/Au layer, after adsorption of layers of PAH, Protein A, Anti-AFB1, and after binding of different concentrations of AFB1.

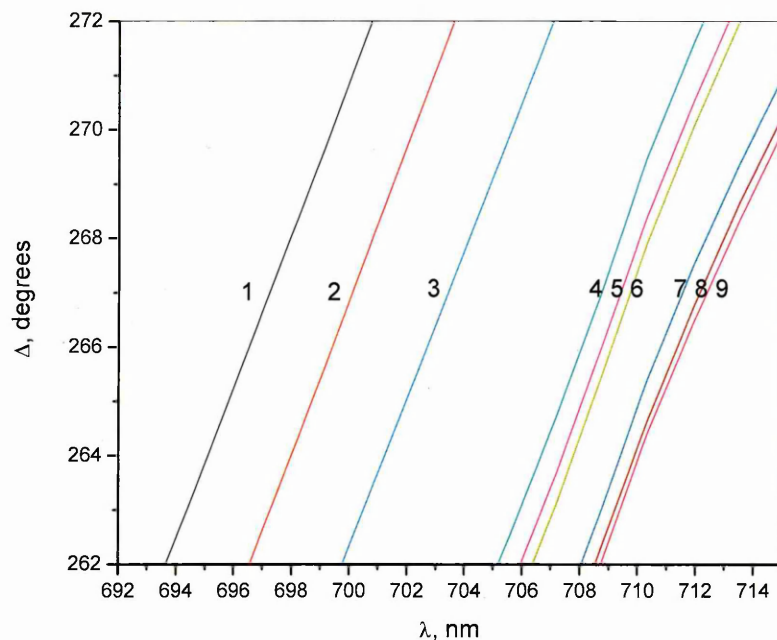


**Fig. 7.3.** Zoomed- in section of corrected  $\Delta(\lambda)$  spectra recorded on bare surface of Cr/Au layer (1), after adsorption of layers of PAH (2), protein A (3), Anti-AFB1 (4), and after binding AFB1 of different concentrations: 0.04ng/ml (5), 0.4ng/ml (6), 4ng/ml(7), 40 ng/ml (8), and 400 ng/ml (9).

**Table 7.1.** The parameters of layers obtained by TIRE fitting

Asterisks in the table indicate that the values were fixed during fitting.

Layer	$d$ (nm)	$\Delta d$ (nm)	$n, k$ (at $\lambda=633$ nm)
Cr/Au	30.349*		
PAH	1.267±0.034	1.267	$n^*=1.42; k^*=0$
Protein A	2.660±0.015	1.393	$n^*=1.42; k^*=0$
Anti-AFT	4.994±0.004	2.334	$n^*=1.42; k^*=0$
AFT, accumulated concentration (ng/ml)			
0.04	5.277±0.094	0.283	$n^*=1.42; k^*=0$
0.44	5.440±0.050	0.446	$n^*=1.42; k^*=0$
4.44	6.292±0.036	1.298	$n^*=1.42; k^*=0$
44.44	6.456±0.043	1.462	$n^*=1.42; k^*=0$
444.44	6.544±0.049	1.550	$n^*=1.42; k^*=0$

### 7.3 TIRE data fitting for Aflatoxin B1 direct immunoassay

The calibration curve for aflatoxin binding is shown in Fig. 7.4 as a dependence of the thickness increment *vs.* accumulated concentration of aflatoxin. The minimal detected concentration of aflatoxin was found to be 0.04 ng/ml. The sigmoid-type calibration curve in Fig. 7.4 is typical for immune reactions and was observed earlier for other mycotoxins [152,153,182].

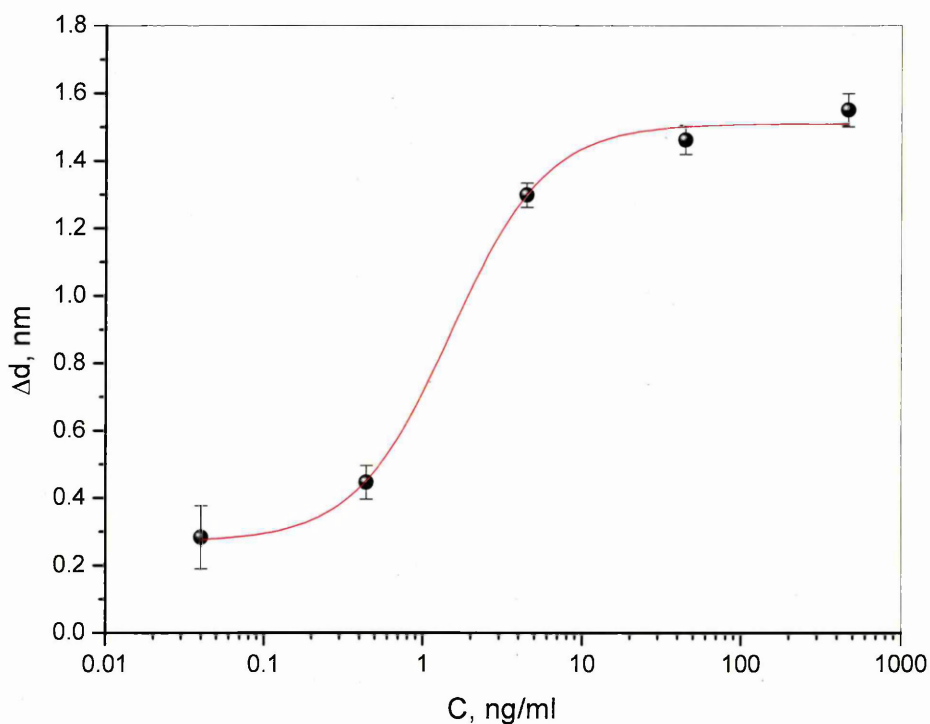


**Fig. 7.4.** Changes in the adsorbed layer thickness *vs.* accumulated concentration of aflatoxin obtained by fitting the TIRE data.

The linear range is quite narrow (from 0.4 ng/ml to 40 ng/ml) and appears to be characteristic for binding other mycotoxins to specific monoclonal antibodies. The maximal thickness increment (at saturation) is about 1.5 nm which is larger than expected for binding rather small molecules of aflatoxin (having dimensions about 0.8×0.5 nm). Similar observations were reported earlier for T-2 mycotoxins (5.5 nm thickness increase) [152], zearalenone (2.5 – 2.7 nm) [182], and nonylphenol (25 nm) [153]. The explanation of this fact lies in the hydrophobicity of the investigated molecules and thus their property to form aggregates in aqueous solutions when the

original stock solution of mycotoxins in methanol was diluted in water. As a result, the antibodies capture not individual molecules of aflatoxin but their aggregates; this effect enhances significantly the sensor response. Such mechanism of the sensitivity boost was proposed earlier for T-2 mycotoxin and particularly for amphiphilic molecules of nonylphenol which form micelles in aqueous solutions [146,153].

Pseudo-3D AFM images in Fig. 7.5 and Fig. 7.6 directly confirm the formation of aggregates of T-2 mycotoxin molecules [152]. The same model can be applied here to explain the observed 1.5 nm thickness increase for aflatoxin, as shown in Table 7.1.

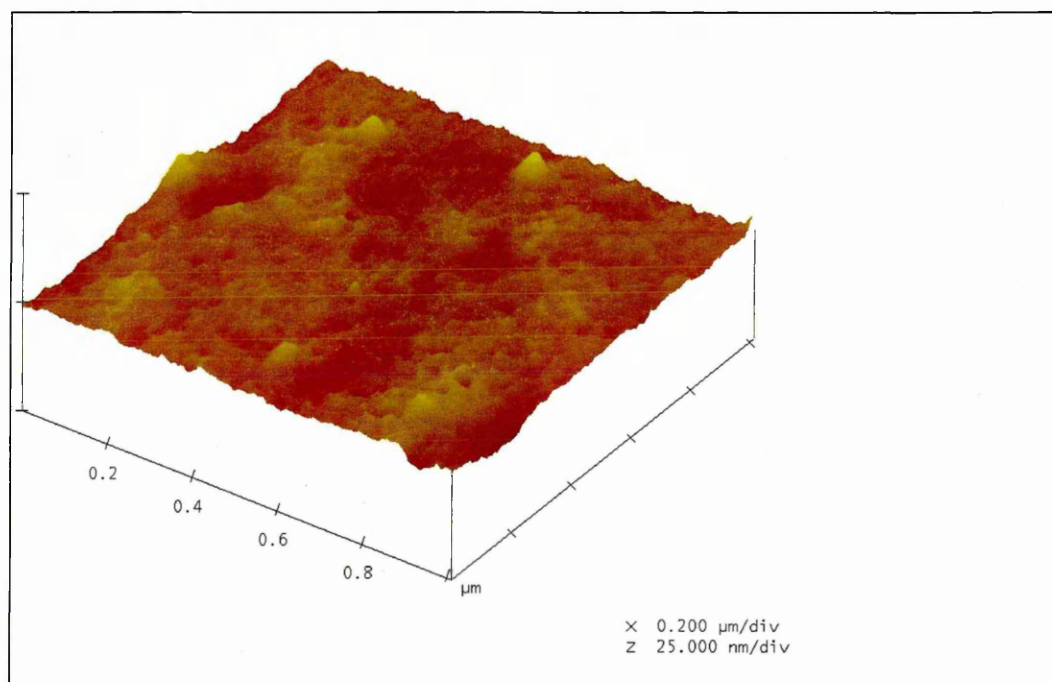


**Fig. 7.5.** Tapping mode AFM images of a layer of monoclonal antibodies to T-2 mycotoxin immobilized on the surface of gold via PAH-Protein A [152].

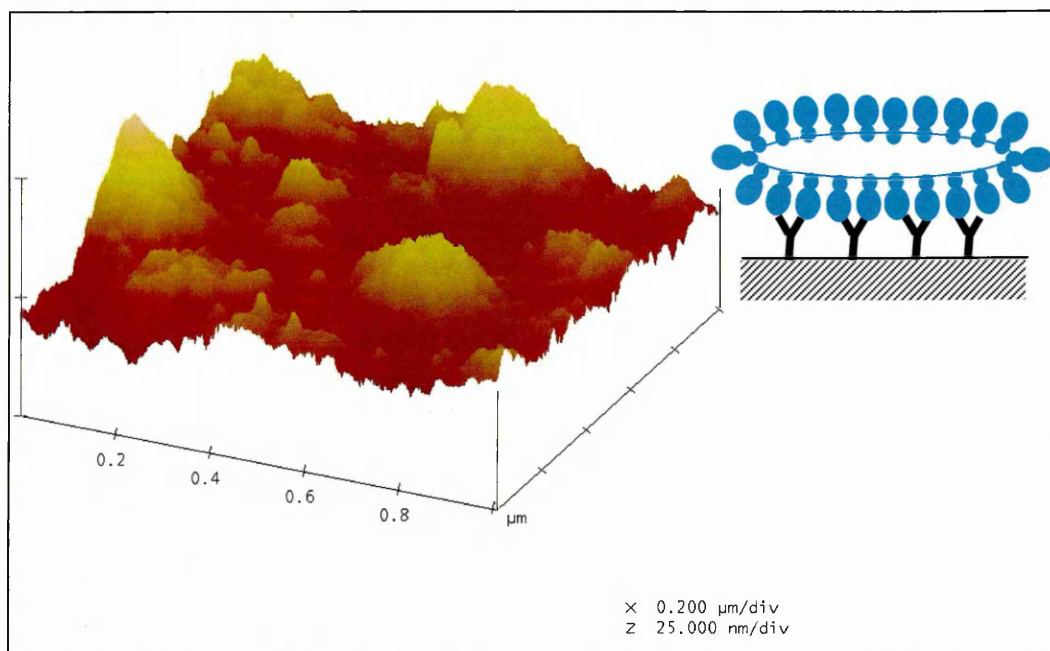


**Fig. 7.6.** The same sample after binding T-2 mycotoxin from 0.5  $\mu\text{g/ml}$  aqueous solution. Inset shows a model of mycotoxins aggregate (micelle) bound to specific antibodies [152].

#### 7.4 Kinetics of the Aflatoxin Immune Reaction

Typical kinetics of the binding of aflatoxin at 400 ng/ml to specific monoclonal antibodies is shown in Fig. 7.7. The binding of aflatoxin causes about  $0.6^\circ$  variation (decrease) in  $\Delta$ , while the variation (increase) in  $\Psi$  is much smaller ( $\sim 0.08^\circ$ ) with the same noise level of about  $0.03^\circ$  for both  $\Delta$  and  $\Psi$ . As a result, a signal-to-noise ratio of 20 for  $\Delta$  measurements appeared to be much better than 2.6 for  $\Psi$  measurements. This proves once again the advantages of using  $\Delta$  measurements in TIRE.

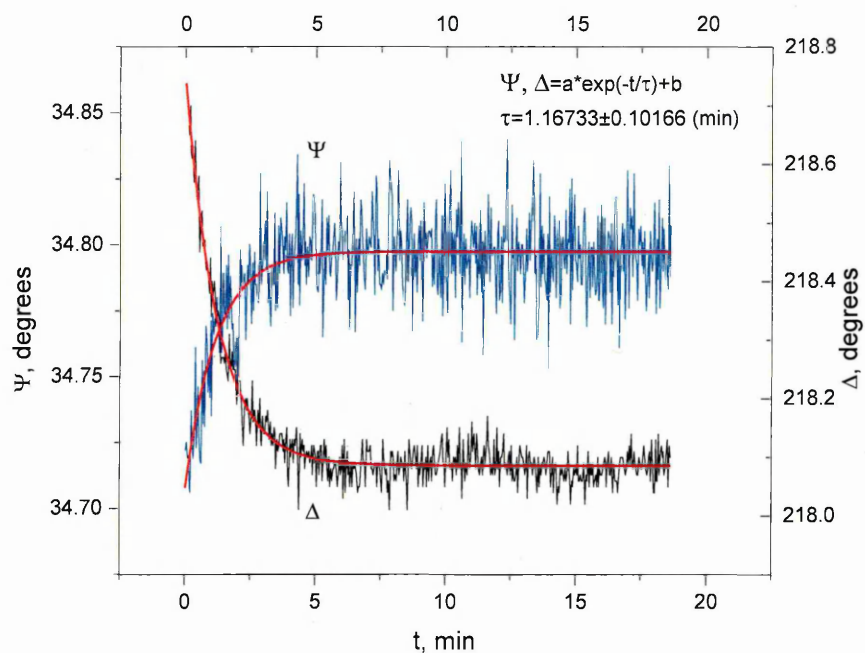


**Fig. 7.7.** Typical time dependencies of  $\Psi$  and  $\Delta$  caused by binding of 400 ng/ml of aflatoxin to specific antibodies immobilised on the surface.

The quite laborious procedure of dynamic measurements and graphical solving of the differential equation for adsorption was simplified in this work. First of all, instead of investigating the adsorption kinetics starting from a fresh surface (free from adsorbed molecules), we used consecutive adsorptions in steps starting from the smallest concentration of the toxin (in our case: 0.04, 0.4, 4, 40, 200, 300 and 400 ng/ml). Such an approach saves both time and expensive bio-chemicals (antibodies).

The kinetic curves for adsorption of aflatoxin of different concentrations (see example in Fig. 7.7) were fitted to exponential function  $\psi$  and  $\Delta = a \cdot \exp(-t/\tau) + b$  in order to evaluate the values of time constant ( $\tau$ ).

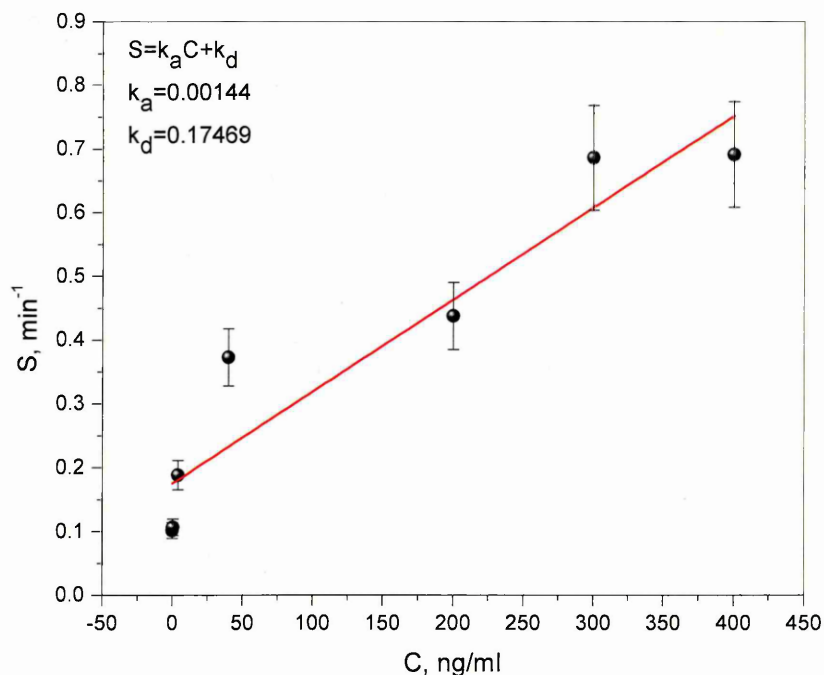


**Fig. 7.8.** Graphical evaluation of parameters  $k_a$  and  $k_d$ .

The obtained dependence of  $1/\tau = k_a C + k_d$  vs.  $C$  shown in Fig. 7.8 was treated as linear, and the values of  $k_a = 7488$  ( $l \text{ mol}^{-1} \cdot s^{-1}$ ) and  $k_d = 2.9115 \cdot 10^{-3}$  ( $s^{-1}$ ) were obtained, respectively, from the gradient and intercept of this line. The association constant  $K_A = k_d/k_d = 2.5719 \cdot 10^6$  ( $l \text{ mol}^{-1}$ ) and affinity constant  $K_D = k_d/k_a = 3.8882 \cdot 10^{-7}$  ( $\text{mol} \text{ l}^{-1}$ ) were therefore evaluated for the immune reaction of binding aflatoxin to specific antibodies (as in Table 7.2). The values obtained are similar to those discussed in Chapter 6 for zearalenone and reported previously for T-2 mycotoxin [152] which is typical for highly specific immune reactions. This is an interesting fact which confirms that binding of large aggregates of aflatoxin molecules to antibodies is still highly specific.

Table 7.2. Affinity constant analysis from TIRE kinetic data

$C$ , ng/ml	$S$ , 1/min	$k_a$ , $\text{mol}^{-1} \cdot \text{l} \cdot \text{s}^{-1}$ $k_d$ , $\text{s}^{-1}$
0.04	0.1018	$k_a = 0.00144 \left[ \frac{\text{ml}}{\text{ng} \cdot \text{min}} \right] =$ $= 0.00144 \cdot \frac{10^{-3}}{10^{-9} \cdot 60} \left[ \frac{\text{l}}{\text{g} \cdot \text{s}} \right] = 24 \left[ \frac{\text{l}}{\text{g} \cdot \text{s}} \right]$ $k_a = 24 \cdot 312 = 7488 \left[ \frac{\text{l}}{\text{mol} \cdot \text{s}} \right]$ $k_d = 0.17469 \left[ \frac{1}{\text{min}} \right] = \frac{0.17469}{60} = 0.002911 \left[ \frac{1}{\text{s}} \right]$ $MW = 312 \text{ Da}$
0.4	0.1068	
4	0.1885	
40	0.3728	
200	0.4376	
300	0.6860	
400	0.6912	
$y_{\text{result}} = 0.00144x + 0.174$		
		$K_A$ , l/mol, $K_D$ , mol/l
		$K_A = \frac{k_a}{k_d} \left[ \frac{\text{l} \cdot \text{s}}{\text{mol} \cdot \text{s}} \right]$ $K_A = \frac{7488}{0.00291} = 2.5719 \cdot 10^6 \left[ \frac{\text{l}}{\text{mol}} \right]$ $K_D = \frac{1}{K_A} = \frac{1}{2.5719 \cdot 10^6} = 3.8886 \cdot 10^{-7} \left[ \frac{\text{mol}}{\text{l}} \right]$

## 7.5 Summary

The method of TIRE once again proved to be very useful for detection of aflatoxin, which is another low molecular weight toxin analyte from the mycotoxin family. The minimal detected concentration of aflatoxin B1 is 0.04 ng/ml, which is quite remarkable and well-below the EU legislated limit. An additional boost of sensitivity can be attributed to the hydrophobic nature of aflatoxin molecules which tend to form aggregates in aqueous solutions. Such behaviour is typical for other hydrophobic toxins, such as mycotoxins (T-2 and zearalenone) and alkylphenols (nonylphenol) [152,153,182]. The method of preparation of aflatoxin solutions used in this work, i.e.

dilution of the original stock solution in organic solvents with deionised water, can be used in future for boosting the sensitivity of the immunosensing of other hydrophobic molecules.

The study of the kinetics of the immune reaction between aflatoxin aggregates and specific monoclonal antibodies allowed the evaluation of the association and affinity constants, which were found to be of  $2.5719 \cdot 10^6$  ( $l \cdot mol^{-1}$ ) and  $3.8882 \cdot 10^{-7}$  ( $mol/l$ ), respectively. Such values are similar to those obtained for other mycotoxins and, in general, typical for immune reactions, which confirms once again that immune binding of aggregates of hydrophobic molecules (such as aflatoxin) is still highly specific.

# CHAPTER 8

## CONCLUSIONS AND FUTURE WORK

### 8.1 Conclusions

The volume of chemicals required for performing bio-sensing is one of the important criteria to consider in minimizing the cost of raw materials and preparation time. The typical volume used for bio-sensing applications devices is in the microlitre range. In this work, a new total internal reflection ellipsometry (TIRE) cell that consumes about 200  $\mu\text{l}$  (ten times smaller than the older version) of the bio-chemicals was designed. By using a small capillary tube and a special needle for connection to the syringe the effect of bubbles produced during injection was minimized. A bracket which fixed the cell to the J. A. Woollam ellipsometer sample stage was able to reduce the problem of cell movement during injection.

The cell was successfully used in TIRE immunosensing. In this work, TIRE was used as the main detection method for Alzheimer's disease diagnostic. The binding of monoclonal DE2 antibodies towards Amyloid Precursor Protein 770 (APP770) was investigated in direct immune assay. It was shown that this method is able to detect a small concentrations (16-times diluted sock solution of unknown concentration) of Amyloid Precursor Protein (APP 770) in a complex medium (containing salts, minerals and other proteins). Complementary quartz crystal microbalance (QCM) method enabled the estimation of the original concentration of APP as 121  $\text{pmol l}^{-1}$ .

The detection of  $\text{A}\beta_{1-16}$  is very low concentrations of 0.05 ng/ml in direct immune assay is very impressive. This remarkable fact is due, first of all, to the high sensitivity of the TIRE method and, secondly, to improved data analysis. The affinity constant for the

reaction of  $A\beta_{1-16}$  towards monoclonal DE2 antibodies  $K_A = 1.78 \cdot 10^6 \text{ l/mol}$  calculated from kinetic measurements confirmed highly specific interaction. The detection of  $A\beta_{1-16}$  (Mw = 1950 Da) in very low concentrations opens a possibility of detecting the actual AD biomarker,  $A\beta_{1-42}$ , which has a higher molecular size (Mw = 4500 Da).

Two types of quartz crystal microbalance (QCM) measurements in liquid were explored for studying binding of APP770 to DE2 antibodies. First, a fully-automated, commercial QCM instrument (Sierra Sensors) with microfluidic flow was employed and showed that it was enable *in-situ* detection of APP770 in up to 16 times dilutions. Secondly, QCM impedance measurements were used to provide qualitative and quantitative information about the effect of viscosity of liquid on the oscillation damping. In this work, qualitative analysis of polynomial fit clearly showed the shift of frequency and the changes of spectral peaks after each injection. A similar (to QCM in air) pattern was observed for frequency changes after the absorption of PAH, Protein G, DE2 antibodies and APP770. The decrease in the resonance frequency was caused by adsorption (or binding) of analyte molecules on the surface of quartz crystal.

The changes in the surface morphology caused by consecutive absorption of PAH, Protein G, DE2 antibodies and APP were analyzed with AFM technique. It was quite difficult to judge the nature of the binding from the 2D and pseudo-3D images, but the analysis of surface roughness validated the relation of surface roughness with molecular size.

The second part of this work was dedicated to detection of low molecular weight mycotoxins, Zearalenone (ZON) and Aflatoxin B1 (AFT). The detection of zearalenone using TIRE method was performed in both direct and competitive inhibition immunoassay. A minimal detected concentrations of ZON of 0.1 ng/ml and 0.01 ng/ml were found for direct and competitive inhibition assay, respectively. A small difference (in only one order of magnitude) between these assays can be explained by the formation of aggregates of zearalenone molecules in aqueous solutions. As a result, the antibodies do not bind individual ZON molecules but rather large aggregates; this increases the response in direct immunoassay but decreases it in competitive assay format.

A remarkably low detection limit of 0.04 ng/ml has been achieved for aflatoxin B1 in direct immunoassay format. A comparison of TIRE direct immunoassay of ZON and AFT by TIRE method has been made. The results clearly showed that the effective thickness increment is larger than the molecular size for both toxins, which again confirms the idea of the formation of aggregates of hydrophobic mycotoxin molecules. A larger response (e.g. thickness increment) for ZON as compared to AFT B1 can be caused either by the formation of larger aggregates of ZON molecules, or by the use of less specific polyclonal antibodies to ZON in contrast to highly specific monoclonal antibodies to AFT B1. The dilution of mycotoxins stock solutions in methanol with water causes aggregation of hydrophobic mycotoxin molecules and boosted the sensitivity of detection. Such dilution technique can therefore be recommended for boosting the sensitivity of direct immunoassay for other small hydrophobic molecules.

A new approach to purifying mycotoxins in contaminated liquid was described in this work. Polyelectrolyte microcapsules (6  $\mu\text{m}$  in diameter) functionalized with antibodies for zearalenone were prepared. The morphology of polyelectrolyte microcapsules was studied with SEM; and the formation of protein aggregates was clearly observed on SEM images. Such functionalized capsules were used for purification of solutions containing ZON. The capsules were simply added to the solution containing ZON, after binding ZON molecules heavy capsules sediment on the bottom of test tube leaving purified solution above. The fact of reduction of concentration of ZON was confirmed by UV-vis absorption spectra measurements. This approach is believed to be cost effective as compared to other conventional techniques. Based on this fact, modified microcapsules could be used in biomedical application to purify body liquids contaminated with mycotoxins.

The method of TIRE was successfully used in this work as an analytical tool for immune analysis. Apart from high sensitivity, the proposed method has several other advantages of being label-free, using cost-effective direct immunoassay format, and providing fast measurements. The results reported in this thesis give a clear possibility for using TIRE method for diagnostics of Alzheimer's Disease at early stages.

## 8.2 Recommendations for future work

The method of TIRE proved to be a very promising analytical tool in biosensing and showed great potential for a number of applications including bio-medical and environmental applications. Several recommendations are made here for future development:

1. The work on Alzheimer's Disease diagnostics should be expanded to detection of actual AD biomarker in biological fluids from an Alzheimer's Disease patients.
2. TIRE method based on spectroscopic ellipsometry is expensive bench-top instrument for suitable in-lab testing method. In order to be used for in medical practice, portable, hand-held are required. This could be achieved using planar waveguide devices which are based on similar physical principles (evanescent wave) but much smaller, cheaper, and at the same time more sensitive. This R&D possibility should be explored in near future.
3. For other applications in which the volume of chemicals is not an issue, the measurements in a constant flow of could be used. This will provide an opportunity of simultaneous spectroscopic and dynamic TIRE measurements.
4. The stability and consistency of QCM impedance measurements could be improved by measuring at the second or third harmonics of the resonance frequency. This could be done either using crystals with a smaller fundamental frequency or using a spectrum analyzer operating in a wide spectral range.
5. Further analysis of QCM impedance spectra in liquids using BVD circuit model could be undertaken to evaluate precisely the added mass as well as changes in the physical properties of the molecular coating, e. g. energy losses, elasticity, etc.

## References

- [1] J. L. Cummings, "Treatment of alzheimer's disease," *Clin. Cornerstone*, vol. 3, pp. 27-39, 2001.
- [2] G. Waldemar, B. Dubois, M. Emre, J. Georges, I. G. McKeith, M. Rossor, P. Scheltens, P. Tariska and B. Winblad, "Recommendations for the diagnosis and management of Alzheimer's disease and other disorders associated with dementia: EFNS guideline," *Eur. J. Neurol.*, vol. 14, pp. E1-E26, JAN, 2007.
- [3] I. Mebane-Sims, "2009 Alzheimer's disease facts and figures," *Alzheimer's and Dementia*, vol. 5, pp. 234-270, 5, 2009.
- [4] A. Wimo, B. Winblad, H. Aguero-Torres and E. von Strauss, "The magnitude of dementia occurrence in the world," *Alzheimer Dis. Assoc. Dis.*, vol. 17, pp. 63-67, APR-JUN, 2003.
- [5] World Health Organisation, "The world health report 2003, shaping the future," World Health Organisation, Switzerland, 2003.
- [6] C. P. Ferri, M. Prince, C. Brayne, H. Brodaty, L. Fratiglioni, M. Ganguli, K. Hall, K. Hasegawa, H. Hendrie, Y. Q. Huang, A. Jorm, C. Mathers, P. R. Menezes, E. Rimmer, M. Sczufca and *Alzheimers Dis Intl*, "Global prevalence of dementia: a Delphi consensus study," *Lancet*, vol. 366, pp. 2112-2117, DEC-JAN, 2005.
- [7] M. J. Clark, J. Gagnon, A. F. Williams and A. N. Barclay, "Mrc Ox-2 Antigen - a Lymphoid Neuronal Membrane Glycoprotein with a Structure Like a Single Immunoglobulin Light Chain," *EMBO J.*, vol. 4, pp. 113-118, 1985.

- [8] G. G. Glenner and C. W. Wong, "Alzheimers-Disease - Initial Report of the Purification and Characterization of a Novel Cerebrovascular Amyloid Protein," *Biochem. Biophys. Res. Commun.*, vol. 120, pp. 885-890, 1984.
- [9] C. Haass, M. G. Schlossmacher, A. Y. Hung, C. Vigopelfrey, A. Mellon, B. L. Ostaszewski, I. Lieberburg, E. H. Koo, D. Schenk, D. B. Teplow and D. J. Selkoe, "Amyloid Beta-Peptide is Produced by Cultured-Cells during Normal Metabolism," *Nature*, vol. 359, pp. 322-325, SEP 24, 1992.
- [10] B. T. Hyman and R. E. Tanzi, "Amyloid, Dementia and Alzheimers-Disease," *Curr. Opin. Neurol. Neurosurg.*, vol. 5, pp. 88-93, FEB, 1992.
- [11] P. Seubert, C. Vigopelfrey, F. Esch, M. Lee, H. Dovey, D. Davis, S. Sinha, M. Schlossmacher, J. Whaley, C. Swindlehurst, R. McCormack, R. Wolfert, D. Selkoe, I. Lieberburg and D. Schenk, "Isolation and Quantification of Soluble Alzheimers Beta-Peptide from Biological-Fluids," *Nature*, vol. 359, pp. 325-327, SEP 24, 1992.
- [12] N. Ramakrishna, M. Smedman and B. Gillam, "Suppression of Alzheimer amyloid precursor protein (APP) expression by exogenous APP mRNA," *Arch. Biochem. Biophys.*, vol. 326, pp. 243-251, FEB 15, 1996.
- [13] J. Kang, H. G. Lemaire, A. Unterbeck, J. M. Salbaum, C. L. Masters, K. H. Grzeschik, G. Multhaup, K. Beyreuther and B. Mullerhill, "The Precursor of Alzheimers-Disease Amyloid-A4 Protein Resembles a Cell-Surface Receptor," *Nature*, vol. 325, pp. 733-736, FEB 19, 1987.
- [14] <http://www.nia.nih.gov/Alzheimers/Resources/HighRes.htm> "Alzheimers", vol. 2010. .
- [15] C. L. Masters, G. Simms, N. A. Weinman, G. Multhaup, B. L. McDonald and K. Beyreuther, "Amyloid Plaque Core Protein in Alzheimer-Disease and Down Syndrome," *Proc. Natl. Acad. Sci. U. S. A.*, vol. 82, pp. 4245-4249, 1985.

- [16] B. Ibach, H. Binder, M. Dragon, S. Poljansky, E. Haen, E. Schmitz, H. Koch, A. Putzhammer, H. Klauenemann, W. Wieland and G. Hajak, "Cerebrospinal fluid tau and beta-amyloid in Alzheimer patients, disease controls and an age-matched random sample," *Neurobiol. Aging*, vol. 27, pp. 1202-1211, SEP, 2006.
- [17] W. Xia, T. Yang, G. Shankar, I. M. Smith, Y. Shen, D. M. Walsh and D. J. Selkoe, "A Specific Enzyme-Linked Immunosorbent Assay for Measuring beta-Amyloid Protein Oligomers in Human Plasma and Brain Tissue of Patients With Alzheimer Disease," *Arch. Neurol.*, vol. 66, pp. 190-199, FEB, 2009.
- [18] G. Grasso, P. Mineo, E. Rizzarelli and G. Spoto, "MALDI, AP/MALDI and ESI techniques for the MS detection of amyloid  $\beta$ -peptides," *International Journal of Mass Spectrometry*, vol. 282, pp. 50-55, 4/15, 2009.
- [19] D. A. White, A. K. Buell, C. M. Dobson, M. E. Welland and T. P. J. Knowles, "Biosensor-based label-free assays of amyloid growth," *FEBS Lett.*, vol. 583, pp. 2587-2592, AUG 20, 2009.
- [20] I. Chou, M. Benford, H. T. Beier, G. L. Cote, M. Wang, N. Jing, J. Kameoka and T. A. Good, "Nanofluidic biosensing for beta-amyloid detection using surface enhanced Raman spectroscopy," *Nano Lett.*, vol. 8, pp. 1729-1735, JUN, 2008.
- [21] K. Hegnerova, M. Bockova, H. Vaisocherova, Z. Kristofikova, J. Ricny, D. Ripova and J. Homola, "Surface plasmon resonance biosensors for detection of Alzheimer disease biomarker," *Sens. Actuator B-Chem.*, vol. 139, pp. 69-73, MAY 20, 2009.
- [22] K. Skerget, A. Taler-Vercic, A. Bavdek, V. Hodnik, S. Ceru, M. Tusek-Znidaric, T. Kumm, D. Pitsi, M. Pompe-Novak, P. Palumaa, S. Soriano, N. Kopitar-Jerala, V. Turk, G. Anderluh and E. Zerovnik, "Interaction between Oligomers of Stefin B and Amyloid-beta in Vitro and in Cells," *J. Biol. Chem.*, vol. 285, pp. 3201-3210, JAN 29, 2010.

- [23] A. J. Haes, L. Chang, W. L. Klein and R. P. Van Duyne, "Detection of a biomarker for Alzheimer's disease from synthetic and clinical samples using a nanoscale optical biosensor," *J. Am. Chem. Soc.*, vol. 127, pp. 2264-2271, 2005.
- [24] M. Malmsten, U. Kassner, K. Winkler, A. Schmidt, E. Buddecke, R. Saunders and G. Siegel, "An ellipsometry-based Alzheimer plaque mimic: Effect of beta-amyloid, lipoprotein identity and apolipoprotein E isoform," *J. Colloid Interface Sci.*, vol. 276, pp. 503-506, AUG 15, 2004.
- [25] <http://www.aflatoxin.info/aflatoxin.asp> "Aflatoxin," vol. 2010.
- [26] S. Cho, C. Lee, M. Jang, Y. Son, S. Lee, I. Choi, S. Kim and D. Kim, "Aflatoxins contamination in spices and processed spice products commercialized in Korea," *Food Chem.*, vol. 107, pp. 1283-1288, 4/1, 2008.
- [27] Saleemullah, A. Iqbal, I. A. Khalil and H. Shah, "Aflatoxin contents of stored and artificially inoculated cereals and nuts," *Food Chem.*, vol. 98, pp. 699-703, 2006.
- [28] S. J. Kershaw, "Occurrence of Aflatoxins in Oilseeds Providing Cocoa-Butter Substitutes," *Appl. Environ. Microbiol.*, vol. 43, pp. 1210-1212, 1982.
- [29] M. O. Moss, "Risk assessment for aflatoxins in foodstuffs," *Int. Biodeterior. Biodegrad.*, vol. 50, pp. 137-142, 10, 2002.
- [30] J. C. C. Yu and E. P. C. Lai, "Polypyrrole film on miniaturized surface plasmon resonance sensor for ochratoxin A detection," *Synth. Met.*, vol. 143, pp. 253-258, JUN 21, 2004.
- [31] C. P. Wild and Y. Y. Gong, "Mycotoxins and human disease: a largely ignored global health issue," *Carcinogenesis*, vol. 31, pp. 71-82, JAN, 2010.

- [32] M. T. Webster, N. Groome, P. T. Francis, B. R. Pearce, F. E. Sherriff, G. Thinakaran, K. M. Felsenstein, W. Wasco, R. E. Tanzi and D. M. Bowen, "A Novel Protein, Amyloid Precursor-Like Protein-2, is Present in Human Brain, Cerebrospinal-Fluid and Conditioned Media," *Biochem. J.*, vol. 310, pp. 95-99, AUG 15, 1995.
- [33] G. W. Hudler, *Magical Mushrooms, Mischievous Mold*. New Jersey: Princeton University Press, 1998.
- [34] M. Peraica, B. Radic, A. Lucic and M. Pavlovic, "Toxic effects of mycotoxins in humans," *Bull. World Health Organ.*, vol. 77, pp. 754-766, 1999.
- [35] J. H. Williams, T. D. Phillips, P. E. Jolly, J. K. Stiles, C. M. Jolly and D. Aggarwal, "Human aflatoxicosis in developing countries: a review of toxicology, exposure, potential health consequences, and interventions," *Am. J. Clin. Nutr.*, vol. 80, pp. 1106-1122, NOV, 2004.
- [36] D. M. Parkin, "The global health burden of infection -associated cancers in the year 2002," *Int. J. Cancer*, vol. 118, pp. 3030-3044, JUN 15, 2006.
- [37] T. Kuiper-Goodman, P. M. Scott and H. Watanabe, "Risk assessment of the mycotoxin zearalenone," *Regulatory Toxicology and Pharmacology*, vol. 7, pp. 253-306, 9, 1987.
- [38] European Commission, "Commission Regulation (EC) No. 856/2005 of 6 June 2005, amending Regulation (EC) No 466/2001 as regards Fusarium Toxins," vol. 143, pp. 3-8, 2005.
- [39] European Commission, "Commission Regulation No (EC) No. 1881/2006 of 19 December 2006 setting maximum levels for certain contaminants in foodstuffs," vol. L364, pp. 5-24, 2006.
- [40] European Commission, "Commission Regulation (EC) No. 1126/2007 of 28 September 2007, amending Regulation (EC) No. 1881/2006 setting maximum

levels for certain contaminants in foodstuff as regards Fusarium toxins in maize and maize products," vol. L255, pp. 14-17, 2007.

- [41] IARC (International Agency for Research and Cancer), "Some Naturally Occuring Substances; Foods Items and Constituents, Heterocyclic Aromatic Amines and Mycotoxins." vol. 56, 1993.
- [42] European Commission, "Commission Regulation (EC) No 1525/98," vol. L201, pp. 43, 1998.
- [43] L. D. Mello and L. T. Kubota, "Review of the use of biosensors as analytical tools in the food and drink industries," *Food Chem.*, vol. 77, pp. 237-256, MAY, 2002.
- [44] J. Stroka, R. v. Otterdijk and E. Anklam, "Immunoaffinity column clean-up prior to thin-layer chromatography for the determination of aflatoxins in various food matrices," *Journal of Chromatography A*, vol. 904, pp. 251-256, 12/29, 2000.
- [45] R. J. Garcia-Villanova, C. Cordon, A. M. G. Paramas, P. Aparicio and M. E. G. Rosales, "Simultaneous immunoaffinity column cleanup and HPLC analysis of aflatoxins and ochratoxin A in Spanish bee pollen," *J. Agric. Food Chem.*, vol. 52, pp. 7235-7239, DEC 1, 2004.
- [46] M. Sulyok, R. Krska and R. Schuhmacher, "A liquid chromatography/tandem mass spectrometric multi-mycotoxin method for the quantification of 87 analytes and its application to semi-quantitative screening of moldy food samples," *Anal. Bioanal. Chem.*, vol. 389, pp. 1505-1523, NOV, 2007.
- [47] L. K. Sørensen and T. H. Elbæk, "Determination of mycotoxins in bovine milk by liquid chromatography tandem mass spectrometry," *Journal of Chromatography B*, vol. 820, pp. 183-196, 6/25, 2005.
- [48] B. Delmulle, S. De Saeger, A. Adams, N. De Kimpe and C. Van Peteghem, "Development of a liquid chromatography/tandem mass spectrometry method

for the simultaneous determination of 16 mycotoxins on cellulose filters and in fungal cultures," *Rapid Commun. Mass Spectrom.*, vol. 20, pp. 771-776, 2006.

- [49] X. Jin, X. Jin, X. Liu, L. Chen, J. Jiang, G. Shen and R. Yu, "Biocatalyzed deposition amplification for detection of aflatoxin B1 based on quartz crystal microbalance," *Anal. Chim. Acta*, vol. 645, pp. 92-97, 7/10, 2009.
- [50] X. Jin, X. Jin, L. Chen, J. Jiang, G. Shen and R. Yu, "Piezoelectric immunosensor with gold nanoparticles enhanced competitive immunoreaction technique for quantification of aflatoxin B1," *Biosensors and Bioelectronics*, vol. 24, pp. 2580-2585, 4/15, 2009.
- [51] B. van der Gaag, S. Spath, H. Dietrich, E. Stigter, G. Boonzaaijer, T. van Osenbruggen and K. Koopal, "Biosensors and multiple mycotoxin analysis," *Food Control*, vol. 14, pp. 251-254, JUN, 2003.
- [52] S. J. Daly, G. J. Keating, P. P. Dillon, B. M. Manning, R. O'Kennedy, H. A. Lee and M. R. A. Morgan, "Development of surface plasmon resonance-based immunoassay for aflatoxin B-1," *J. Agric. Food Chem.*, vol. 48, pp. 5097-5104, NOV, 2000.
- [53] W. Mullett, E. P. C. Lai and J. M. Yeung, "Immunoassay of fumonisins by a surface plasmon resonance biosensor," *Anal. Biochem.*, vol. 258, pp. 161-167, MAY 1, 1998.
- [54] A. J. Tudos, E. R. Lucas-van den Bos and E. C. A. Stigter, "Rapid surface plasmon resonance-based inhibition assay of deoxynivalenol," *J. Agric. Food Chem.*, vol. 51, pp. 5843-5848, SEP 24, 2003.
- [55] J. C. C. Yu and E. P. C. Lai, "Polypyrrole film on miniaturized surface plasmon resonance sensor for ochratoxin A detection," *Synth. Met.*, vol. 143, pp. 253-258, JUN 21, 2004.

- [56] C. M. Maragos and V. S. Thompson, "Fiber-optic immunosensor for mycotoxins," *Nat. Toxins*, vol. 7, pp. 371-376, 1999.
- [57] N. Adányi, I. A. Levkovets, S. Rodriguez-Gil, A. Ronald, M. Váradi and I. Szendrő, "Development of immunosensor based on OWLS technique for determining Aflatoxin B1 and Ochratoxin A," *Biosensors and Bioelectronics*, vol. 22, pp. 797-802, 1/15, 2007.
- [58] D. Abramson, J. D. House and C. M. Nyachoti, "Reduction of deoxynivalenol in barley by treatment with aqueous sodium carbonate and heat," *Mycopathologia*, vol. 160, pp. 297-301, NOV, 2005.
- [59] S. Herzallah, K. Alshwabkeh and A. Al Fataftah, "Aflatoxin Decontamination of Artificially Contaminated Feeds by Sunlight, gamma-Radiation, and Microwave Heating," *J. Appl. Poult. Res.*, vol. 17, pp. 515-521, WIN, 2008.
- [60] G. Piva, F. Galvano, A. Pietri and A. Piva, "Detoxification methods of aflatoxins. A review," *Nutr. Res.*, vol. 15, pp. 767-776, 5, 1995.
- [61] U. Samarajeewa, A. C. Sen, M. D. Cohen and C. I. Wei, "Detoxification of Aflatoxins in Foods and Feeds by Physical and Chemical Methods," *J. Food Prot.*, vol. 53, pp. 489-501, JUN, 1990.
- [62] N. Takahashi-Ando, T. Tokai, H. Hamamoto, I. Yamaguchi and M. Kimura, "Efficient decontamination of zearalenone, the mycotoxin of cereal pathogen, by transgenic yeasts through the expression of a synthetic lactonohydrolase gene," *Appl. Microbiol. Biotechnol.*, vol. 67, pp. 838-844, JUN, 2005.
- [63] G. Schatzmayr, F. Zehner, M. Taubel, D. Schatzmayr, A. Klimitsch, A. P. Loibner and E. M. Binder, "Microbiologicals for deactivating mycotoxins," *Mol. Nutr. Food Res.*, vol. 50, pp. 543-551, MAY, 2006.

- [64] E. Donath, G. B. Sukhorukov, F. Caruso, S. A. Davis and H. Mohwald, "Novel hollow polymer shells by colloid-templated assembly of polyelectrolytes," *Angew. Chem. -Int. Edit.*, vol. 37, pp. 2202-2205, AUG 17, 1998.
- [65] F. Caruso, R. A. Caruso and H. Mohwald, "Nanoengineering of inorganic and hybrid hollow spheres by colloidal templating," *Science*, vol. 282, pp. 1111-1114, NOV 6, 1998.
- [66] G. Decher, "Fuzzy nanoassemblies: Toward layered polymeric multicomposites," *Science*, vol. 277, pp. 1232-1237, AUG 29, 1997.
- [67] J. J. Kulys, V. V. Sorochinskii and R. A. Vidziunaite, "Transient response of bienzyme electrodes," *Biosensors*, vol. 2, pp. 135-146, 1986.
- [68] B. R. Eggins, *Biosensors: An Introduction*. UK: John Wiley & Sons, 1996.
- [69] R. Thusu. (2010, 1 Oct). Strong growth predicted for biosensors market. *Weekly*
- [70] Global industry Analyst Inc., "Biosensors in medical diagnostics-global bussiness report," US, 2008.
- [71] I. V. Turko, G. I. Lepesheva and V. L. Chashchin, "Direct Antigen-Detection in Langmuir-Blodgett-Films of Immunoglobulin-G Modified with Coproporphyrin-i," *Anal. Chim. Acta*, vol. 265, pp. 21-26, AUG 1, 1992.
- [72] K. A. Defillipo and M. L. Grayeski, "Flow-Injection Chemiluminescent Method for an Enzyme-Labeled Dna Probe," *Anal. Chim. Acta*, vol. 249, pp. 155-162, AUG 15, 1991.
- [73] G. F. Blackburn, H. P. Shah, J. H. Kenten, J. Leland, R. A. Kamin, J. Link, J. Peterman, M. J. Powell, A. Shah, D. B. Talley, S. K. Tyagi, E. Wilkins, T. G. Wu and R. J. Massey, "Electrochemiluminescence Detection for Development of Immunoassays and Dna Probe Assays for Clinical Diagnostics," *Clin. Chem.*, vol. 37, pp. 1534-1539, SEP, 1991.

- [74] B. F. Rocks, N. Patel and M. P. Bailey, "Use of a Silver-Enhanced Gold-Labeled Immunoassay for Detection of Antibodies to the Human-Immunodeficiency-Virus in Whole-Blood Samples," *Ann. Clin. Biochem.*, vol. 28, pp. 155-159, MAR, 1991.
- [75] E. H. J. M. Jansen, R. H. Vandenberg and G. Zomer, "Characteristics and Detection Principles of a New Enzyme Label Producing a Long-Term Chemiluminescent Signal," *J. Biolumin. Chemilumin.*, vol. 4, pp. 129-135, JUL, 1989.
- [76] Bertazzo.U, S. D. Ehrlich and G. Bernardi, "Radioactive Labeling and Analysis of 3'-Terminal Nucleotides of Dna Fragments," *Biochim. Biophys. Acta*, vol. 312, pp. 192-201, 1973.
- [77] T. Hyypia, "Detection of Adenovirus in Nasopharyngeal Specimens by Radioactive and Nonradioactive Dna Probes," *J. Clin. Microbiol.*, vol. 21, pp. 730-733, 1985.
- [78] K. R. Rogers, "Principles of affinity-based biosensors," *Mol. Biotechnol.*, vol. 14, pp. 109-129, FEB, 2000.
- [79] M. L. Yarmush, K. P. Antonsen, S. Sundaram and D. M. Yarmush, "Immunoabsorption - Strategies for Antigen Elution and Production of Reusable Adsorbents," *Biotechnol. Prog.*, vol. 8, pp. 168-178, MAY-JUN, 1992.
- [80] B. Hock, "Antibodies for immunosensors - A review," *Anal. Chim. Acta*, vol. 347, pp. 177-186, JUL 30, 1997.
- [81] Jason Brownlee, "Antigen-antibody interaction," Australia, Tech. Rep. 070427A, 2007.
- [82] D. Wild, Ed., *The Immunoassay Handbook*. London: Elsevier, 2005.

- [83] David Male, Jonathan Brostoff, David B Roth and Ivan Roitt, Immunology. Canada: Elsevier, 2006.
- [84] F. T. Bosman, M. Vanderploeg, P. Vanduijn and A. Schaberg, "Photometric Determination of Dna Distribution in 24-Human Chromosomes," *Exp. Cell Res.*, vol. 105, pp. 301-311, 1977.
- [85] J. L. Guesdon, "Immunoenzymatic Techniques Applied to the Specific Detection of Nucleic-Acids - a Review," *J. Immunol. Methods*, vol. 150, pp. 33-49, JUN 24, 1992.
- [86] E. Palecek, M. Vojtiskova, F. Jelen and E. Lukasova, "Introduction of an Electroactive Marker into the Polynucleotide Chain - a New Probe for Distorted Regions in the Dna Double Helix," *Bioelectrochem. Bioenerget.*, vol. 12, pp. 135-136, 1984.
- [87] K. Kerman, D. Ozkan, P. Kara, B. Meric, J. J. Gooding and M. Ozsoz, "Voltammetric determination of DNA hybridization using methylene blue and self-assembled alkanethiol monolayer on gold electrodes," *Anal. Chim. Acta*, vol. 462, pp. 39-47, JUN 26, 2002.
- [88] M. Wilchek and E. Bayer, Eds., *Methods in Enzymology; Avidin Biotin Technology*. UK: Academic Press Limited, 1990.
- [89] K. Hofmann and Y. Kiso, "Approach to Targeted Attachment of Peptides and Proteins to Solid Supports," *Proc. Natl. Acad. Sci. U. S. A.*, vol. 73, pp. 3516-3518, 1976.
- [90] E. A. Bayer, M. Wilchek and E. Skutelsky, "Affinity Cytochemistry - Localization of Lectin and Antibody Receptors on Erythrocytes Via Avidin-Biotin Complex," *FEBS Lett.*, vol. 68, pp. 240-244, 1976.

- [91] M. H. Heggeness and J. F. Ash, "Use of Avidin-Biotin Complex for Localization of Actin and Myosin with Fluorescence Microscopy," *J. Cell Biol.*, vol. 73, pp. 783-788, 1977.
- [92] E. A. Bayer, M. G. Zalis and M. Wilchek, "3-(N-Maleimido-Propionyl) Biotin - a Versatile Thiol-Specific Biotinylating Reagent," *Anal. Biochem.*, vol. 149, pp. 529-536, 1985.
- [93] G. Barnard, E. A. Bayer, M. Wilchek, Y. Amirzaltsman and F. Kohen, "Amplified Bioluminescence Assay using Avidin Biotin Technology," *Meth. Enzymol.*, vol. 133, pp. 284-288, 1986.
- [94] F. Ricci, G. Volpe, L. Micheli and G. Palleschi, "A review on novel developments and applications of immunosensors in food analysis," *Anal. Chim. Acta*, vol. 605, pp. 111-129, DEC 19, 2007.
- [95] K. Janis, *Immunology*. W.H.Freeman & Co, 1997.
- [96] A. V. Elgersma, R. L. J. Zsom, W. Norde and J. Lyklema, "The Adsorption of Different Types of Monoclonal Immunoglobulin on Positively and Negatively Charged Polystyrene Lattices," *Colloids and Surfaces*, vol. 54, pp. 89-101, MAR 14, 1991.
- [97] P. Bagchi and S. M. Birnbaum, "Effect of Ph on the Adsorption of Immunoglobulin-G on Anionic Poly(vinyltoluene) Model Latex-Particles," *J. Colloid Interface Sci.*, vol. 83, pp. 460-478, 1981.
- [98] W. Schramm, S. Paek and G. Voss, "Strategies for the Immobilization of Antibodies," *Immunomethods*, vol. 3, pp. 93-103, 10, 1993.
- [99] K. Nakanishi, H. Muguruma and I. Karube, "A novel method of immobilizing antibodies on a quartz crystal microbalance using plasma-polymerized films for immunosensors," *Anal. Chem.*, vol. 68, pp. 1695-1700, MAY 15, 1996.

- [100] Y. Li, Ed., *Biosensors: In Handbook of Agriculture Engineering*. Michigan, USA: Axel Munack, 2006.
- [101] D. R. Shankaran, K. V. Gobi and N. Miura, "Recent advancements in surface plasmon resonance immunosensors for detection of small molecules of biomedical, food and environmental interest," *Sensors and Actuators B: Chemical*, vol. 121, pp. 158-177, 1/30, 2007.
- [102] M. W. Foster, D. J. Ferrel and R. A. Lieberman, "Surface plasmon resonance biosensor miniaturization," in *Chemical, Biochemical, and Environmental Fiber Sensors VI*, 1994, pp. 122-31.
- [103] A. V. Nabok, T. A. A. Holloway, N. F. Starodub, A. Demchenko and O. Gojster, "Registration of low molecular weight environmental toxins with total internal reflection ellipsometry," in *Sensors, 2004. Proceedings of IEEE, 2004*, pp. 1195-1198 vol.3.
- [104] J. Homola, "Surface plasmon resonance sensors for detection of chemical and biological species," *Chem. Rev.*, vol. 108, pp. 462-493, FEB, 2008.
- [105] W. Lukosz, "Principles and sensitivities of integrated optical and surface plasmon sensors for direct affinity sensing and immunosensing," *Biosensors and Bioelectronics*, vol. 6, pp. 215, 1991.
- [106] A. Shons, J. Najarian and F. Dorman, "Immunospecific Microbalance," *J. Biomed. Mater. Res.*, vol. 6, pp. 565-&, 1972.
- [107] S. Babacan, P. Pivarnik, S. Letcher and A. G. Rand, "Evaluation of antibody immobilization methods for piezoelectric biosensor application," *Biosensors and Bioelectronics*, vol. 15, pp. 615-621, 12, 2000.
- [108] S. Kurosawa, H. Aizawa, M. Tozuka, M. Nakamura and J. W. Park, "Immunosensors using a quartz crystal microbalance," *Meas Sci Technol*, vol. 14, pp. 1882-1887, NOV, 2003.

- [109] S. Kurosawa, J. Park, H. Aizawa, S. Wakida, H. Tao and K. Ishihara, "Quartz crystal microbalance immunosensors for environmental monitoring," *Biosensors and Bioelectronics*, vol. 22, pp. 473-481, 10/15, 2006.
- [110] X. L. Su and Y. B. Li, "A self-assembled monolayer-based piezoelectric immunosensor for rapid detection of *Escherichia coli* O157 : H7," *Biosens. Bioelectron.*, vol. 19, pp. 563-574, JAN 15, 2004.
- [111] A. F. Holloway, A. Nabok, M. Thompson, A. K. Ray and T. Wilkop, "Impedance analysis of the thickness shear mode resonator for organic vapour sensing," *Sensors and Actuators B: Chemical*, vol. 99, pp. 355-360, 5/1, 2004.
- [112] J. Zhang, X. D. Su and S. J. O'Shea, "Antibody/antigen affinity behavior in liquid environment with electrical impedance analysis of quartz crystal microbalances," *Biophys. Chem.*, vol. 99, pp. 31-41, SEP 3, 2002.
- [113] H. Q. Zhao, L. Lin, J. R. Li, J. A. Tang, M. X. Duan and L. Jiang, "DNA biosensor with high sensitivity amplified by gold nanoparticles," *Journal of Nanoparticle Research*, vol. 3, pp. 321-3, 08, 2001.
- [114] S. Yukioka and T. Inoue, "Ellipsometric Analysis of Polymer Polymer Interface," *Polymer Communications*, vol. 32, pp. 17-19, 1991.
- [115] T. Mutschler, B. Kieser, R. Frank and G. Gauglitz, "Characterization of thin polymer and biopolymer layers by ellipsometry and evanescent field technology," *Anal. Bioanal. Chem.*, vol. 374, pp. 658-664, OCT, 2002.
- [116] M. A. Hempenius, M. Peter, N. S. Robins, E. S. Kooij and G. J. Vancso, "Water-soluble poly(ferrocenylsilanes) for supramolecular assemblies by layer-by-layer deposition," *Langmuir*, vol. 18, pp. 7629-7634, OCT 1, 2002.

- [117] S. S. Lee, K. B. Lee and J. D. Hong, "Evidence for spin coating electrostatic self-assembly of polyelectrolytes," *Langmuir*, vol. 19, pp. 7592-7596, SEP 2, 2003.
- [118] A. V. Nabok, N. V. Lavrik, Z. I. Kazantseva, B. A. Nesterenko, L. N. Markovskiy, V. I. Kalchenko and A. N. Shivaniuk, "Complexing Properties of Calix[4]resorcinolarene Lb Films," *Thin Solid Films*, vol. 259, pp. 244-247, APR 15, 1995.
- [119] T. Riedl, W. Nitsch and T. Michel, "Gas permeability of Langmuir-Blodgett (LB) films: characterisation and application," *Thin Solid Films*, vol. 379, pp. 240-252, DEC 8, 2000.
- [120] C. C. Tsai, C. Chou, C. Y. Han, C. H. Hsieh, K. Y. Liao and Y. F. Chao, "Determination of optical parameters of a twisted-nematic liquid crystal by phase-sensitive optical heterodyne interferometric ellipsometry," *Appl. Opt.*, vol. 44, pp. 7509-7514, DEC 10, 2005.
- [121] H. Arwin, "Is ellipsometry suitable for sensor applications?" *Sensors and Actuators A: Physical*, vol. 92, pp. 43-51, 8/1, 2001.
- [122] R. M. Ostroff, D. Hopkins, A. B. Haeberli, W. Baouchi and B. Polisky, "Thin Film Biosensor for Rapid Visual Detection of Nucleic Acid Targets," *Clin Chem*, vol. 45, pp. 1659-1664, September 1, 1999.
- [123] B. Trotter, G. Moddel, R. Ostroff and G. R. Bogart, "Fixed-polarizer ellipsometry: a simple technique to measure the thickness of very thin films," *Opt. Eng.*, vol. 38, pp. 902-907, MAY, 1999.
- [124] A. Tsargorodskaya, "Research and Development in Optical Biosensors for Environment Control," 2007.
- [125] T. Laurell, J. Drott and L. Rosengren, "Silicon wafer integrated enzyme reactors," *Biosensors and Bioelectronics*, vol. 10, pp. 289-299, 1995.

- [126] P. Westphal and A. Bornmann, "Biomolecular detection by surface plasmon enhanced ellipsometry," *Sensors and Actuators, B: Chemical*, vol. 84, pp. 278-282, 2002.
- [127] H. Arwin, M. Poksinski and K. Johansen, "Total internal reflection ellipsometry: principles and applications," *Appl. Opt.*, vol. 43, pp. 3028-3036, MAY 20, 2004.
- [128] A. V. Nabok, A. Tsargorodskaya, A. K. Hassan and N. F. Starodub, "Total internal reflection ellipsometry and SPR detection of low molecular weight environmental toxins," *Applied Surface Science*, vol. 246, pp. 381-386, 6/30, 2005.
- [129] H. Kim, S. Jung, S. Kim, I. Suh, W. J. Kim, J. Jung, J. s. Yuk, Y. Kim and K. Ha, "High-throughput analysis of mumps virus and the virus-specific monoclonal antibody on the arrays of a cationic polyelectrolyte with a spectral SPR biosensor," *Proteomics*, vol. 6, pp. 6426-6432, DEC, 2006.
- [130] A. Tsargorodskaya, S. V. Lishchuk and A. Nabok, "The model of alkylphenol micelles bound to respective antibodies on the solid surface," *Colloid Surf. A-Physicochem. Eng. Asp.*, vol. 324, pp. 117-121, JUL 1, 2008.
- [131] J A Woollam Co. Inc, *Guide to using WVASE32, Software for Spectroscopic Ellipsometry Data Acquisition and Analysis*. New York: Wex Tech Systems Inc., 2001.
- [132] Hiroyuki Fujiwara, *Spectroscopic Ellipsometry: Principles and Applications*. England: John Wiley & Son Ltd., 2007.
- [133] A. Otto, "Excitation of nonradiative surface plasma waves in silver by the method of frustrated total reflection," *Z. Phys.*, vol. 216, pp. 398-410, 1968.

- [134] Kretschm.E, "Determination of Optical Constants of Metals by Excitation of Surface Plasmons," *Zeitschrift Fur Physik*, vol. 241, pp. 313-&, 1971.
- [135] B. Liedberg, I. Lundström and E. Stenberg, "Principles of biosensing with an extended coupling matrix and surface plasmon resonance," *Sensors Actuators B: Chem.*, vol. 11, pp. 63-72, 3/1, 1993.
- [136] B. Liedberg, C. Nylander and I. Lundstrom, "Surface-Plasmon Resonance for Gas-Detection and Biosensing," *Sensors and Actuators*, vol. 4, pp. 299-304, 1983.
- [137] W. M. Mullett, E. P. C. Lai and J. M. Yeung, "Surface Plasmon Resonance-Based Immunoassays," *Methods*, vol. 22, pp. 77-91, 9, 2000.
- [138] R. Karlsson, "SPR for molecular interaction analysis: a review of emerging application areas," *Journal of Molecular Recognition*, vol. 17, pp. 151-161, MAY-JUN, 2004.
- [139] J. Homola, S. S. Yee and G. Gauglitz, "Surface plasmon resonance sensors: review," *Sensors and Actuators B: Chemical*, vol. 54, pp. 3-15, 1/25, 1999.
- [140] J. Homola, J. Dostalek, S. F. Chen, A. Rasooly, S. Y. Jiang and S. S. Yee, "Spectral surface plasmon resonance biosensor for detection of staphylococcal enterotoxin B in milk," *Int. J. Food Microbiol.*, vol. 75, pp. 61-69, MAY 5, 2002.
- [141] E. Brynda, J. Homola, M. Houska, P. Pfeifer and J. Skvor, "Antibody networks for surface plasmon resonance immunosensors," *Sensors and Actuators B: Chemical*, vol. 54, pp. 132-136, 1/25, 1999.
- [142] C. T. Campbell and G. Kim, "SPR microscopy and its applications to high-throughput analyses of biomolecular binding events and their kinetics," *Biomaterials*, vol. 28, pp. 2380-92, 05, 2007.

- [143] M. I. Aguilar, S. Subasinghe and D. H. Small, "Surface plasmon resonance spectroscopy for the analysis of beta-amyloid interactions in Alzheimer's disease research," *J. Neurochem.*, vol. 94, pp. 86-86, AUG, 2005.
- [144] M. Poksinski and H. Arwin, "Protein monolayers monitored by internal reflection ellipsometry," *Thin Solid Films*, vol. 455-456, pp. 716-721, 5/1, 2004.
- [145] A. Nabok and A. Tsargorodskaya, "The method of total internal reflection ellipsometry for thin film characterisation and sensing," *Thin Solid Films*, vol. 516, pp. 8993-9001, OCT 31, 2008.
- [146] A. Nabok, *Organic and Inorganic Nanostructures*. London: Artech House, 2005.
- [147] G. V. Beketov, Y. M. Shirshov, O. V. Shynkarenko and V. I. Chegel, "Surface plasmon resonance spectroscopy: prospects of superstrate refractive index variation for separate extraction of molecular layer parameters," *Sensors and Actuators B: Chemical*, vol. 48, pp. 432-438, 5/30, 1998.
- [148] A. Szekacs, N. Adanyi, I. Szekacs, K. Majer-Baranyi and Istvan Szendro, "Optical waveguide light-mode spectroscopy immunosensors for environmental monitoring," *Appl. Opt.*, vol. 48, pp. B151-B158, FEB 1, 2009.
- [149] C. Striebel, A. Brecht and G. Gauglitz, "Characterization of biomembranes by spectral ellipsometry, surface plasmon resonance and interferometry with regard to biosensor application," *Biosens. Bioelectron.*, vol. 9, pp. 139-146, 1994.
- [150] K. Spaeth, A. Brecht and G. Gauglitz, "Studies on the biotin-avidin multilayer adsorption by spectroscopic ellipsometry," *J. Colloid Interface Sci.*, vol. 196, pp. 128-135, DEC 15, 1997.
- [151] X. Liu, J. Wei, D. Song, Z. Zhang, H. Zhang and G. Luo, "Determination of affinities and antigenic epitopes of bovine cardiac troponin I (cTnI) with

monoclonal antibodies by surface plasmon resonance biosensor," *Anal.*

*Biochem.*, vol. 314, pp. 301-309, 3/15, 2003.

- [152] A. V. Nabok, A. Tsargorodskaya, A. Holloway, N. F. Starodub and O. Gojster, "Registration of T-2 mycotoxin with total internal reflection ellipsometry and QCM impedance methods," *Biosensors and Bioelectronics*, vol. 22, pp. 885-890, 1/15, 2007.
- [153] A. Nabok, A. Tsargorodskaya, A. Holloway, N. F. Starodub and A. Demchenko, "Specific binding of large aggregates of amphiphilic molecules to the respective antibodies," *Langmuir*, vol. 23, pp. 8485-8490, 2007.
- [154] Alan Holloway, "The development of the intelligent QCM sensor array," 2005.
- [155] C. K. O'Sullivan and G. G. Guilbault, "Commercial quartz crystal microbalances - theory and applications," *Biosens. Bioelectron.*, vol. 14, pp. 663-670, DEC, 1999.
- [156] R. C. Ebersole, J. A. Miller, J. R. Moran and M. D. Ward, "Spontaneously Formed Functionally Active Avidin Monolayers on Metal-Surfaces - a Strategy for Immobilizing Biological Reagents and Design of Piezoelectric Biosensors," *J. Am. Chem. Soc.*, vol. 112, pp. 3239-3241, APR 11, 1990.
- [157] S. J. Martin, H. L. Bandey, R. W. Cernosek, A. R. Hillman and M. J. Brown, "Equivalent-circuit model for the thickness-shear mode resonator with a viscoelastic film near film resonance," *Anal. Chem.*, vol. 72, pp. 141-149, JAN 1, 2000.
- [158] G. Sauerbrey, "Verwendung von Schwingquarzen zur Wagung dünner Schichten und zur Mikrowagung," *Zeitschrift Fur Physik*, vol. 155, pp. 206-222, 1959.
- [159] A. Janshoff, H. J. Galla and C. Steinem, "Piezoelectric mass-sensing devices as biosensors - An alternative to optical biosensors?" *Angew. Chem. -Int. Edit.*, vol. 39, pp. 4004-4032, 2000.

- [160] D. A. Buttry and M. D. Ward, "Measurement of Interfacial Processes at Electrode Surfaces with the Electrochemical Quartz Crystal Microbalance," *Chem. Rev.*, vol. 92, pp. 1355-1379, SEP-OCT, 1992.
- [161] T. Nomura and M. Iijima, "Electrolytic Determination of Nanomolar Concentrations of Silver in Solution with a Piezoelectric Quartz Crystal," *Anal. Chim. Acta*, vol. 131, pp. 97-102, 1981.
- [162] R. Lucklum and P. Hauptmann, "The quartz crystal microbalance: mass sensitivity, viscoelasticity and acoustic amplification," *Sensors and Actuators B: Chemical*, vol. 70, pp. 30-36, 11/1, 2000.
- [163] B. Zimmermann, R. Lucklum, P. Hauptmann, J. Rabe and S. Büttgenbach, "Electrical characterisation of high-frequency thickness-shear-mode resonators by impedance analysis," *Sensors and Actuators B: Chemical*, vol. 76, pp. 47-57, 6/1, 2001.
- [164] C. Behling, R. Lucklum and P. Hauptmann, "Response of quartz-crystal resonators to gas and liquid analyte exposure," *Sensors and Actuators A: Physical*, vol. 68, pp. 388-398, 6/15, 1998.
- [165] R. Lucklum, C. Behling and P. Hauptmann, "Gravimetric and non-gravimetric chemical quartz crystal resonators," *Sens. Actuator B-Chem.*, vol. 65, pp. 277-283, JUN 30, 2000.
- [166] R. Lucklum and P. Hauptmann, "The Delta f-Delta R QCM technique: an approach to an advanced sensor signal interpretation," *Electrochim. Acta*, vol. 45, pp. 3907-3916, 2000.
- [167] C. Steinem and A. Janshoff, Eds., *Piezoelectric Sensor*. Berlin: Springer, 2007.

- [168] R. Lucklum, C. Behling, R. W. Cernosek and S. J. Martin, "Determination of complex shear modulus with thickness shear mode resonators," *J. Phys. D-Appl. Phys.*, vol. 30, pp. 346-356, FEB 7, 1997.
- [169] [http://www.sierrasensors.com/index.php?option=com\\_content&task=view&id=23&Itemid=62](http://www.sierrasensors.com/index.php?option=com_content&task=view&id=23&Itemid=62), "Sierra Sensors - QCMA-1 Features and Benefits "vol. 2011, .
- [170] [http://www.sierrasensors.com/index.php?option=com\\_content&task=view&id=75&Itemid=62](http://www.sierrasensors.com/index.php?option=com_content&task=view&id=75&Itemid=62) "Sierra Sensors - QCMA-1 Applications "vol. 2011,
- [171] G. Binnig, C. F. Quate and C. Gerber, "Atomic Force Microscope," *Phys. Rev. Lett.*, vol. 56, pp. 930-933, MAR 3, 1986.
- [172] <http://www.nanoscience.com/education/AFM.html>, "Atomic Force Microscopy overview,"vol. 2008, .
- [173] R. F. Egerton, *Physical Principles of Electron Microscopy :An Introduction to TEM, SEM, and AEM*. New York, NY: Springer, 2005.
- [174] Suryajaya, A. V. Nabok, A. Tsargorodskaya, A. K. Hassan and F. Davis, "Electrostatically self-assembled films containing II-VI semiconductor nanoparticles: Optical and electrical properties," *Thin Solid Films*, vol. 516, pp. 8917-8925, OCT 31, 2008.
- [175] Y. Lvov, K. Ariga and T. Kunitake, "Layer-By-Layer Assembly of Alternate Protein Polyion Ultrathin Films," *Chem. Lett.*, pp. 2323-2326, DEC, 1994.
- [176] N. Alexei, *Organic and Inorganic Nanostructures*. USA: Artech House, INC., 2005.
- [177] N. F. Starodub, L. V. Pirogova, A. Demchenko and A. V. Nabok, "Antibody immobilisation on the metal and silicon surfaces. The use of self-assembled

layers and specific receptors," *Bioelectrochemistry*, vol. 66, pp. 111-115, 4, 2005.

- [178] A. Szekacs, "Enzyme-linked immunosorbent assay for monitoring the Fusarium toxin zearalenone," *Food Technol. Biotechnol.*, vol. 36, pp. 105-110, APR-JUN, 1998.
- [179] I. L. Radtchenko, G. B. Sukhorukov, S. Leporatti, G. B. Khomutov, E. Donath and H. Mohwald, "Assembly of alternated multivalent ion/polyelectrolyte layers on colloidal particles. Stability of the multilayers and encapsulation of macromolecules into polyelectrolyte capsules," *J. Colloid Interface Sci.*, vol. 230, pp. 272-280, OCT 15, 2000.
- [180] G. B. Sukhorukov and H. Moehwald, "Multifunctional cargo systems for biotechnology," *Trends Biotechnol.*, vol. 25, pp. 93-98, MAR, 2007.
- [181] S. Erokhina, L. Benassi, P. Bianchini, A. Diaspro, V. Erokhin and M. P. Fontana, "Light-Driven Release from Polymeric Microcapsules Functionalized with Bacteriorhodopsin," *J. Am. Chem. Soc.*, vol. 131, pp. 9800-9804, JUL 22, 2009.
- [182] A. Nabok, A. Tsargorodskaya, M. K. Mustafa, I. Székács, N. F. Starodub and A. Székács, "Detection of low molecular weight toxins using an optical phase method of ellipsometry," *Sensors Actuators B: Chem.*, vol. In Press, Corrected Proof, Available online 10 Feb 2010.